

Copyright
by
Katherine Hannah Zlotkowski
2015

**The Dissertation Committee for Katherine Hannah Zlotkowski Certifies that this is
the approved version of the following dissertation:**

**Chemical Biology Studies of Neuroregenerative Small Molecules using
*Caenorhabditis elegans***

Committee:

Hung-Wen Liu, Supervisor

Dionicio Siegel, Co-Supervisor

Adrian Keatinge-Clay

Guangbin Dong

Jon Pierce-Shimomura

Chemical Biology Studies of Neuroregenerative Small Molecules using
Caenorhabditis elegans

by

Katherine Hannah Zlotkowski, B.S.

Dissertation

Presented to the Faculty of the Graduate School of

The University of Texas at Austin

in Partial Fulfillment

of the Requirements

for the Degree of

Doctor of Philosophy

The University of Texas at Austin

May 2015

Acknowledgements

Thank you to Professor Dionicio Siegel for allowing me to become a part of his group, for guiding me and providing support throughout my career as a graduate student, and for making the work presented in this dissertation possible. My gratitude outpours to the members of the Siegel lab as well, particularly Anders, Andrew, Drew, Matt, and Trevor. I have learned so much from our conversations and shared experiences, both scientific and otherwise. Most of all, however, your friendship has made graduate school worthwhile. A special thanks also to Professor Jon Pierce-Shimomura and the members of his lab for helpful conversations and instructions regarding anything and everything related to *C. elegans*. You all helped me come to know and love a creature previously unfamiliar to me. Thank you to Professor Adela Ben-Yakar and her lab for an introduction to *C. elegans* laser axotomy and to Professors Hung-Wen Liu, Adrian Keatinge-Clay, and Guangbin Dong for serving on my dissertation committee. Many thanks to the friends I made while living in Austin who saw me through both good times and bad. And finally, thank you to my family, whose unfailing love and support of my dreams, goals, and life ambitions continuously encourage me to explore the world and make the most of my opportunities. It means more to me than you will ever know.

**Chemical Biology Studies of Neuroregenerative Small Molecules using
*Caenorhabditis elegans***

Katherine Hannah Zlotkowski, Ph.D.

The University of Texas at Austin, 2015

Supervisor: Hung-Wen Liu

Co-Supervisor: Dionicio Siegel

The debilitating effects of spinal cord injury can be attributed to a lack of regeneration in the central nervous system. Identification of growth-promoting pathways, particularly ones that can be controlled by small molecules, could provide significant advancements in regenerative science and lead to potential treatments for spinal cord injury. The biological investigations of neuroregenerative small molecules, specifically the natural products clovanemagnolol and vinaxanthone, have been expanded to a whole organism context using the nematode *Caenorhabditis elegans* (*C. elegans*) as a tool for these studies. A straightforward assay using *C. elegans* was developed to screen for compounds that promote neuronal outgrowth *in vivo*. This outgrowth assay was then used to guide the design of chemically edited analogs of clovanemagnolol that maintained biological activity while possessing structures amenable to further modification for mechanism of action studies. Pull-down experiments using affinity reagents synthesized from a neuroactive structural derivative, clovanebisphenol, and the *C. elegans* proteome combined with mass spectrometry-based protein identification and genetic recapitulation using mutant *C. elegans* identified the putative protein target of the small molecule as a kinesin light chain, KLC-1. Furthermore, the small molecule-promoted regeneration of

injured neurons *in vivo* was studied using laser microsurgery to cut specific axons in *C. elegans* followed by treatment with a library of analogs of the growth-promoting natural product vinaxanthone. Enhanced axonal regeneration was observed following small molecule treatment and the results were used to determine the structure-activity relationship of vinaxanthone, which may guide future development of potential drug candidates for the treatment of spinal cord injury.

Table of Contents

List of Figures.....	ix
List of Schemes.....	xiii
Abbreviations	xiv
Chapter 1 – Introduction	1
Spinal Cord Injury.....	1
Growth-Promoting Small Molecules.....	3
The Model Organism <i>Caenorhabditis elegans</i>	9
Drug Discovery in <i>C. elegans</i>	11
<i>C. elegans</i> Neurobiology	13
Conclusion	15
Chapter 2 – Clovanemagnolol and <i>C. elegans</i>	16
Small Molecules in <i>C. elegans</i>	16
Development of an <i>in vivo</i> Outgrowth Assay.....	19
Design of Clovanemagnolol Analogs	26
Mechanism of Action Studies.....	30
Generation of Organismal Lysate	31
Preparation of Reagents for Target Identification	32
Soluble Competition.....	36
Identification of an Unknown Protein Target of Clovanemagnolol....	38
Conclusion	43
Experimental Section.....	44
Chapter 3 – Vinaxanthone and Laser Axotomy	53
Synthesis of Vinaxanthone and Analogs.....	53
Outgrowth Promoted by Vinaxanthone.....	58
Laser Axotomy in <i>C. elegans</i>	58
Regeneration Following Small Molecule Exposure	62
Conclusion	69

Experimental Section.....	70
Appendix: NMR Spectra and HPLC Traces.....	75
References	147

List of Figures

Figure 1.1. Neuronal injury creates a break in the axon (A). The regeneration process requires the initiation of a growth cone followed by axonal regrowth and reconnection to its target (B).	2
Figure 1.2. Current drugs used in the treatment of SCI.	3
Figure 1.3. Structures of several small molecules found to have growth-promoting activity.....	5
Figure 1.4. Neuroactive natural products isolated from magnolia sources.....	6
Figure 1.5. The natural products xanthofulvin and vinaxanthone.	8
Figure 1.6. Laser axotomy in <i>C. elegans</i> results in an induced axonal injury followed by observation for neuronal regeneration.	14
Figure 2.1. Dihydropyridines assessed for accumulation in <i>C. elegans</i> . DHPs in green were found to accumulate by Burns <i>et al.</i> while those in blue were previously not found to accumulate but were detected in <i>C. elegans</i> lysates with reassessment by HPLC. <i>Ortho</i> -nitro DHPs (black) are light sensitive and are found to accumulate when experiments are conducted in the dark. DHPs in red were not detected in the accumulation assessments.	17
Figure 2.2. Cholinergic neurons expressing GFP in <i>C. elegans</i> strain LX929.	21
Figure 2.3. Outgrowth of cholinergic neurons in <i>C. elegans</i> exposed to clovanemagnolol (A,B) or caryolanemagnolol (C-F).....	22
Figure 2.4. Small molecules screened for outgrowth in <i>C. elegans</i> , shown as differences from control (set at zero).....	24

Figure 2.5. Outgrowth of <i>C. elegans</i> treated with 2 μ M small molecules, with the frequency compared to controls (A). Branching and sprouting of cholinergic neurons observed following exposure to dibutyryl-cAMP (B1), carnosic acid (B2), garcinol (B3), trigonelline (B4), and amphotericin B (B5).	25
Figure 2.6. Outgrowth of <i>C. elegans</i> exposed to clovanebisphenol (A-C) or caryolanebisphenol (D-F).	29
Figure 2.7. Representative molecules that have been shown to bind FKBP.	33
Figure 2.8. Representative section of proteins identified as binding to pipercolyl α -ketoamide following pull-down experiments.	36
Figure 2.9. Soluble competition pull-down methods using <i>C. elegans</i> lysate and pipercolyl α -ketoamide free in solution as well as attached to beaded agarose.	37
Figure 2.10. Proteins identified as putative targets following clovane affinity matrix pull-down and soluble competition.....	40
Figure 2.11. The structure of the kinesin motor protein moving along a microtubule.	41
Figure 2.12. Outgrowth of <i>C. elegans</i> exposed to clovane-based small molecules and <i>klc-1</i> genetic mutants compared to control worms (* $P \leq 0.03$, ** $P \leq 0.005$) (A). Control cholinergic neurons (B1) and outgrowth observed in worms treated with clovanemagnolol (B2,B3) and <i>klc-1</i> mutants (B4,B5).....	43
Figure 3.1. The five parent ynones used to generate vinaxanthone analogs.....	57

Figure 3.2. Vinaxanthone and the 24 analogs generated through ynone coupling reactions. Xanthone and chromone cores with identical aryl functionality are coded the same color.57

Figure 3.3. Commissures of control cholinergic neurons in *C. elegans* (A). Outgrowth caused by treatment with vinaxanthone includes commissural branching (B) as well as sprouting from nerve cords (C,D).58

Figure 3.4. Morphology of the mechanosensory neurons in *C. elegans*.59

Figure 3.5. Laser axotomy of the PLM neuron in *C. elegans* was performed ~15 μm after the synaptic branch when the branch point was $\leq 100 \mu\text{m}$ from the cell body (A), leaving behind a small break in the axon (B). No regrowth from the severed axon at 24 hours post-surgery resulted in a proximal stump and distal fragment degeneration (C). Regrowth of the severed proximal axon was observed on occasion 24 hours post-axotomy (D). Arrows indicate the site of axotomy and arrowheads indicate the synaptic branch.61

Figure 3.6. Following laser axotomy, worms exposed to vinaxanthone analogs displayed varying neuronal regrowth rates relative to controls. Colors correspond to structures in Figure 3.2 for SAR comparison.64

Figure 3.7. Branching regrowth of PLM neuron 24 hours following laser axotomy and treatment with 2 μM vinaxanthone (A). Regeneration morphologies promoted by post-axotomy treatment with 2 μM analog **98** included branching regrowth (B), arching regrowth (C), linear regrowth (D), regrowth with branching to the ventral nerve cord (E), and regrowth with reconnection to the distal fragment (F). Arrows indicate beginning of new growth and arrowheads indicate the synaptic branch.65

Figure 3.8. Lengths of regrowing PLM neuronal processes following laser axotomy and treatment with the library of vinaxanthone analogs.....	66
Figure 3.9. The dose-response relationships of <i>C. elegans</i> treated with vinaxanthone or analog 98	67
Figure 3.10. Regeneration following laser axotomy and treatment with 2 μ M clovanemagnolol (A-D). Arrows indicate beginning of regrowth and arrowheads indicate the synaptic branch.	68
Figure 3.11. Regeneration following laser axotomy and treatment with 2 μ M clovanebisphenol (A-D). Arrows indicate beginning of regrowth and arrowheads indicate the synaptic branch.	69

List of Schemes

- Scheme 1.1.** Syntheses of caryolanemagnolol and clovanemagnolol.7
- Scheme 2.1.** Synthesis of clovanebisphenol, a clovanemagnolol derivative.26
- Scheme 2.2.** Mechanism of caryolanebisphenol and clovanebisphenol formation.28
- Scheme 2.3.** Synthesis of pipercolyl α -ketoamide and the FKBP affinity matrix.35
- Scheme 2.4.** Synthesis of clovanetriol and the clovane-based affinity matrix.39
- Scheme 3.1.** Mechanism of 5,6-dehydropolivione dimerization to form
vinaxanthone.54
- Scheme 3.2.** One-step laboratory synthesis of vinaxanthone from 5,6-
dehydropolivione.55
- Scheme 3.3.** Mechanism for synthesizing vinaxanthone analogs through an ynone
coupling reaction (A). Reversing the order of the ynone addition
generates the analog with opposite core functionality (B).....56

Abbreviations

μL	microliter
μm	micrometer
μM	micromolar
AChEI	acetylcholinesterase inhibitor
ACN	acetonitrile
ALS	amyotrophic lateral sclerosis
BHT	butylated hydroxytoluene
CAEEL	<i>C. elegans</i> protein database
cAMP	cyclic adenosine monophosphate
CDI	carbonyldiimidazole
<i>C. elegans</i>	<i>Caenorhabditis elegans</i>
CGC	Caenorhabditis Genetics Center
CNS	central nervous system
DCC	<i>N,N'</i> -dicyclohexylcarbodiimide
DHP	1,4-dihydropyridine
DIPEA	<i>N,N</i> -diisopropylethylamine
DMAP	4-dimethylaminopyridine
DMF	dimethylformamide
DMSO	dimethyl sulfoxide
<i>E. coli</i>	<i>Escherichia coli</i>
EDTA	ethylenediaminetetraacetic acid
eq./equiv.	equivalent
ERK	extracellular signal-regulated kinase

Et	ethyl
EtOAc	ethyl acetate
FKBP	FK506 binding protein
FTI	farnesyltransferase inhibitor
GABA	γ -aminobutyric acid
GFP	green fluorescent protein
HPLC	high-performance liquid chromatography
<i>i</i> -Pr	isopropyl
IR	infrared
KHC	kinesin heavy chain
KLC	kinesin light chain
L4	larval stage 4
MAP	mitogen-activated protein
<i>m</i> -CPBA	<i>meta</i> -chloroperoxybenzoic acid
Me	methyl
mg	milligram
mL	milliliter
mm	millimeter
mM	millimolar
MOM	methoxymethyl
MS	mass spectrometry
N	normal
NACTN	North American Clinical Trials Network
NGM	nematode growth medium
nm	nanometer

NMM	<i>N</i> -methylnorpholine
NMR	nuclear magnetic resonance
PAGE	polyacrylamide gel electrophoresis
PBS	phosphate buffered saline
PKC	protein kinase C
PLM	posterior lateral microtubule
PMSF	phenylmethylsulfonyl fluoride
PNS	peripheral nervous system
ppm	parts per million
R_f	retention factor
RNAi	ribonucleic acid interference
SAR	structure-activity relationship
SCI	spinal cord injury
SDS	sodium dodecyl sulfate
Sema3A	semaphorin 3A
SSRI	selective serotonin reuptake inhibitor
TBS	tris buffered saline
<i>t</i> -Bu	<i>tert</i> -butyl
TFA	trifluoroacetic acid
THF	tetrahydrofuran
TLC	thin-layer chromatography

Chapter 1 – Introduction

Spinal Cord Injury

Spinal cord injury (SCI) is the second leading cause of paralysis, affects approximately 1.3 million people in the United States¹, and totals an annual associated cost of over \$7.7 billion². There is currently no cure. The lack of regeneration in the adult mammalian central nervous system (CNS) presents a significant obstacle in overcoming spinal cord injury. This lack of CNS regeneration has been attributed to the inhibitory extrinsic environment formed after injury as well as the absence of intrinsic growth signals. It has been shown that successful axonal regrowth in the mammalian CNS depends not only on mitigation of the inhibitory environment but also requires activation of growth pathways for recovery following SCI.³ The ability to enhance these regenerative pathways, or suppress the biological pathways inhibiting regeneration, could promote the development of therapeutic treatments for SCI.

Nerve cells are composed primarily of a soma (cell body), dendrites, and an axon. Damage to neurons that results in debilitating injury most often occurs to the axons, which are the neuronal projections that allow communication between nerve cells as well as with other cells such as muscles. Injury disrupts and prevents the transmission of information in the form of electrical pulses along the axon. Functional recovery and restoration of the ability to convey neuronal signals depend upon the axon regrowing and re-establishing contact with its target. This regeneration of damaged neurons requires the severed axon to

surmount its inhibitory surroundings via growth cone formation and neurite extension emanating in response to signals from the injured environment (Figure 1.1).

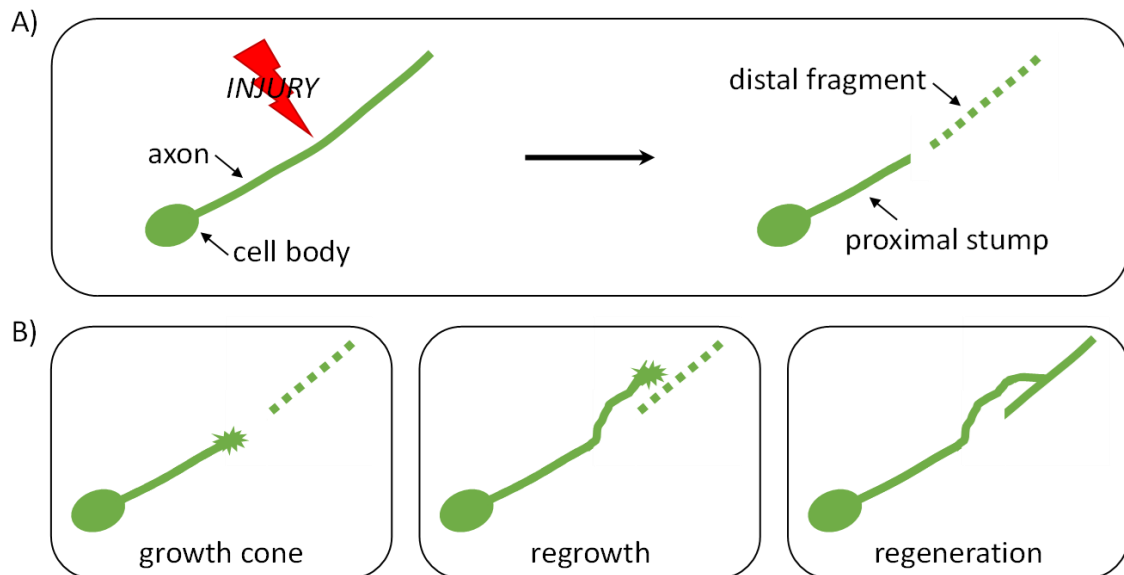


Figure 1.1. Neuronal injury creates a break in the axon (A). The regeneration process requires the initiation of a growth cone followed by axonal regrowth and reconnection to its target (B).

Most current treatments for SCI focus on reducing the secondary effects immediately following injury, subsequent rehabilitation, and long-term palliative care. Methylprednisolone (**1**), if given within the first eight hours after SCI, can ameliorate the secondary effects of injury by reducing inflammation and further damage to nerve cells (Figure 1.2).⁴ Pregabalin (Lyrica) (**2**) is often prescribed for the management of neuropathic pain resulting from SCI but does not provide any functionally remedial gain. The development of approaches for inducing regeneration has largely focused on the use

of gene therapy, growth factors, and stem cells while small molecules and natural products have traditionally received less attention.⁵ Although various clinical trials for SCI treatments have been initiated in recent years, only a few have advanced to the final phase.⁶ The North American Clinical Trials Network (NACTN) has initiated Phase I clinical trials of the neuroprotective drug riluzole (**3**), currently used in the treatment of amyotrophic lateral sclerosis (ALS).⁷ The antibiotic minocycline (**4**) was investigated in Phase II clinical trials and found to enhance motor recovery⁸; Phase III trials are currently ongoing. These drugs provide hope for the use of small molecules as favorable SCI treatments, but given the high failure rates of medicinal agents in clinical trials the need for novel compounds still exists.⁹

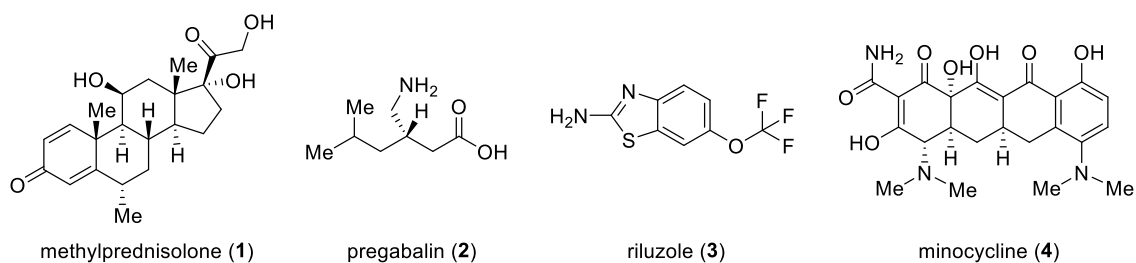


Figure 1.2. Current drugs used in the treatment of SCI.

Growth-Promoting Small Molecules

The identification of growth-promoting pathways, particularly ones that can be controlled by small molecules, could provide significant advancements in regenerative medicine. Numerous growth-promoting small molecules have already been discovered

(Figure 1.3). The vitamin A metabolite retinoic acid (**5**) is a well-known signaling molecule involved in the differentiation and patterning of neurons, axon outgrowth, and the maintenance of established neurons.¹⁰ Increased retinoic acid and upregulation of the retinoic acid receptor have been shown to improve regeneration in the peripheral nervous system (PNS) both *in vitro*¹¹ and *in vivo*¹²⁻¹⁴. Paclitaxel (Taxol) (**6**), originally isolated from the bark of the Pacific Yew tree¹⁵, has been shown to have a dramatic effect on regenerating PNS axons¹⁶ and has recently been reported useful in axon regeneration therapy¹⁷. Paclitaxel is thought to function through microtubule stabilization, thereby resulting in enhanced axon sprouting and regeneration after spinal cord injury in rodent models.¹⁷ Additional studies have suggested that the regenerative ability displayed by axons of injured nerves exposed to paclitaxel applies to the CNS as well.¹⁸⁻²⁰ The antifungal compound amphotericin B (**7**) has been shown to promote CNS axon growth by overcoming the inhibitory injured environment through serine/threonine-specific protein kinase (Akt pathway) activation.²¹ Garcinol (**8**) promotes neurogenesis of rat cortical progenitor cells through extracellular signal-regulated kinase (ERK) activation.²² The natural product was also shown to induce neurite outgrowth in the developing nerve cells and enhance neuronal survival via ERK pathway regulation.

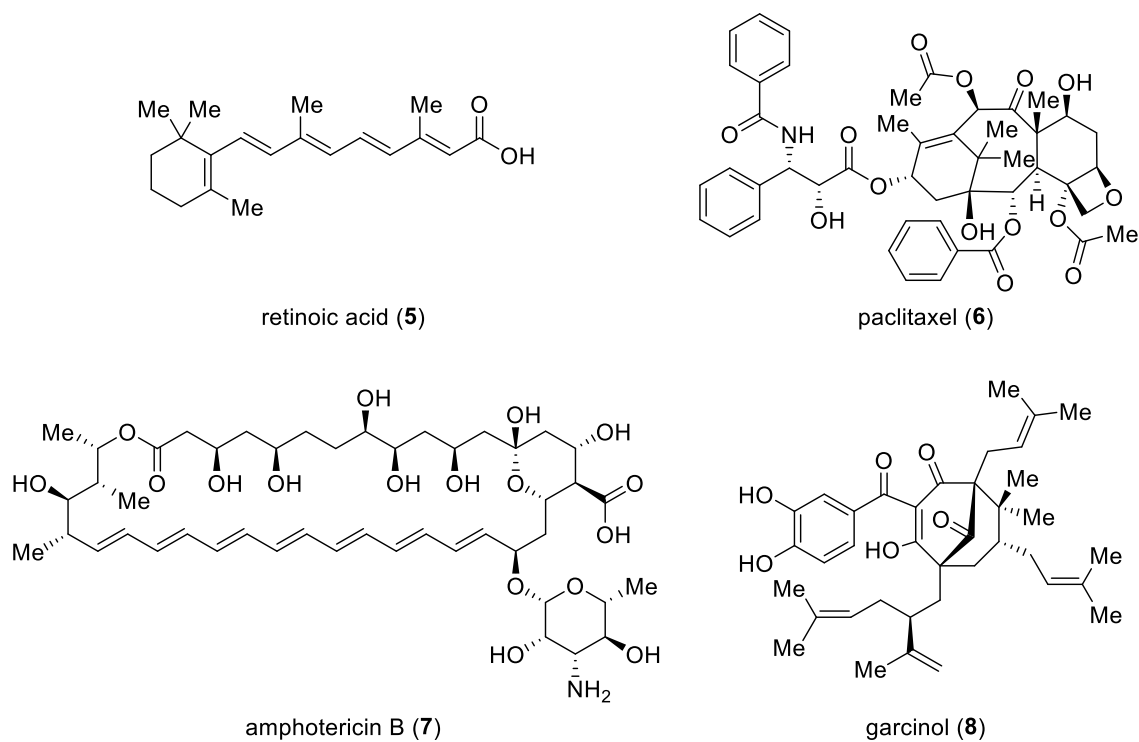


Figure 1.3. Structures of several small molecules found to have growth-promoting activity.

Several neurotrophic natural products have been isolated from the bark of magnolia trees used in traditional Chinese medicine, including *Magnolia obovata* and *Magnolia officinalis* (Figure 1.4).²³ The biphenyl neolignan honokiol (**9**) and its structural isomer magnolol (**10**) were identified as two of the active components contributing to the growth-promoting effects of these magnolia sources. Honokiol has been shown to induce neurite outgrowth in rat cortical neurons at a concentration of 0.1 μM .²⁴ Magnolol has induced outgrowth of cortical neurons at 1 μM , exhibiting a weaker effect on neurite extension.²⁴ Additionally, the structurally related sesquiterpene-neolignan natural products

clovanemagnolol (**11**) and caryolanemagnolol (**12**) have been isolated from these magnolia species and shown to enhance neurite outgrowth in primary neuronal cultures, with clovanemagnolol exhibiting effects at 10 nM concentration.²⁵⁻²⁸ One-step syntheses of these natural products have been reported by Siegel *et al.* (Scheme 1.1).²⁹

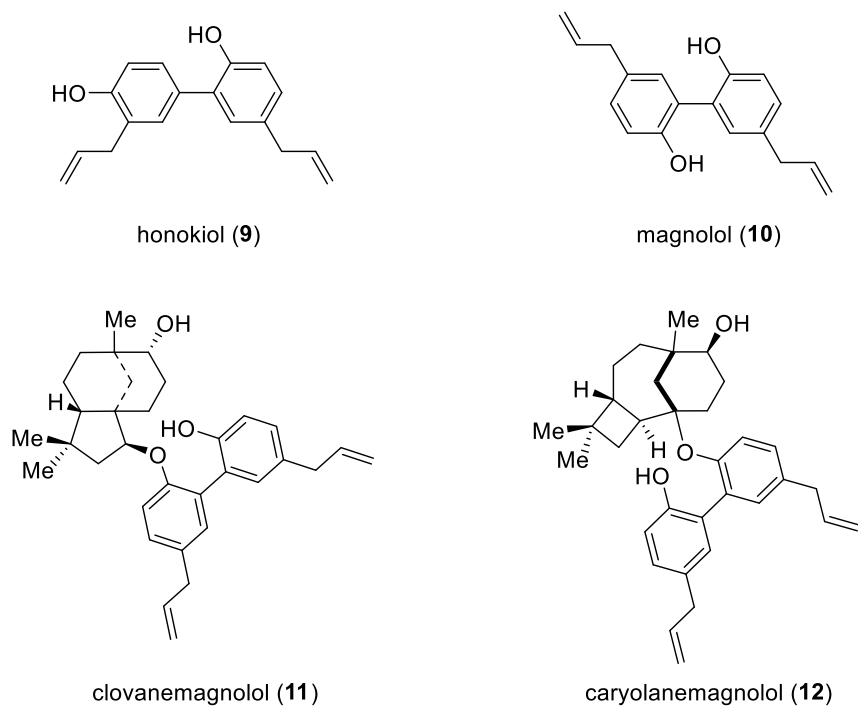
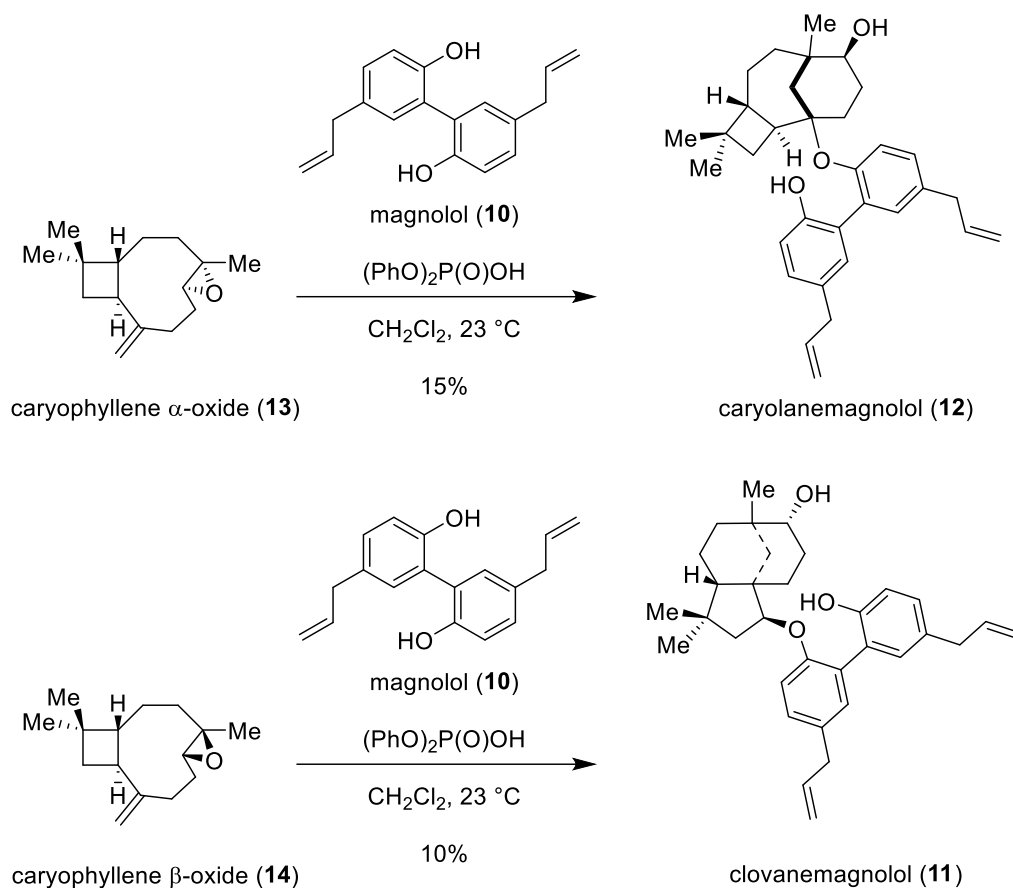


Figure 1.4. Neuroactive natural products isolated from magnolia sources.



Scheme 1.1. Syntheses of caryolanemagnolol and clovanemagnolol.

Reported in 2003 by Saji and coworkers from fungal extracts of *Penicillium* sp. SPF-3059, xanthofulvin (SM-216289) (**15**) was shown to have 0.9-1.1 $\mu\text{g}/\text{mL}$ activity towards blocking semaphorin 3A (Sema3A), an inhibitor of axonal regeneration, with no cytotoxicity observed at over 1,000 times the effective concentration (Figure 1.5).³⁰ Sema3A, a chemorepulsive agent secreted as a guidance cue to inhibit axonal outgrowth, binds to the plexin receptor in complex with neuropilin-1 and mediates growth cone collapse, which leads to failed regeneration of injured neurons.³¹ Xanthofulvin is believed

to act by disrupting Sema3A/plexin interactions, thereby preventing Sema3A-mediated growth cone collapse. The structurally related natural product vinaxanthone (SM-345431) (**16**) was co-isolated from these fungal extracts and possesses similar growth-promoting activity.³² Murine models treated with xanthofulvin or vinaxanthone following complete spinal cord transection exhibited dramatic axonal regeneration, remyelination, and functional recovery compared to control animals.³³⁻³⁵ Vinaxanthone has also been shown to promote corneal nerve growth following transplant. Mice that received post-transplant treatment with vinaxanthone showed significantly higher peripheral nerve regeneration as well as improved functional recovery of corneal sensitivity compared to control mice.³⁶ Interestingly, mice deficient in the plexin receptors for semaphorin do not show enhanced regeneration in complete spinal cord transection models, indicating that removal of semaphorin-mediated inhibition is insufficient to promote axon growth.³⁷ Although their mechanisms of action have been thought to result from Sema3A inhibition, xanthofulvin and vinaxanthone possibly possess polypharmacological activity since functional removal of Sema3A alone does not enhance regeneration following SCI.

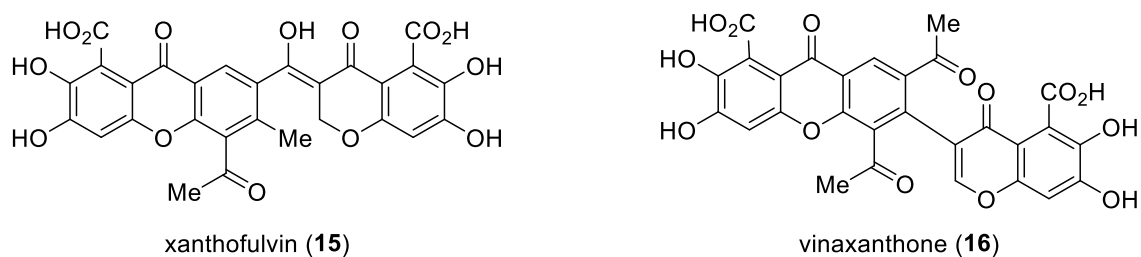


Figure 1.5. The natural products xanthofulvin and vinaxanthone.

While most screens for novel compounds that promote neuronal growth employ *in vitro* cell cultures, these methods have limitations. The isolated neuronal conditions of *in vitro* cultures disregard drug metabolism, target tissue availability, and toxicity. Consequently, lead molecules identified through *in vitro* screens often present issues with absorption, distribution, and stability in subsequent animal studies, resulting in their ultimate abandonment and a deficit of time and money.³⁸ An effective *in vivo* model for examining growth-promoting small molecules in a whole-organism context would therefore be advantageous in screening endeavors. Furthermore, assays employing whole animals allow for monitoring of any behavioral responses and increase the chances of identifying off-target effects.

The Model Organism *Caenorhabditis elegans*

The nematode *Caenorhabditis elegans* (*C. elegans*) has become a well-established model organism since its introduction to the scientific community by Sydney Brenner in 1974.³⁹ This free-living roundworm has many advantages over other, higher level model organisms. Its short generation time to adulthood (~3 days at 20 °C) and total lifespan (2-3 weeks) combined with the low cost and ease of maintenance make it particularly useful for high-throughput screens, compared to mice which require a considerably longer generation time (9-10 weeks) and significant maintenance resources. In the lab, these nematodes can easily be cultured on solid agar or in liquid media with a diet of *Escherichia coli* (*E. coli*) and develop through four larval stages (L1-L4) before becoming 1 mm-long

adults. *C. elegans* are primarily hermaphrodites, with males arising spontaneously in approximately 0.1% of the population.⁴⁰ Hermaphroditic reproduction via self-fertilization allows for genetically identical offspring, yet the presence of males maintains the ability to generate genetic crosses through mating. The nematodes are comprised of an invariant cell number with their complete lineages and developmental processes mapped.⁴¹⁻⁴² These multicellular animals feature various organs and tissue types including intestines, muscles, hypodermis, reproductive systems, and nervous systems, giving them physiological complexity while maintaining the simplicity of easily scored phenotypes ideal for chemical biology studies.⁴³ They also exhibit behavioral complexity and have been shown to display learning⁴⁴, memory⁴⁴, and sleep patterns⁴⁵. Their transparent nature and facile incorporation of green fluorescent protein (GFP) allow for the visualization of biological structures and processes occurring in living organisms at the single cell level.⁴⁶ Additionally, the worms produce a large number of progeny (>300 offspring) and can be frozen at cryogenic temperatures for indefinite storage with viable recovery.⁴⁷

With the entire genome of *C. elegans* sequenced in 1998, the worm rose to the forefront of genetic biology.⁴⁸ Numerous fundamental biological and medically relevant discoveries were made possible using *C. elegans*. Genes regulating aging⁴⁹ and apoptosis⁵⁰ were originally discovered using the worm and subsequently linked to their corresponding human phenomena. Significantly, *C. elegans* possess between 60-80% of genes homologous to human genes.⁵¹⁻⁵² Gene expression can be controlled through the use of RNA interference (RNAi), also discovered using the worm, and the facile construct of mutants, which are then made available to the scientific community and can readily be

obtained from the Caenorhabditis Genetics Center (CGC).⁵³⁻⁵⁴ This conservation of genes and fundamental cellular processes coupled with the ability to control their expression further established the worm as a relevant model organism. Several Nobel Prizes awarded for discoveries made using *C. elegans*, including the 2002 and 2006 Nobel Prizes in Physiology or Medicine and the 2008 Nobel Prize in Chemistry, attest to their validity as an invaluable resource for discovery in biomedical research.

Invertebrate model organisms like *C. elegans* provide an advantage in early research by delivering rapid discoveries. Revealing physiologically relevant information in a high-throughput manner, they bridge the gap between *in vitro* assays and higher level *in vivo* models.⁵⁵ *C. elegans* have been used for numerous models of human diseases and hold potential as a tool for drug discovery.⁵⁶ Worm models have been established for neurodegenerative diseases⁵⁷⁻⁵⁸, mental illnesses such as depression⁵⁹, bacterial infections⁶⁰, and cancer⁶¹. Over 40% of genes implicated in human diseases possess a *C. elegans* homolog, spanning a wide array of ailments from Alzheimer's to breast cancer, diabetes, and even deafness.⁶² Despite the fact that most work with the worm has traditionally had a genetic focus, many drug candidates have been studied in these disease models and shown effective.⁵⁵

Drug Discovery in *C. elegans*

The identification and development of biologically active small molecules are key components of drug discovery. Before a candidate drug can elicit the desired response, however, it must enter the body and reach the target tissues. In the case of *C. elegans*, it

has been reported that drugs enter the worm through ingestion as well as uptake through the hypodermis or through exposed sensory neuronal endings.⁶³⁻⁶⁵ Once inside, the normal biological function of the target must be altered by the drug to evoke a physiological response. Organismal-based drug screens are therefore superior to cell-based methods since only bioavailable compounds exhibiting *in vivo* activity will result in measurable effects. Numerous bioactive compounds have been shown to elicit responses in the worm.⁶⁶ For example, the steroid prednisone was identified in a blind compound screen as reducing muscle degeneration in dystrophin-deficient *C. elegans*.⁶⁷ This compound, already in use as a treatment for muscular dystrophy, validated chemical screening in worms for drug discovery by showcasing the conservation between worms and humans.

Many small molecules exhibit useful biological activity, but their mechanisms of action are often unknown. Notably, the use of a whole organism allows for screening of small molecules without prior identification of targets.⁶⁸ Target identification, however, provides a better understanding of the molecule's mechanism of action as well as enables optimization of lead compounds for increased activity and reduced negative side effects. Many drug, chemical, and biotechnology companies employ *C. elegans* in their research endeavors.⁶⁹ Researchers from Bristol-Myers Squibb Pharmaceuticals and Exelixis have used the worm to better understand the mechanism of action and identify targets of farnesyltransferase inhibitors (FTIs) used in cancer therapy.⁷⁰ The 1,4-dihydropyridine (DHP) nemadipine A was discovered in a bioactivity screen using *C. elegans* to identify compounds that elicit phenotypic responses.⁷¹ DHPs act as antagonists of the α_1 subunit of L-type calcium channels. A subsequent genetic suppressor screen was conducted in *C.*

elegans and the target gene of nepadipine A was identified as *egl-19*, the sole L-type calcium channel α_1 subunit in *C. elegans*, thus confirming the worm as a viable platform for target validation.⁷¹

***C. elegans* Neurobiology**

Many compounds that exhibit neuroactivity in humans, such as nicotine⁷², ethanol⁷³, anesthetics⁷⁴, selective serotonin reuptake inhibitors (SSRIs)⁷⁵, and acetylcholinesterase inhibitors (AChEIs)⁷⁶, also elicit responses in the worm. Of the 959 cells in the adult hermaphrodite, roughly one third are neurons. *C. elegans* possess multiple neuronal types and employ many of the same neurotransmitters as humans, including acetylcholine, dopamine, γ -aminobutyric acid (GABA), glutamate, and serotonin.⁷⁷ *C. elegans* is currently the only organism with its full connectome, or wiring diagram of its entire neuronal connectivity, mapped.⁷⁸⁻⁷⁹ The various neurons come together in the head region of the worm to form a brain-like structure known as the nerve ring. As a genetic system, *C. elegans* have been widely used to identify cellular and molecular mechanisms of neuronal growth, uncovering determinants of growth cone formation⁸⁰, axonal guidance⁸¹, and regeneration⁸².

Many factors that affect axon regeneration in vertebrate neurons have similar counterparts in *C. elegans*, supporting its use as a biologically relevant model organism.⁸³ *C. elegans* have been developed as a model for studying axon regeneration following injury.⁸⁴⁻⁸⁵ Axonal injury is induced by severing individual GFP-labeled neurons in live worms using highly precise laser microsurgery; neurons have been shown to functionally

regrow following these laser axotomy procedures (Figure 1.6).⁸⁴ The laser causes plasma formation and generates cavitation bubbles at the site of contact which damage the nerve cell and create a break in the axon.⁸⁶ The intrinsic regeneration ability following laser axotomy depends on many factors including the type of neuron, transgenic background, developmental stage of the worm, method of axotomy, and location of the neuronal injury.^{82, 85, 87}

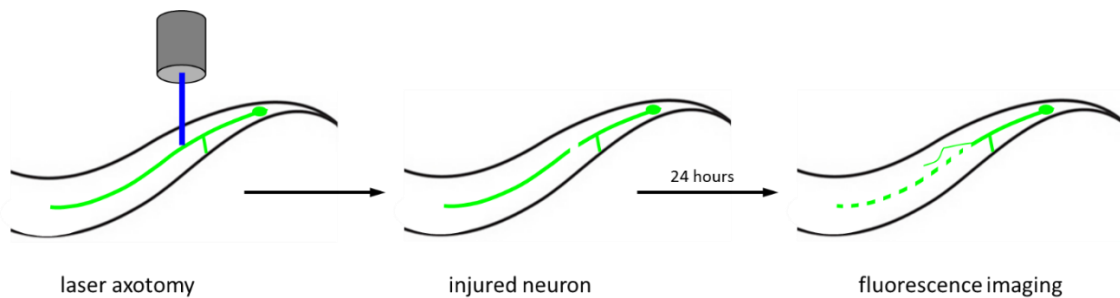


Figure 1.6. Laser axotomy in *C. elegans* results in an induced axonal injury followed by observation for neuronal regeneration.

The genetic determinants of axon regeneration have been extensively screened using laser axotomy in *C. elegans*, investigating over 650 conserved genes to identify both promoters and repressors of growth.⁸⁸ These positive and negative effectors have been identified for elements ranging from second messengers to kinases and axon guidance molecules such as ephrin, netrin, and semaphorin. Laser axotomy in *C. elegans* has aided in the identification of both genetic and molecular pathways controlling regeneration⁸⁹, including the DLK-1 mitogen-activated protein (MAP) kinase pathway⁹⁰ and calcium or

cyclic adenosine monophosphate (cAMP) signaling⁹¹. While most of the axonal regeneration studies in *C. elegans* have primarily focused on genetically manipulated models, small molecules hold great potential for affecting regeneration pathways. Previous small molecule screens, although limited in number, have identified compounds able to enhance regeneration following laser axotomy.⁹² The protein kinase C (PKC) activator prostratin was found to enhance regeneration in the nematode through the first large-scale *in vivo* screen for compounds that affect neurite growth, establishing *C. elegans* as an instrument for neuroregenerative drug discovery.⁹²

Conclusion

The combination of biologically active small molecules with the amenable model organism *C. elegans* uniquely establishes a position for chemical biology studies. The neurobiology of the nematode provides a further advantage for investigations regarding regeneration pathways. Enhanced methods for the discovery of novel neuroactive compounds via *in vivo* screening followed by the ability to conduct target identification studies utilizing the same organism make an ideal platform for studying growth-promoting compounds.

Chapter 2 – Clovanemagnolol and *C. elegans*

Small Molecules in *C. elegans*

Organism-based screening hinges on the identification of small molecules that modulate biological function through *in vivo* phenotypic assays. A recent small molecule screen in *C. elegans* by Kwok *et al.* investigated members of the 1,4-dihydropyridine (DHP) family of compounds.⁷¹ DHPs are commonly used in the treatment of hypertension due to their L-type calcium channel antagonistic activity. Of the 12 molecules from the DHP family that were screened, it was found that one third of those tested accumulated. The authors stated that this was a similar hit rate to those obtained in other whole-organism screens, thus demonstrating that the worm was a suitable model for the identification of new bioactive compounds.⁷¹

Comparatively, a following study by Burns *et al.* presented a model for predicting drug accumulation in *C. elegans* based on the functional groups present on the molecule, using a high-throughput high-performance liquid chromatography (HPLC) method to measure the accumulation of 21 structurally related DHPs as proof of principle.⁹³ Only five of these DHPs were found to accumulate. Subsequent large-scale analysis of a chemical library of over 1,000 compounds placed the accumulation in *C. elegans* below 10%, suggesting that most molecules do not accumulate inside *C. elegans* likely due to difficulty entering the worms through their outer physical barrier, the cuticle.⁹³

Structural comparison of the DHPs **17** - **37** shows a high degree of similarity, with minor differences between the compounds found to accumulate and those that did not such as a methyl ester in place of an ethyl ester (**19** vs **22**), addition of a single fluorine to the aromatic ring (**20** vs **23**, **24**, and **25**), and substitution of the halogen present (chlorine in **21** vs fluorine in **26**) (Figure 2.1). Although the absorption of small molecules by *C. elegans* might be low, accumulation, which is influenced by the overall size, shape, and polarity of molecules, unlikely selects between the minor structural differences of these DHPs.⁹⁴

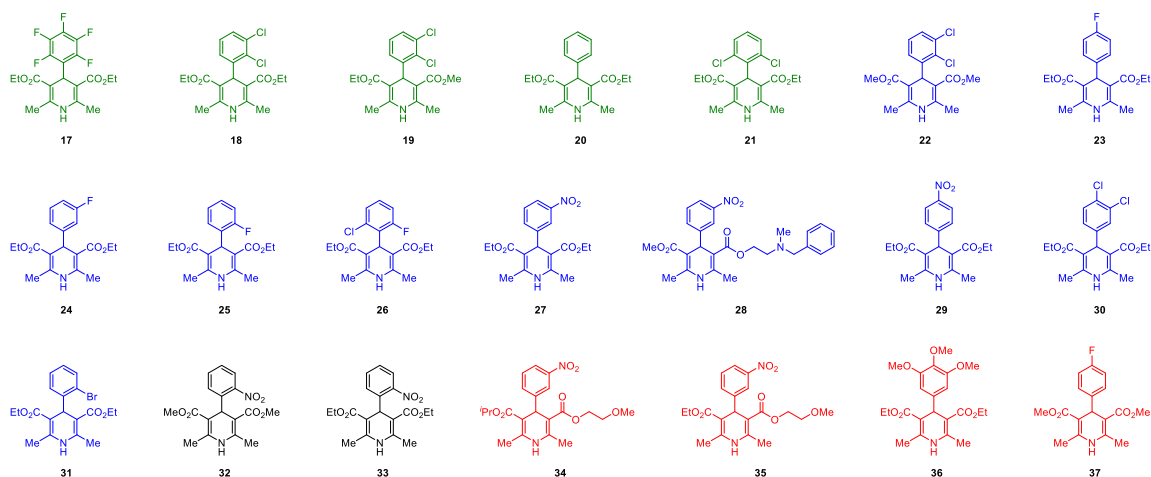


Figure 2.1. Dihydropyridines assessed for accumulation in *C. elegans*. DHPs in green were found to accumulate by Burns *et al.* while those in blue were previously not found to accumulate but were detected in *C. elegans* lysates with reassessment by HPLC. *Ortho*-nitro DHPs (black) are light sensitive and are found to accumulate when experiments are conducted in the dark. DHPs in red were not detected in the accumulation assessments.

Neuroactive small molecules, as well as many other drugs, have been shown to elicit phenotypic responses in *C. elegans*, indicating that a large number of compounds do in fact enter the worm. The widespread claim that compounds do not easily cross the nematode cuticle was therefore investigated by reassessing the accumulation of the same 21 DHPs according to the HPLC method of worm lysates presented by Burns *et al.* In addition to the five DHPs reported to accumulate by Burns *et al.*, it was discovered that ten of the DHPs not previously found to accumulate were detectable after 6 hour incubation. This suggested that there was a potentially large number of false negatives in the previous report, underestimating the accumulation of compounds in *C. elegans*.

Dihydropyridines, also known as Hantzsch esters, are susceptible to mild oxidative aromatization, so the compounds were carefully analyzed for purity.⁹⁵⁻⁹⁶ The number of worms used in each trial was doubled from the amount reported by Burns *et al.* to ensure that the samples would be above the HPLC limits of detection and the HPLC solvent gradient was slightly altered from the one originally used in their paper. Using a slower gradient with a longer run time ensured that the DHP peaks were visible against the changing background absorbance of the solvents throughout the HPLC run. In addition, pyridine derivatives corresponding to each of the DHPs as well as other known or possible metabolites were synthesized for comparison. The new solvent gradient also allowed for the separation of the DHPs, pyridines, and other metabolites, enabling the identification of any DHP metabolites at detectable levels in the worm lysates.

Following the improved assessment it was found that 81% of the DHPs (**17** - **33**) accumulated, compared to the 24% previously reported. Interestingly, DHPs **32** and **33** are

light sensitive and rapidly degraded in the incubation buffer, which accounted for their initial apparent lack of accumulation.⁹⁷ While they were not detected if the accumulation was evaluated in the presence of light, the *ortho*-nitro compounds were found to accumulate in *C. elegans* when the incubation and subsequent preparation of samples for HPLC analysis were conducted in the dark. The four compounds that were not detected, **34**, **35**, **36**, and **37**, may also accumulate but undergo metabolic degradation as the ethylethoxy esters, accessible methyl esters, and aryl methyl ethers are metabolically labile. In addition, when dihydropyridines undergo oxidative aromatization through metabolism the resulting penta-substituted pyridines possess a new, distinct UV chromophore that was not detected by analogy to the parent compound absorbance.⁹⁸ In light of these findings regarding the bioaccumulation of DHPs it was concluded that small molecules do in fact readily enter *C. elegans* and thus it is both a useful and justifiable organism for small molecule studies.

Development of an *in vivo* Outgrowth Assay

Neuronal networks form through highly regulated axonal branching, a dynamic process that involves both extension and retraction.⁹⁹⁻¹⁰¹ Formation of new branches through a net extension of neuronal outgrowth results in the establishment of functional neuronal circuits. An assay was desired that would detect the branching and outgrowth of networked neurons promoted by bioactive compounds. In the development of an assay for screening neurotrophic small molecules *in vivo*, the natural product clovanemagnolol was selected as a positive control due to its previously established potent neurotrophic activity.

The effects of clovanemagnolol were observed in various neuronal classes in *C. elegans* through the use of GFP-labeled nerve cells. Nematodes with fluorescent cholinergic neurons, GABAergic neurons, dopaminergic neurons, or mechanosensory (glutamatergic) neurons were treated with clovanemagnolol and observed for aberrant growth 48 hours later. No significant additional or abnormal growth was observable in the GABAergic, dopaminergic, or mechanosensory neurons of treated worms. Significant additional growth deviations from untreated control worms, including increased sprouting and branching, were observed in GFP-labeled cholinergic neurons of nematodes treated with clovanemagnolol. The cholinergic strain was therefore carried forward in the outgrowth assay development due to easily observed abnormal deviations from control worms.

C. elegans expressing GFP in cholinergic motor neurons (LX929 (*vsIs48[unc-17::GFP]*)) exhibit fluorescence in the nerve ring, laterally along the worm in the dorsal and ventral nerve cords, and in commissures that run ventrodorsally across the body (Figure 2.2). Due to complex fluorescence in the nerve ring, investigations for abnormalities of cholinergic neurons were focused on regions posterior to the pharynx.

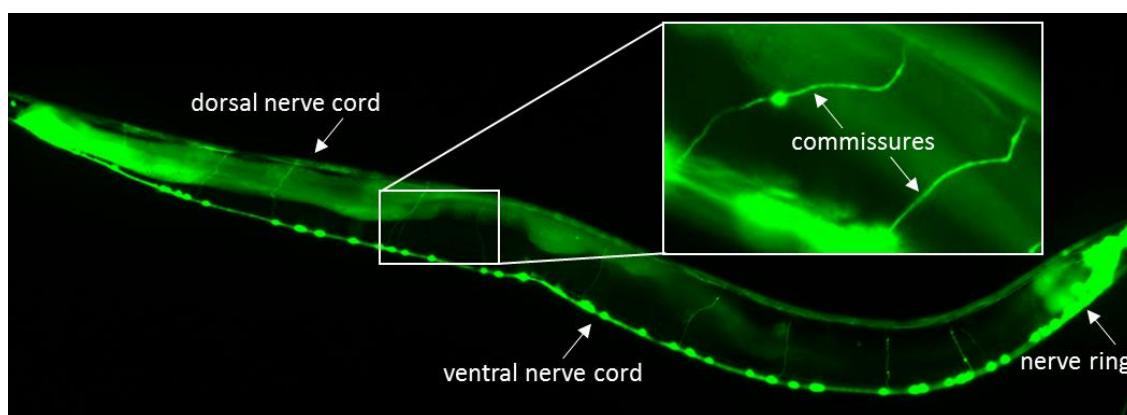


Figure 2.2. Cholinergic neurons expressing GFP in *C. elegans* strain LX929.

Increased sprouting, branching, and abnormal neuronal growth morphologies were observed in the small molecule treated nematodes compared to controls (Figure 2.3). Sprouting, both single process and occasionally Y-shaped growths, was observed from both the ventral and dorsal nerve cords as well as sublateral nerve cords. Commissural branching and aberrant growth were observed as well. These neuronal outgrowth effects were observed in nematodes exposed to clovanemagnolol at concentrations as low as 0.02 μM . Worms exposed to 0.02 μM clovanemagnolol showed a slight increase in abnormal growths compared to controls, while those exposed to 2 μM showed a distinctive increase in the frequency of outgrowth. Exposure to clovanemagnolol as well as the isomeric natural product caryolanemagnolol at 2 μM concentrations caused outgrowth in 35% and 38% of *C. elegans*, respectively, compared to a background rate of branching of 18% in untreated control worms.

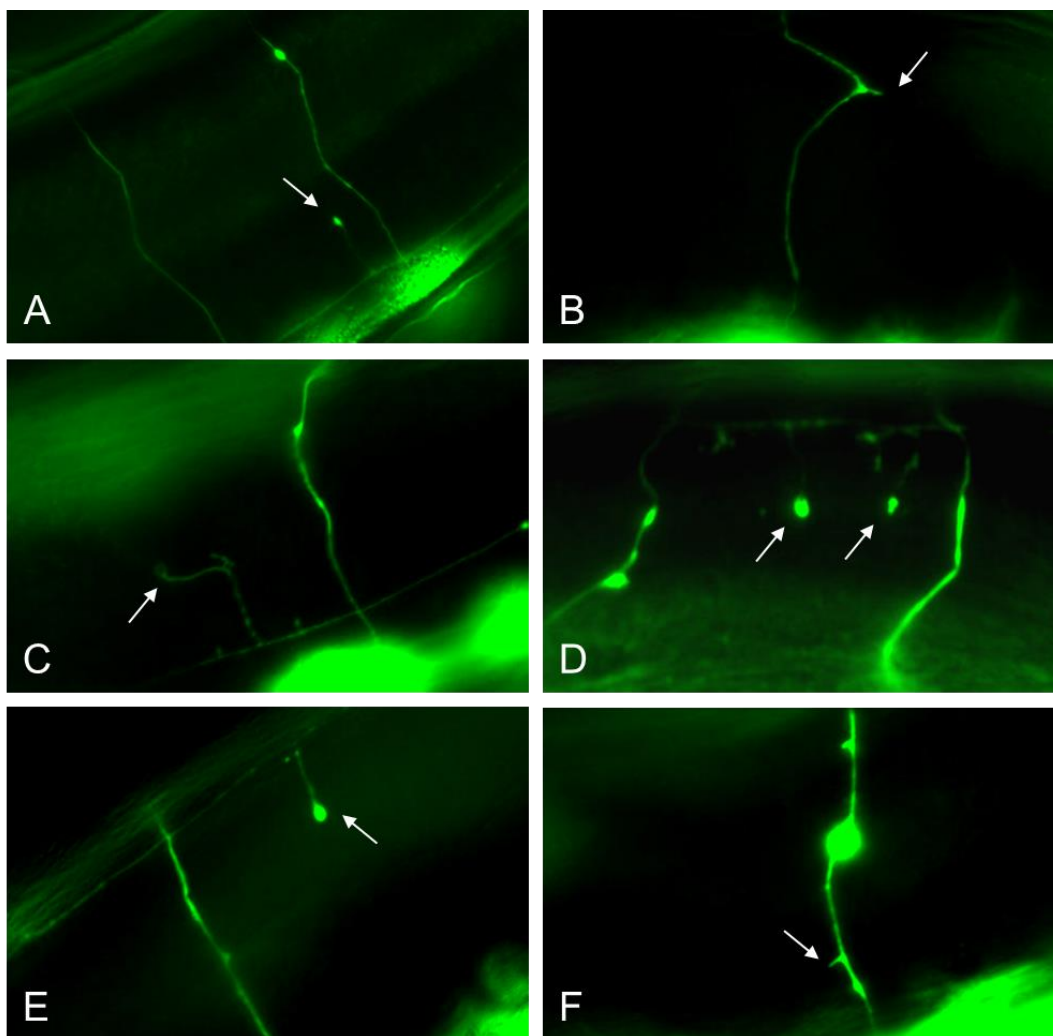


Figure 2.3. Outgrowth of cholinergic neurons in *C. elegans* exposed to clovanemagnolol (A,B) or caryolanemagnolol (C-F).

The method of exposure of the worms to small molecules affects the required dosage. For these experiments, *C. elegans* were allowed to crawl on an agar plate treated with the neurotrophic compound. The tough outer cuticle of *C. elegans* presents a difficult barrier for small molecules to cross into the worm.^{93, 102} For this reason, compounds often

have to be administered at concentrations orders of magnitude higher than those for *in vitro* cell cultures. As the concentrations of the compounds were increased orders of magnitude above 2 μ M solubility became an issue and significant increases in the extent of resultant outgrowth effects were not observed, so this was used as the standard concentration.

To ensure that the observed branching was not caused by experimental factors other than small molecule exposure, several control experiments were performed. Branching was not increased by physical stress to the worms, nor was there evidence of severed or injured axons caused by changes in conditioning of the worms. Branching was independent of worm age up to one week old adults. Past this point, background branching increased, so experiments were limited to late larval and early adult stages. The exposure time was optimized to 48 hours to allow for a sufficient exposure period without introducing the likelihood of age-related branching. Experiments were performed with both living and dead *E. coli* as a food source to examine the possibility of drug metabolism by the bacteria. Branching of *C. elegans* was found to be similar under both conditions, indicating that the presence of live *E. coli* was not detrimental to the experimental conditions.

In developing the *in vivo* screening protocol for detecting small molecule-induced neuronal outgrowth in cholinergic neurons of *C. elegans* several previously reported, commercially available neuroactive compounds were investigated (Figure 2.4). *C. elegans* were treated with a compound via environmental exposure by adding them to an agar plate containing the drug. Their fluorescent neurons were subsequently observed for evidence of outgrowth. The presence of growth abnormalities in a significantly higher frequency of

nematodes compared to untreated control worms was characterized as indicative of small molecule-induced effects. In order to account for the variable nature of using living organisms, individual experiments were repeated in triplicate and the results averaged as percentages of worms showing abnormal morphologies. Several compounds were found to induce higher levels of neuronal outgrowth in cholinergic neurons.

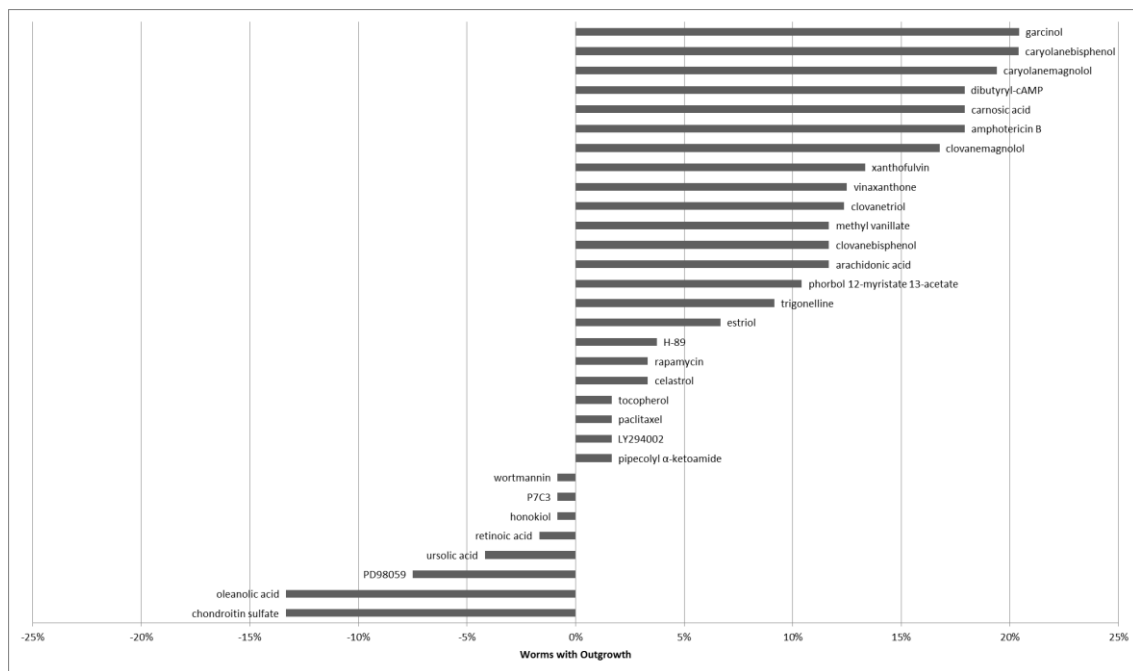


Figure 2.4. Small molecules screened for outgrowth in *C. elegans*, shown as differences from control (set at zero).

Observed abnormalities following exposure to the growth-promoting small molecules included sprouting, branching, and aberrant growth (Figure 2.5). Most significantly, new sprouts were observed to originate from the dorsal nerve cord, the ventral

nerve cord, and sublateral nerve cords. Wandering commissural growth and branching from commissures were also observed, although less frequently. Untreated control worms rarely exhibited these complex morphologies, with similar background abnormalities arising only occasionally in approximately 18% of control worms. The highest frequency of outgrowth was observed in nematodes treated with garcinol, with 39% exhibiting branching or sprouting.

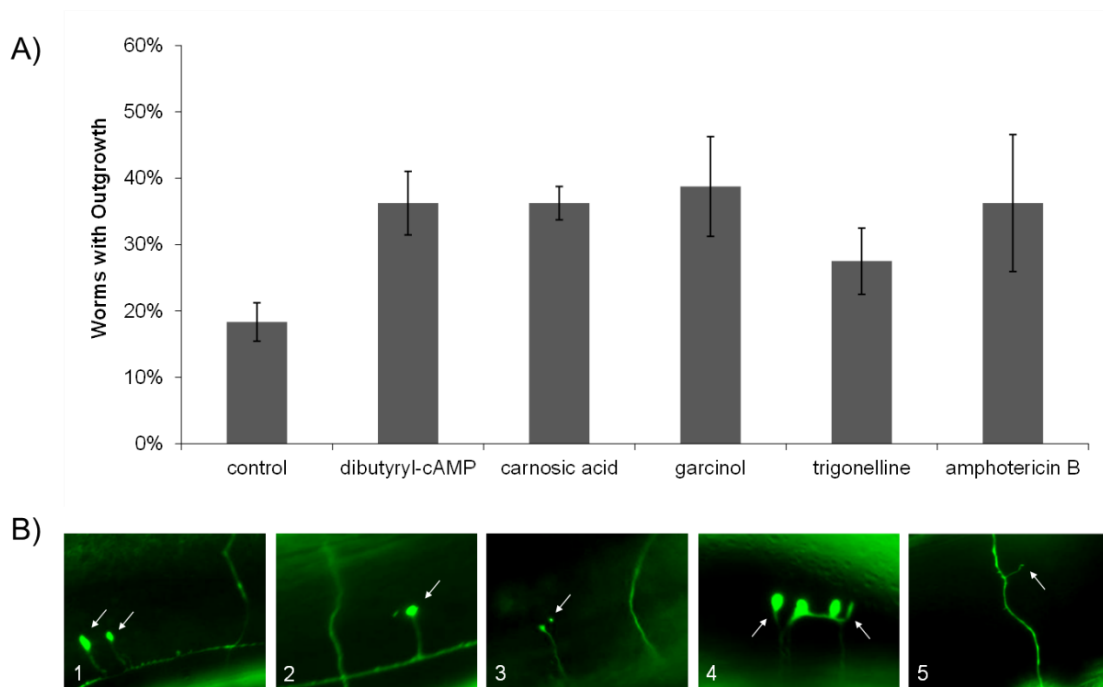
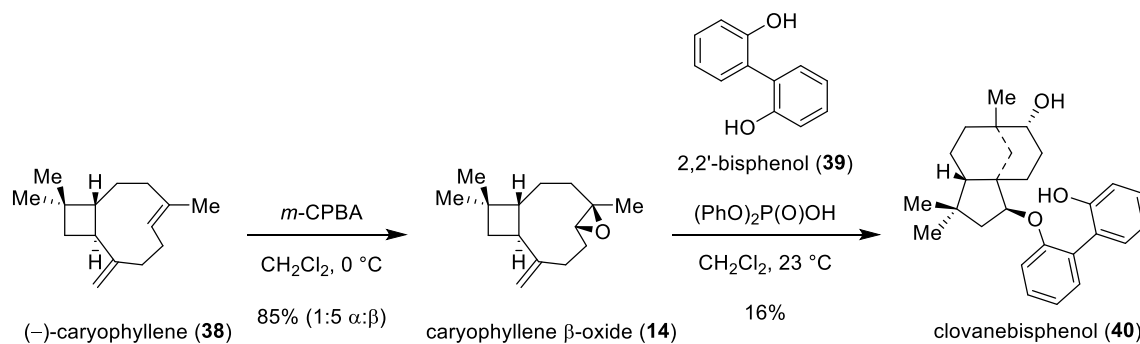


Figure 2.5. Outgrowth of *C. elegans* treated with 2 μ M small molecules, with the frequency compared to controls (A). Branching and sprouting of cholinergic neurons observed following exposure to dibutyryl-cAMP (B1), carnosic acid (B2), garcinol (B3), trigonelline (B4), and amphotericin B (B5).

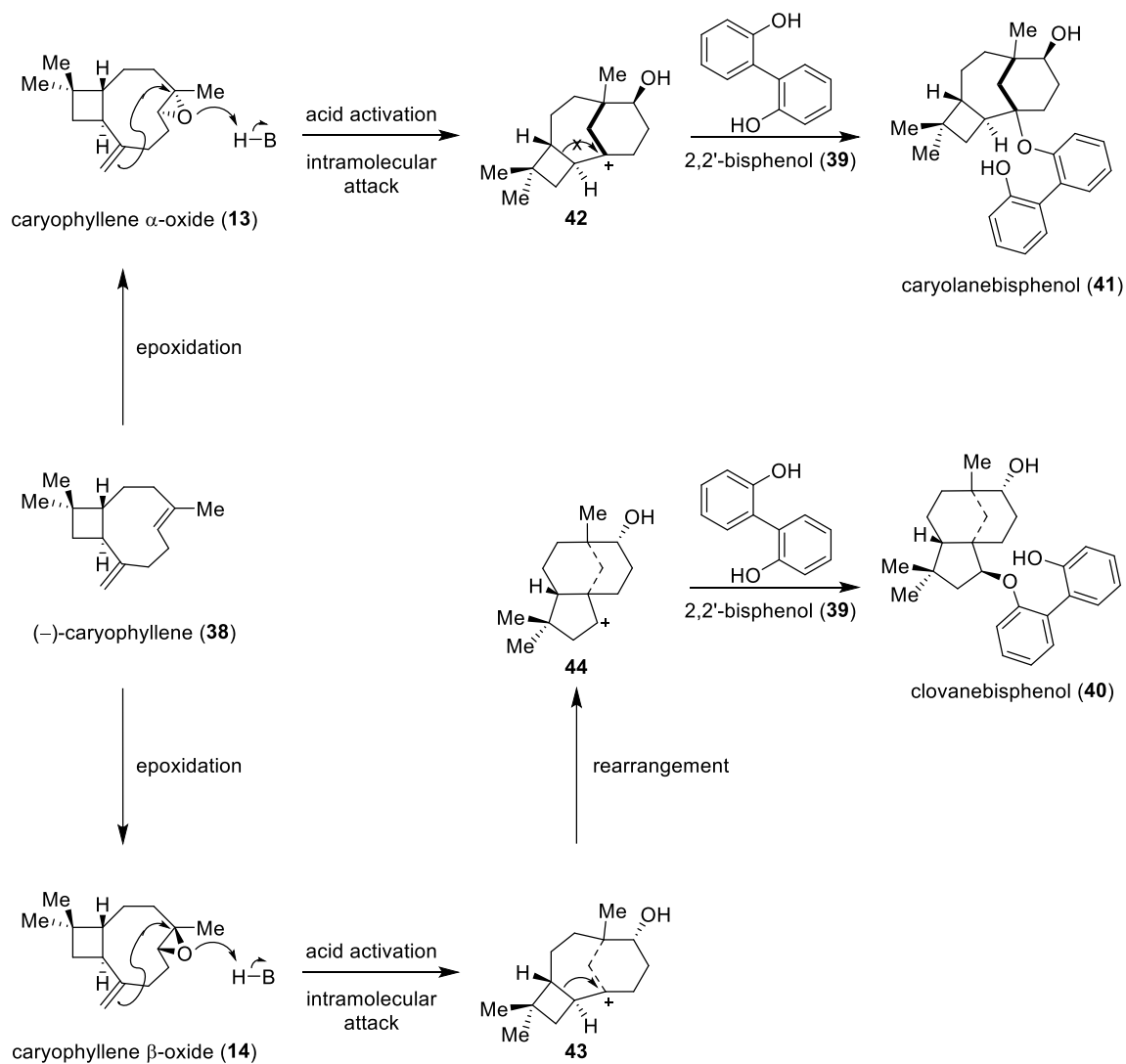
Design of Clovanemagnolol Analogs

The observed *in vivo* neuronal outgrowth of both clovanemagnolol and caryolanemagnolol as well as other growth-promoting compounds was promising considering the reported difficulty of many small molecules passing through the *C. elegans* cuticle. Previously developed synthetic routes to access these natural products and derivatives on multi-gram scales favorably positioned the preparation of structural analogs.²⁸⁻²⁹ To develop additional analogs for biological testing and target identification studies, the synthesis of a structural derivative of clovanemagnolol amenable to modification was designed from the readily available starting materials (–)-caryophyllene (**38**) and 2,2'-bisphenol (**39**) based on the previously reported synthesis by the Siegel group (Scheme 2.1).²⁹ This derivative possessed the same structural core derived from caryophyllene, but lacked the allyl appendages on the aryl rings. It was reasoned that these positions could be used later as a handle for chemical modification and would provide the ideal location for designing further analogs for mechanism of action studies.



Scheme 2.1. Synthesis of clovanebisphenol, a clovanemagnolol derivative.

Oxidation of (–)-caryophyllene (**38**) produced diastereomeric epoxides caryophyllene α -oxide (**13**) and caryophyllene β -oxide (**14**). First proposed by Barton and coworkers, the caryophyllene epoxides rearrange to generate the clovane and caryolane core structures as a result of Brønsted acid activation followed by intramolecular attack of the alkene (Scheme 2.2).¹⁰³⁻¹⁰⁴ Reaction of the tricyclic carbocation intermediates with 2,2'-bisphenol (**39**) generated the derivative compounds. The intermediate bridgehead carbocation derived from caryophyllene α -oxide was trapped directly by bisphenol to form the caryolanebisphenol (**41**) diastereomer with 48% yield. The carbocation intermediate resulting from caryophyllene β -oxide possessed favorable orbital overlap to undergo rearrangement, whereby the cyclobutane ring expanded to relieve ring strain, generating the clovane core. This rearranged cation was then trapped by bisphenol to generate the clovanebisphenol (**40**) analog in 16% yield.¹⁰⁵



Scheme 2.2. Mechanism of caryolanebisphenol and clovanebisphenol formation.

These newly synthesized derivatives combined with the cholinergic neuronal outgrowth assay in *C. elegans* allowed for investigations into the biological activity of chemically edited analogs possessing the clovane or caryolane core. It was found that the derivatives clovanebisphenol and caryolanebisphenol caused sprouting from multiple

nerve cords and commissural branching morphologies at concentrations as low as 0.02 μM in cholinergic neurons. Caryolanebisphenol showed outgrowth in 39% of nematodes, while clovanebisphenol showed outgrowth in 30% at 2 μM concentrations (Figure 2.6). These levels of branching were similar to those found after exposure to the parent natural products. When the concentration of clovanebisphenol was increased to 20 μM , 43% of the worms showed outgrowth morphologies. The modified derivatives clovanebisphenol and caryolanebisphenol retained biological activity, and established a position for making further derivatives of the natural products.

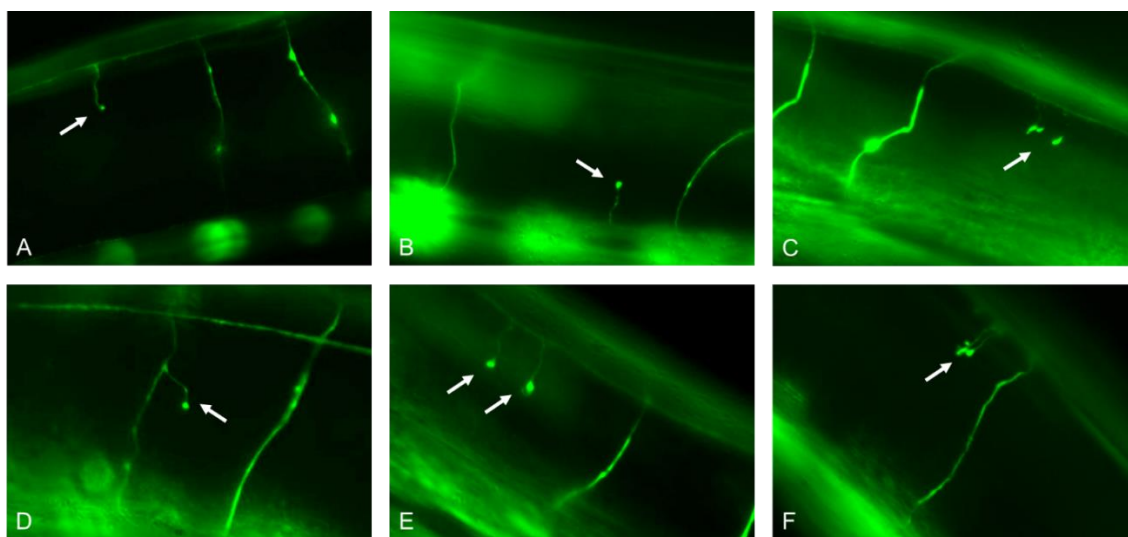


Figure 2.6. Outgrowth of *C. elegans* exposed to clovanebisphenol (A-C) or caryolanebisphenol (D-F).

A simplified method for determining the biological effects of small molecules on neuronal outgrowth was desired, and the use of *C. elegans* as a model system allowed for

examining *in vivo* activity as well as overcoming many of the problems associated with primary neuronal cultures. A strain of GFP-fluorescing nematodes was discovered where neuronal outgrowth could easily be examined in cholinergic neurons. The exposure of nematodes to potentially neuroactive compounds was accomplished with minimal effort, and within 48 hours the results of outgrowth assays were obtained. Various compounds were found to cause outgrowth in the *C. elegans* model, including the clovane scaffold, providing a simple technique for assessing the neurotrophic activity of small molecules and facilitating the design and screening of biologically optimized analogs in the development of potential therapeutics.

Mechanism of Action Studies

The ability to transition from early screening stages to mechanism of action studies within the same model organism provides significant advantages in target identification. The use of a protein set from an entire organism surpasses the use of individual cell lines as protein targets that exist in only one type of cell might be missed. *C. elegans* are well suited for generating organismal lysates since they can be cultivated easily on a large scale, allowing for the production of sizable protein samples.¹⁰⁶⁻¹⁰⁷ The hermaphroditic nature of the worms generates a uniform pool of proteins. Furthermore, upon discovery of a putative protein target RNAi coupled with *C. elegans*' well-studied genetics could be used for target validation. The use of *C. elegans* lysates in target identification allows for organismal mechanism of action studies, providing a link between small molecule screening and genetic manipulations.

Generation of Organismal Lysate

The nematodes' tough outer cuticles have presented a challenge in generating organismal lysates. *C. elegans* possess a resilient exoskeleton, known as the cuticle, made up of cross-linked collagens, cuticlins, glycoproteins, and lipids.¹⁰² The cuticle is synthesized five times throughout the development of the worm and, among other functions, provides environmental protection.¹⁰² This tough extracellular matrix has proven to be a barrier to methods of lysis, especially under non-denaturing conditions. Several methods for lysing *C. elegans* have been reported, including proteinase K digestion, sonication, boiling, freezing and pulverizing, and homogenization techniques.¹⁰⁸ After investigating these, continuous sonication at low power using a microtip probe was found to be the best method for easily and sufficiently fragmenting cuticles and extracting worm innards under non-denaturing conditions.¹⁰⁸

C. elegans were grown in large-scale liquid cultures to provide substantial whole-organism protein lysates for mode of action studies. Lysates were generated from wild-type *C. elegans* (N2) after incubation in buffer for 30 minutes to allow for complete digestion of their *E. coli* food source, thereby avoiding bacterial contamination. Worms were collected by washing with a cold buffer solution, and the samples were subsequently maintained at ~5 °C to ensure protein integrity. After centrifugation at low speed, the supernatant was discarded and the worms were washed with a series of buffers. Cold lysis buffer containing protease inhibitors was added to the worm pellet following the final wash/centrifugation cycle. The worms were then sonicated using a microtip probe until “ghost cuticles” were observed microscopically as evidence of lysis. The organismal lysate

was then cleared by a final centrifugation and the supernatant was collected for target identification.

Preparation of Reagents for Target Identification

Various strategies for direct target identification exist, including methods involving affinity matrices, biotinylation, radiolabeling/imaging, and photoaffinity probes.¹⁰⁹ Previous target identification studies using *C. elegans* have employed chemistry-to-gene screens^{69, 110} and affinity chromatography¹¹¹. Affinity purification, or “pull-down”, methods employ a molecule of interest conjugated to a solid support which is then incubated with a cellular lysate. Affinity purification pull-down methods have been successful in identifying protein targets of bioactive molecules.¹¹¹ The use of solid support resins for pull-down experiments is advantageous due to the low cost, simple procedures (combine, wash, and elute), and environmental benignity. Recently, small molecules containing primary alcohols have been linked successfully to beaded agarose containing terminal amines via carbamate formation following activation with carbonyldiimidazole (CDI).¹¹²

Affinity purification was chosen from among small molecule target identification strategies due to synthetic advantages following structure-activity relationship (SAR) determination.¹⁰⁹ The validity of using *C. elegans* proteome for mode of action studies was first established through identifying the known protein targets of a synthetic small molecule derivative of the macrolide lactone FK506 (**45**)¹¹³, pipercolyl α -ketoamide (**46**)¹¹⁴, which is recognized by the human immunophilin FKBP12¹¹⁵ (Figure 2.7). Isolated from

the soil bacterium *Streptomyces tsukubaensis*, FK506 exhibits potent immunosuppressive activity. The natural product FK506, the structurally related macrolide rapamycin (**47**), and small molecule derivatives possessing the binding domain such as pipercolyl α -ketoamide bind with high affinity to the immunophilin FKBP12 (FK506 binding protein 12) as well as several other members of the FKBP family of proteins which possess peptidyl-prolyl cis-trans isomerase activity, thereby generating a small molecule/protein complex that inhibits T-cell functions.^{116-117, 118} The simplified ligand allows for exploitation of this strong binding along with manipulation of the small molecule structure to generate affinity reagents. The well-known FKBP binding targets of the small molecule FK506 and derivative ligands like pipercolyl α -ketoamide allow for validation of novel target identification methods, such as the desired use of the *C. elegans* proteome for pull-down experiments.

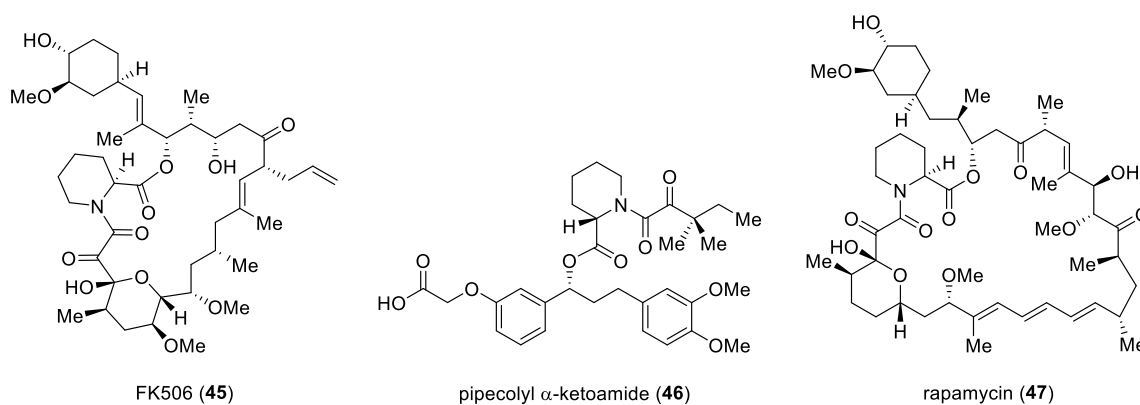
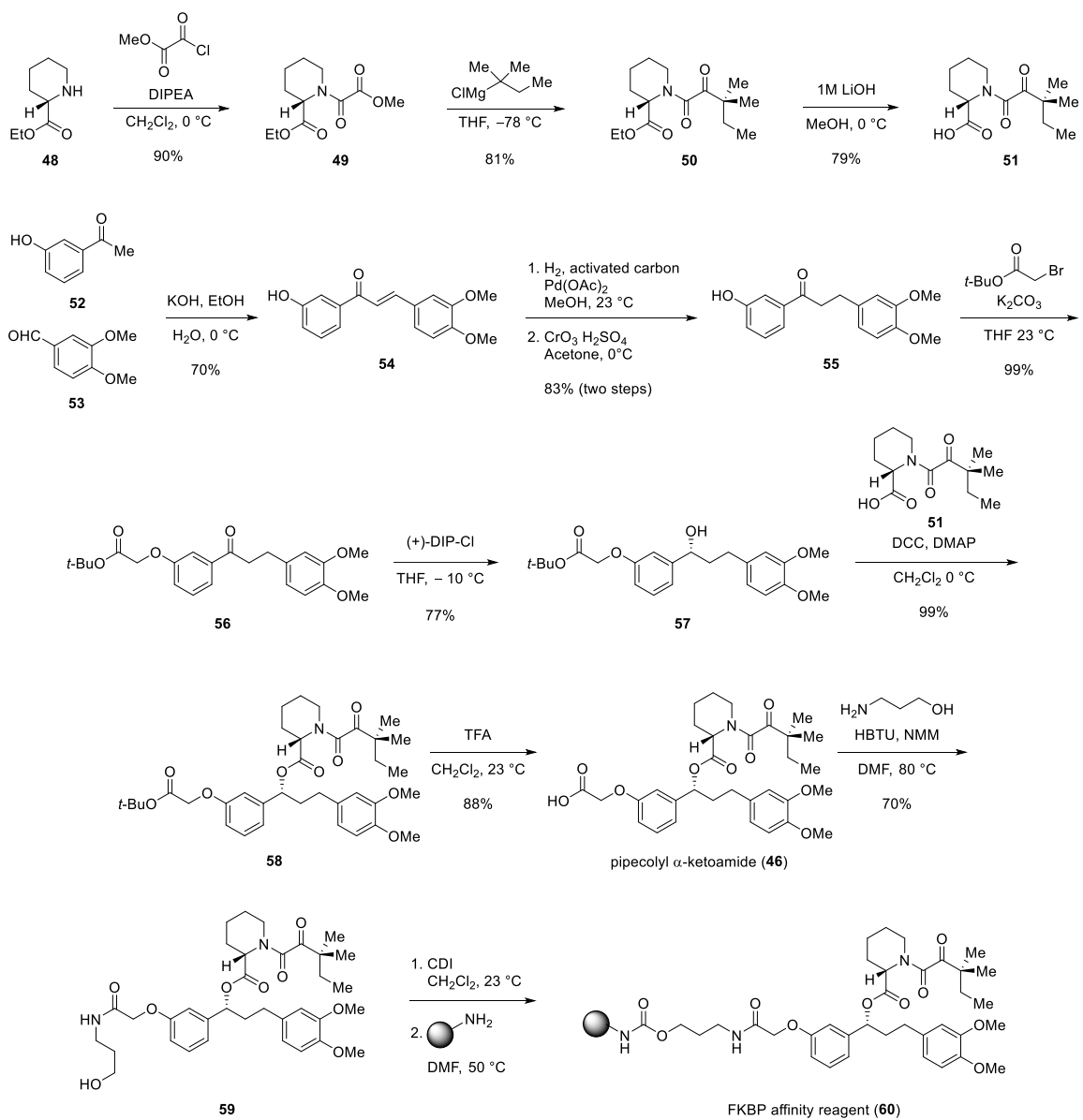


Figure 2.7. Representative molecules that have been shown to bind FKBP.

The synthesis of the pipercolyl α -ketoamide **46** was achieved by a minor modification of the existing route (Scheme 2.3).¹¹⁴⁻¹¹⁵ Following amide bond formation with 3-aminopropanol, the primary alcohol-containing pipercolyl α -ketoamide **59** was conjugated to immobilized diaminodipropylamine on beaded agarose through carbamate bond formation according to previously established procedures.¹¹² Capping of unreacted amines as an acetoxy group was achieved by the use of *N*-acetoxy succinimide.¹¹⁷ The affinity reagent (**60**) was then combined with the prepared *C. elegans* crude proteome generated by sonication of the worms. Proteins that bound to the beads were denatured, separated by sodium dodecyl sulfate polyacrylamide gel electrophoresis (SDS-PAGE), and bands were excised from the gel for mass spectrometry (MS)-based protein identification. Mass spectrometry data compared to a database of *C. elegans* protein sequences (CAEEL) revealed that proteins corresponding to the *fkB-3*, *fkB-4*, and *fkB-5* genes were isolated in the gel bands (Figure 2.8). These genes encode a peptidyl-prolyl cis-trans isomerase homologous to a mammalian FK506 immunosuppressant binding protein.



Scheme 2.3. Synthesis of pipecolyl α -ketoamide and the FKBP affinity matrix.

Identified Proteins (226)	Accession Number	MW
Peptidyl-prolyl cis-trans isomerase OS=Caenorhabditis elegans GN=fkb-5 PE=2 SV=1	P91180_CAEEL (+1)	30 kDa
Peptidyl-prolyl cis-trans isomerase OS=Caenorhabditis elegans GN=fkb-3 PE=2 SV=1	O16309_CAEEL	29 kDa
Protein Y47G6A.22 OS=Caenorhabditis elegans GN=CELE_Y47G6A.22 PE=2 SV=1	Q8MXS8_CAEEL	27 kDa
Anamorsin homolog OS=Caenorhabditis elegans GN=T20B12.7 PE=2 SV=1	DRE2_CAEEL	26 kDa
Protein Y82E9BR.14, isoform b OS=Caenorhabditis elegans GN=CELE_Y82E9BR.14 PE=4 SV=1	H2LOG7_CAEEL (+1)	36 kDa
Serine/threonine-protein phosphatase Pgam5, mitochondrial OS=Caenorhabditis elegans GN=pgam-5 PE=2 SV=2	PGAM5_CAEEL	32 kDa
ICln1 OS=Caenorhabditis elegans GN=icln-1 PE=2 SV=1	G5EFZ5_CAEEL (+1)	23 kDa
Protein Y116A8C.27, isoform a OS=Caenorhabditis elegans GN=CELE_Y116A8C.27 PE=4 SV=2	Q9U2U3_CAEEL	30 kDa
Histone H1.5 OS=Caenorhabditis elegans GN=hil-5 PE=2 SV=3	H15_CAEEL	23 kDa
Peptidyl-prolyl cis-trans isomerase OS=Caenorhabditis elegans GN=fkb-4 PE=2 SV=2	Q23338_CAEEL	29 kDa
Protein F48B9.8 OS=Caenorhabditis elegans GN=CELE_F48B9.8 PE=2 SV=1	Q20557_CAEEL	30 kDa
SPARC OS=Caenorhabditis elegans GN=ost-1 PE=1 SV=1	SPRC_CAEEL	30 kDa
Protein CEY-2 OS=Caenorhabditis elegans GN=cey-2 PE=2 SV=1	P91306_CAEEL	29 kDa
rRNA 2'-O-methyltransferase fibrillar OS=Caenorhabditis elegans GN=fib-1 PE=2 SV=1	FBRL_CAEEL	36 kDa

Figure 2.8. Representative section of proteins identified as binding to pipecolyl α -ketoamide following pull-down experiments.

Soluble Competition

Another application of the pull-down method combined the small molecule-bound beads with free, soluble small molecule ligand able to engage in competitive binding.^{117,}
¹¹⁹ Protein lysates were combined with either the small molecule-bound beads alone or the small molecule beads plus a high concentration of unbound ligand in solution. The free ligand competes for target binding with the immobilized compound, and should preferentially bind to the target due to the concentration disparity. Soluble competition experiments were performed using affinity resin-bound pipecolyl α -ketoamide (**60**) combined with the free, soluble ligand **46** in *C. elegans* lysate. Following the soluble competition experiment, SDS-PAGE and mass spectrometry-based protein identification

were used to identify proteins in each sample and the two sets of data were compared (Figure 2.9). Proteins that were absent from the sample containing free ligand but bound to the sample of small molecule-immobilized beads alone were noted, while proteins that bound to both samples were discarded.

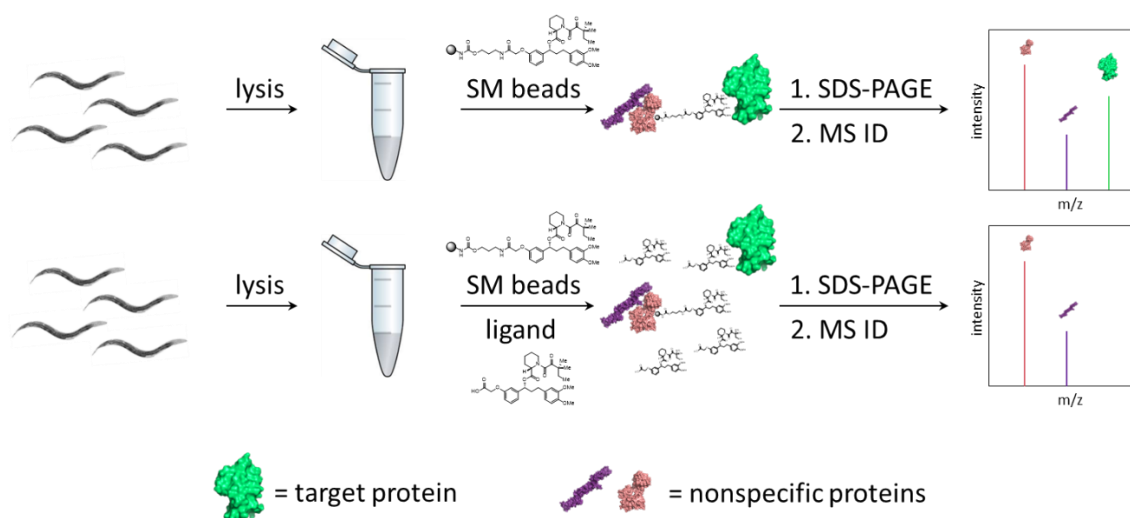


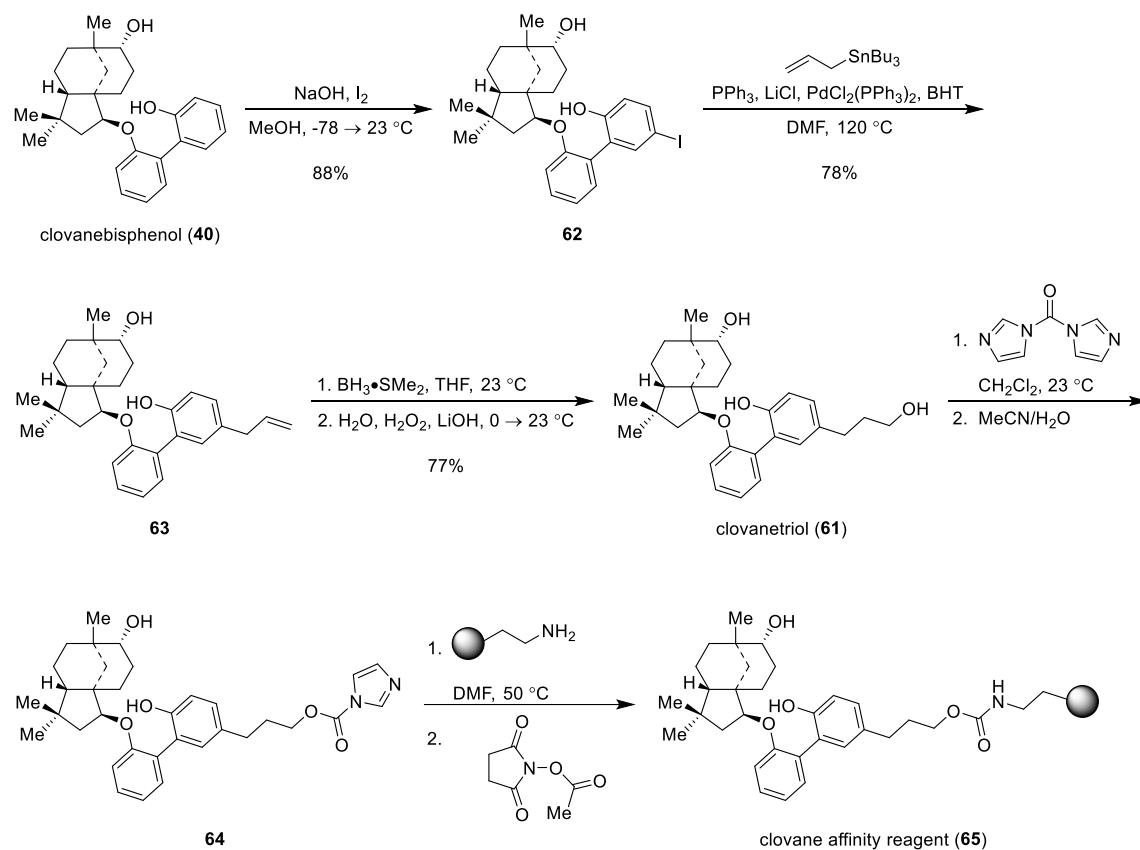
Figure 2.9. Soluble competition pull-down methods using *C. elegans* lysate and pipercolyl α -ketoamide free in solution as well as attached to beaded agarose.

Mass spectrometry protein identification revealed three FKBP s that were present in the bead only sample but absent from the bead plus free ligand sample, corresponding to *C. elegans* genes *fbk-1*, *fbk-2*, and *fbk-5*, all of which are homologs of human FKBP s.¹²⁰ Additionally, proteins corresponding to *fbk-6* were enriched in the bead only sample, but found in both likely due to incomplete soluble competition in the control. Successful identification of the expected FKBP s using these soluble competition methods provided a

foundation for the discovery of unknown protein targets of small molecules utilizing *C. elegans* proteome.

Identification of an Unknown Protein Target of Clovanemagnolol

These soluble competition pull-down and identification techniques were then applied to clovanebisphenol, which possessed unknown targets. This analog of the natural product clovanemagnolol was identified as a promoter of nerve growth using the previously described phenotypic cholinergic outgrowth assay.¹²¹ It was determined through SAR investigations that the allyl appendages were not required for activity, establishing a structural position for attachment to a solid support. To apply the affinity purification pull-down methods to this molecule, a derivative containing a primary alcohol, clovanetriol (**61**), was synthesized for coupling to beaded agarose (Scheme 2.4). After acid-catalyzed rearrangement of caryophyllene β -oxide and trapping of the cationic intermediate with 2,2'-bisphenol, the resultant clovanebisphenol underwent selective iodination with sodium hydroxide and iodine, generating aryl iodide **62** *para* to the phenol in 88% yield. The mono-allyl clovanemagnolol derivative **63** was then formed by Stille reaction with allyl tributylstannane. After hydroboration and oxidation, clovanetriol (**61**) was obtained in 77% yield. The clovane-based affinity reagent (**65**) could then be accessed by CDI coupling to amino-beaded agarose.¹¹²



Scheme 2.4. Synthesis of clovanetriol and the clovane-based affinity matrix.

The clovanetriol analog **61**, which retained its neuroactive properties according to assessment with the outgrowth assay by inducing branching in 29% of worms, possessed improved aqueous solubility. Clovanetriol was conjugated to amine-bound agarose beads and mixed with *C. elegans* lysate alone as well as lysate combined with free clovanetriol for soluble competition experiments. Following SDS-PAGE and mass spectrometry-based protein identification, several proteins were identified as present in the bead-alone sample but not the sample containing free molecule, providing putative targets (Figure 2.10).¹⁰⁵

Possible target proteins from clovane affinity matrix only (absent from soluble competition with free clovanetriol)

ALP-1

F54A3.2

KLC-1

M142.8

XRN-1

Y32H12A.8

Probability $\geq 99\%$ with 2 peptides at 80% minimum threshold analyzed using Scaffold Proteome Software.

Sample nonspecific binding proteins pulled down in soluble competition experiments

ACT-4

ATP-2

H28O16.1

TBB-1

VIT-6

VHA-13

DAF-21

PCK-2

R05G6.7

ZYG-1

Figure 2.10. Proteins identified as putative targets following clovane affinity matrix pull-down and soluble competition.

From these identified proteins, KLC-1 proved to be the most reproducibly isolated target relevant to axonal regeneration and was therefore selected for further investigation.

The *klc-1* gene codes for a kinesin light chain, which together with kinesin heavy chain forms part of the kinesin complex, a motor protein involved in cellular transport (Figure 2.11). Kinesin facilitates anterograde transport, meaning it migrates unidirectionally toward the plus end of microtubules and carries axonal cargo toward the periphery of the cell. Generally, the light chain of kinesin is involved in cargo binding.

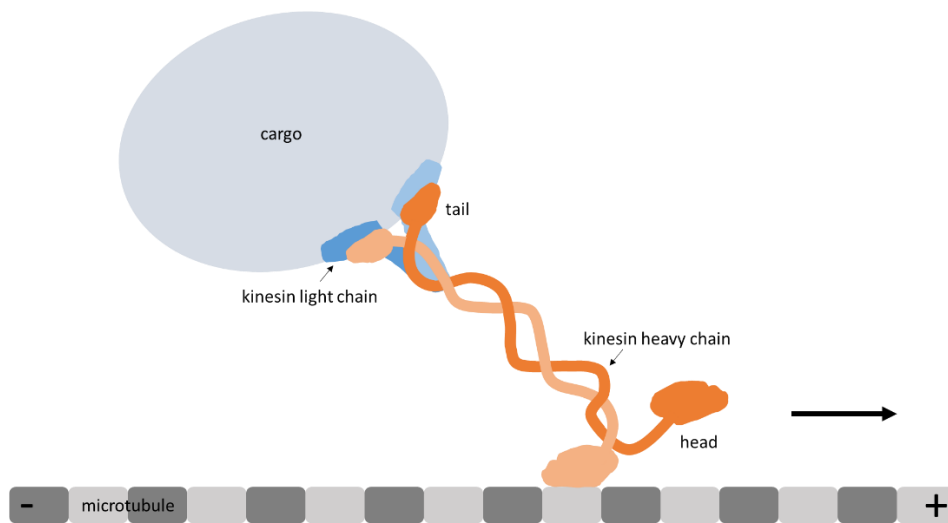


Figure 2.11. The structure of the kinesin motor protein moving along a microtubule.

C. elegans contain two genes that code for kinesin light chains, *klc-1* and *klc-2*. Kinesin-1, a complex of *C. elegans* proteins UNC-116/KHC and KLC-2, has been identified as playing a role in axonal transport and outgrowth in yeast two-hybrid assays.¹²² Although limited, previous reports have identified *klc-1* as a gene affecting axonal regeneration in *C. elegans* following laser microsurgery.⁸⁸ Additionally, inhibition of a

kinesin protein, kinesin-5, in adult mouse dorsal root ganglion neurons has been shown to enhance axonal regeneration.¹²³

To lend support to the role of *klc-1* in neuronal outgrowth and branching, genetic validation of the identified target through the use of either mutants or RNAi can be investigated to reproduce the phenotypic effects observed with small molecule treatment. *C. elegans*' well-studied genome along with efforts by the *C. elegans* Gene Knockout Consortium to generate a large number of readily available genetic knockouts make this organism ideal for these studies. When coupled with the previously developed *in vivo* outgrowth assay, any altered branching phenotypes caused by the functional absence of this gene can be observed.¹²¹ Mutant *klc-1* worms (RB1975 (*klc-1(ok2609)*)) were crossed with worms containing GFP-labeling in cholinergic neurons (LX929 (*vsIs48[unc-17::GFP]*)) and observed for outgrowth. While control worms possessed only 18% of background branching, 43% of the fluorescent cholinergic *klc-1* mutant worms exhibited a branching phenotype (Figure 2.12).¹⁰⁵ This branching emanated from both the nerve cords and commissures that extend across the worm, with many commissures containing several branches. Treatment with clovanebisphenol had little effect on the rate of branching of *klc-1* mutant worms. As previously reported, control worms treated with clovanebisphenol exhibited 30% branching while *klc-1* mutant worms treated with clovanebisphenol exhibited 36% outgrowth. Genetic validation via RNAi was also attempted but failed to produce either positive or negative results. The difficulty of RNAi with nerve cells has been reported and was possibly the reason behind a lack of observed effects.^{54, 124}

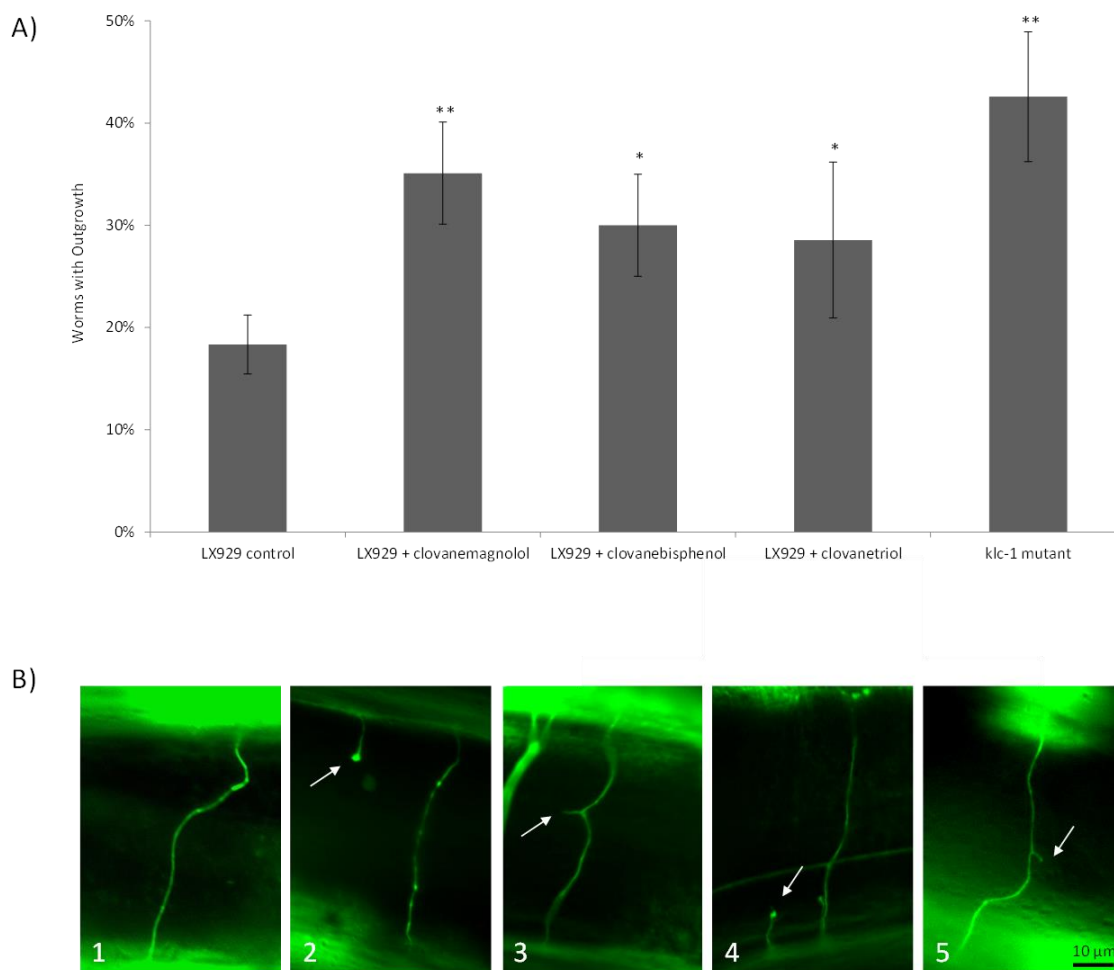


Figure 2.12. Outgrowth of *C. elegans* exposed to clovane-based small molecules and *klc-1* genetic mutants compared to control worms (* $P \leq 0.03$, ** $P \leq 0.005$) (A). Control cholinergic neurons (B1) and outgrowth observed in worms treated with clovanemagnolol (B2,B3) and *klc-1* mutants (B4,B5).

Conclusion

C. elegans allow for chemical biology investigations of small molecules from initial phenotypic screening *in vivo* to synthetic design of analogs, mechanism of action studies

for the identification of unknown protein targets, and genetic validation. Pull-down experiments combined with genetic methods using *C. elegans* exhibited the versatility of this model organism for identifying and validating biological targets of small molecules and provided a powerful basis for mode of action studies. The worm provided a useful vehicle for connecting high-throughput screening, mode of action studies, and genetic recapitulation within the same organism.

Experimental Section

Bioaccumulation of DHPs. *C. elegans* were grown at 23 °C in liquid culture according to established procedures from synchronized first larval stage worms using OP50 *Escherichia coli* as a food source.⁴⁷ The worms were harvested at the fourth larval stage, washed at least twice, and resuspended in M9 buffer to give a concentration of about 10 worms per μL . The worm suspension was divided into wells of a 48-well microplate (1 mL each, about 10,000 worms per trial) and DHPs were added to a final concentration of 40 μM (0.4% DMSO, v/v). Worms were incubated in the solutions at 23 °C for 6 hours. The worm solutions were then transferred to microcentrifugation tubes, pelleted by centrifugation, and the incubation solution removed. The worms were washed three times with M9 buffer (1 mL), centrifuged, and the liquid above the pellet removed following the final washing. The worms were then stored frozen at -20 °C until ready for HPLC processing. The samples were lysed by adding lysis buffer (50 μL of 100 mM KCl, 20 mM Tris pH 8.3, 0.4% SDS), proteinase K (10 μL of 3 mg/mL), and heating at 60 °C for 1 hour. After lysis the worm solutions were diluted with acetonitrile (150 μL), briefly

sonicated, and filtered using a syringe filter (0.2 μ m reconstituted cellulose membrane). The samples were then processed the same day by HPLC. Samples (100 μ L) were injected onto a 150x4.6 mm C18 (5 μ m) analytical column and analyzed at 230 nm using an Agilent 1260 Infinity Quaternary LC system equipped with an autosampler and diode array detector. A solvent gradient (0% to 100% B, increasing by 10% every 2 minutes) was used to elute the samples over 24 minutes at a flow rate of 1.5 mL/minute (Solvent A: 4.9% ACN, 95% H₂O, 0.1% TFA; Solvent B: 95% ACN, 4.9% H₂O, 0.1% TFA). Experiments were repeated in triplicate. To account for the possibility of false positives, several control experiments were conducted. The accumulation procedure was repeated with an additional washing using 0.1% SDS after incubation, without worms, or using heat-killed worms (overnight incubation at 37 °C). Worms washed with SDS still showed accumulation of DHPs. No DHP was observed in HPLC traces of experiments without worms. Dead worm trials did show DHP accumulation, which could be due to diffusion of compounds into the worm body.

Nematode Cultures and Microscopy. General maintenance of *C. elegans* was performed using an Olympus SZX16 stereomicroscope. GFP-labeled nematodes from outgrowth assays were visualized using an Olympus IX73 inverted microscope with a Prior Lumen 200 fluorescence illumination system. Images were captured using a Hamamatsu Orca-flash2.8 digital camera. *C. elegans* cultures were maintained on nematode growth medium (NGM) agar plates seeded with *Escherichia coli* OP50 bacteria at 23 °C according to established procedures.³⁹ Wild-type Bristol N2 strain was used for generating lysates. Other strains used include LX929 (vsIs48[unc-17::GFP]), EG1285 (oxIs12[Punc-47::GFP];

lin-15(+)), BZ555 (egIs1[Pdat-1::GFP]), SK4005 (zdIs5[Pmec-4::GFP; lin-15(+)], LX959 (vsIs13[lin-11::pes-10::GFP; lin-15(+)], and RB1975 (*klc-1(ok2609)*), which can be obtained from the Caenorhabditis Genetics Center.

Outgrowth Assay. Stock solutions (20 mM) of various chemicals were prepared in DMSO and subsequently diluted in M9 buffer to a final concentration of 0.04 mM (0.2% DMSO, v/v). Diluted solutions (200 μ L) were spread over seeded NGM plates (35x10 mm, containing 4 mL of agar) and allowed to absorb to a final concentration of 2 μ M. Approximately thirty fourth-larval-stage nematodes were picked from age-synchronized populations to prepared chemical plates. Worms were allowed to grow at 23°C on the chemical plates for approximately 48 hours, after which time the Day 2 Adults ($n \geq 20$) were mounted in M9 buffer (10 μ L) on 2% agarose pads containing sodium azide (5 mM) and observed for neuronal outgrowth compared to untreated control worms.

Generating C. elegans Lysates. Worms were transferred from starved plates to fifteen 60x15 mm NGM agar plates seeded with *E. coli* OP50 and allowed to grow until a large number of adults were present and the plates were freshly starved (about 3 days). The plates were washed with cold M9 buffer to collect the worms. Everything was kept cold from this point forward. The collected worm suspension was centrifuged at 300 rpm for 5 minutes to pellet the worms. The supernatant was discarded and the worms were washed with cold M9 three times, 0.1 M NaCl once, and TBS once, centrifuging between cycles. After the final washing the supernatant was discarded and 2 mL cold lysis buffer (TBS pH 7.5 containing 1 mM EDTA, 1.5% n-octyl glucoside, 1 mM PMSF, 1 mM NaF, and protease inhibitors (Amresco Protease Inhibitor Cocktail, General Use)) was added to the

worm pellet. The worms were sonicated using a microtip probe for 3 minute continuous cycles at 7-8 W power until “ghost cuticles” were observed microscopically as evidence of lysis. Organismal lysates were incubated on ice for 10 minutes then cleared by centrifugation at 15000 rpm for 10 minutes and the supernatant collected.

Soluble Competition and Pull-Down Experiments. The soluble competitor was dissolved in TBS to create a 5 mM stock ligand solution. Prepared affinity beads (10 μ L) were combined with either *C. elegans* lysate (500 μ L) and TBS buffer (200 μ L) or *C. elegans* lysate (500 μ L) premixed with 5 mM ligand solution (200 μ L). The suspensions were mixed with gentle shaking at 4 °C for 18 hours. The lysate mixtures were then centrifuged at 15000 rpm for 2 minutes to pellet the beads. The supernatant was removed and the beads were washed with 1 mL TBS four times and 1 mL water once. After the final washing the liquid was removed and 20 μ L SDS loading buffer was added to the beads. The solutions were heated at 100 °C for 5 minutes and SDS-PAGE was performed (12% gel run at 150 V for 10 minutes). The entire lanes were excised and submitted for mass spectrometry analysis and protein identification. Mass spectrometry and protein identification were performed by the Protein and Metabolite Analysis Facility at the University of Texas at Austin. Probability scores were analyzed by Scaffold Proteome Software.

General Chemistry. All reactions were performed in flame dried round bottom flasks under a positive pressure of nitrogen unless otherwise indicated. Pipecolyl α -ketoamide **46** and the corresponding pipecolyl ketoamide-based solid phase reagent **60** were prepared as previously described.^{112, 114} Dichloromethane (CH_2Cl_2) and

tetrahydrofuran (THF) were purified using a Pure-Solv MD-5 Solvent Purification System (Innovative Technology). All commercial reagents were used directly without further purification unless otherwise noted. Analytical thin-layer chromatography (TLC) was carried out using 0.2 mm commercial silica gel plates (silica gel 60, F254, EMD Chemical). TLC plates were visualized by exposure to ultraviolet light and/or stained with ceric ammonium molybdate or potassium permanganate. Flash chromatography was performed using Silicycle SiliaFlash P60 (230-400 mesh) silica gel. Organic solutions were concentrated by rotary evaporation at ~20 Torr. Nuclear magnetic resonance spectra (^1H NMR and ^{13}C NMR) were recorded with a Varian Mercury 400 MHz or Varian DirectDrive 400 MHz spectrometer. Chemical shifts are reported as parts per million (ppm) downfield of tetramethylsilane and referenced relative to residual protium in NMR solvents or carbon resonances of the solvent (CDCl_3 ^1H δ 7.26 ppm and CDCl_3 ^{13}C δ 77.0 ppm). Coupling constants are reported in Hertz (Hz). Data for ^1H NMR spectra are reported as follows: chemical shift (ppm, referenced to protium; s = singlet, d = doublet, t = triplet, q = quartet, m = multiplet, bs = broad singlet, coupling constant (Hz), and integration). Infrared spectra (IR) were recorded on a Thermo Scientific Nicolet 380 FTIR using neat thin film technique. High-resolution mass spectra (HRMS) were performed at The University of Texas at Austin Mass Spectrometry Center on an Agilent 6530 QTOF system and reported as m/z (relative intensity).

Synthesis of Clovanebisphenol (40). To a solution of caryophyllene oxide (**14**) (1.1 g, 4.5 mmol, 1.0 equiv.) and 2,2'-bisphenol (**39**) (4.2 g, 22 mmol, 5 equiv.) in CH_2Cl_2 (30 mL) was added a solution of diphenyl phosphate (0.57 g, 2.3 mmol, 0.5 equiv.) in CH_2Cl_2

(20 mL) over 10 minutes. The reaction was stirred at 38 °C for 2 hours then allowed to cool to 23 °C. The solvent was removed and the residue diluted with hexane (250 mL). The organic solution was washed with aqueous phosphate buffer (pH 7, 3 x 150 mL), 1 N NaOH (5 x 150 mL), brine (1 x 150 mL), dried over Na₂SO₄, and concentrated. The material was purified by silica gel chromatography (hexanes/EtOAc 80:20 as eluent) followed by another round of silica gel chromatography (100% CH₂Cl₂ as eluent), providing clovanebisphenol **40** (292 mg, 0.42 mmol) as a white foam. **R_f** = 0.22 (100% CH₂Cl₂); **¹H NMR** (400 MHz, CDCl₃) δ 0.84 (s, 3H), 0.87 (bs, 1H), 0.90 (s, 3H), 0.94 (s, 3H), 1.02-1.2 (m, 2H), 1.20-1.47 (m, 6H), 1.48-1.72 (m, 4H), 1.79 (dd, *J* = 5.4 and 12.1 Hz, 1H), 1.86-2.02 (m, 1H), 3.25 (bs, 1H), 4.22 (dd, *J* = 5.8 and 9.3 Hz), 6.33 (s, 1H), 7.00 (t, *J* = 8.2, 2H), 7.04-7.16(m, 2H), 7.2-7.4 (m, 4H); **¹³C NMR** (100 MHz, CDCl₃) δ 20.5, 25.3, 25.9, 26.4, 28.3, 31.1, 32.8, 34.5, 35.4, 37.5, 44.2, 44.7, 49.8, 74.7, 89.4, 115.8, 116.9, 120.6, 122.2, 126.7, 128.6, 128.9, 129.0, 131.1, 132.2, 153.5, 155.5; **IR** (film, ν cm⁻¹) 3378, 2947, 1478, 752; **HRMS** calc. for C₂₇H₃₄O₃+Na⁺([M+Na⁺]) 429.2508, obs. 429.2406.

Synthesis of Iodo-Clovanebisphenol (62). A solution of clovanebisphenol (**40**) (990 mg, 2.43 mmol, 1.0 equiv.) and NaOH (177 mg, 4.43 mmol, 2.0 equiv.) in MeOH (250 mL) was cooled to -78 °C. Once cooled, a solution of iodine (617 mg, 2.44 mmol, 1.0 equiv.) in MeOH (250 mL) was added over 5 minutes and stirred at -78 °C for 30 minutes. The reaction was allowed to warm to 23 °C over 1 hour. The reaction mixture was concentrated under reduced pressure to form a viscous oil, diluted with EtOAc (300 mL), aqueous phosphate buffer (pH 3, 200 mL), and saturated Na₂SO₃ (300 mL). The organic layer was separated and washed with saturated Na₂SO₃ (100 mL) and brine (100 mL). The

organic solution was dried over Na₂SO₄, filtered, and concentrated. The resulting iodophenol was purified by silica gel chromatography (90% CH₂Cl₂/hexanes → 100% CH₂Cl₂ → 5% MeOH/CH₂Cl₂) to afford **62** as a white foam (1.14 g, 2.14 mmol). **R_f** = 0.2 (100% CH₂Cl₂); **¹H NMR** (400 MHz, CDCl₃) δ 0.87 (s, 3H), 0.93 (s, 3H), 0.95 (s, 3H), 1.02-1.2 (m, 2H), 1.21-1.69 (m, 9H), 1.80 (dd, *J* = 5.8 and 12.5, 1H), 1.86-2.02 (m, 1H), 3.28 (bs, 1H), 4.25 (dd, *J* = 5.4 and 9, 1H), 6.52 (d, *J* = 8 Hz), 6.77 (d, *J* = 8.2 Hz, 1H), 7.03 (d, *J* = 8.2, 1H), 7.07 (t, *J* = 7.5 Hz, 1H), 7.27 (d, *J* = 1.9, 1H), 7.29 (dd, *J* = 1.5 and 7.52, 1H), 7.33-7.42 (m, 1H), 7.53 (dd, *J* = 2.3 and 10.5, 1H), 7.54 (d, *J* = 2.0 Hz, 1H); **¹³C NMR** (100 MHz, CDCl₃) δ 20.5, 25.3, 25.9, 26.5, 28.2, 31.0, 32.7, 34.3, 35.4, 37.6, 43.8, 44.7, 49.8, 74.8, 82.2, 88.6, 115.1, 119.0, 121.8, 126.7, 129.0, 129.4, 131.8, 137.3, 139.3, 153.5, 155.2; **IR** (film, ν cm⁻¹) 3400, 2949, 1478, 753; **HRMS** calc. for C₂₇H₃₃O₃I⁺ ([M⁺]) 532.1474, obs. 532.1475.

Synthesis of Des-Allyl-Clovanemagnolol (63). Triphenyl phosphine (2.21 g, 8.42 mmol, 6 equiv.), lithium chloride (960 mg, 22.6 mmol, 16 equiv.), bis(triphenylphosphine)palladium(II) dichloride (98 mg, 0.14 mmol, 0.1 equiv.), 2,6-di-*tert*butyl-4-methyl phenol (BHT) (2 mg, 0.01 mmol, 0.007 equiv.), and iodophenol **62** (747 mg, 1.4 mmol, 1 equiv.) were combined and placed under N₂. To the reaction vessel was added N,N'-dimethylformamide (14 mL) followed by allyltributylstannane (1.39 g, 1.28 mL, 4.21 mmol, 3 equiv.). The reaction was heated at 120 °C for 15 minutes then allowed to cool to 23 °C. Once cool, the reaction was diluted with EtOAc (50 mL) and washed with 3 N LiCl (5 x 15 mL) and brine (15 mL). The organic layer was dried over Na₂SO₄, filtered, and concentrated. The resulting allylphenol was purified by silica gel chromatography

(50% CH₂Cl₂/hexanes → 100% CH₂Cl₂ → 10% EtOAc/CH₂Cl₂) to afford **63** as a white foam (488 mg, 1.09 mmol). $R_f = 0.47$ (35% EtOAc/hexanes); **¹H NMR** (400 MHz, CDCl₃) δ 0.84 (s, 3H), 0.91 (s, 3H), 0.95 (s, 3H), 1.02-1.20 (m, 2H), 1.20-1.47 (m, 6H), 1.48-1.67 (m, 4H), 1.79 (dd, $J = 5.4$ and 12.1 Hz, 1H), 1.86-2.02 (m, 1H), 3.24 (bs, 1H), 3.36 (d, $J = 6.6$ Hz, 2H), 4.21 (dd, $J = 5.4$ and 9.3 Hz, 1H), 4.88-5.1 (m, 2H), 4.97-5.1 (m, 2H), 6.31 (s, 1H), 6.94 (d, $J = 8.2$ Hz, 1H), 7.03-7.16 (m, 4H), 7.29-7.39 (m, 1H); **¹³C NMR** (100 MHz, CDCl₃) δ 20.5, 25.3, 26.0, 26.4, 28.2, 31.1, 32.8, 34.4, 35.3, 37.5, 39.2, 44.1, 44.7, 49.8, 74.7, 89.4, 115.2, 115.8, 116.9, 122.1, 126.6, 128.7, 128.9, 129.0, 131.1, 131.8, 132.0, 137.8, 151.8, 155.4; **IR** (film, ν cm⁻¹) 3421, 2948, 1497, 732; **HRMS** calc. for C₃₈H₃₈O₃⁺([M⁺]) 446.2821, obs. 446.2822.

Synthesis of Clovanetriol (61). To a solution of **63** (488 mg, 1.09 mmol, 1.0 equiv.) in dry THF (10.9 mL) was added 1M BH₃·SMe₂ (7.1 mL, 7.1 mmol, 6.5 equiv.) via syringe. After 10 minutes at 23 °C, the reaction was placed in a 0 °C ice bath and H₂O (1 mL) was slowly added. Once gas evolution had subsided, 30% H₂O₂ (5 mL) and 4 N LiOH (5 mL) were added, the ice bath removed, and the reaction allowed to stir for 10 minutes. The reaction was then diluted with phosphate buffer (pH 3, 30 mL) and brine (30 mL). The organic layer was separated and the aqueous layer was extracted with EtOAc (4 x 50 mL). The combined extracts were dried over Na₂SO₄, filtered, and concentrated. The resulting compound was purified by silica gel chromatography (30% EtOAc/hexanes → 60% EtOAc/hexanes) to afford clovanetriol (**61**) as a white foam (399 mg, 0.839 mmol). $R_f = 0.13$ (35% EtOAc/hexanes); **¹H NMR** (400 MHz, CDCl₃) δ 0.86 (s, 3H), 0.88 (s, 3H), 0.96 (s, 3H), 1.01-1.14 (m, 2H), 1.16-1.58 (m, 7H), 1.61 (t, $J = 10.6$ Hz, 1H), 1.76-1.98 (m,

3H), 2.35 (s, 1H), 2.68 (t, $J = 7$ Hz, 2H), 3.2 (bs, 1H), 3.64 (t, $J = 6.5$ Hz, 2H), 4.23 (dd, $J = 5$ Hz and 9 Hz, 1H), 6.9 (bs, 1H), 6.92 (d, $J = 7.8$ Hz, 1H), 7.02-7.12 (m, 3H), 7.14-7.22 (m, 1H), 7.30-7.40 (m, 2H); ^{13}C NMR (100 MHz, CDCl_3) δ 20.5, 25.2, 25.2, 25.8, 26.4, 28.2, 31.0, 32.8, 34.0, 34.4, 35.4, 37.5, 44.1, 44.6, 49.7, 61.7, 74.6, 88.9, 115.3, 116.6, 125.1, 126.5, 128.0, 128.5, 128.8, 130.9, 131.9, 133.6, 151.6, 155.5; IR (film, v cm^{-1}) 3383, 2946, 1036, 736; HRMS calc. for $\text{C}_{30}\text{H}_{40}\text{O}_4^+$ ($[\text{M}^+]$) 464.2927, obs. 464.2924.

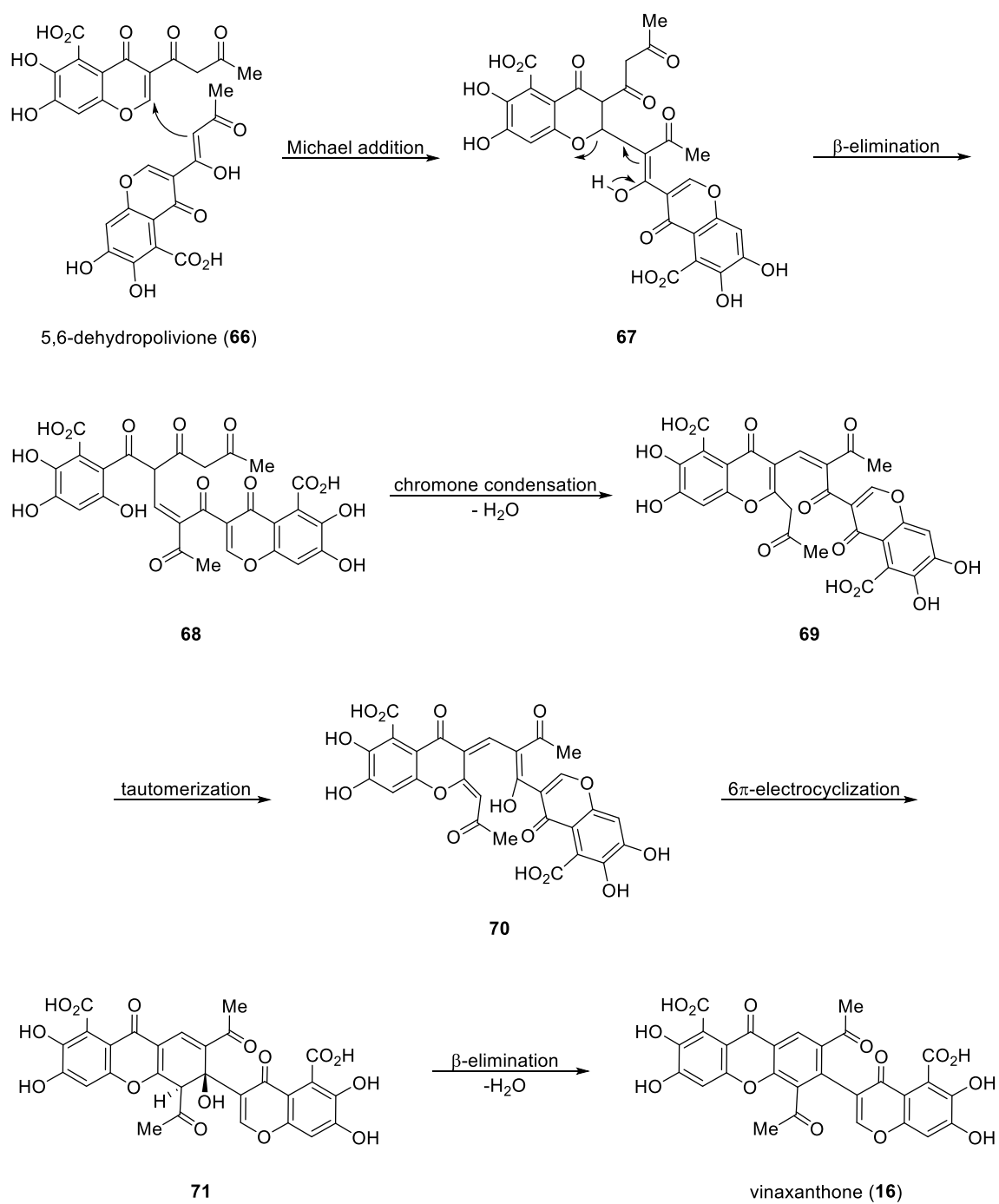
Synthesis of Clovane-Based Affinity Reagent (65). The primary alcohol **61** (1.3 mg, 2.0 μmol , 1.0 equiv.) was combined with carbonyldiimidazole (CDI) (8.1 mg, 50 μmol , 25 equiv.) in CH_2Cl_2 (200 μL) and shaken on a vortex mixer at 23 $^\circ\text{C}$ for 1 hour. The excess CDI was then quenched by the addition of a 1:1 acetonitrile/water solution (100 μL) and shaken for 30 minutes. The liquids were removed under reduced pressure and the resulting residue dissolved in DMF (400 μL). ThermoScientific CarboxyLink Coupling Gel (immobilized diaminodipropylamine on 4% cross-linked beaded agarose) (1 mL) was washed with DMF (3 x 1 mL), centrifuged, and the solvent removed. The solution of activated carbamate in DMF was added to the agarose beads and shaken at 50 $^\circ\text{C}$ overnight. A 1 M *N*-acetoxy succinimide solution in DMF (400 μL) was added to the beads and shaken at room temperature for 2 hours. The beads were washed with DMF (3 x 1 mL), PBS (phosphate buffered saline) buffer (3 x 1 mL), and water (3 x 1 mL) then suspended in 0.05% sodium azide in water (1 mL).

Chapter 3 – Vinaxanthone and Laser Axotomy

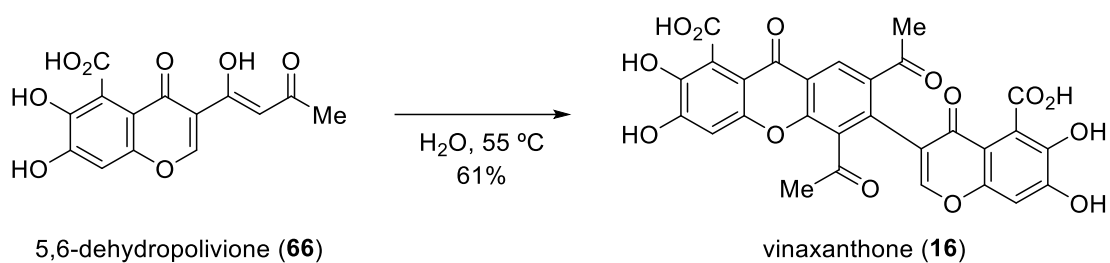
Synthesis of Vinaxanthone and Analogs

Due to previously reported dramatic CNS regenerative properties and high stability, the natural product vinaxanthone was selected for regeneration studies utilizing laser axotomy in *C. elegans*. Vinaxanthone and a library of synthetic analogs were tested for the potential to promote regeneration following laser axotomy in *C. elegans* in order to analyze the structure-activity relationship (SAR) of the molecule. This enabled the determination of structural moieties leading to enhanced biological activity so that more potent promoters of neuronal growth could be designed, optimized, and developed. Structure-activity relationship studies in *C. elegans* provide many advantages over other model organisms, particularly the capability for rapid, large scale screenings made possible by their small size, short life cycle, and procedural simplicity.

Vinaxanthone was synthesized by Siegel *et al.* through a biologically-inspired dimerization of 5,6-dehydropolivione (**66**), a putative derivative of the known natural product polivione (Scheme 3.1).¹²⁵ This reaction is proposed to occur in nature via Michael addition of one molecule of 5,6-dehydropolivione to another, followed by β -elimination and chromone condensation. After tautomerization, a 6π -electrocyclization reaction yields the final core and subsequent β -elimination with loss of water gives the natural product vinaxanthone. Simply heating 5,6-dehydropolivione to 55 °C in aqueous solution under neutral laboratory conditions generates vinaxanthone in 61% yield (Scheme 3.2).¹²⁵

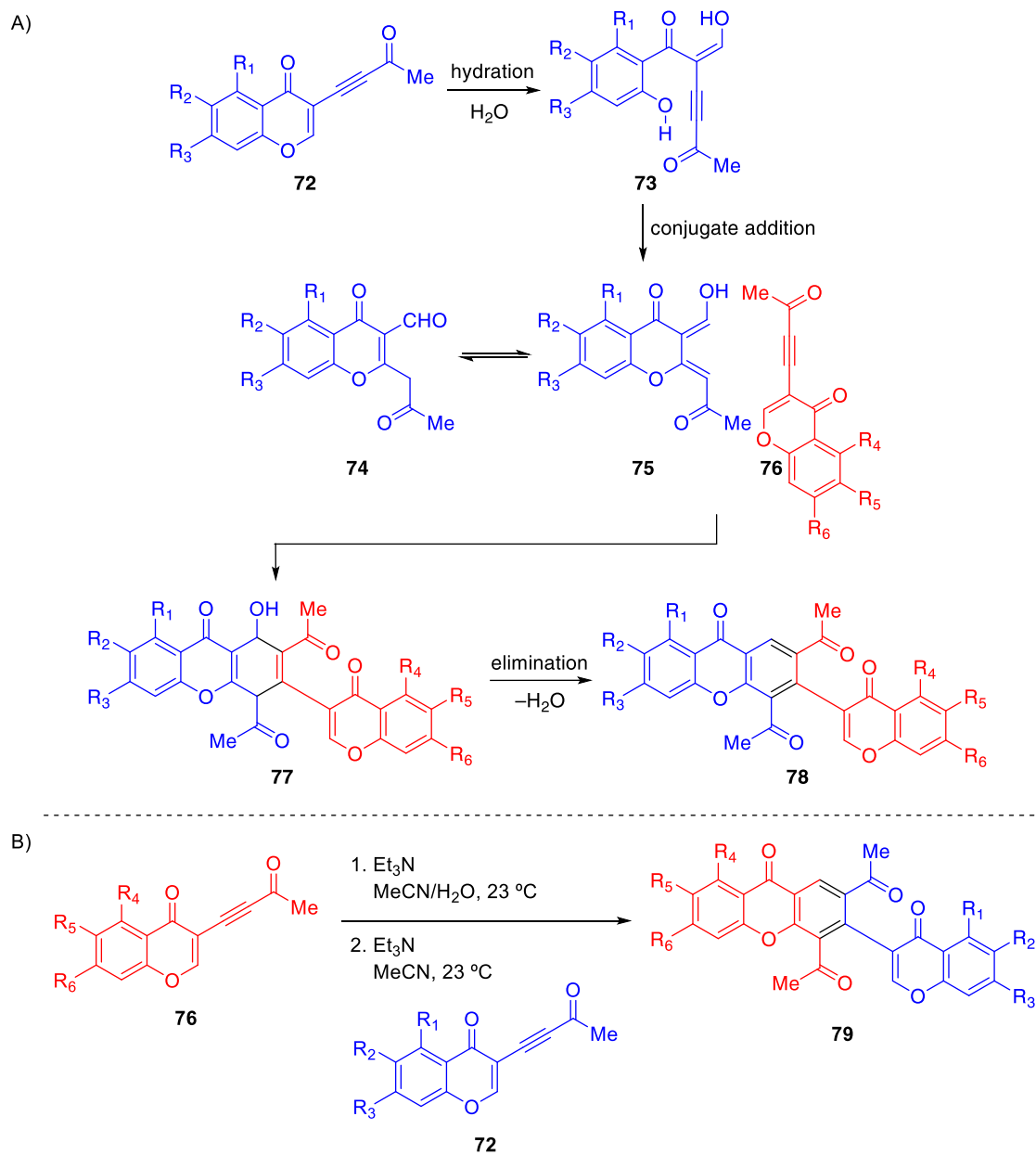


Scheme 3.1. Mechanism of 5,6-dehydropolivione dimerization to form vinaxanthone.



Scheme 3.2. One-step laboratory synthesis of vinaxanthone from 5,6-dehydropolivione.

Analogs of vinaxanthone were synthesized through an ynone coupling reaction (Scheme 3.3).¹²⁶ This allowed for the effective production of derivatives with distinct xanthone and chromone cores, utilizing ynones with modified aryl ring functionality. For this reaction, a parent ynone undergoes hydration and conjugate addition to form a diene which then reacts with another ynone through a cycloaddition/dehydrative elimination process to generate the xanthone core. Starting from n ynones, the generation of n^2 analogs is possible. Five different 3-ynone chromones (Figure 3.1) were systematically coupled to generate vinaxanthone and 24 analogs (Figure 3.2).



Scheme 3.3. Mechanism for synthesizing vinaxanthone analogs through an ynone coupling reaction (A). Reversing the order of the ynone addition generates the analog with opposite core functionality (B).

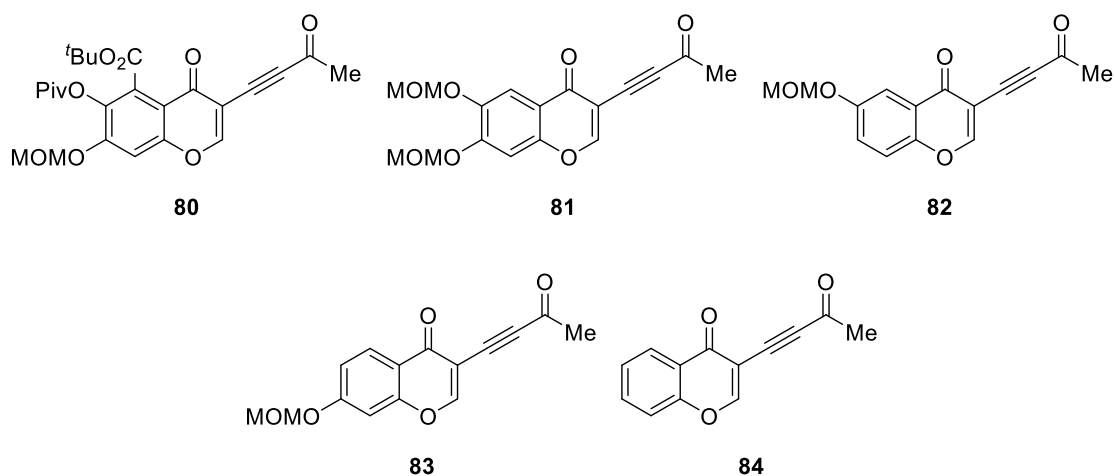


Figure 3.1. The five parent ynone used to generate vinaxanthone analogs.

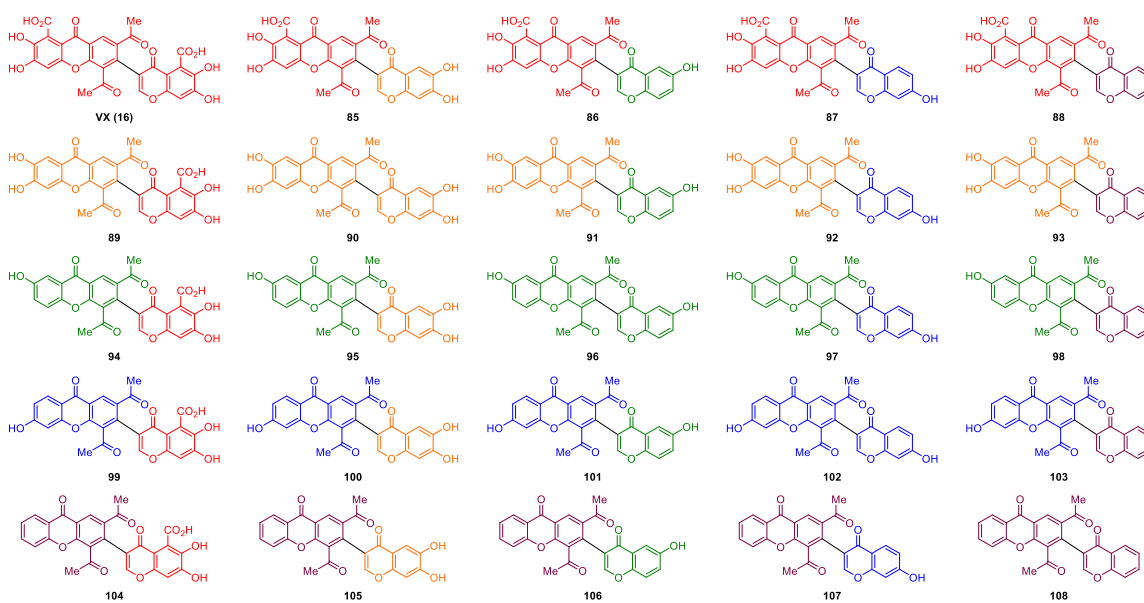


Figure 3.2. Vinaxanthone and the 24 analogs generated through ynone coupling reactions. Xanthone and chromone cores with identical aryl functionality are coded the same color.

Outgrowth Promoted by Vinaxanthone

Prior to the laser axotomy regeneration studies, the growth-promoting properties of vinaxanthone were evaluated using the *in vivo* outgrowth assay of cholinergic neurons. Vinaxanthone was found to enhance neuronal outgrowth in *C. elegans*, with 31% of treated worms exhibiting branching morphologies at 2 μM concentration (Figure 3.3).¹²⁵ These results were similar to the levels of cholinergic branching induced by other neurotrophic compounds such as amphotericin B, which promoted outgrowth in 36% of nematodes at 2 μM .¹²¹

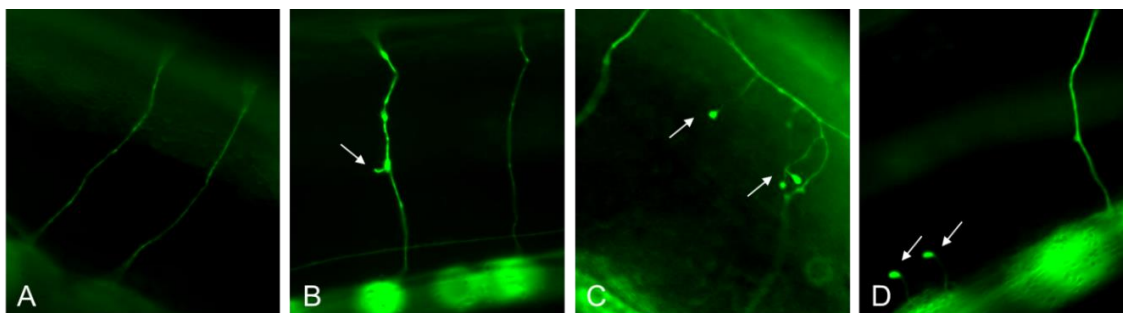


Figure 3.3. Commissures of control cholinergic neurons in *C. elegans* (A). Outgrowth caused by treatment with vinaxanthone includes commissural branching (B) as well as sprouting from nerve cords (C,D).

Laser Axotomy in *C. elegans*

Laser axotomy provides a method for further investigations into the neuroregenerative properties of small molecules *in vivo* following a simulated axonal injury. The mechanosensory neurons, which are responsible for the worm's reaction to

light touch, have been used extensively in laser axotomy experiments due to their relatively large size and distinctive axonal morphology.¹²⁷ Furthermore, these neurons have been employed in human disease investigations involving neurodegeneration, establishing a relevant connection for the model system.¹²⁸⁻¹²⁹ The axon of one of the two posterior lateral microtubule (PLM) cells, the mechanosensory neurons located along the left and right sides of the tail of *C. elegans*, was severed during laser axotomy. These neurons extend processes longitudinally from the tail toward the midbody, and each of the PLM neurites forms a single synaptic branch with the ventral nerve cord (Figure 3.4).¹³⁰⁻¹³¹

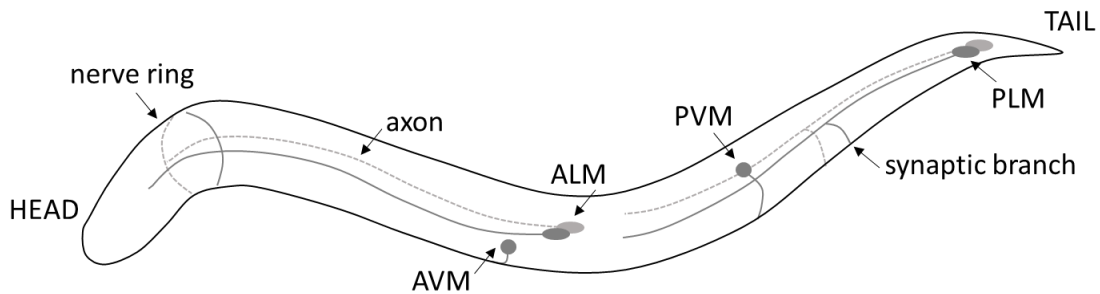


Figure 3.4. Morphology of the mechanosensory neurons in *C. elegans*.

Previous studies have indicated that the mechanosensory synaptic branch may serve in regulating neuronal growth as PLM neurons are able to regrow when severed proximal to their synaptic branch but not when severed distal to the branch site, thus marking a transition point in innate regenerative ability.¹²⁷ As many spinal cord neurons possess collateral branches that have been shown to influence regrowth potential, this inhibitory

branching environment would be a particularly useful model.¹³²⁻¹³³ Therefore, mechanosensory neurons severed beyond their branch point provided an experimental starting point which would result in a standard with limited intrinsic regrowth following axonal injury.

Late L4-stage *C. elegans* expressing GFP in mechanosensory neurons (*zDIs5*) were anesthetized using levamisole (1 mM) and their PLM was severed via laser axotomy at a point approximately 15 μm distal to the synaptic branch (Figure 3.5A). The distance of the synaptic branch point from the cell body in the *zDIs5* nematodes was not consistent between worms. It has been found that the greater the distance of injury from the cell body, the less likely regeneration is to occur from the severed axon.¹²⁷ Thus, in order to standardize the location of axotomy and to maintain the potential for regrowth, experimental nematodes were selected as having the desired PLM morphology only if they possessed a synaptic branch within a maximum distance of 100 μm from the cell body.

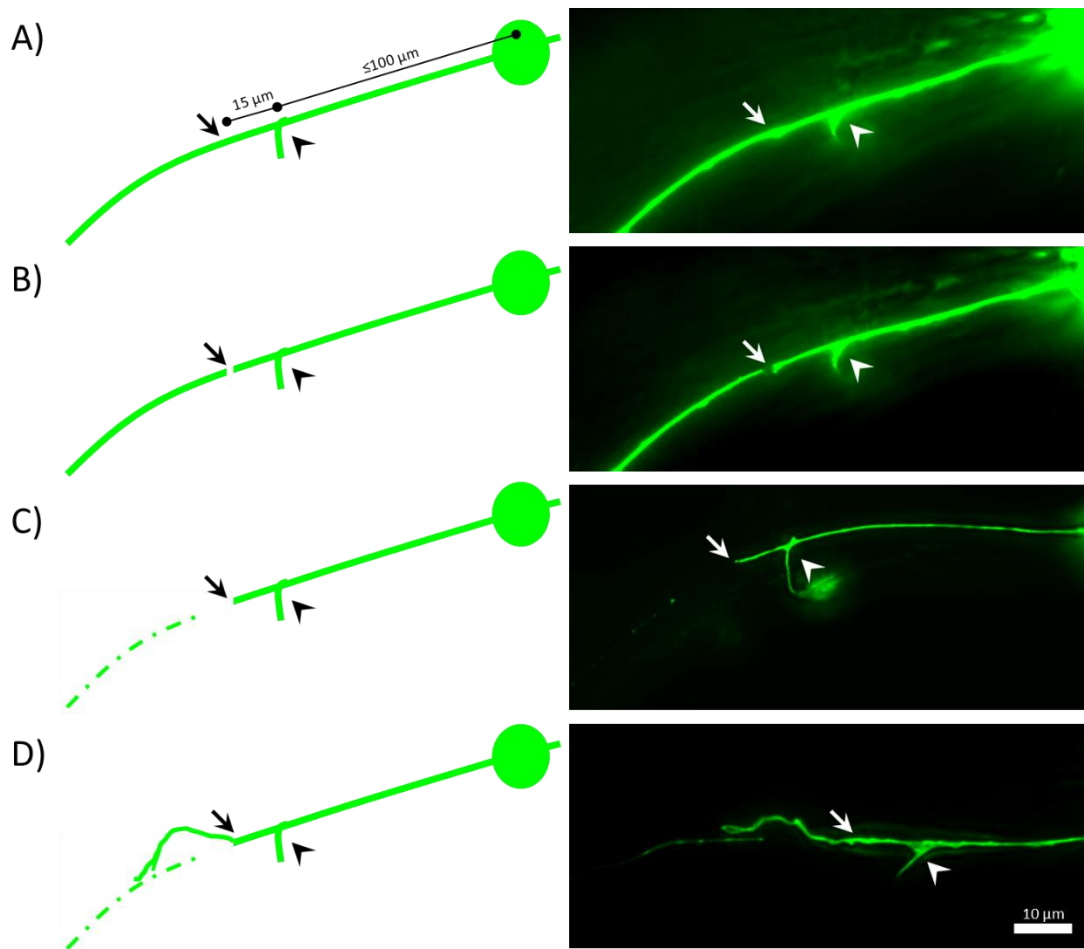


Figure 3.5. Laser axotomy of the PLM neuron in *C. elegans* was performed $\sim 15 \mu\text{m}$ after the synaptic branch when the branch point was $\leq 100 \mu\text{m}$ from the cell body (A), leaving behind a small break in the axon (B). No regrowth from the severed axon at 24 hours post-surgery resulted in a proximal stump and distal fragment degeneration (C). Regrowth of the severed proximal axon was observed on occasion 24 hours post-axotomy (D). Arrows indicate the site of axotomy and arrowheads indicate the synaptic branch.

Axotomy is accompanied by a characteristic series of events. The laser injures the neuron by creating a small break in the axon (Figure 3.5B), leaving a gap which expands over the next few hours as the ends of the severed fragments retract. The distal fragment

begins to undergo degeneration, characterized by the beading and disappearance of GFP, when the proximal end does not reconnect within 24 hours after axotomy and, if no proximal fragment regrowth occurs, an axonal stump remains (Figure 3.5C). The distal fragment degeneration can be likened to Wallerian degeneration described in other organisms and once onset of degeneration occurs the process is irreversible.⁸⁹ Alternately, formation of a growth cone on the proximal fragment can initiate the regeneration process, causing the axon to extend (Figure 3.5D). Sometimes the regrowing axonal process is able to find its distal fragment and fusion occurs, with this reconnection consequently preventing distal degeneration.¹³⁴

Regeneration Following Small Molecule Exposure

Axons severed distal to the synaptic branch point were found to be able to regrow in a small number of control worms (average 27%), and this potential for regrowth could be enhanced by small molecule treatment. After laser microsurgery nematodes ($n \geq 20$ per compound) were exposed to a small molecule library of vinaxanthone analogs at 2 μM concentrations. Regrowth of the severed proximal axon was quantified 24 hours after axotomy by measuring from the beginning of new growth at the axonal injury site to the tip of the longest regrowing process. Initial experiments indicated that if regrowth was to occur, it was observable within 24 hours. Although axonal regeneration involves both exploratory outgrowth and pruning, observation at 48 hours indicated that any difference in regrowth length was not substantial enough to warrant the increased experimental time. If no growth was observed from the proximal portion of the cut axon at 24 hours post-

axotomy it was therefore regarded as negative for regrowth. Growth of the synaptic branch was sometimes observed but was not included in the regeneration measurements; only regeneration from the severed axon was recorded as positive for regrowth. Regrowth usually occurred without connection to the distal fragment, but when, on occasion, reconnection to the distal portion was observed it was counted as positive for regrowth with its length being measured to the point of reconnection.

Varying degrees of regeneration, including both the lengths of the regrowing processes and the overall number of worms exhibiting regrowth compared to controls, were observed in worms treated with vinaxanthone analogs. Analog **98**, which possesses a monohydroxylated xanthone core and lacks functionality on its chromone core, had the highest rate of regrowth, with a 130% increase in the number of worms exhibiting regrowth morphologies from controls (Figure 3.6).¹²⁶ Comparatively, vinaxanthone showed a 21% increase in regrowth rate. While most of the analogs promoted the level of regeneration, analog **95** interestingly had no significant change in regrowth potential and analog **96** had a 15% decrease in regrowth rate compared to controls.

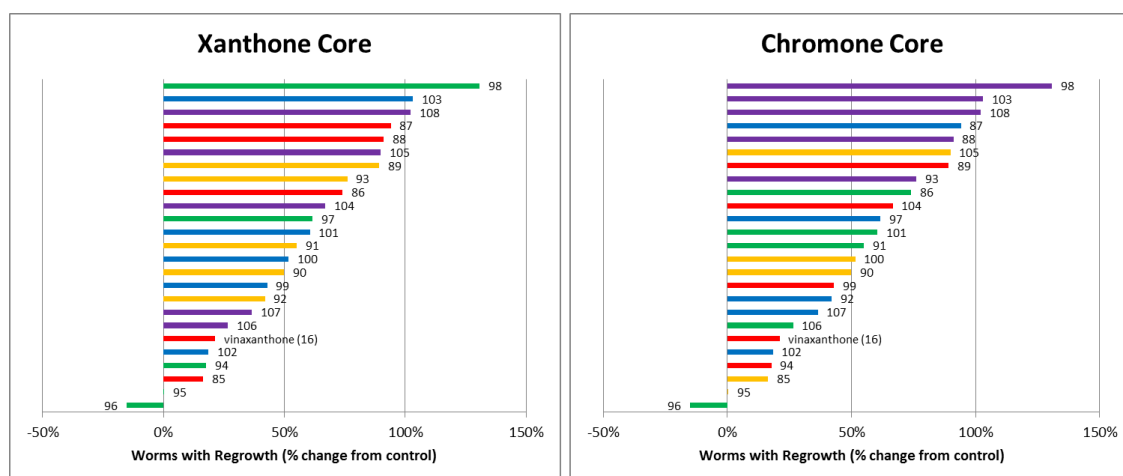


Figure 3.6. Following laser axotomy, worms exposed to vinaxanthone analogs displayed varying neuronal regrowth rates relative to controls. Colors correspond to structures in Figure 3.2 for SAR comparison.

The regrowing processes exhibited a variety of morphologies from virtually linear extension across the site of injury to arching growths around the axotomy scar as well as branching in search of their distal fragments (Figure 3.7). Occasionally the regrowing axon reconnected to its distal fragment or grew to the ventral cord in a manner similar to its synaptic branch. In examining the data for SAR correlations, it was found that analogs **87**, **88**, **98**, **103**, and **108** exhibited over 90% increase in regrowth from controls. The chromone cores of four of these molecules are identical, lacking any functionality on the aryl rings. This indicated that the chromone core, and specifically the bare structural motif, was significant in inducing the observed drug-promoted regeneration process. The structure of the xanthone core did not seem to have a strong relationship to the regeneration potential of PLM neurons post-axotomy.

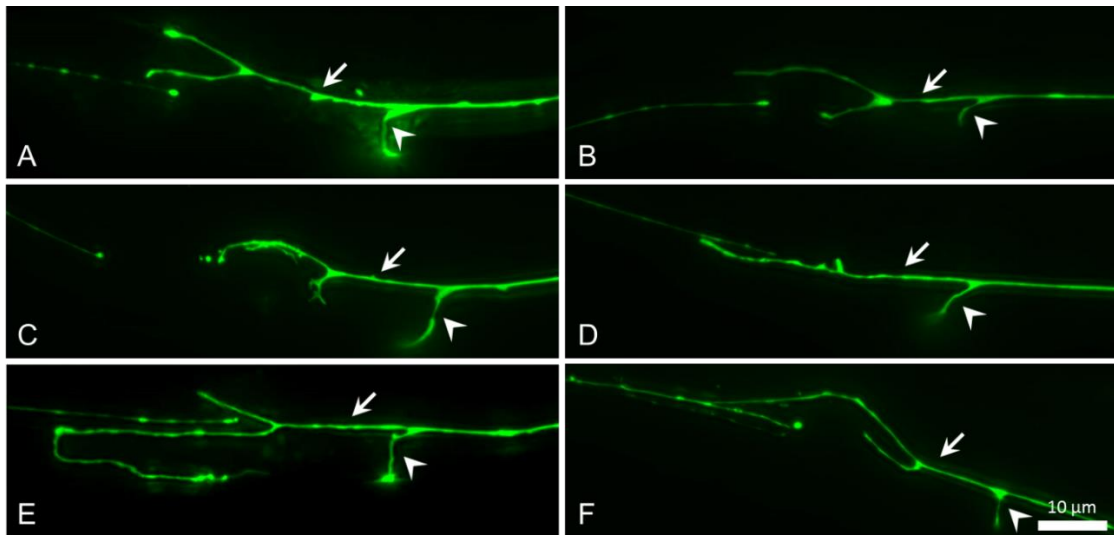


Figure 3.7. Branching regrowth of PLM neuron 24 hours following laser axotomy and treatment with 2 μM vinaxanthone (A). Regeneration morphologies promoted by post-axotomy treatment with 2 μM analog **98** included branching regrowth (B), arching regrowth (C), linear regrowth (D), regrowth with branching to the ventral nerve cord (E), and regrowth with reconnection to the distal fragment (F). Arrows indicate beginning of new growth and arrowheads indicate the synaptic branch.

Although varied, the lengths of the regrowing axons did not appear to have any correlation to the analogs' growth-promoting abilities nor was any pattern observed between the lengths of the regrowing processes and analogs with similar molecular structures (Figure 3.8). Even though wild-type *C. elegans* possess a virtually identical genetic background and standardized axotomy procedures are typically employed the highly variable extent of axonal regrowth between individual worms has been noted previously, with the exact reasons behind this variability unknown.⁸⁹

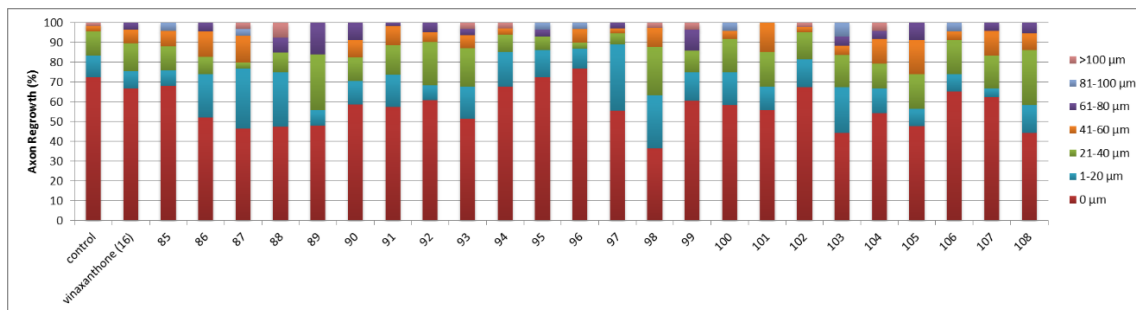


Figure 3.8. Lengths of regrowing PLM neuronal processes following laser axotomy and treatment with the library of vinaxanthone analogs.

The dose-response relationships for vinaxanthone and analog **98**, the most potent analog found following laser axotomy, were investigated (Figure 3.9). Although analog **98** induced an overall greater biological response at the standard concentration used in the axotomy experiments (2 μM), vinaxanthone produced a maximum biological activity at lower concentration (0.2 μM). Both compounds exhibited a biphasic dose-response curve, with decreased activity at higher concentrations (20 μM).

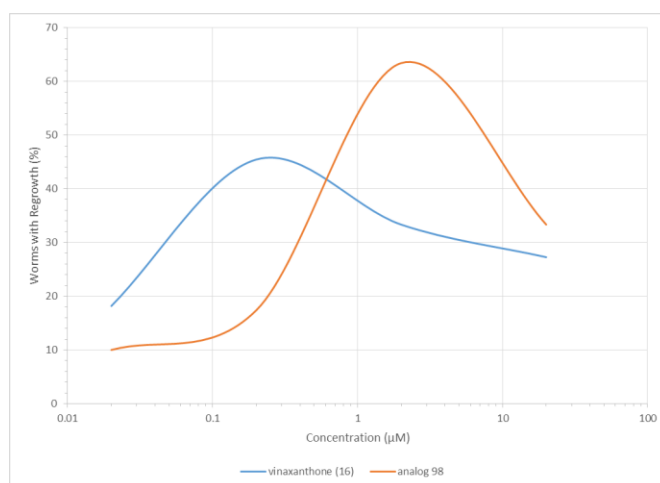


Figure 3.9. The dose-response relationships of *C. elegans* treated with vinaxanthone or analog **98**.

The regenerative potentials of the growth-promoting small molecules clovanemagnolol and clovanebisphenol were also explored. *C. elegans* were exposed to the compounds following injury simulated by laser microsurgery of mechanosensory neurons (Figure 3.10 and Figure 3.11). Regrowth and/or reconnection to the distal portion of the severed axon was classified as effective nerve regeneration. Worms were imaged 24 hours after axotomy, so the absence of degeneration in distal portions of the severed axons was taken as a positive indication of reconnection. Both compounds were found to improve successful axonal regeneration compared to untreated worms, where treated nematodes showed significantly increased regrowth and reconnection of the severed axon to its distal end. Following laser axotomy, worms treated with clovanemagnolol exhibited a regrowth rate of 63% (n = 16) while those treated with clovanebisphenol showed 56% regrowth (n = 16) compared to a regrowth rate of 40% observed in untreated control worms

(n = 10). It is significant to note that in previous experiments outgrowth was not observed when undamaged mechanosensory neurons of *C. elegans* were exposed to these compounds.

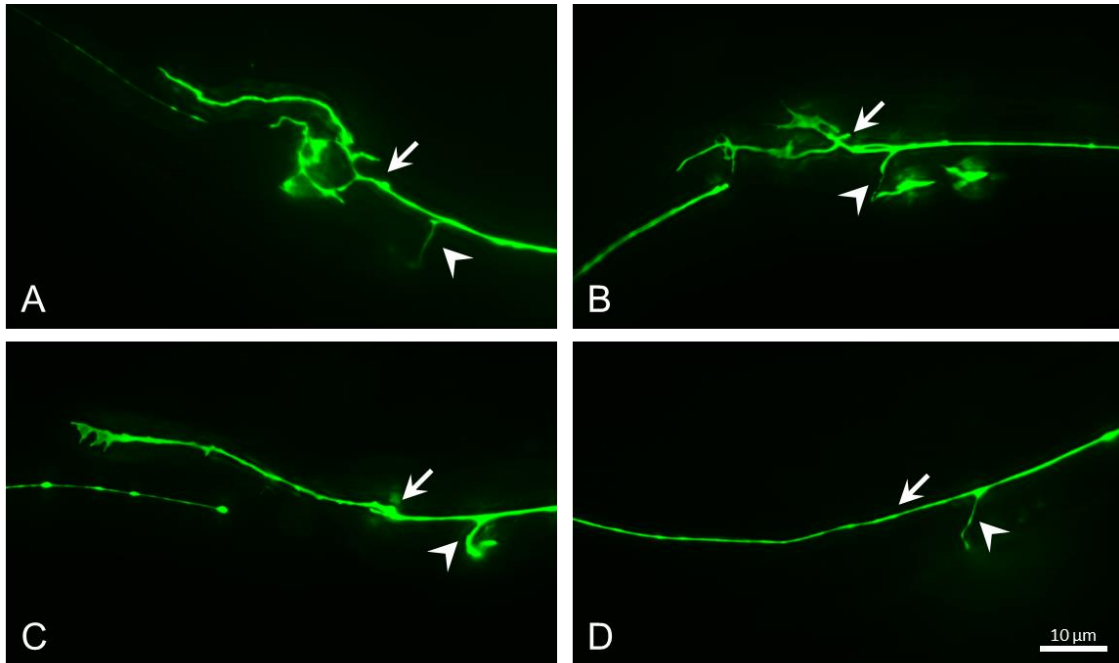


Figure 3.10. Regeneration following laser axotomy and treatment with 2 μ M clovanemagnolol (A-D). Arrows indicate beginning of regrowth and arrowheads indicate the synaptic branch.

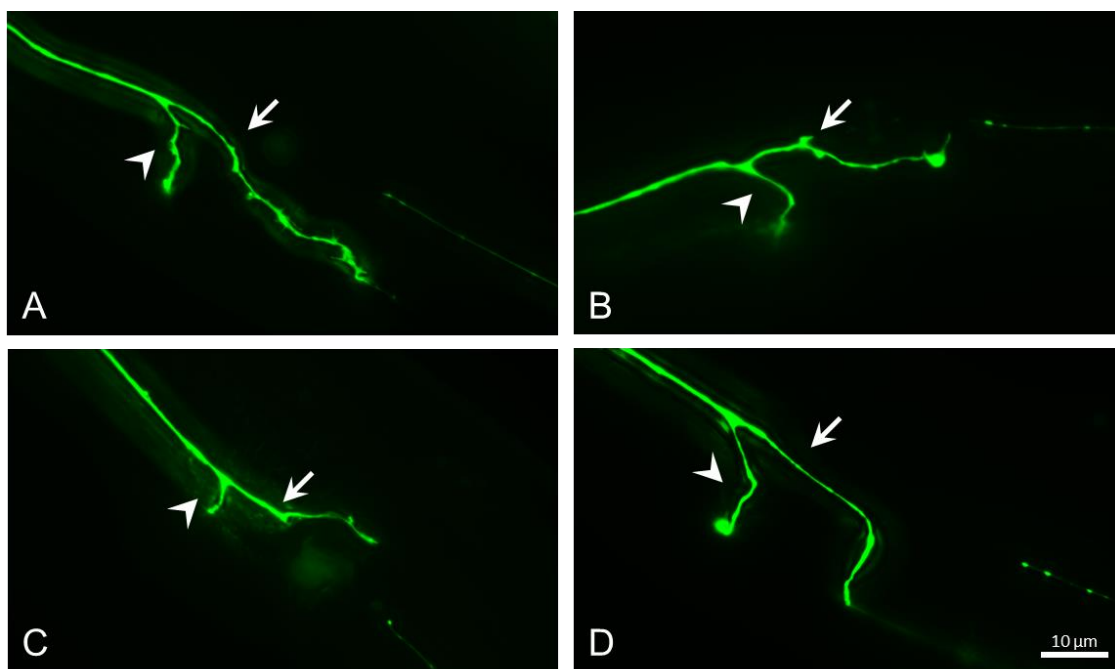


Figure 3.11. Regeneration following laser axotomy and treatment with 2 μM clovanebisphenol (A-D). Arrows indicate beginning of regrowth and arrowheads indicate the synaptic branch.

Conclusion

Laser axotomy in *C. elegans* has allowed the *in vivo* neuroregenerative potentials of vinaxanthone and a library of novel small molecule analogs to be determined, the SAR of the molecules to be analyzed within a relatively short time span, and can be used to assess further chemically-edited compounds for growth-promoting activity. The development of synthetic routes to vinaxanthone and altered precursors allowed for the systematic production of analogs. Analysis of the analogs resulting in enhanced regeneration of mechanosensory neurons post-injury indicated that a chromone core

lacking functionality could be a significant structural design for the development of further small molecule drugs and provided the early stages for the design of spinal cord injury treatments via identification of regeneration-promoting small molecules.

Experimental Section

Nematode Cultures and Microscopy. *C. elegans* cultures were maintained on nematode growth medium (NGM) agar plates seeded with *Escherichia coli* OP50 bacteria at 23 °C according to established procedures.³⁹ The strain used for axotomy experiments was SK4005 (zdIs5 [mec-4::GFP + lin-15(+)] (pSK1)), which can be obtained from the Caenorhabditis Genetics Center. General maintenance of *C. elegans* was performed using an Olympus SZX16 stereomicroscope. GFP-labeled nematodes were visualized using an Olympus IX73 inverted microscope with a Prior Lumen 200 fluorescence illumination system. Laser axotomies were performed using the Olympus IX73 microscope (100x/1.40 NA objective) equipped with an Andor MicroPoint nitrogen pulsed dye laser (435 nm). Images were captured using a Hamamatsu Orca-flash2.8 digital camera and cellSens Dimension imaging software.

Laser Axotomy. Stock solutions of the small molecules were prepared in DMSO (12.5 mM) and subsequently diluted in M9 buffer to a final concentration of 0.04 mM (0.32% DMSO, v/v). Diluted solutions (200 μ L) were spread over seeded NGM plates (35x10 mm, containing 4 mL of agar) and allowed to absorb to a final concentration of 2 μ M. The plates were set aside until nematodes were added for small molecule treatment post-surgery. Surgery was performed on late L4-stage *C. elegans* immobilized on 5%

agarose pads and anesthetized with levamisole (3 μ L, 1 mM in M9 buffer). Axons of the PLM were cut using a single laser pulse approximately 15 μ m after the synaptic branch, but only when the branch point was ≤ 100 μ m from the cell body. Only nematodes whose synaptic branch morphology met this requirement were used in the experiments. Nematodes were transferred to prepared NGM plates after the surgery, washed twice with M9 buffer (3 μ L), and allowed to recover at 23 °C overnight. Axon regrowth was measured 24 hours post-axotomy from the site of axotomy to the tip of the longest regrowing process ($n \geq 23$ worms). No growth from the proximal portion of the cut axon was recorded as zero regrowth. Growth of the synaptic branch was sometimes observed but was not included in regrowth measurements.

General Chemistry. All reactions were performed in flame dried round bottom or modified Schlenk (Kjeldahl shape) flasks fitted with rubber septa under a positive pressure of argon, unless otherwise indicated. Air- and moisture-sensitive liquids and solutions were transferred via syringe or cannula. Organic solutions were concentrated by rotary evaporation at 20 torr. Methylene chloride (CH_2Cl_2) and tetrahydrofuran (THF) were purified using a Pure-Solv MD-5 Solvent Purification System (Innovative Technology). Acetonitrile (MeCN) was purified using a Vac 103991 Solvent Purification System (Vacuum Atmospheres). Dimethoxyethane (DME) was purchased from Acros (99+%, stabilized with BHT), methanol (MeOH) was purchased from Sigma-Aldrich (99.8%, anhydrous), ethanol (EtOH) was purchased from Pharmco-Aaper (200 proof, absolute). All other reagents were used directly from the supplier without further purification unless noted. Analytical thin-layer chromatography (TLC) was carried out using 0.2 mm

commercial silica gel plates (silica gel 60, F254, EMD chemical) and visualized using a UV lamp and/or aqueous ceric ammonium molybdate (CAM) or aqueous potassium permanganate (KMnO₄) stain. Infrared spectra were recorded on a Nicolet 380 FTIR using neat thin film or KBr pellet technique. High-resolution mass spectra (HRMS) were recorded on a Karatos MS9 and are reported as m/z (relative intensity). Accurate masses are reported for the molecular ion [M+Na]⁺, [M+H], [M⁺], or [M-H]. Nuclear magnetic resonance spectra (¹H NMR and ¹³C NMR) were recorded with a Varian Gemini [(400 MHz, ¹H at 400 MHz, ¹³C at 100 MHz), (500 MHz, ¹³C at 125 MHz), (600 MHz, ¹³C at 150 MHz)]. For CDCl₃ solutions the chemical shifts are reported as parts per million (ppm) referenced to residual protium or carbon of the solvent; CHCl₃ δ H (7.26 ppm) and CDCl₃ δ D (77.0 ppm). For (CD₃)₂SO solutions the chemical shifts are reported as parts per million (ppm) referenced to residual protium or carbon of the solvents; (CD₃)(CHD₂)SO δ H (2.50 ppm) or (CD₃)₂SO δ C (39.5 ppm). Coupling constants are reported in Hertz (Hz). Data for ¹H-NMR spectra are reported as follows: chemical shift (ppm, referenced to protium; s = singlet, d = doublet, t = triplet, q = quartet, dd = doublet of doublets, td = triplet of doublets, ddd = doublet of doublet of doublets, m = multiplet, coupling constant (Hz), and integration). Melting points were measured on a MEL-TEMP device without corrections.

General Procedure A for Ynone Dimerization. To a stirred solution of ynone (1.0 equiv.) (intended xanthone side of protected vinaxanthone) and H₂O (1,000 equiv.) in MeCN (0.01 M) at 23 °C was added triethylamine (10 equiv.). After 1 hour, the reaction mixture was diluted with EtOAc, dried over Na₂SO₄ and concentrated *in vacuo* to give an

amber oil. The crude aldehyde was diluted to 0.1 M with MeCN before the second ynone (1.0 equiv.) (intended chromone side of protected vinaxanthone) and triethylamine (2 equiv.) were added. The reaction mixture was stirred at 23 °C for 16 hours. The reaction mixture was then concentrated to give crude protected vinaxanthone. The crude material was purified via silica gel column chromatography to give pure protected vinaxanthone.¹²⁶

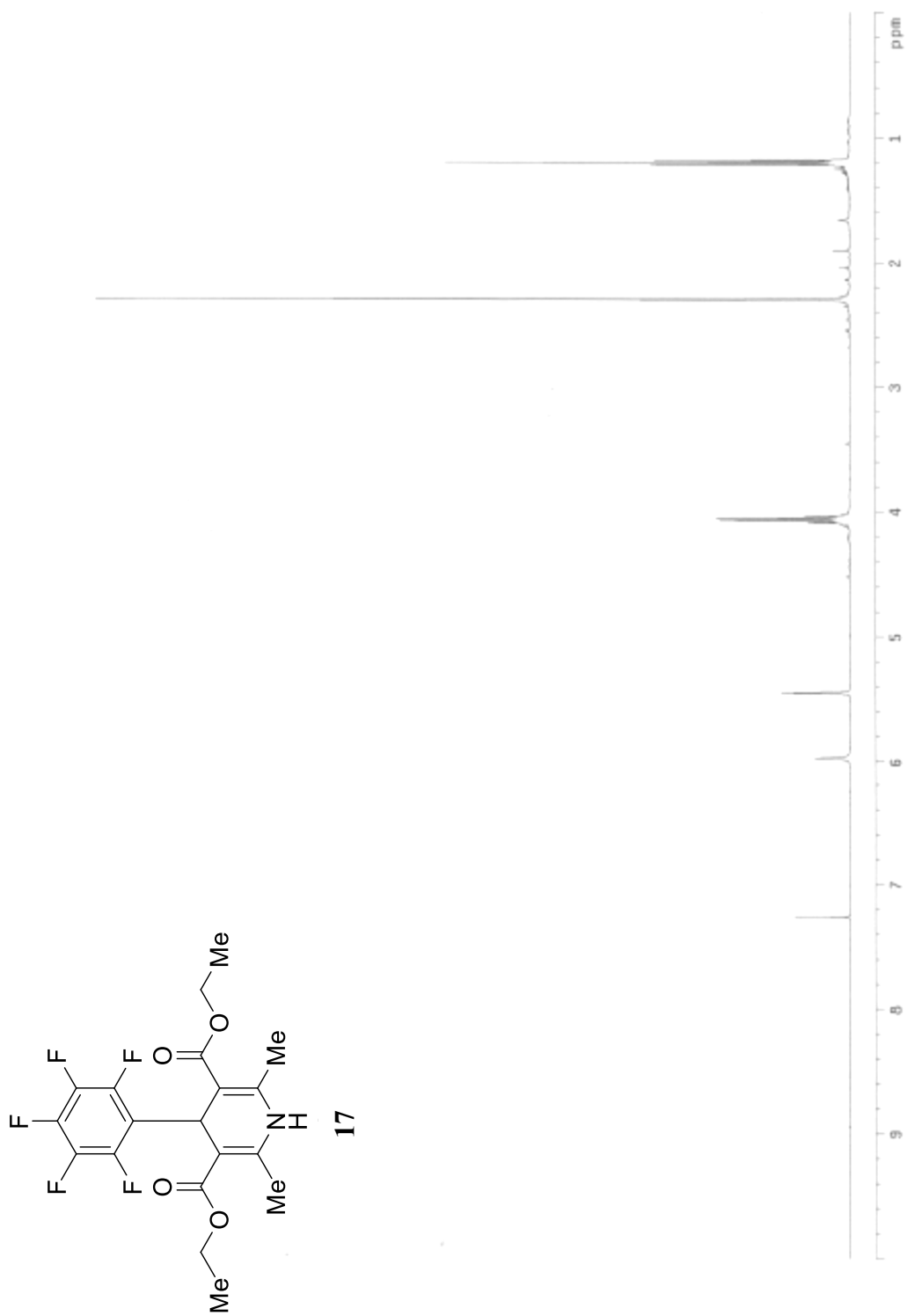
General Procedure B for Ynone Dimerization. To a stirred solution of ynone (1.0 equiv.) in MeCN (0.1 M) at 23 °C was added a 1.0 M solution of H₂O in MeCN (0.5 equiv.) and triethylamine (10 equiv.). After 16 hours, the reaction mixture was concentrated *in vacuo* to give crude protected vinaxanthone. The crude material was purified via silica gel column chromatography to give pure protected vinaxanthone.¹²⁶

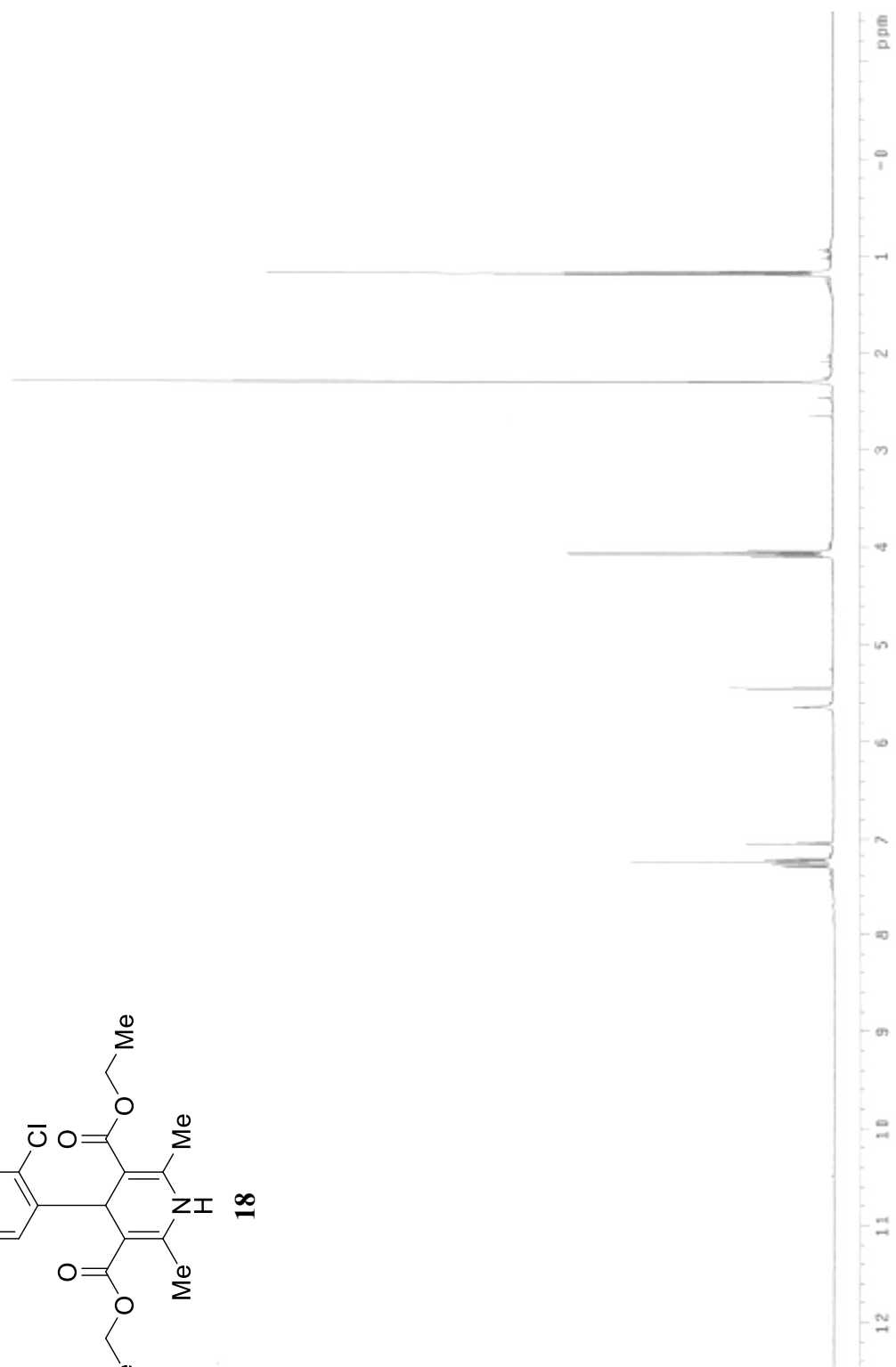
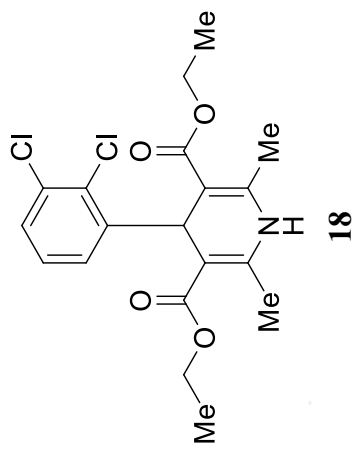
General Procedure A for Protected Vinaxanthone Deprotection. To a stirred solution of protected vinaxanthone (1.0 equiv.) in CH₂Cl₂ at 0 °C was added a 1.0 M solution of boron trichloride in CH₂Cl₂ (2.0 equiv. per protecting group). The reaction mixture was stirred at 23 °C for 1 hour. The reaction mixture was then diluted with EtOAc and washed with brine (5x). The organic layer was dried over Na₂SO₄ and concentrated *in vacuo* to give crude vinaxanthone. Trituration with pentane:MeOH (ratio varies depending on substrate solubility) gave pure vinaxanthone.¹²⁶

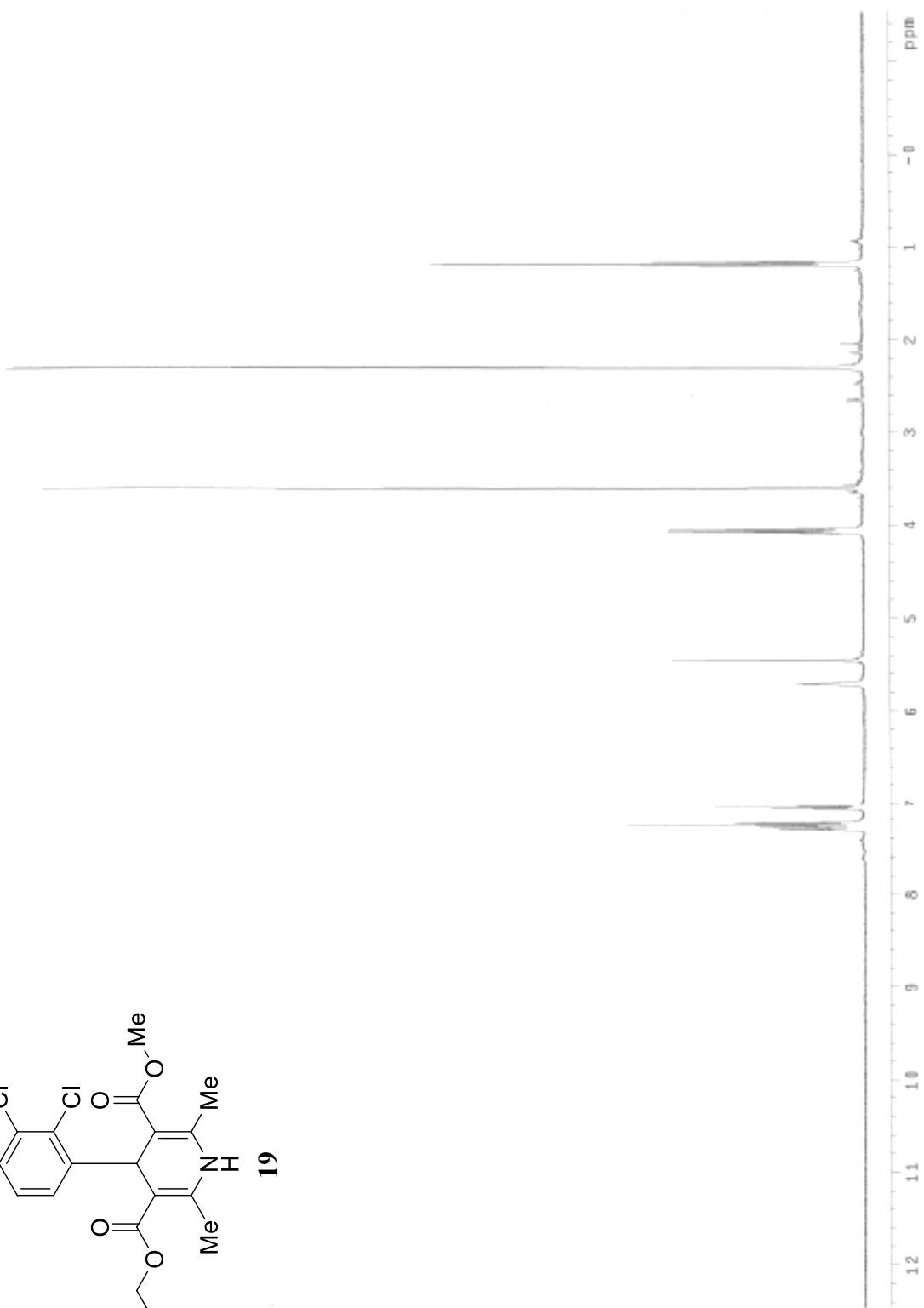
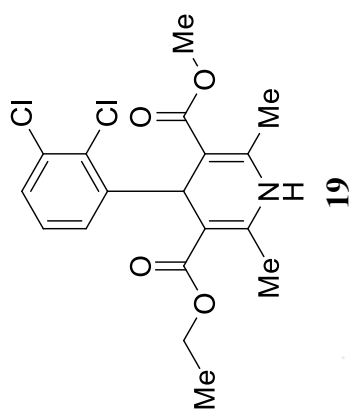
General Procedure B for Protected Vinaxanthone Deprotection. A solution of protected vinaxanthone (1.0 equiv.) in 1.25 M methanolic HCl (10 equiv. per protecting group) was stirred at 65 °C for 8 hrs. The reaction was followed by aliquot ¹H NMR. The reaction mixture was then purged with N₂ and concentrated *in vacuo* to give crude

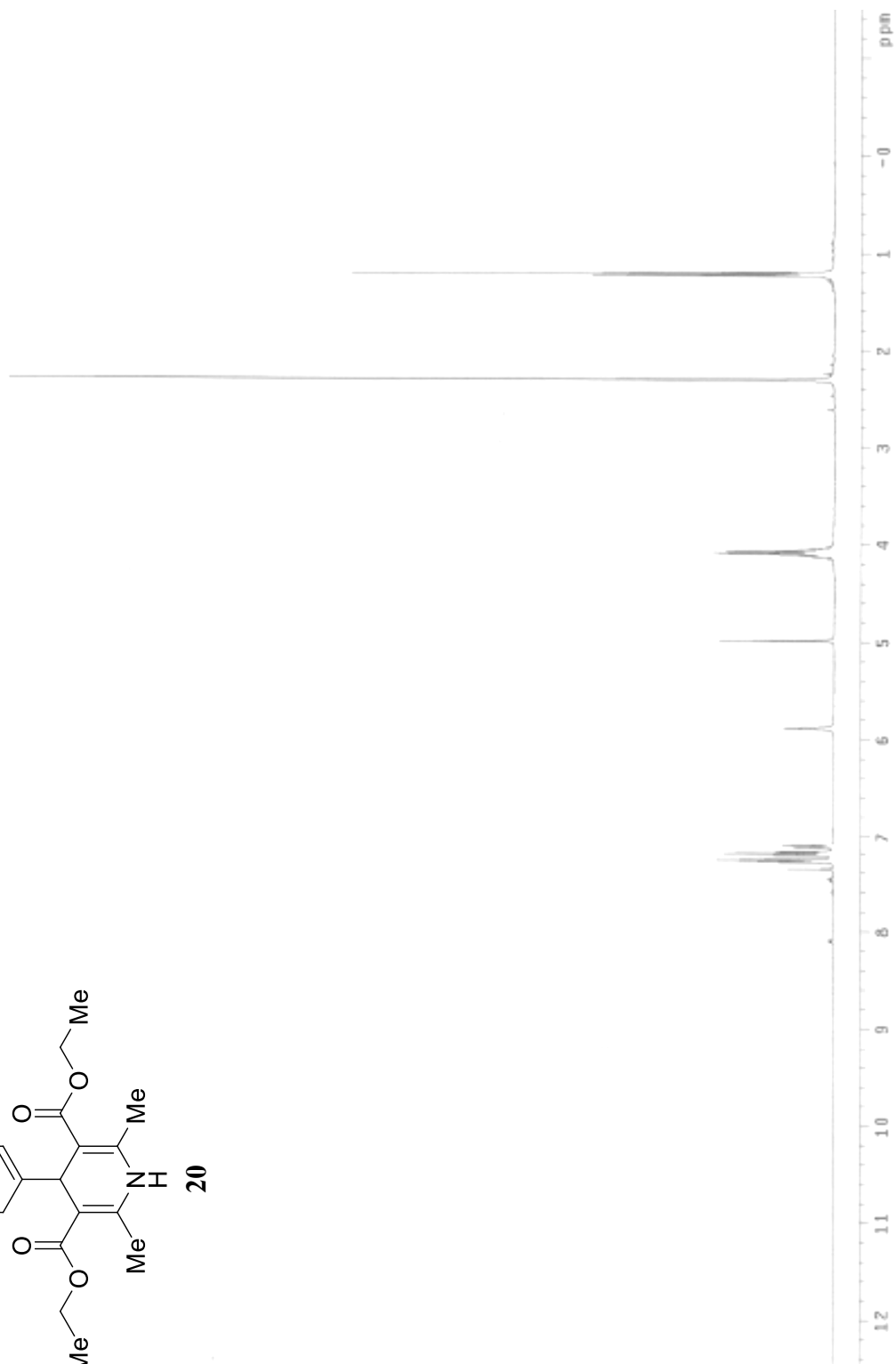
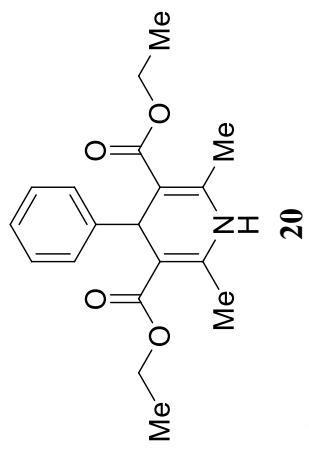
vinaxanthone. Trituration with pentane:MeOH (ratio varies depending on substrate solubility) gave pure vinaxanthone.¹²⁶

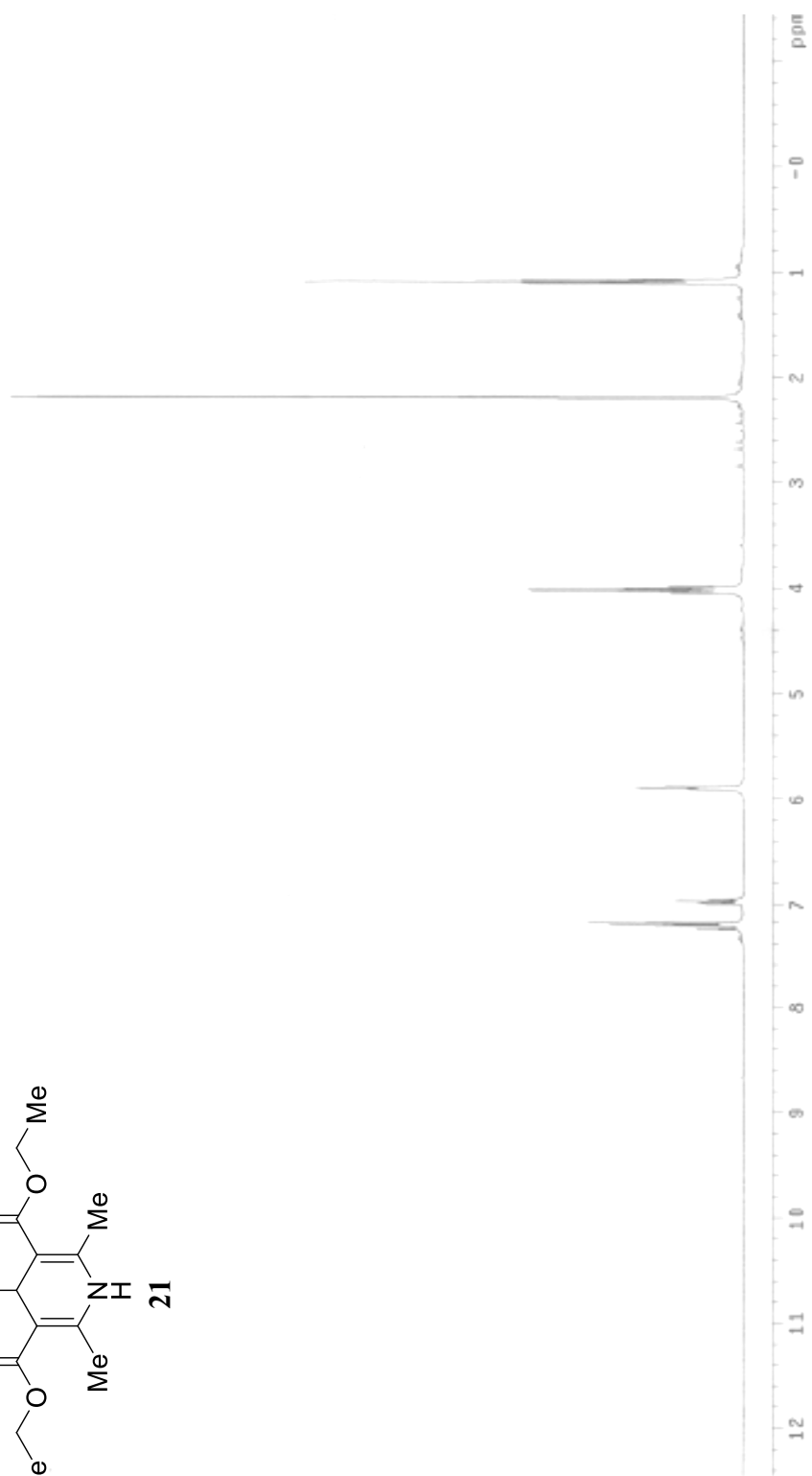
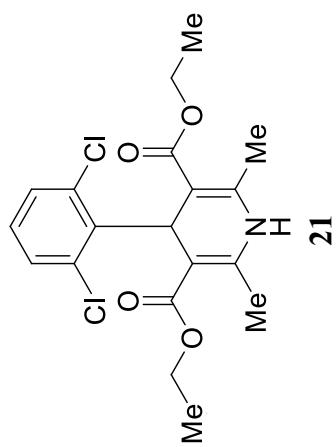
Appendix: NMR Spectra and HPLC Traces

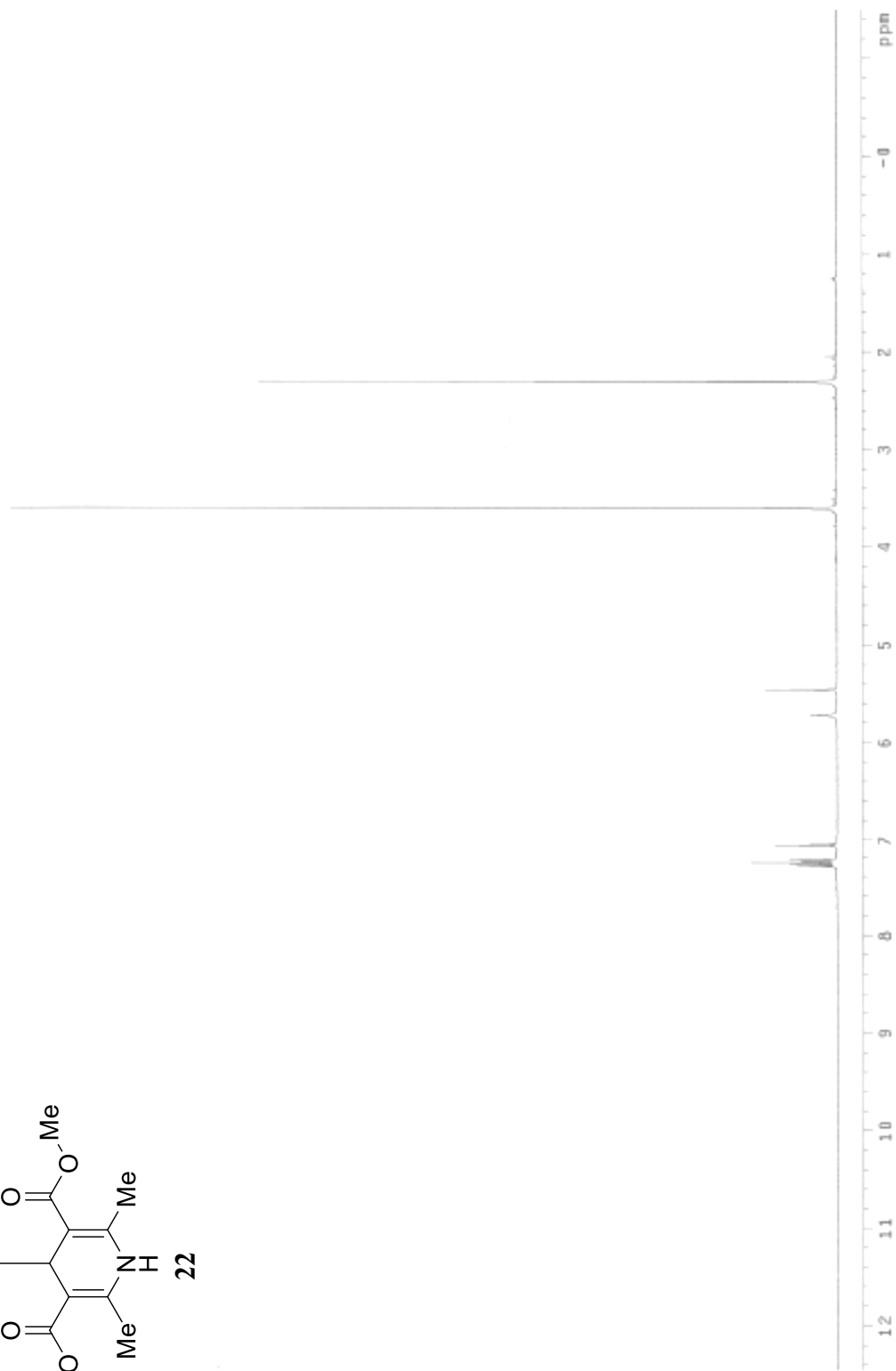
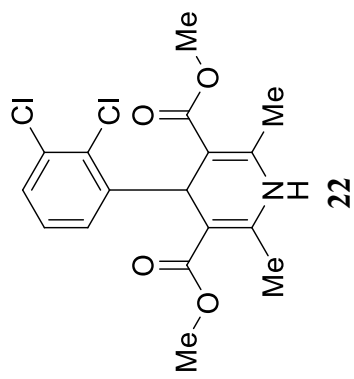


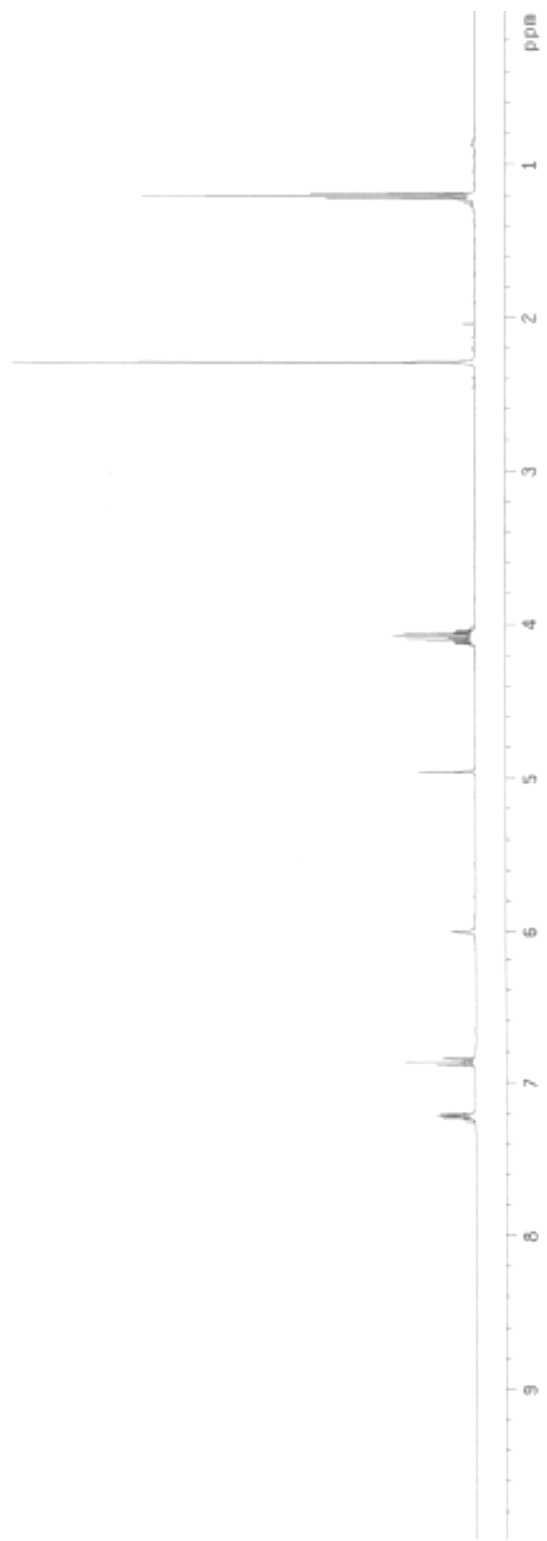
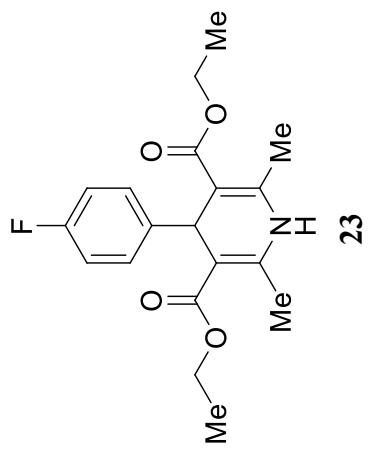


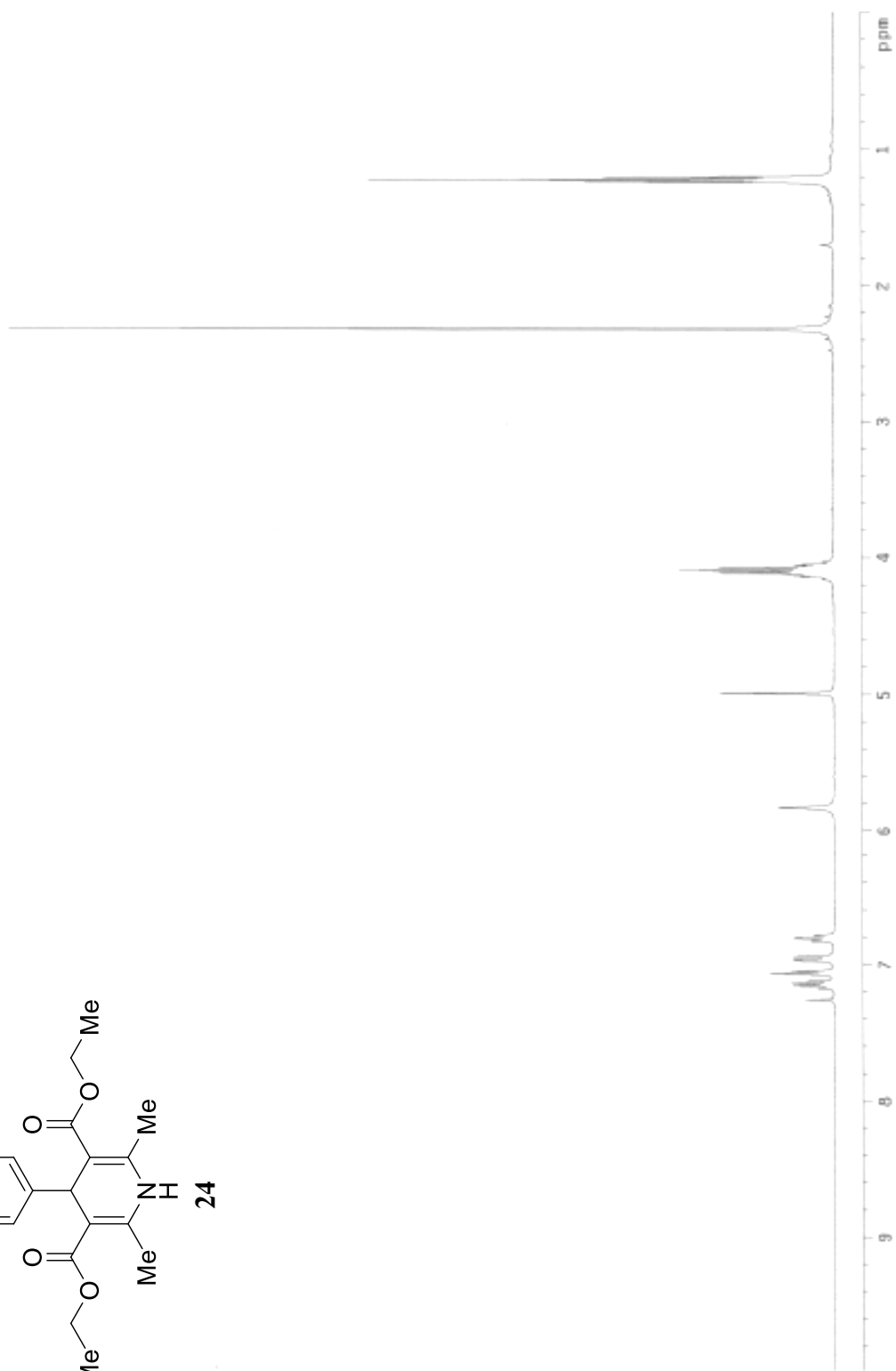
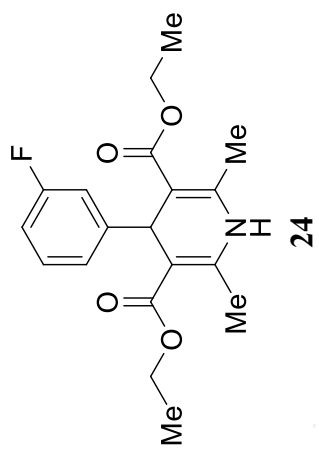


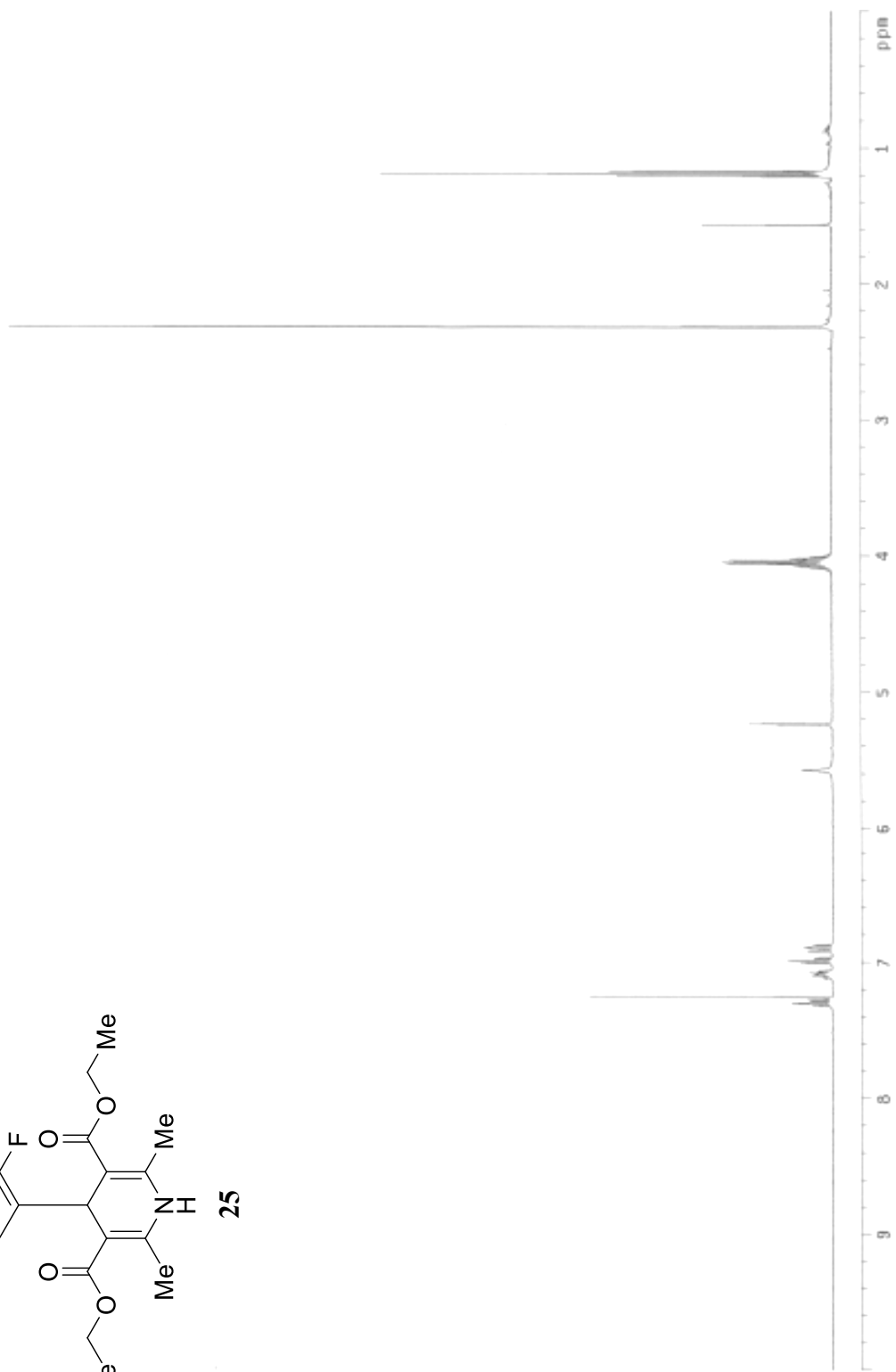
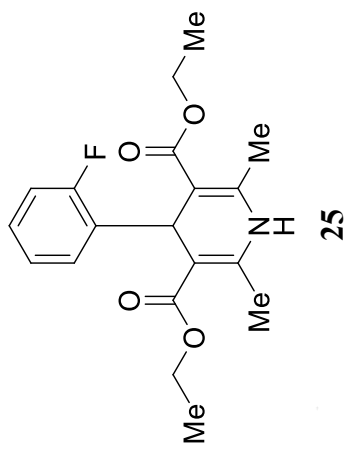


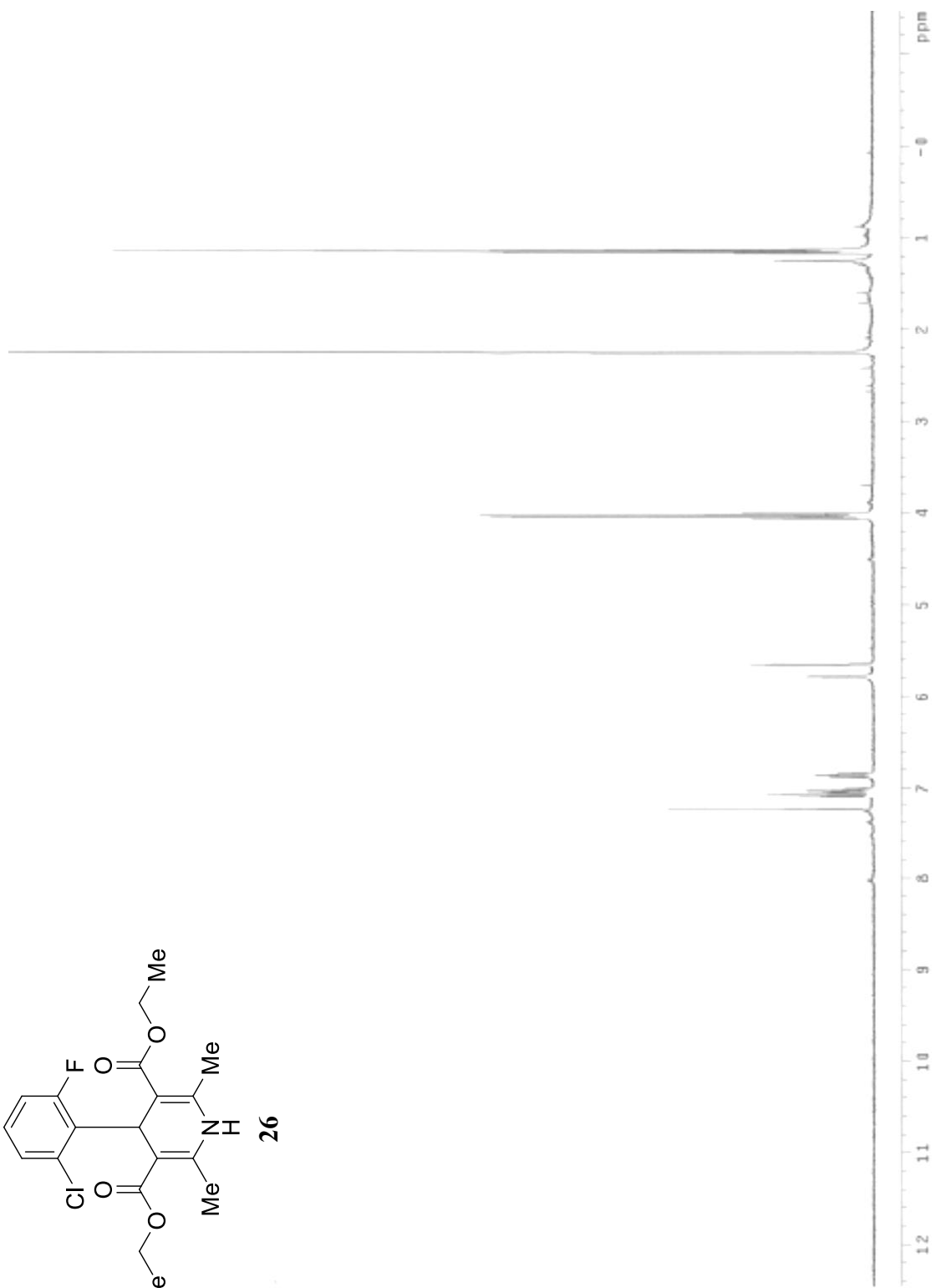
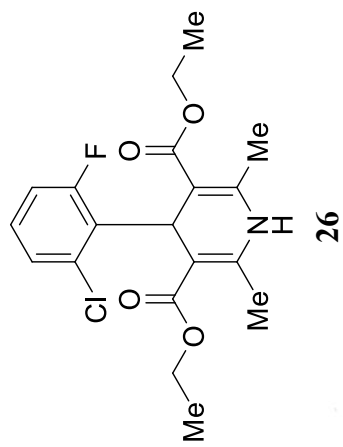


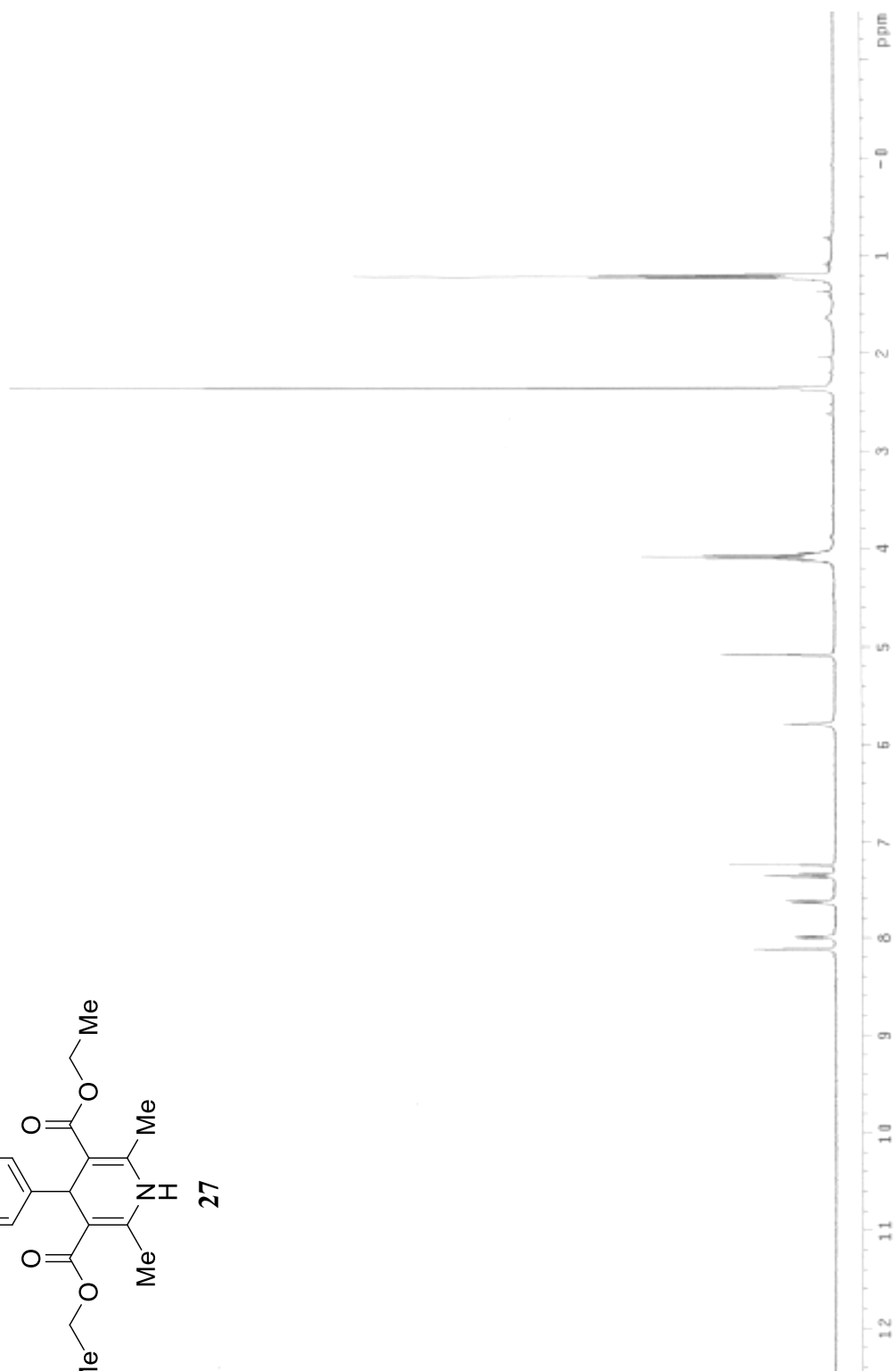
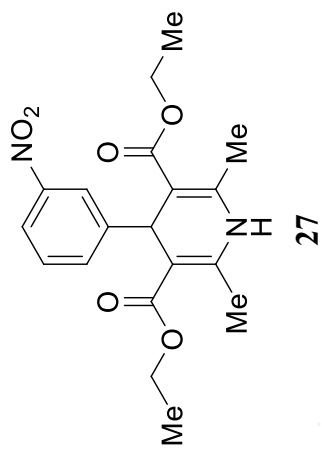


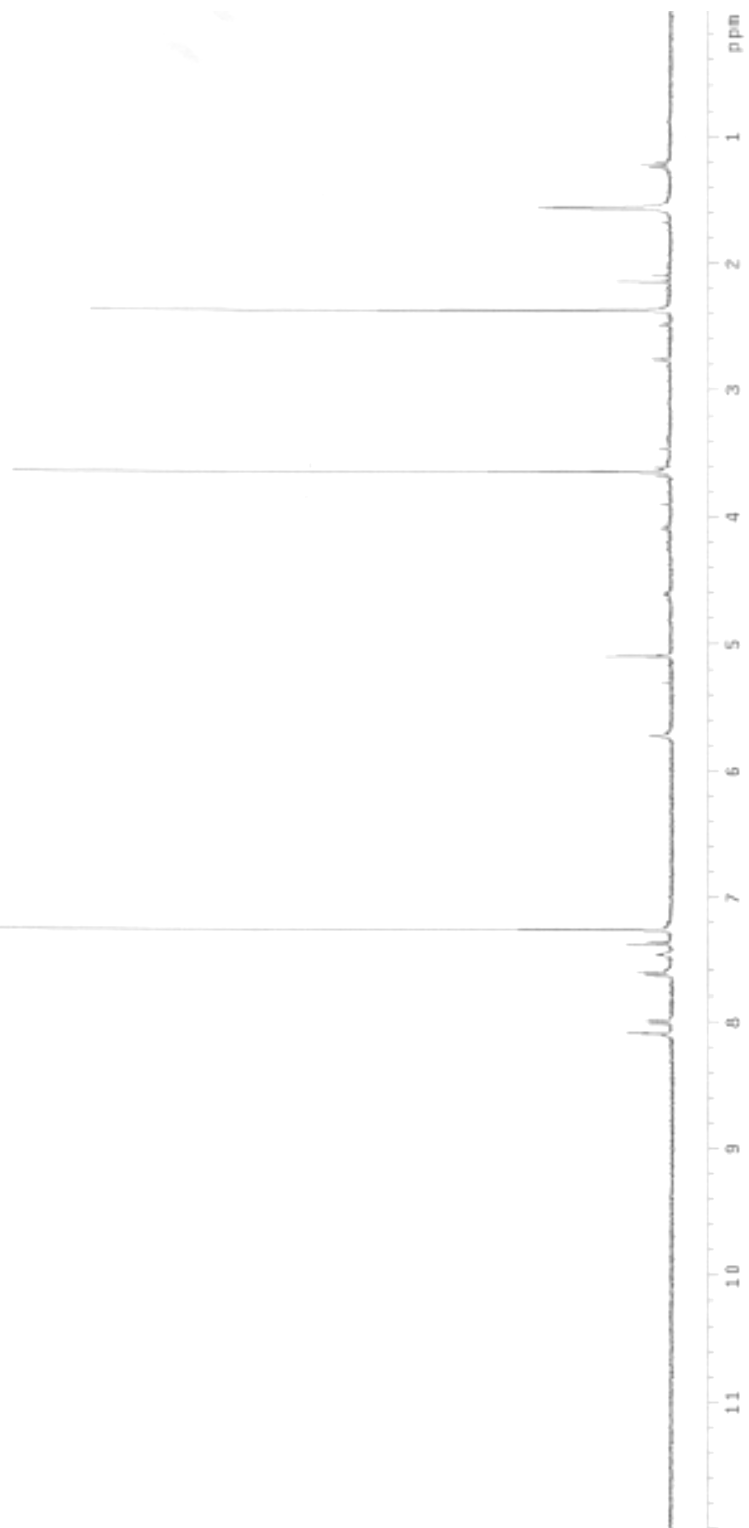
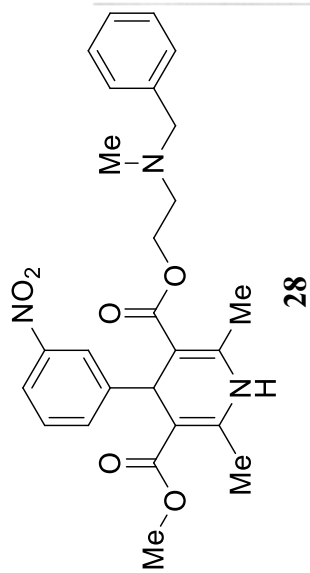


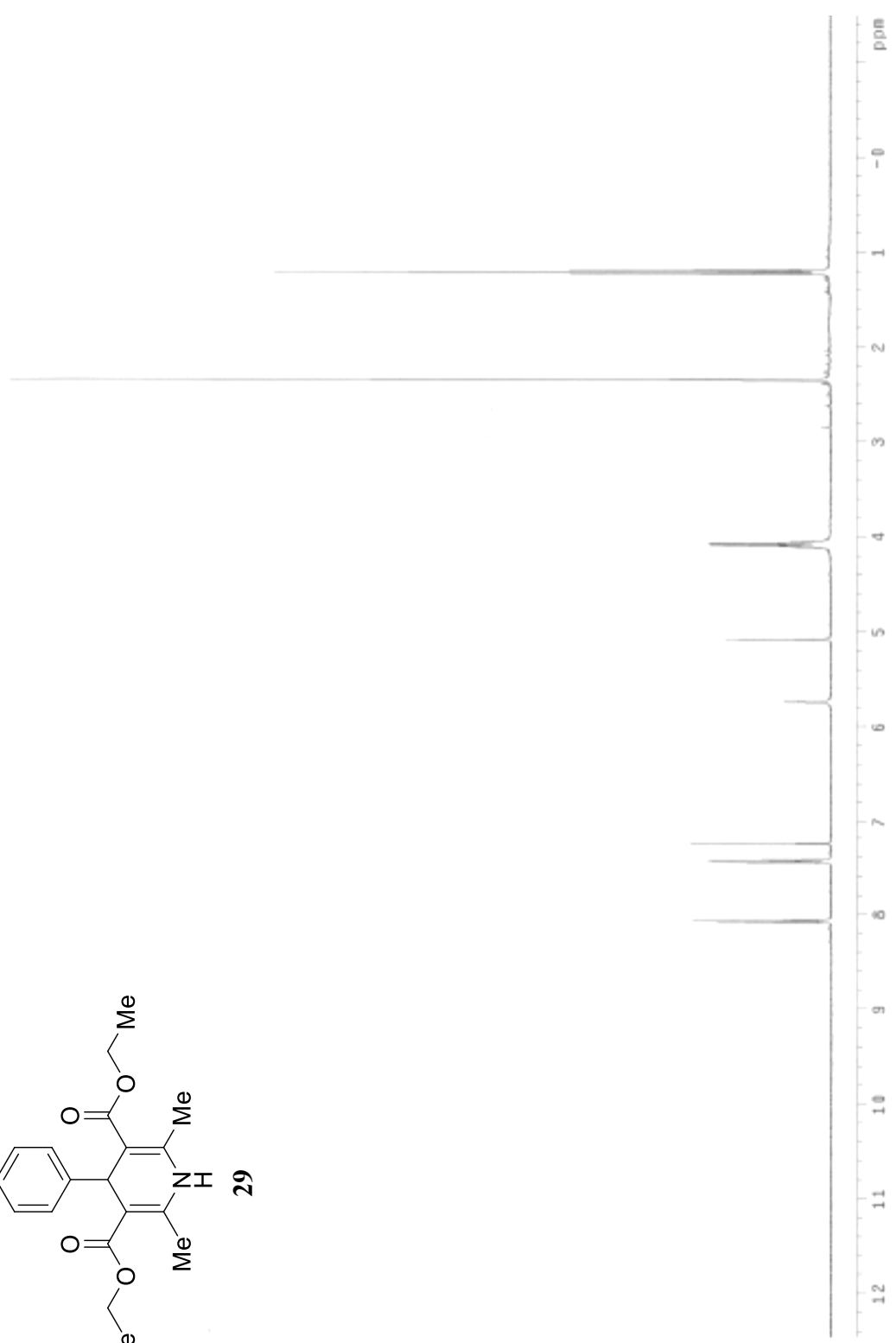
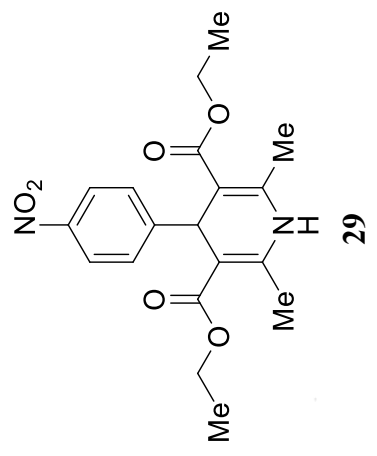


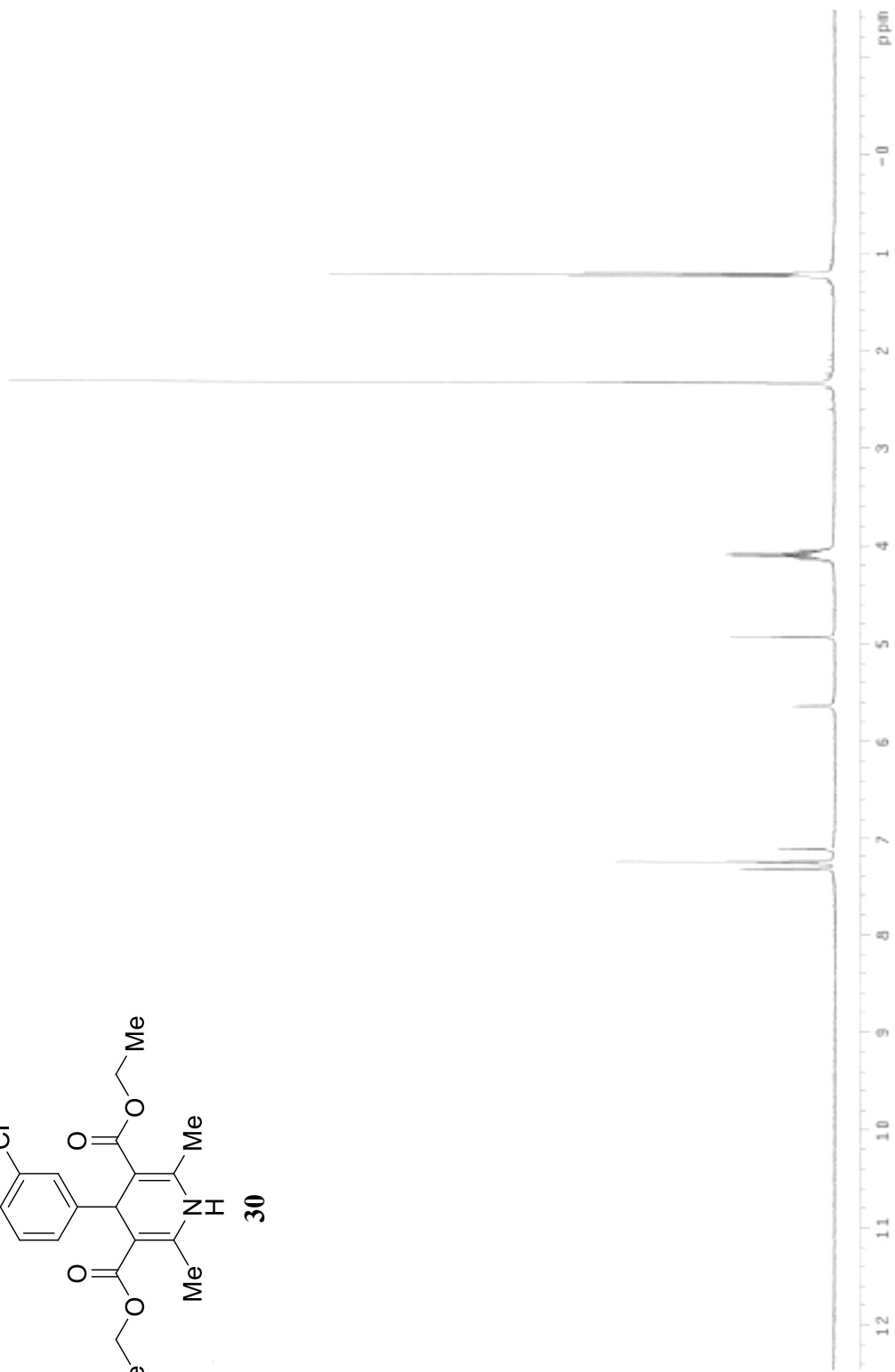
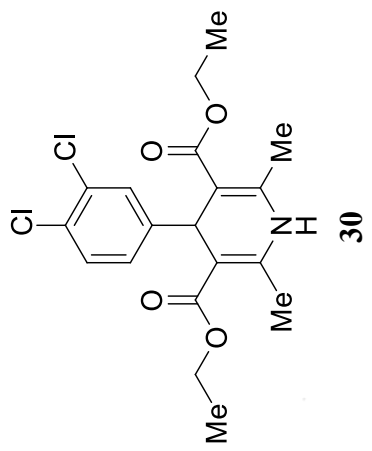


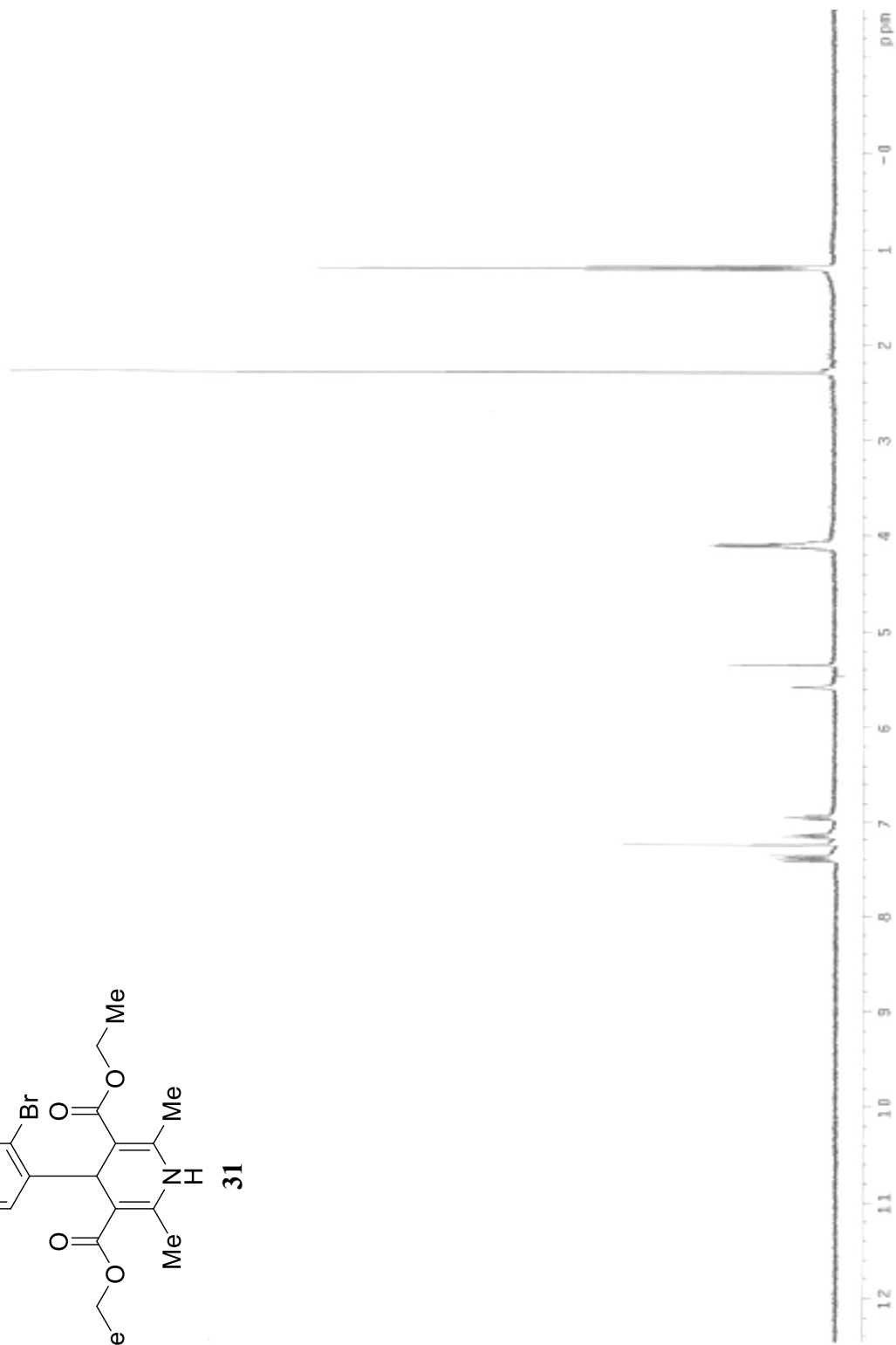
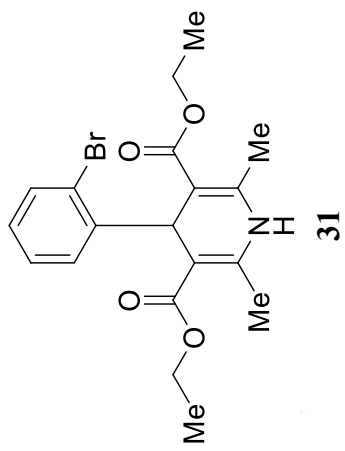


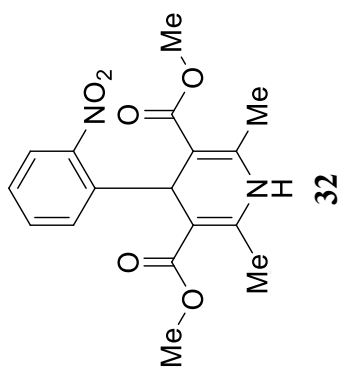


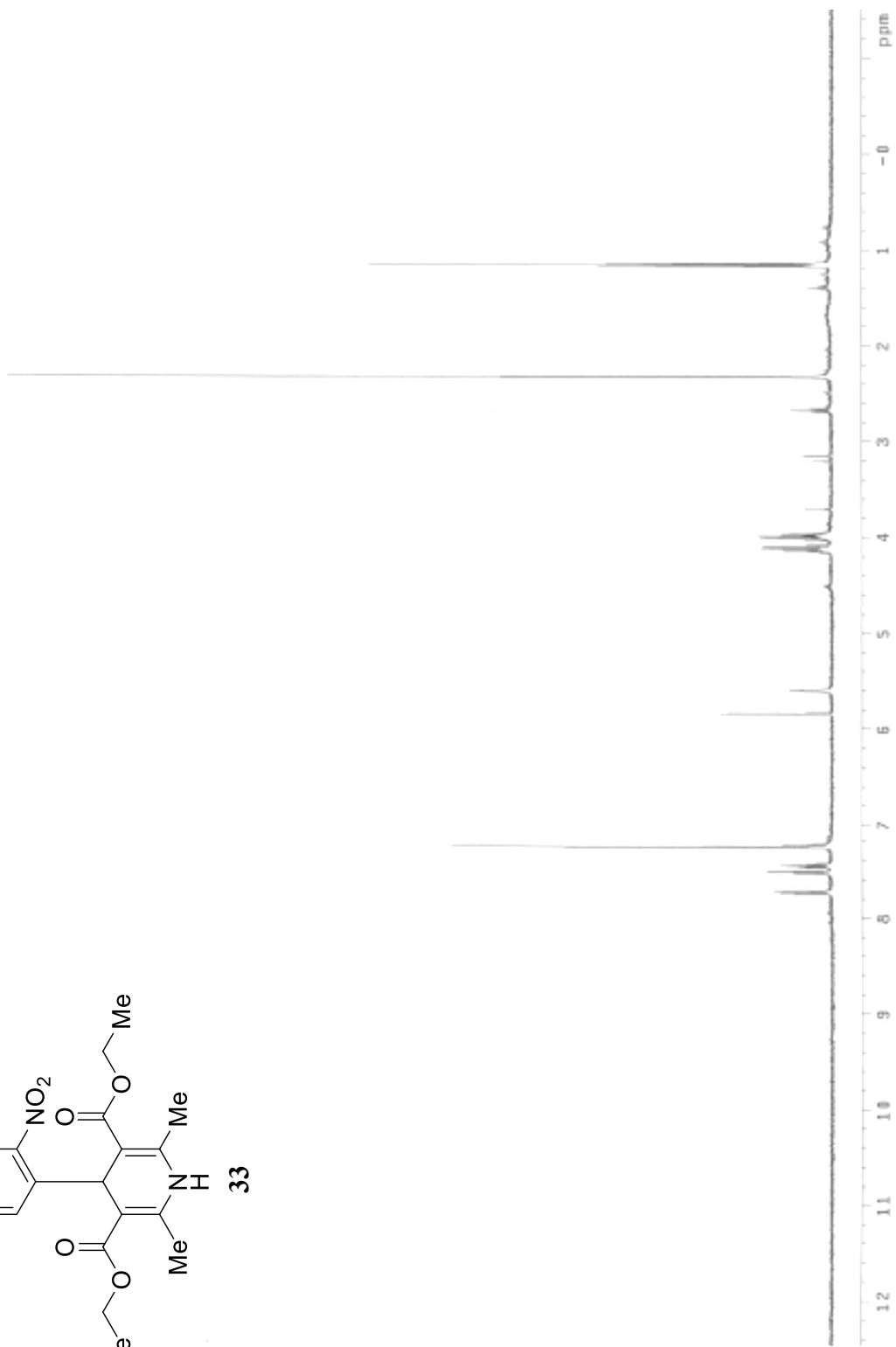
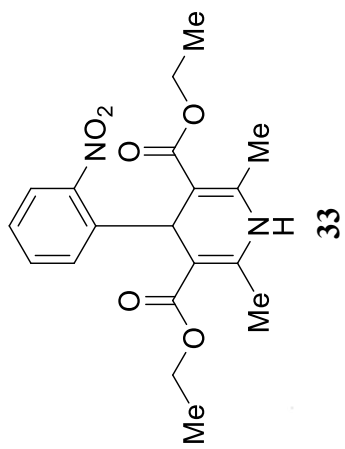


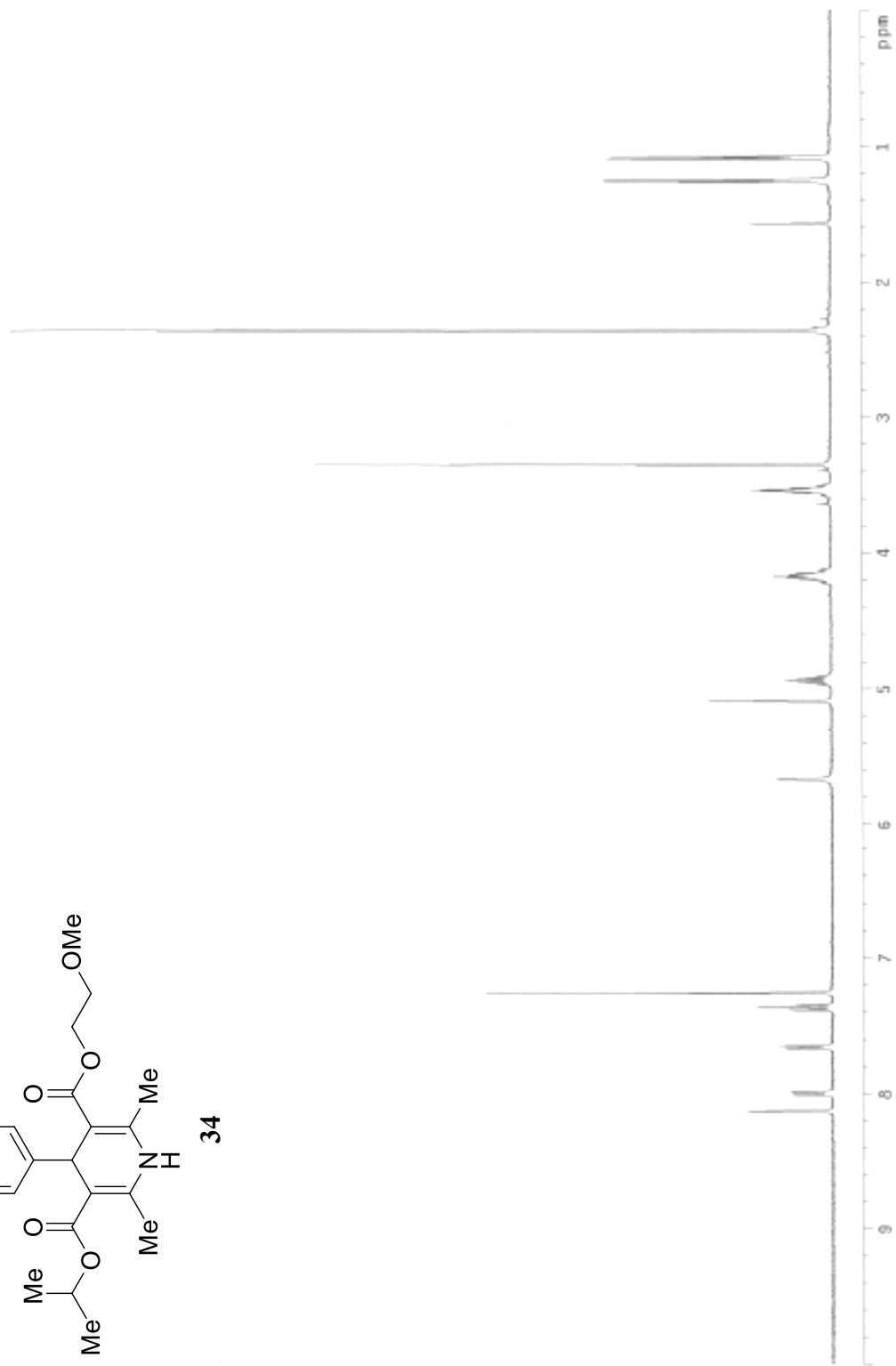
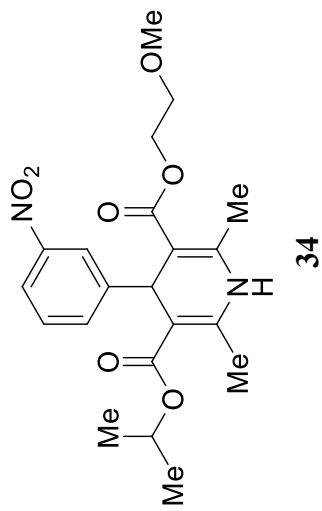


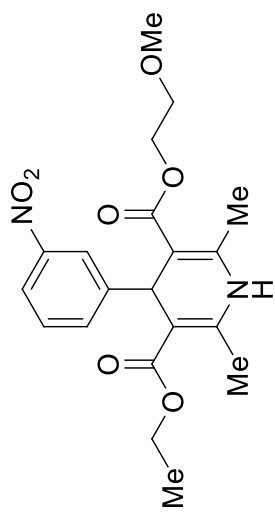




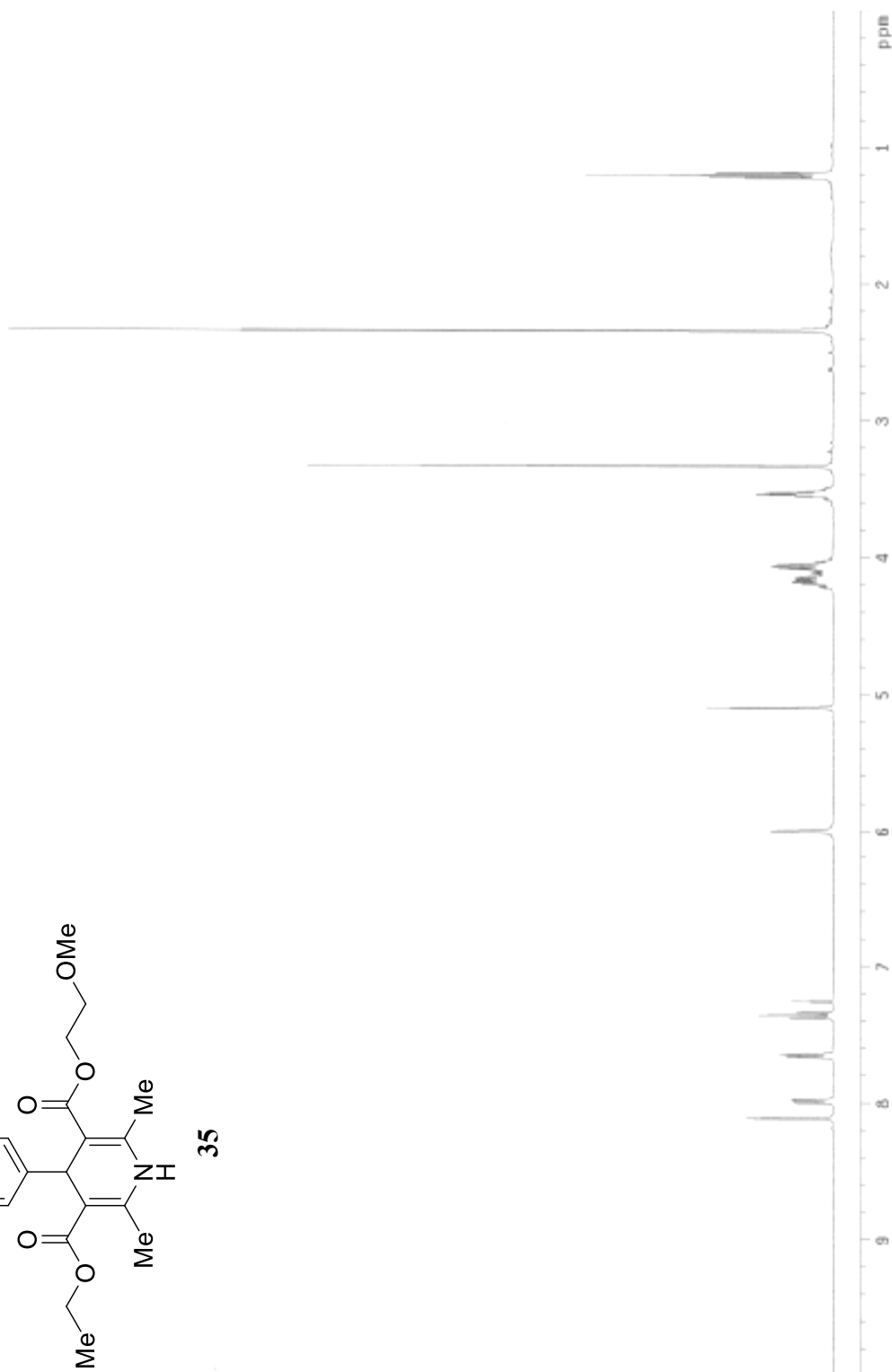


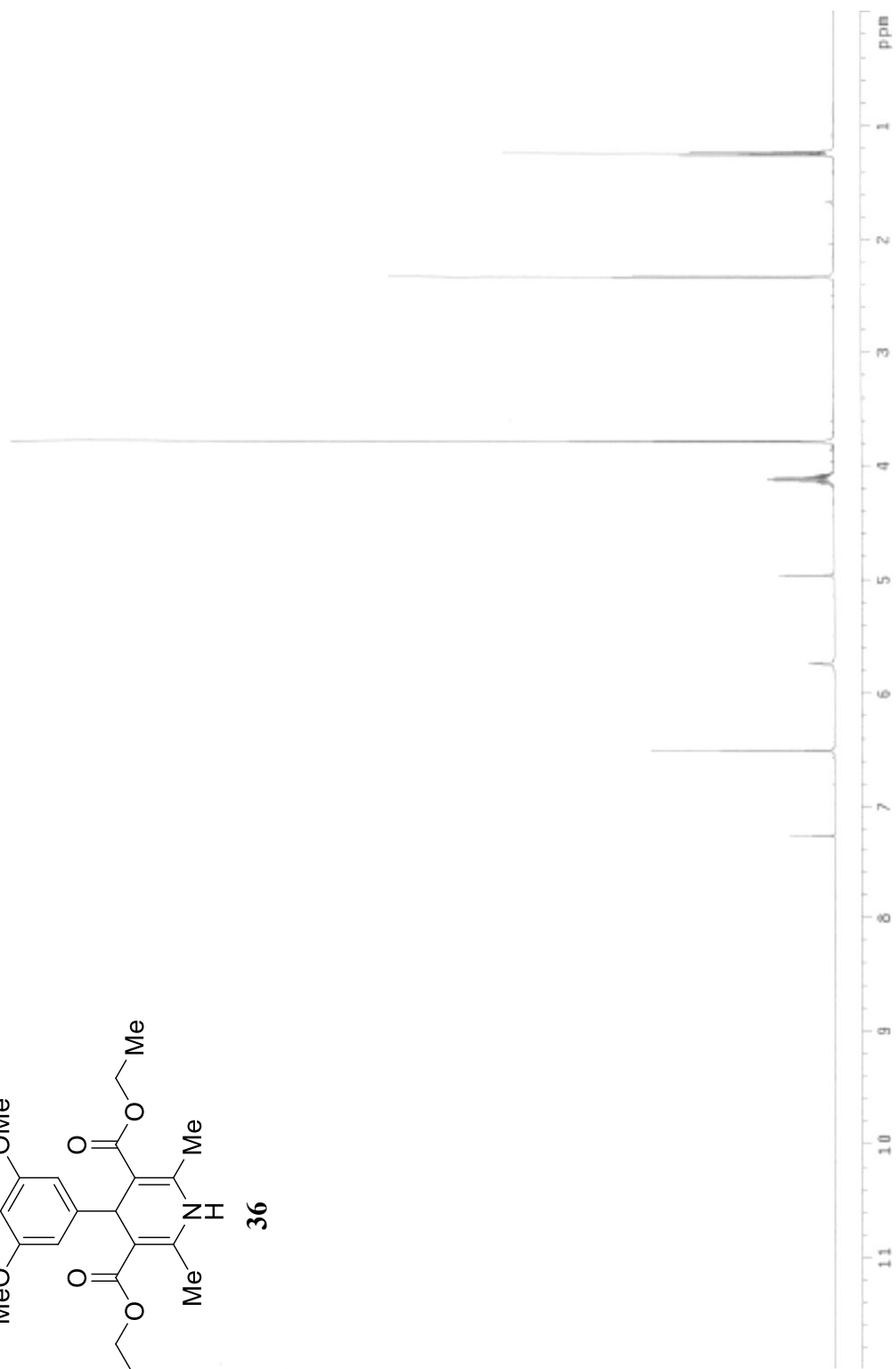
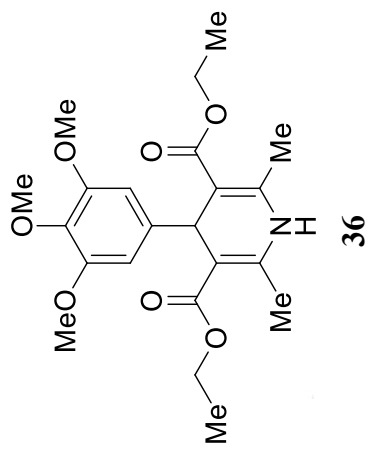


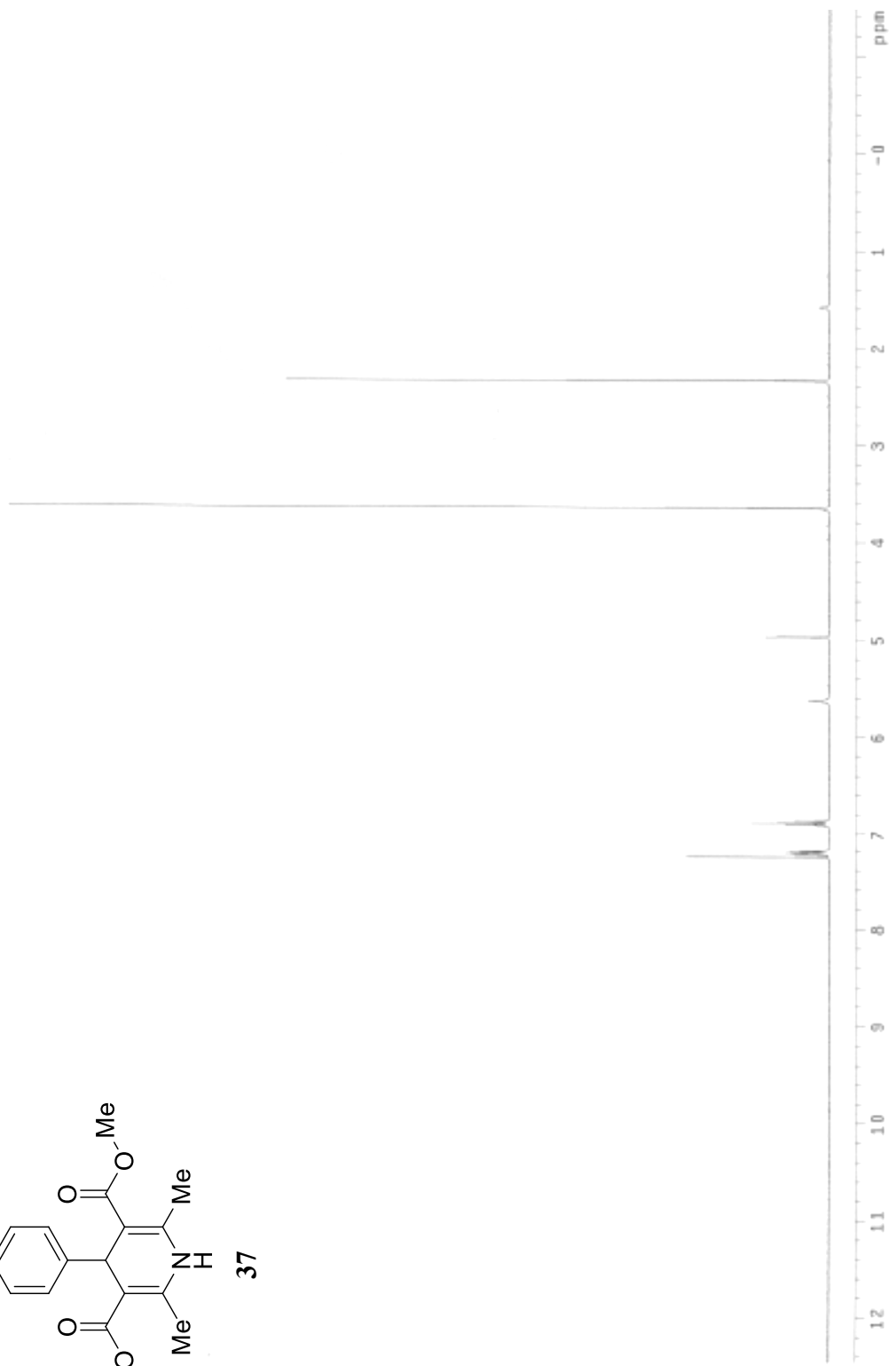
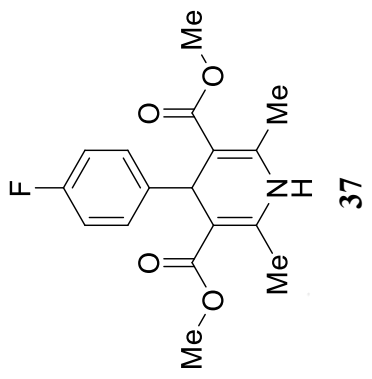




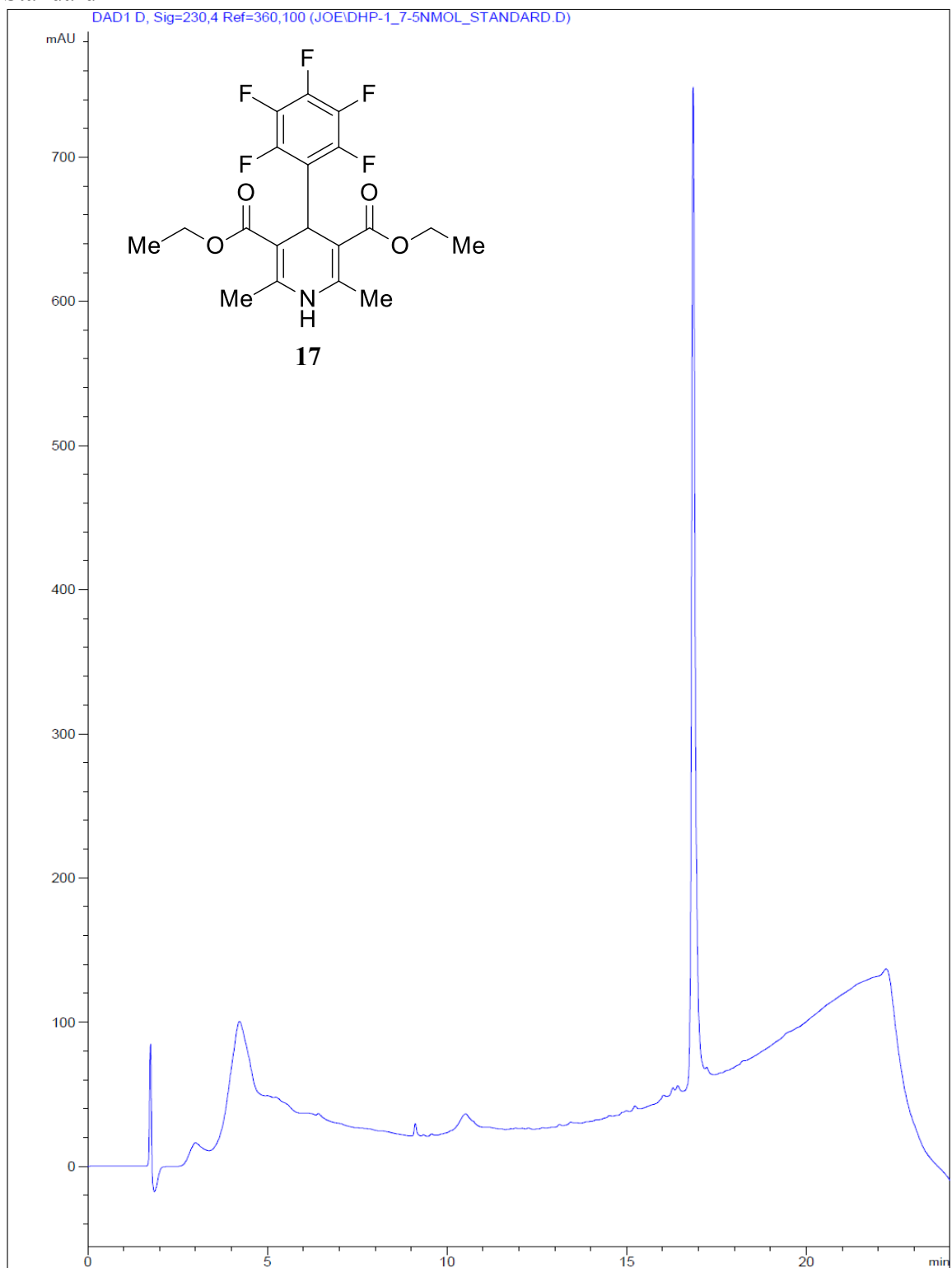
35



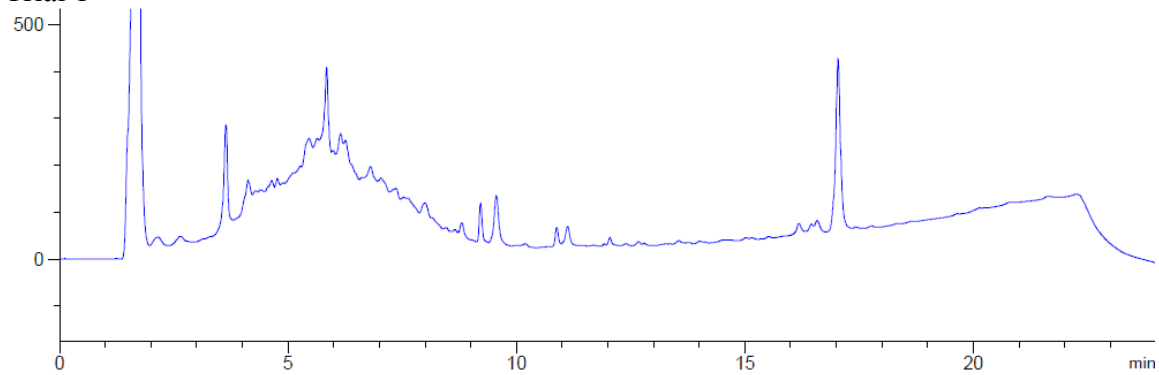




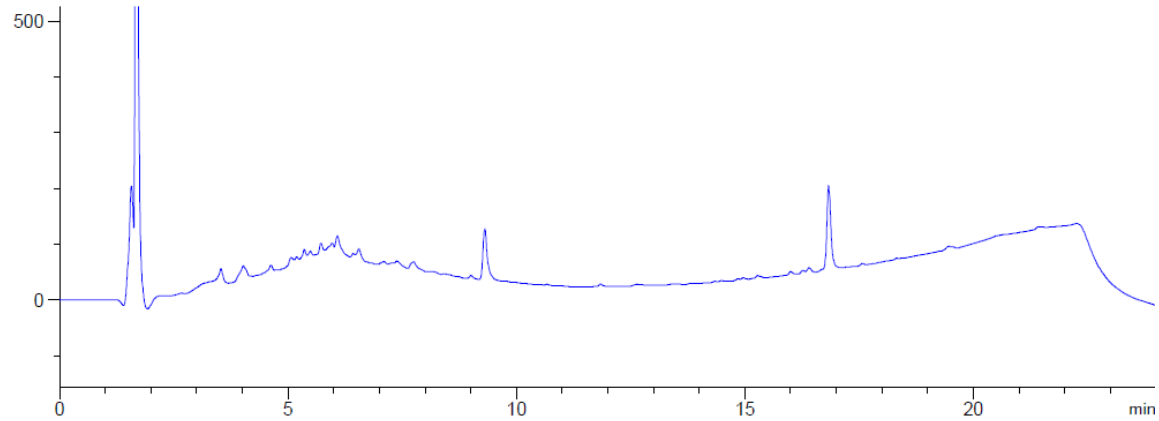
Standard



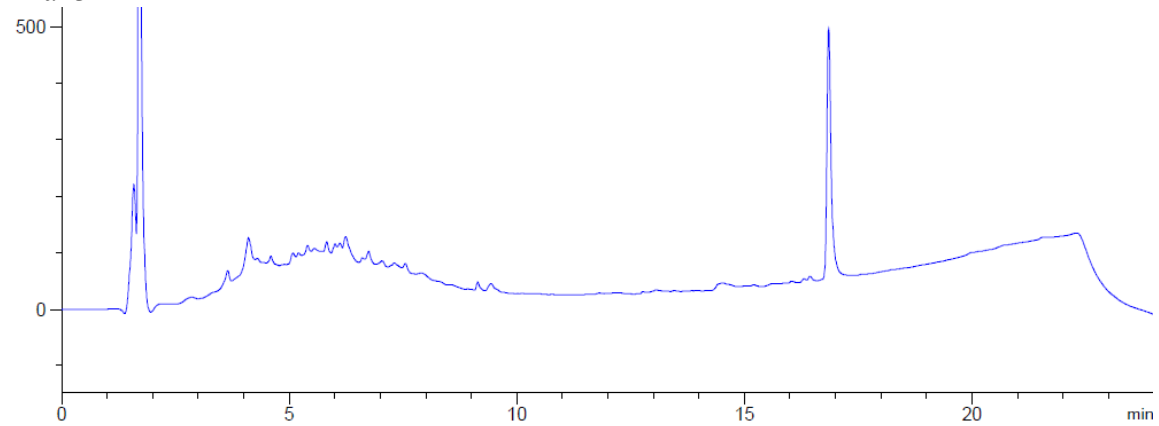
Trial 1



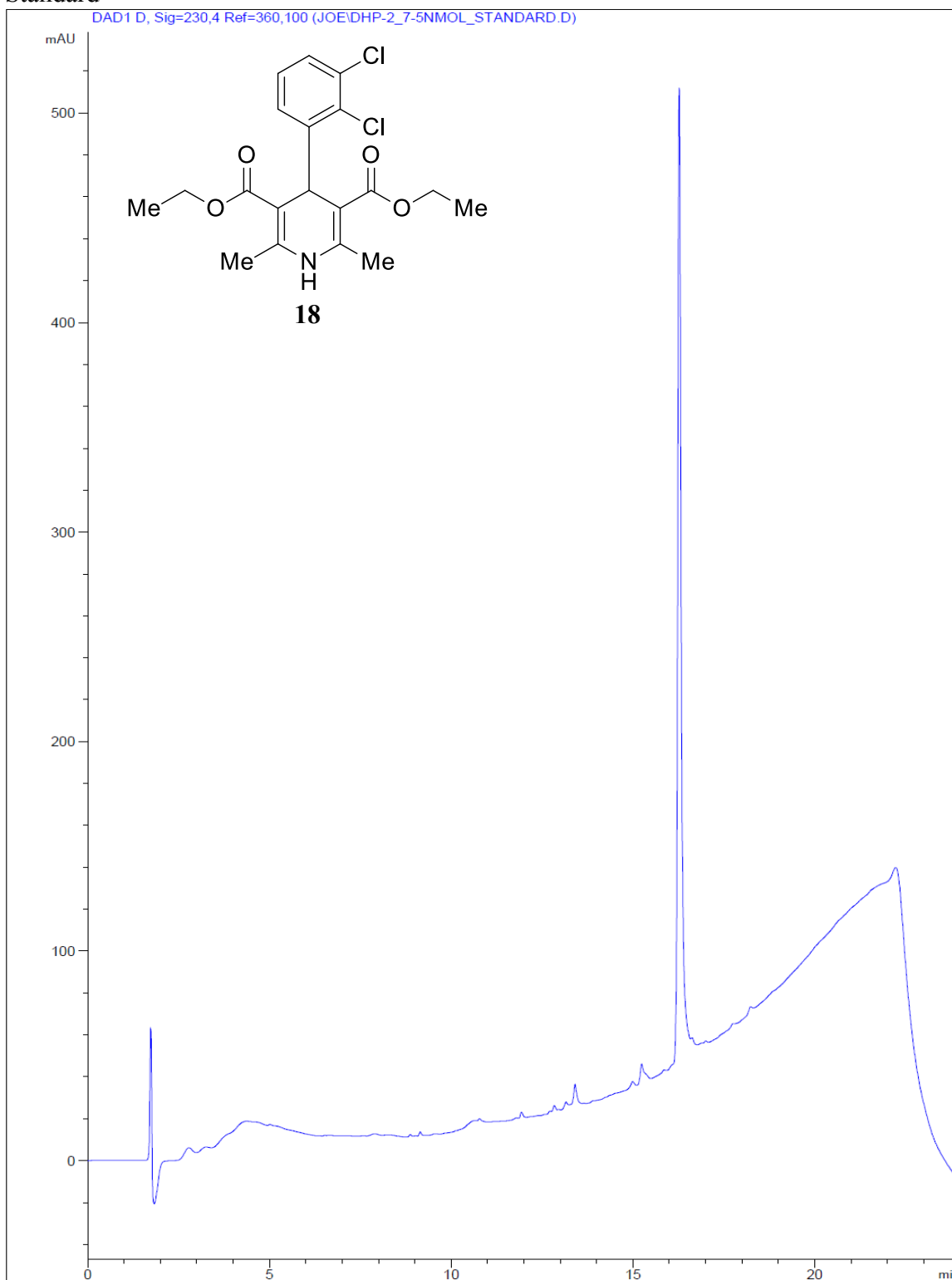
Trial 2



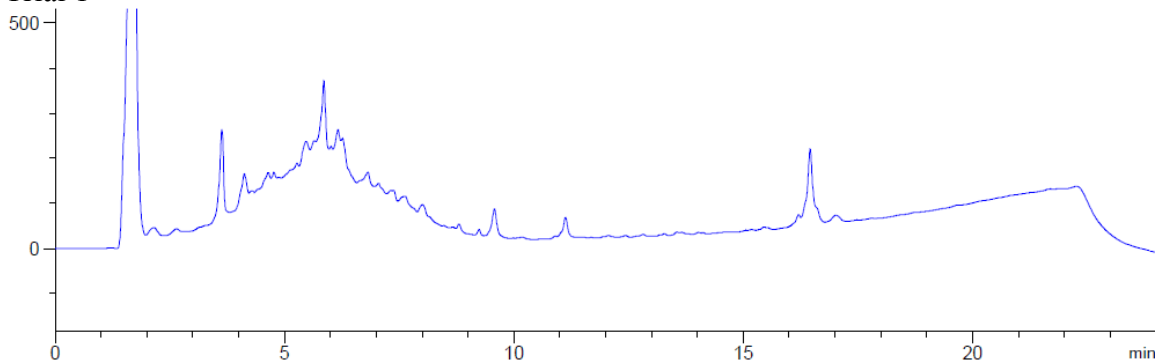
Trial 3



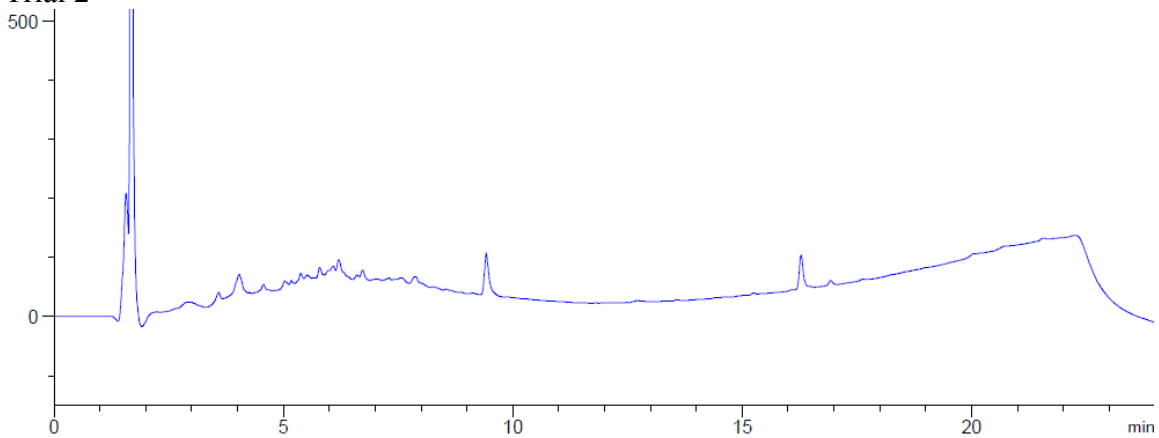
Standard



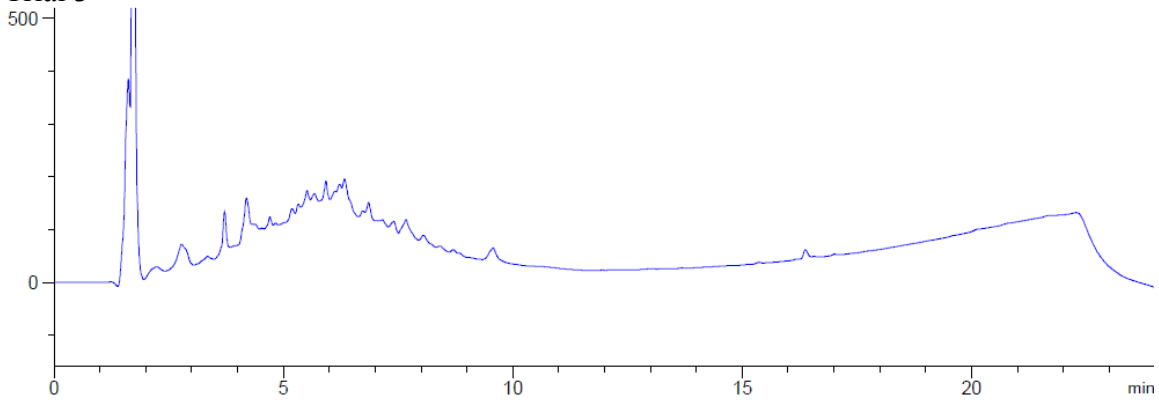
Trial 1



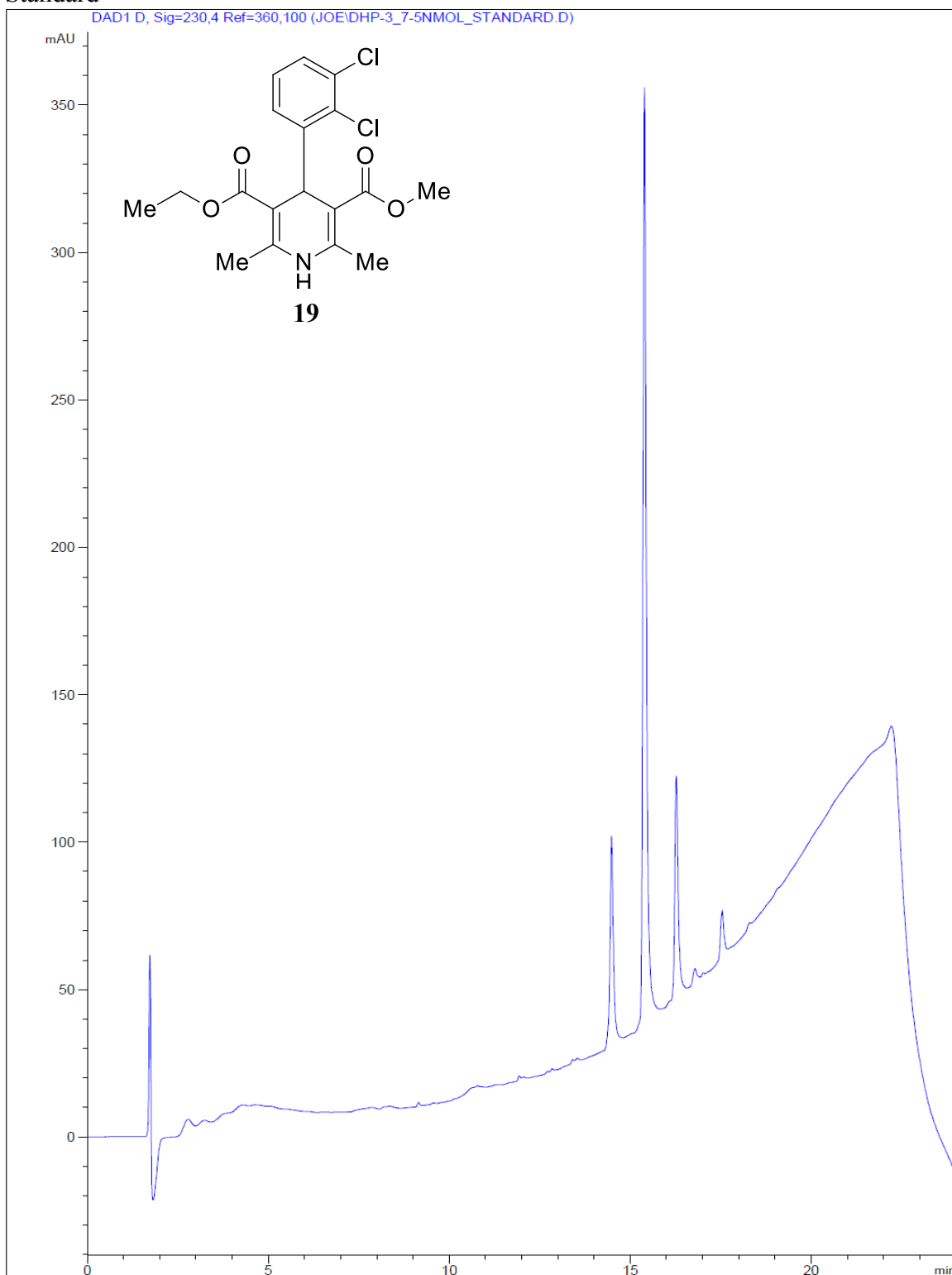
Trial 2

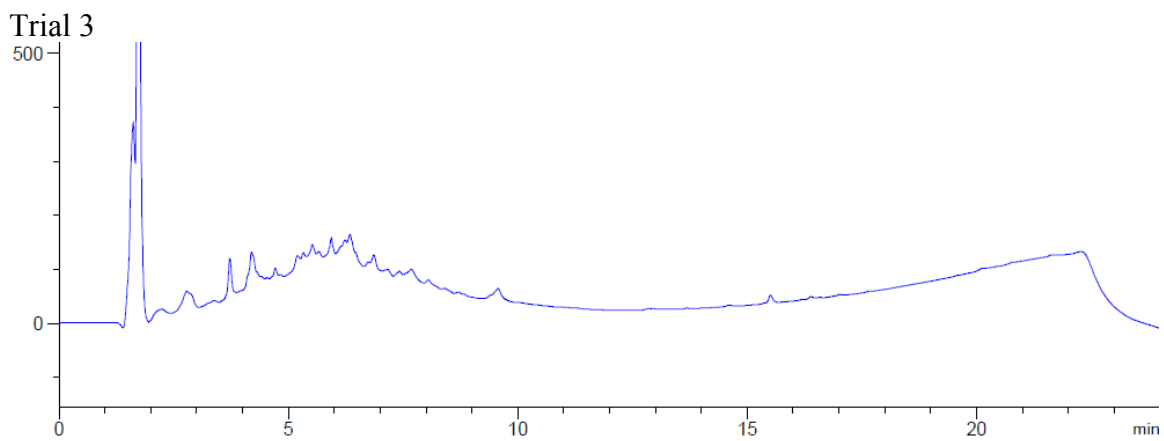
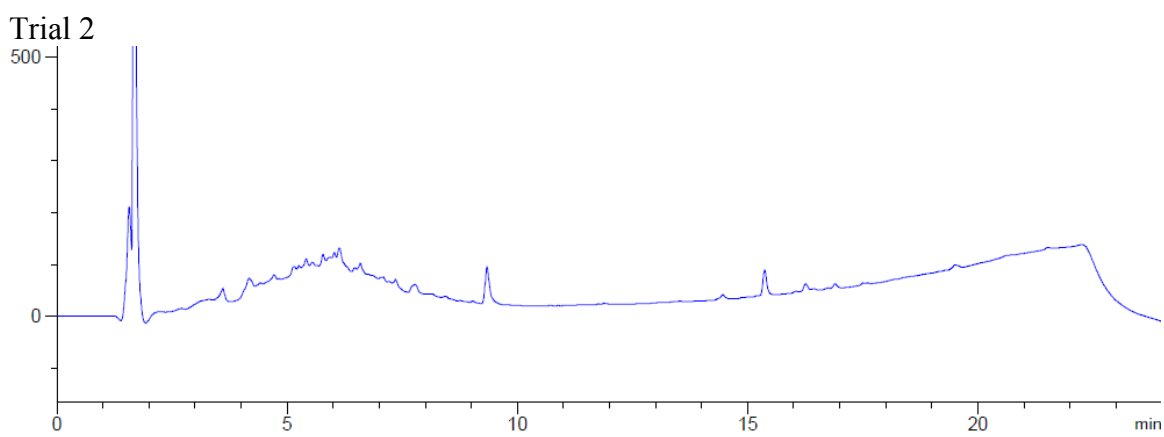
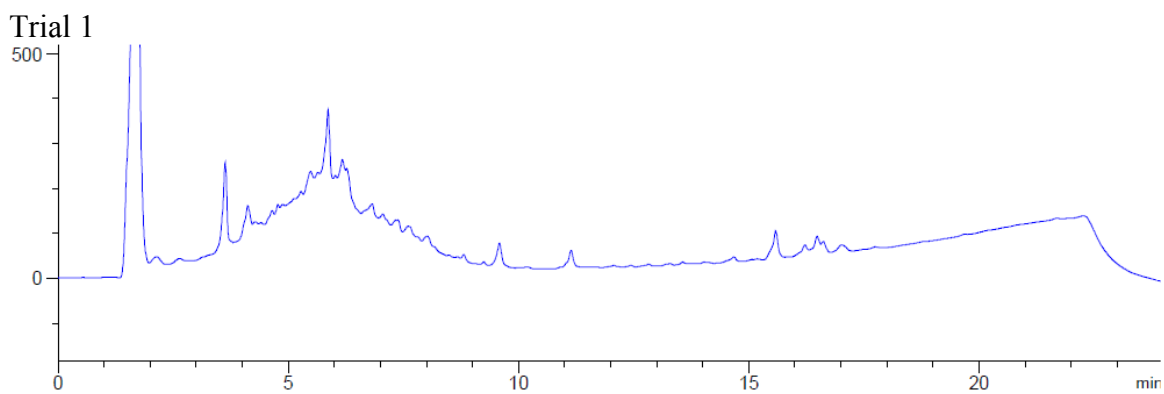


Trial 3

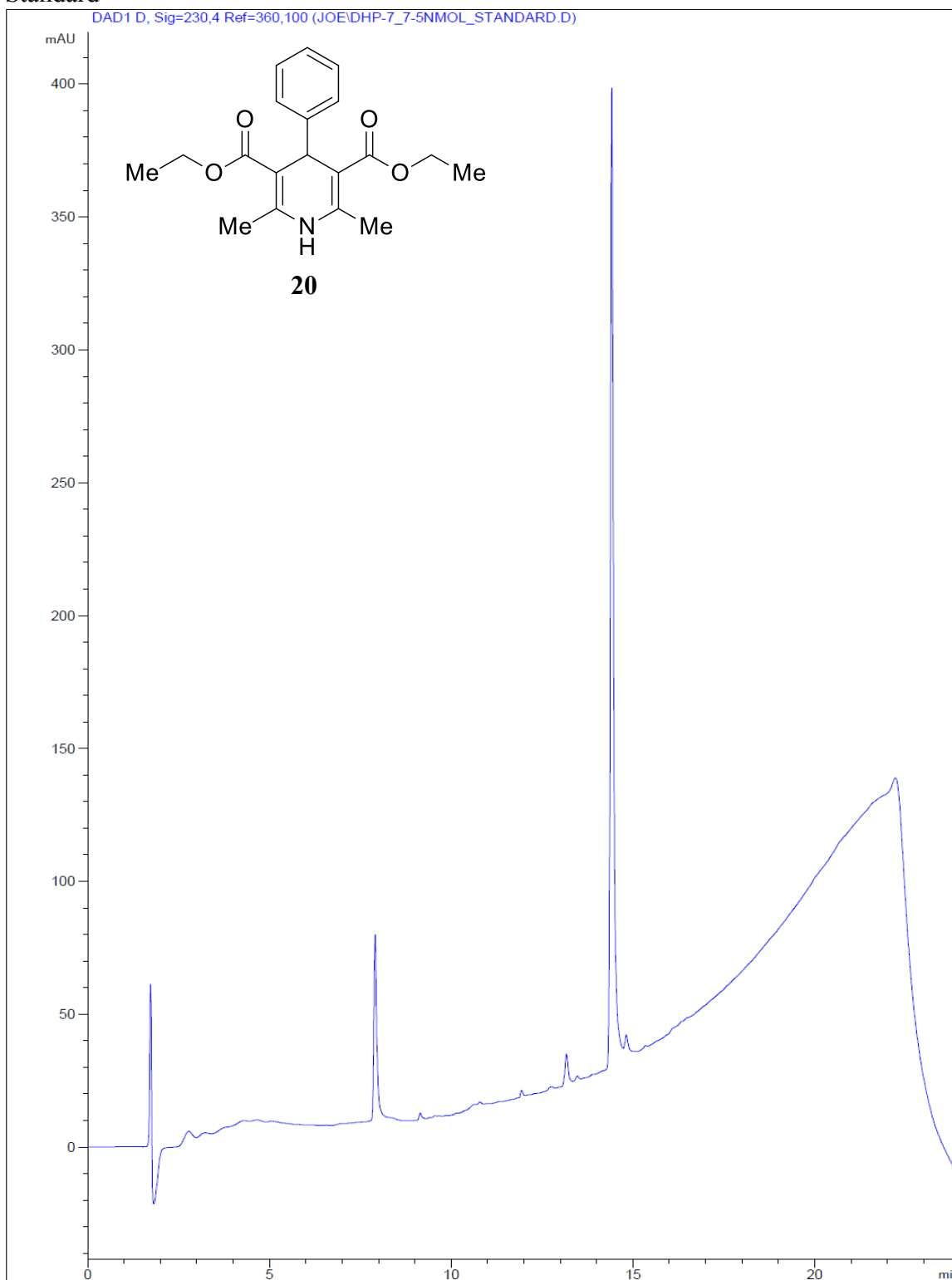


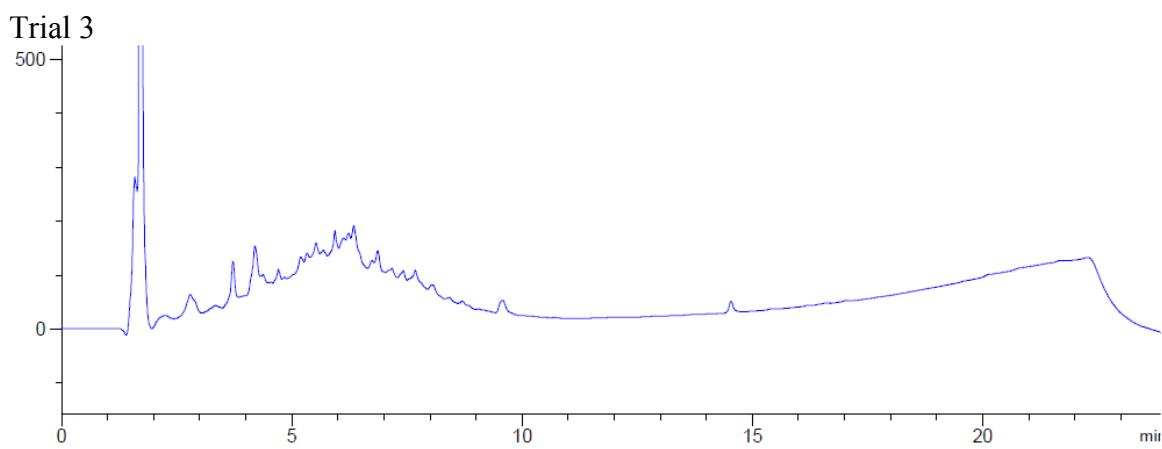
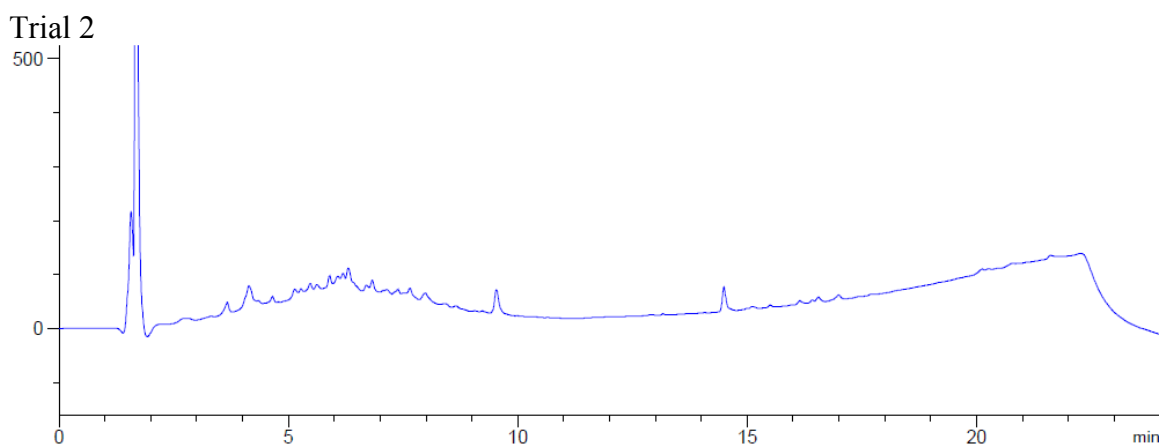
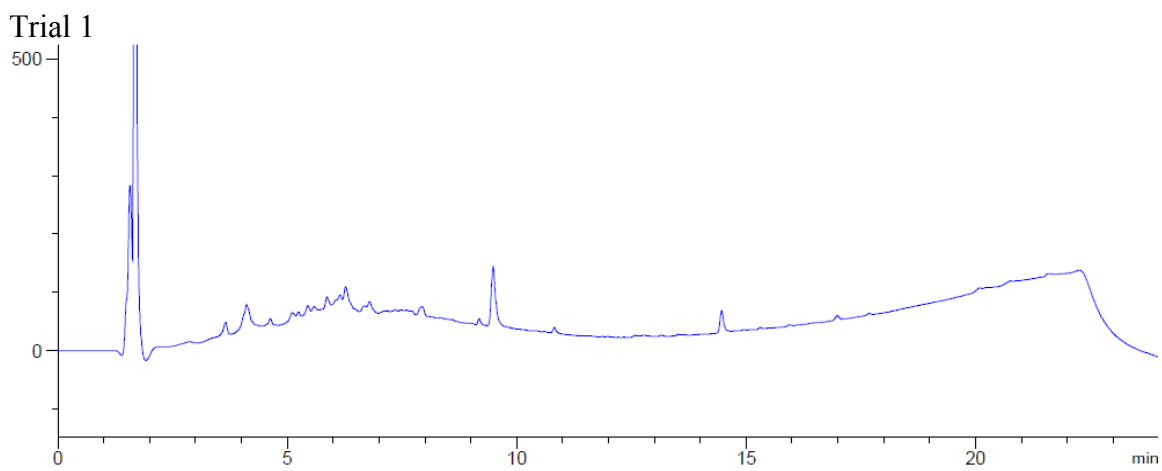
Standard





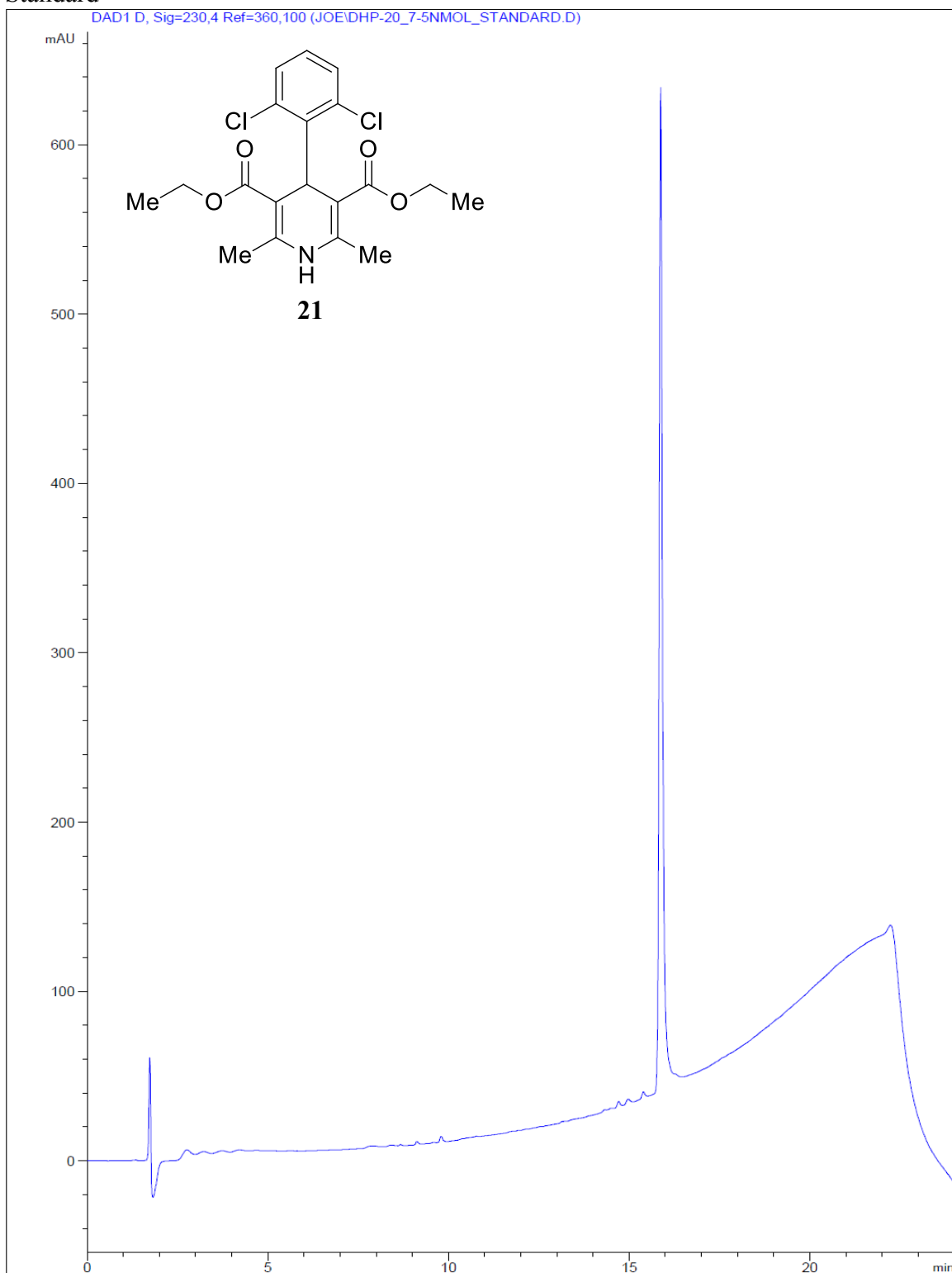
Standard



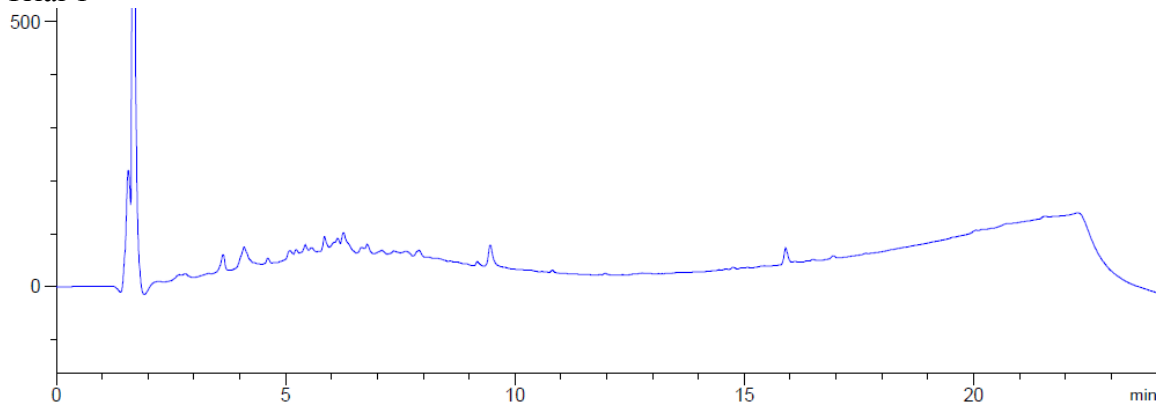


Standard

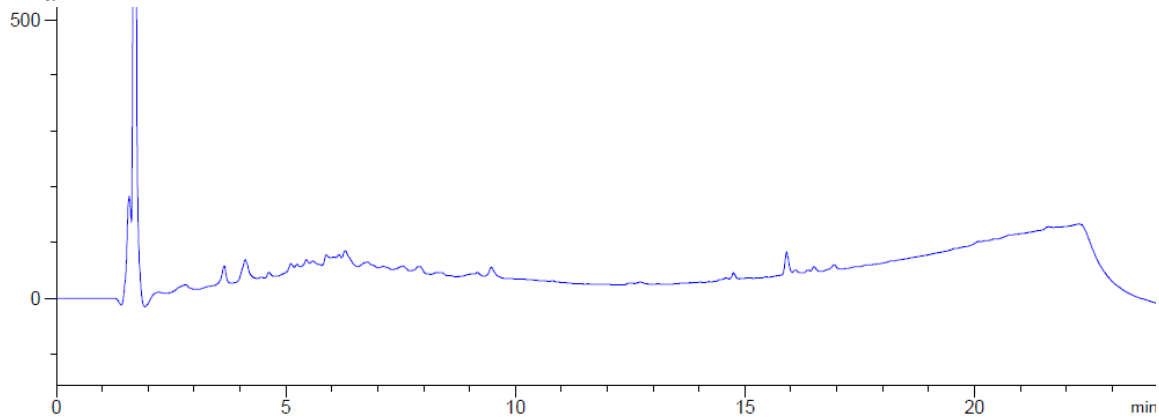
DAD1 D, Sig=230,4 Ref=360,100 (JOE\DHP-20_7-5NMOL_STANDARD.D)



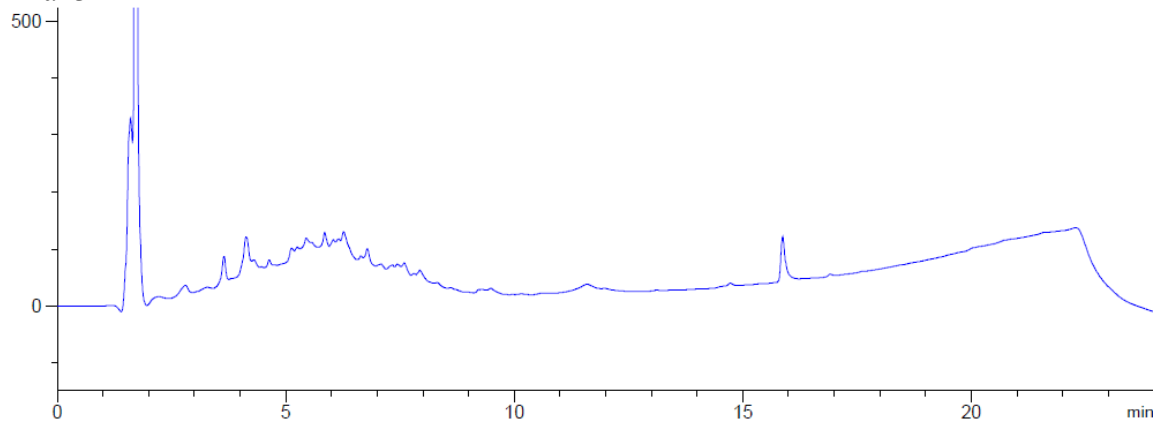
Trial 1



Trial 2

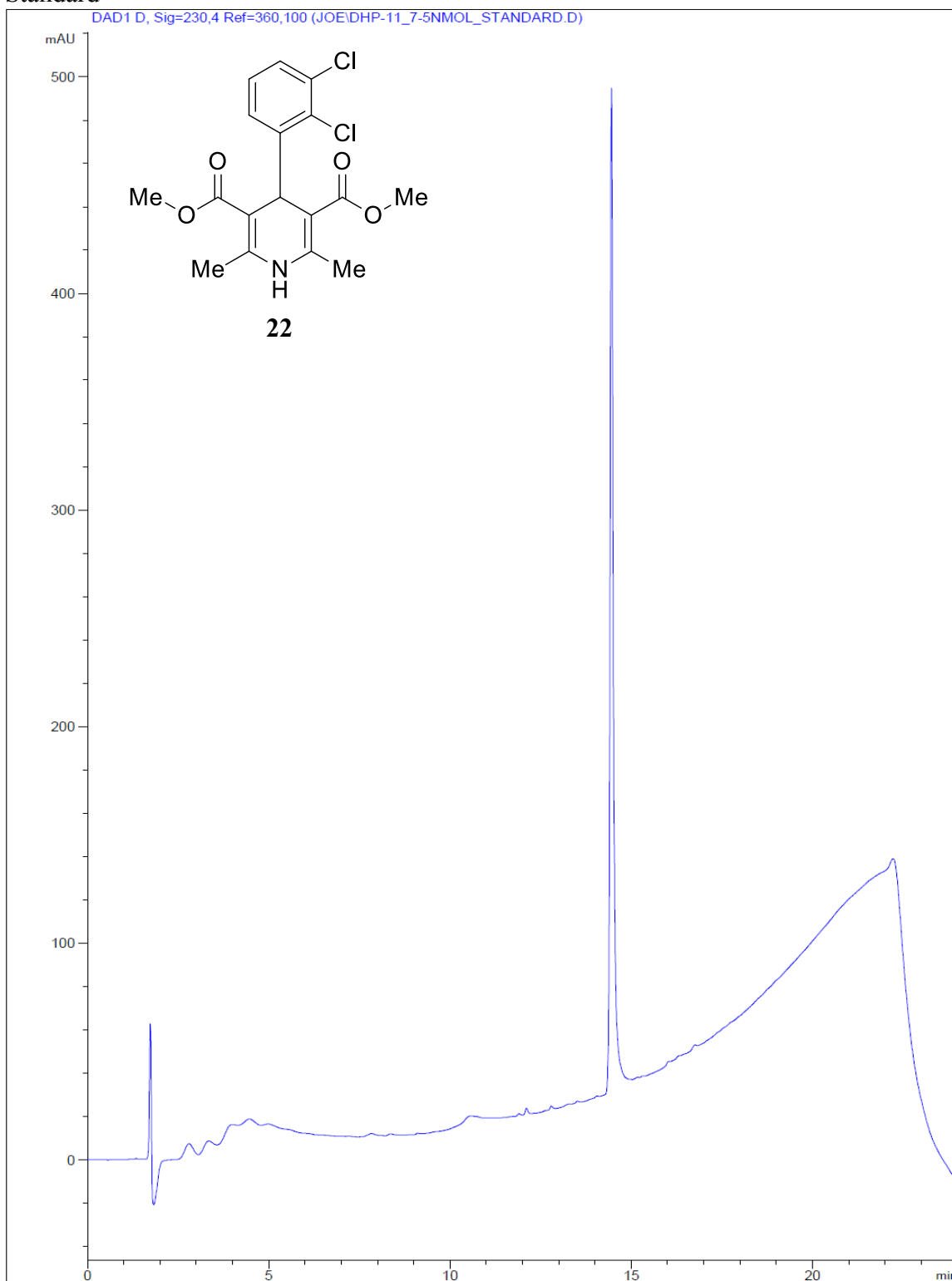


Trial 3

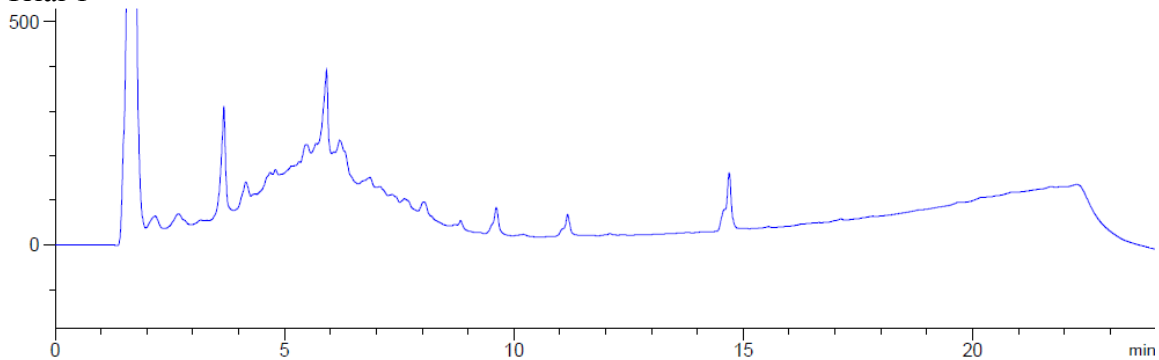


Standard

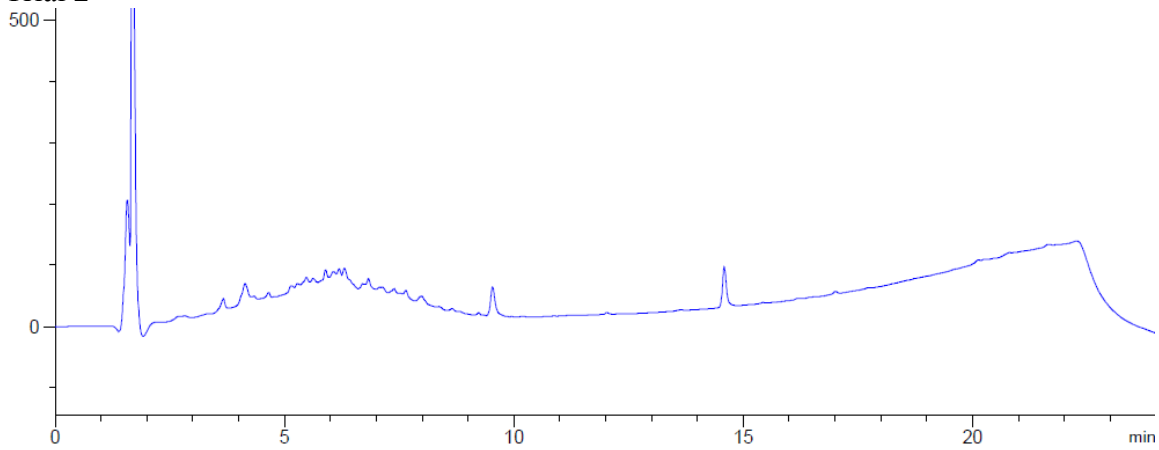
DAD1 D, Sig=230,4 Ref=360,100 (JOE\DHP-11_7-5NMOL_STANDARD.D)



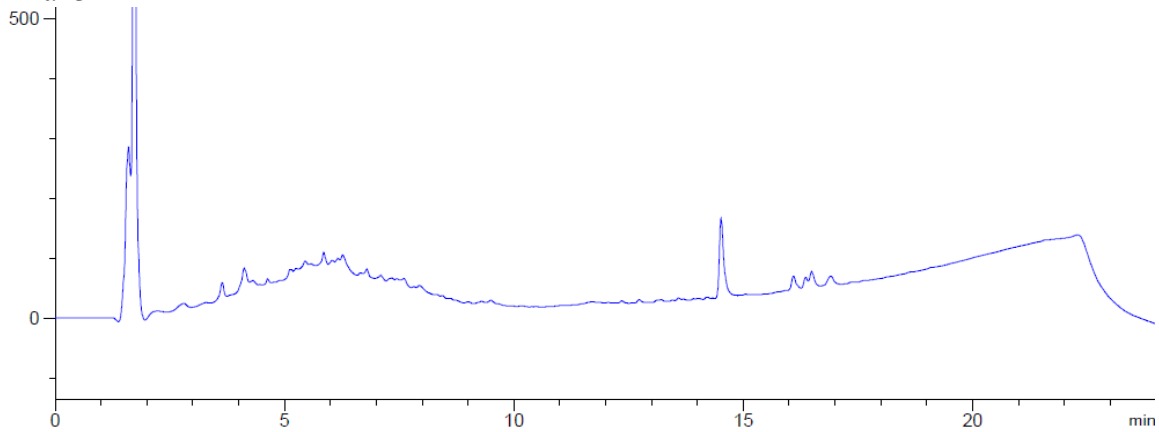
Trial 1



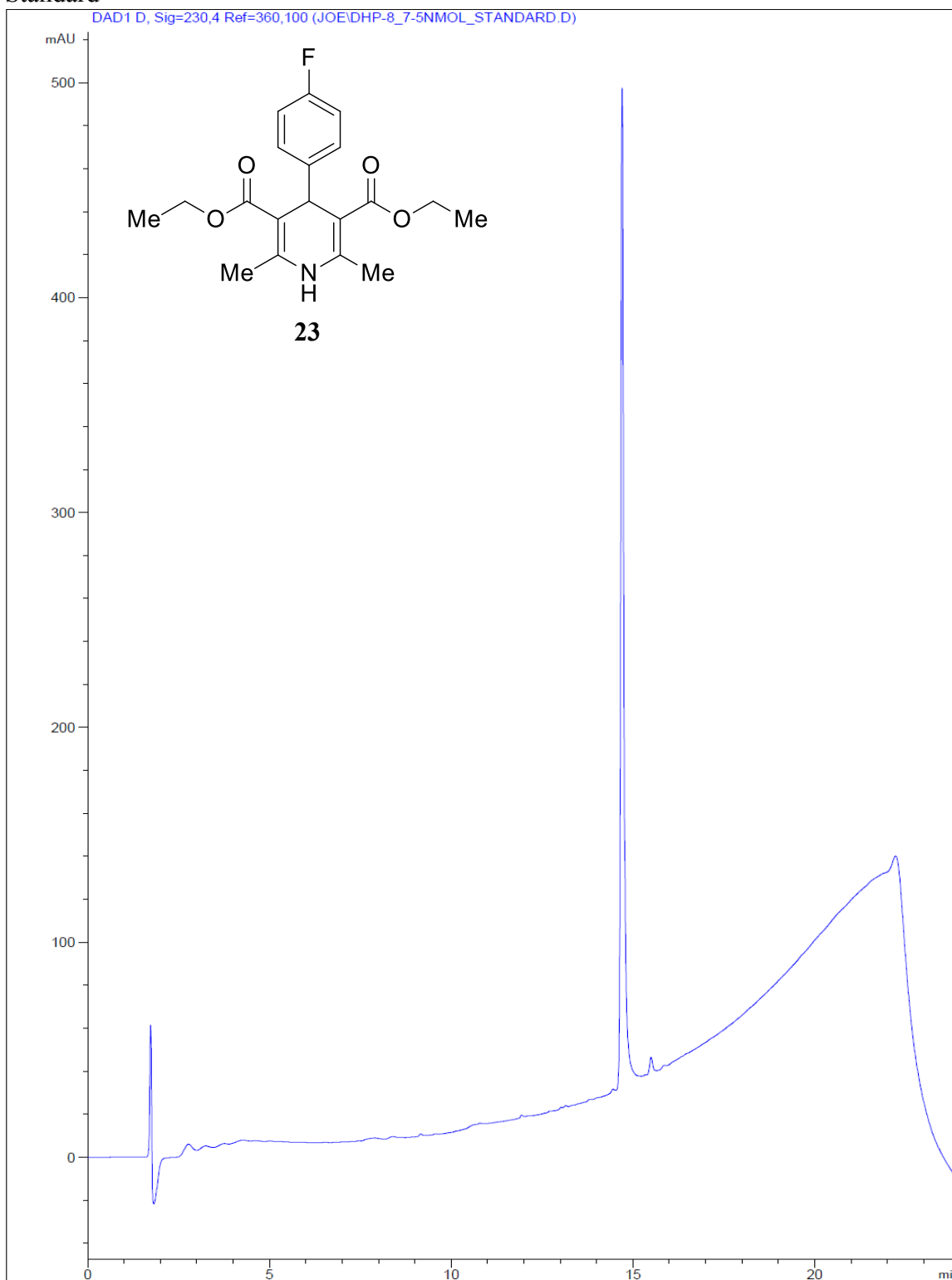
Trial 2



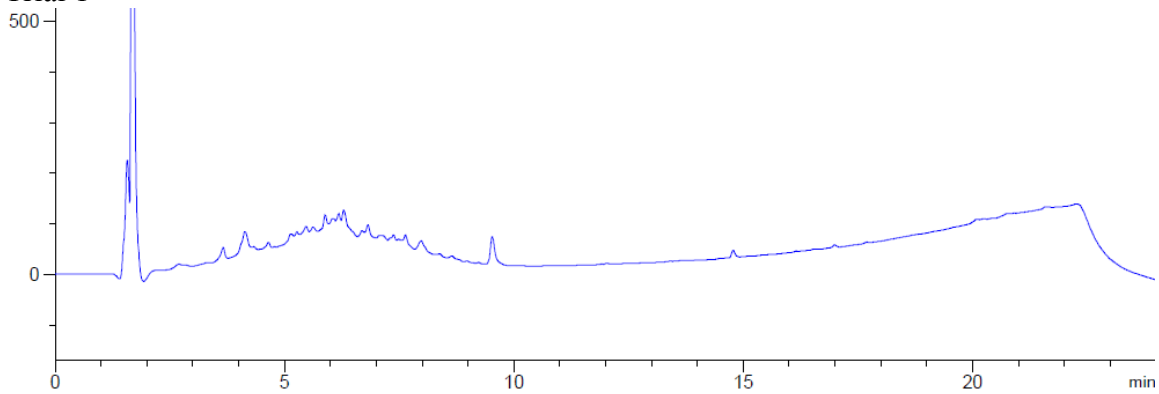
Trial 3



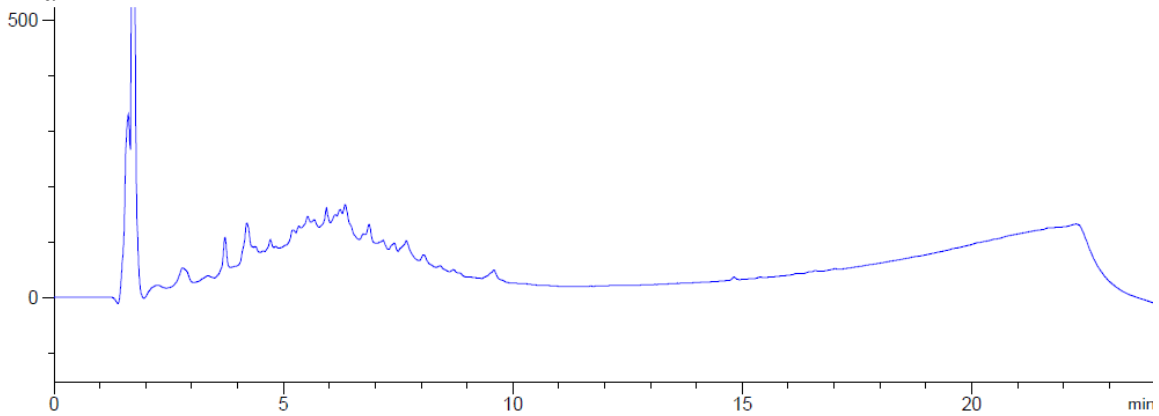
Standard



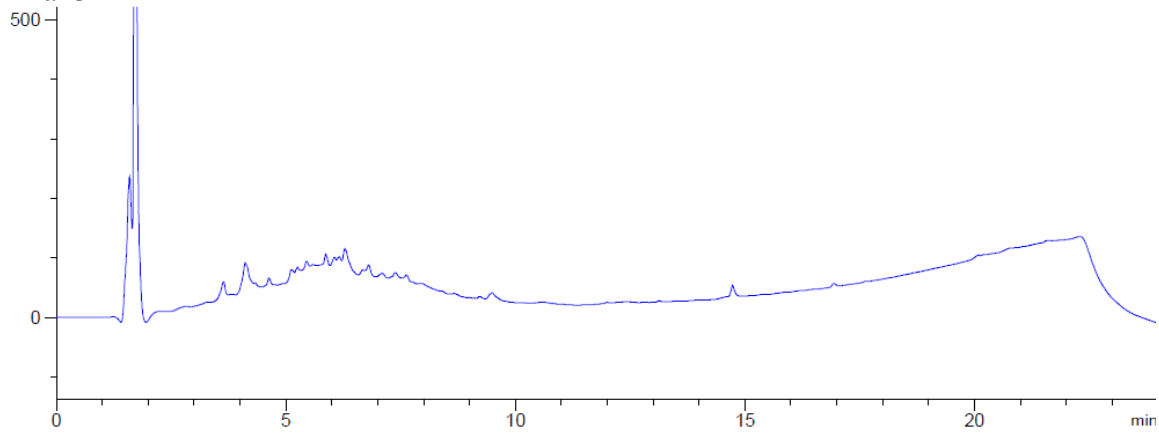
Trial 1



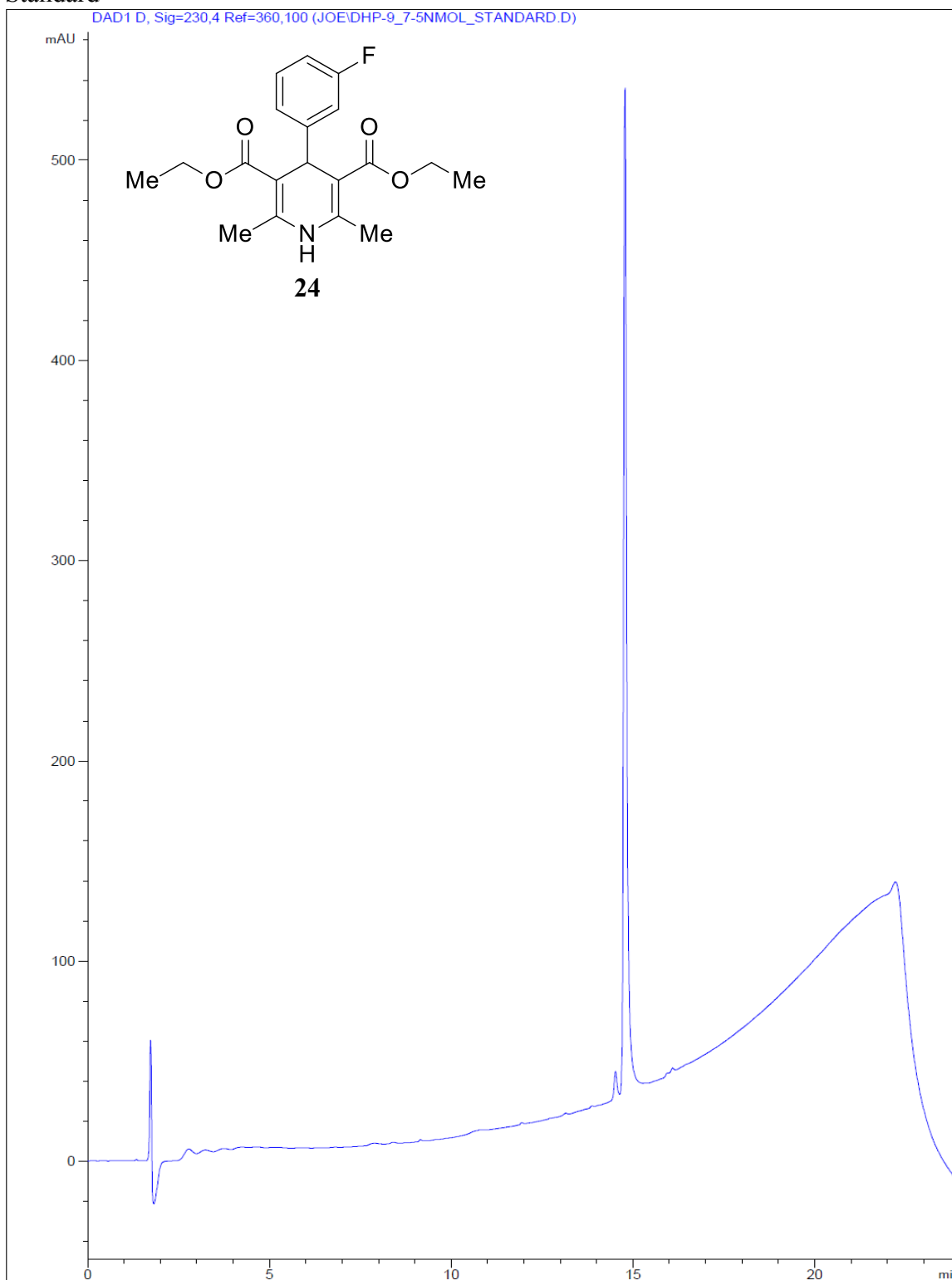
Trial 2



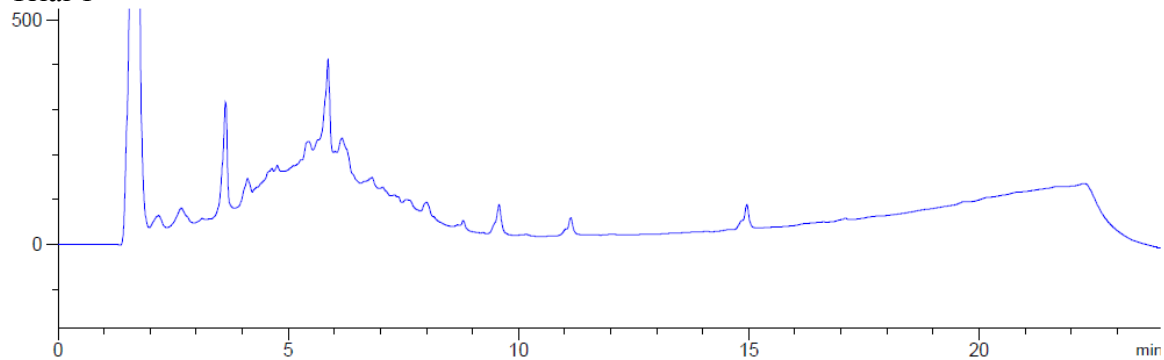
Trial 3



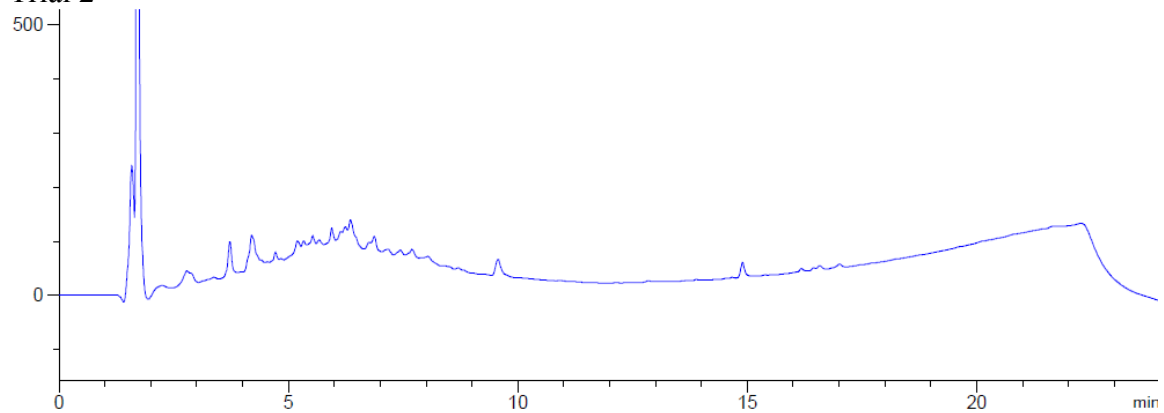
Standard



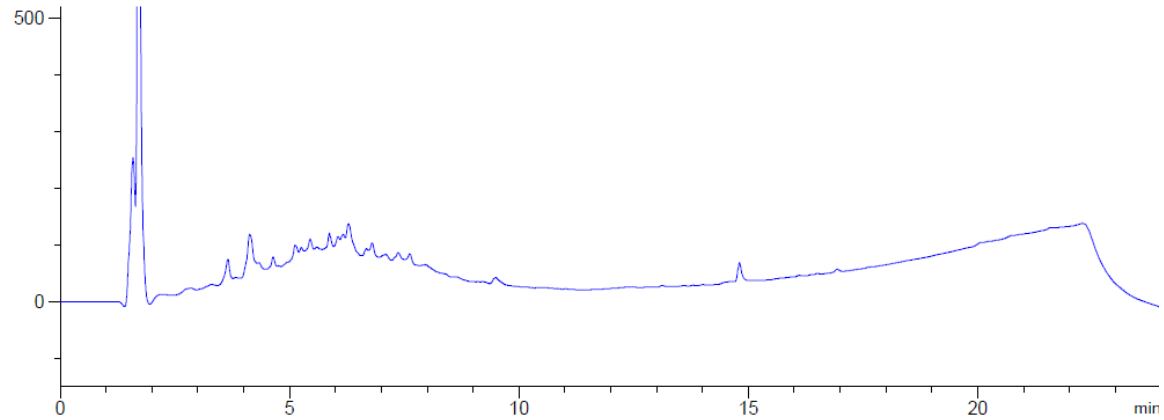
Trial 1



Trial 2

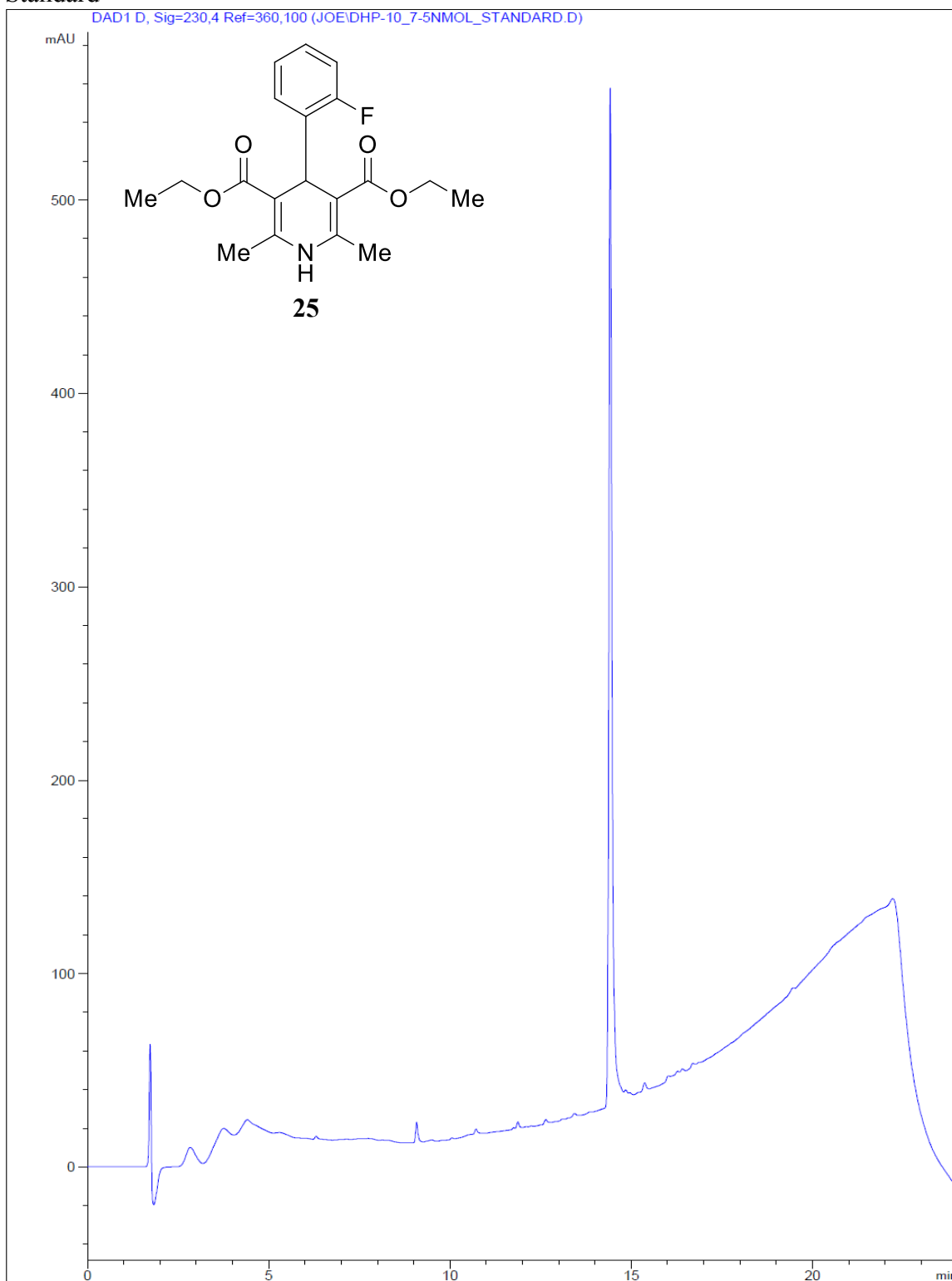


Trial 3

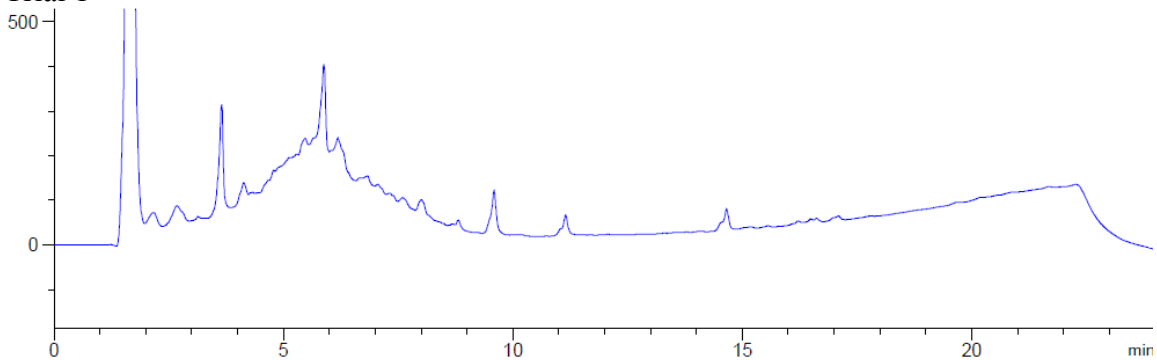


Standard

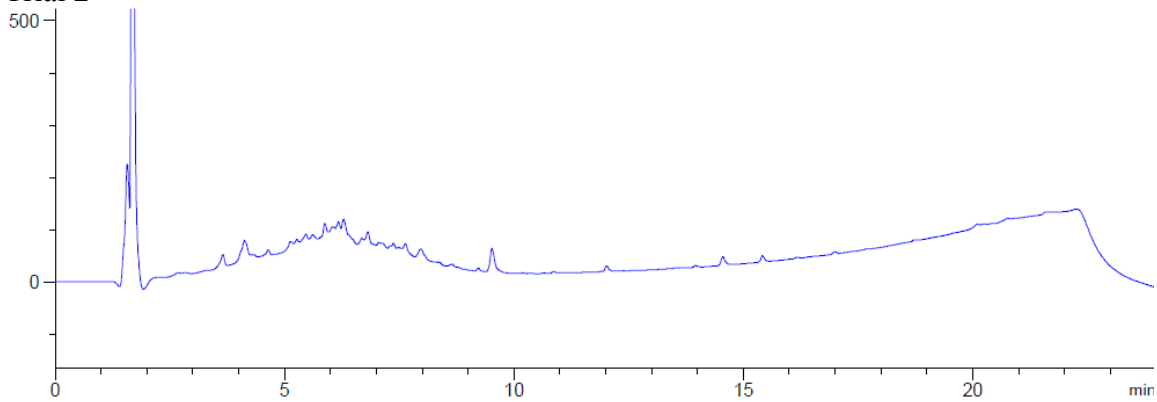
DAD1 D, Sig=230,4 Ref=360,100 (JOE\DHP-10_7-5NMOL_STANDARD.D)



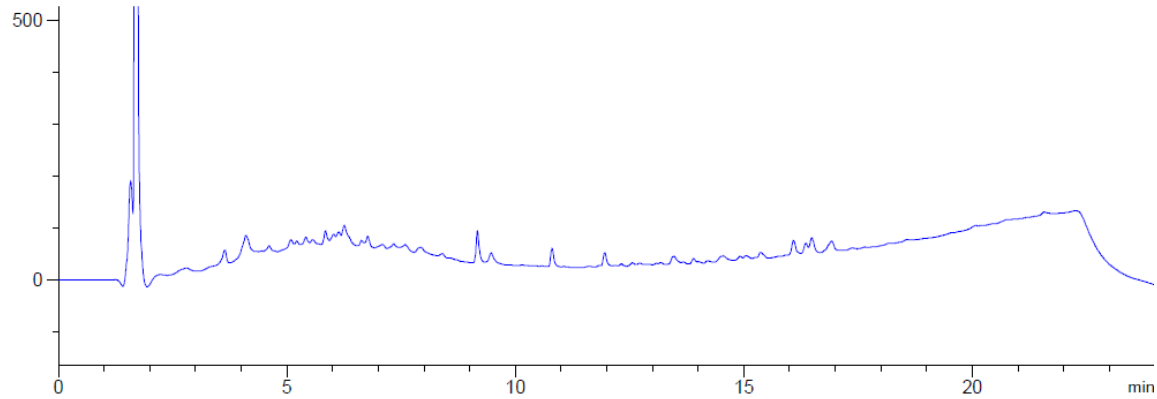
Trial 1



Trial 2

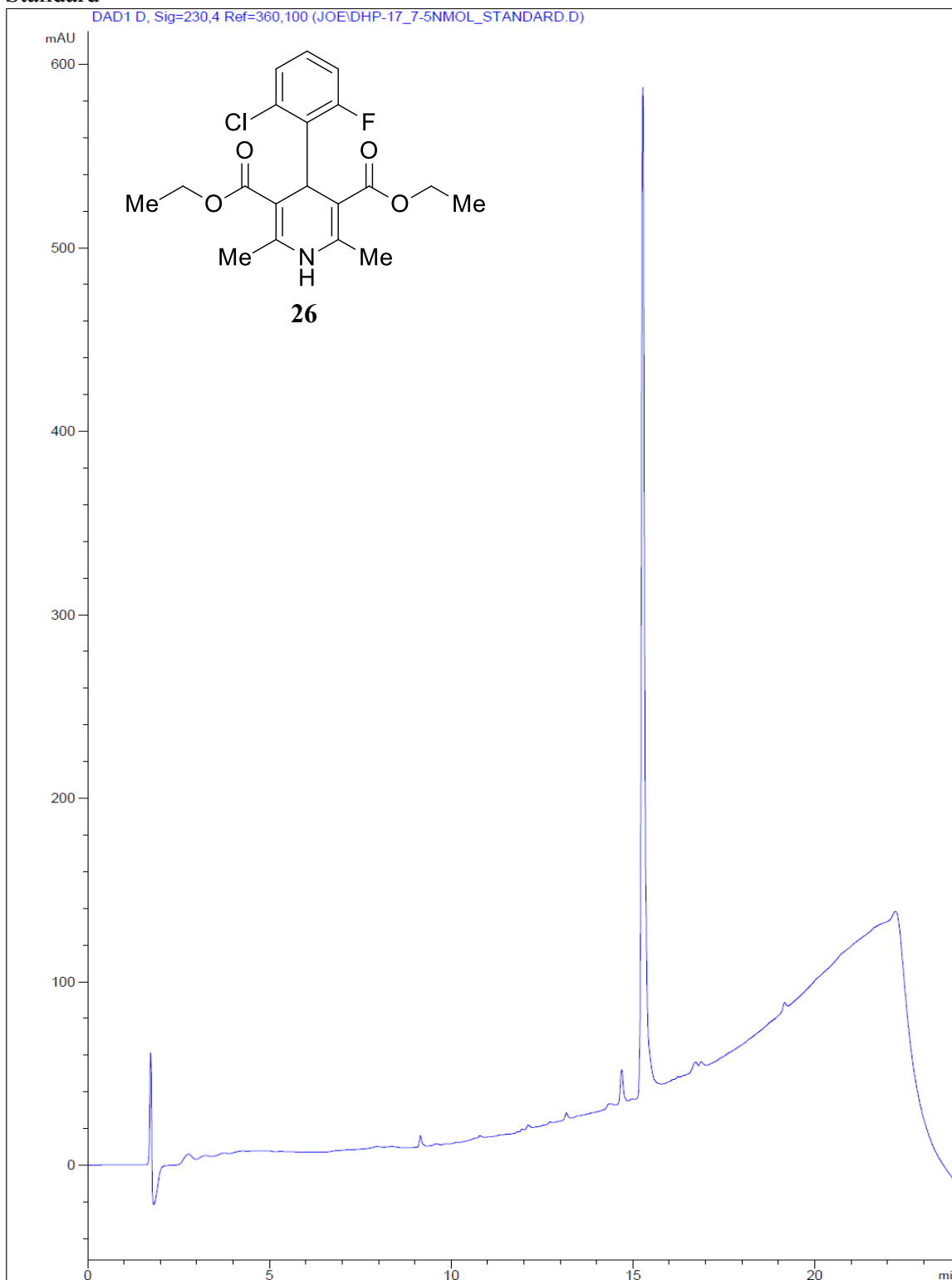


Trial 3

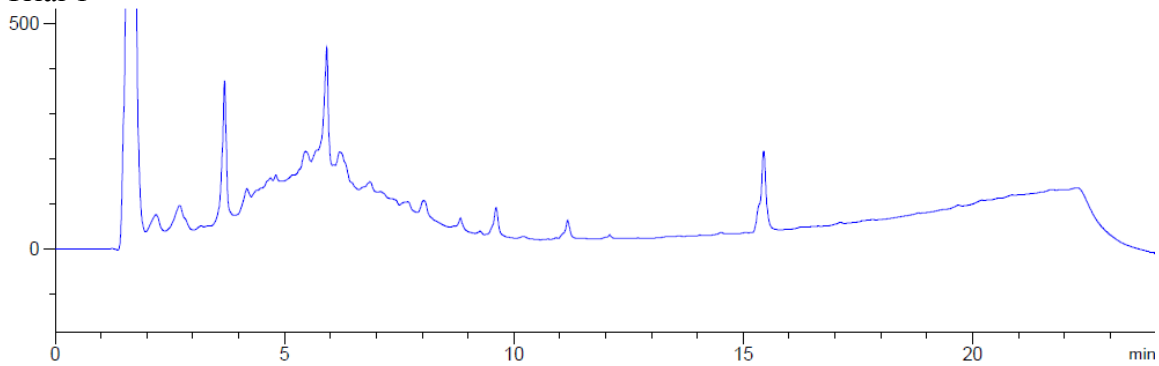


Standard

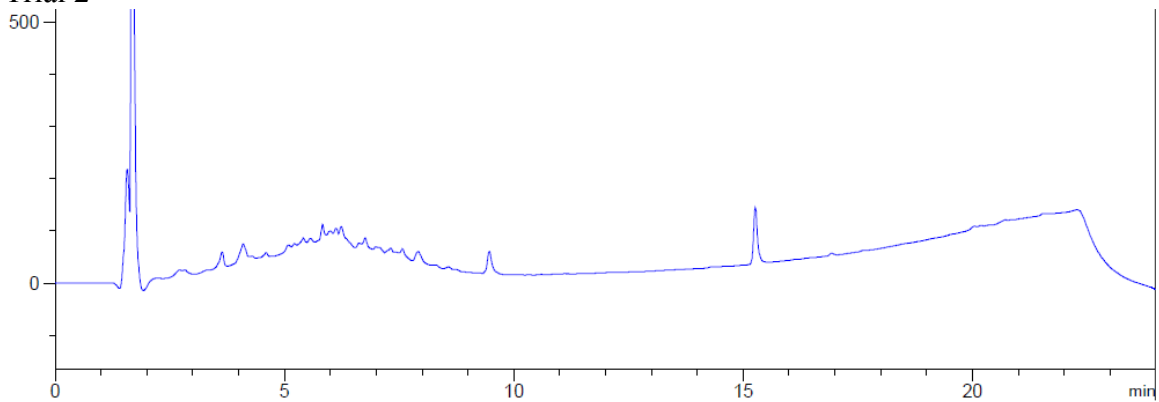
DAD1 D, Sig=230,4 Ref=360,100 (JOE\DHP-17_7-5NMOL_STANDARD.D)



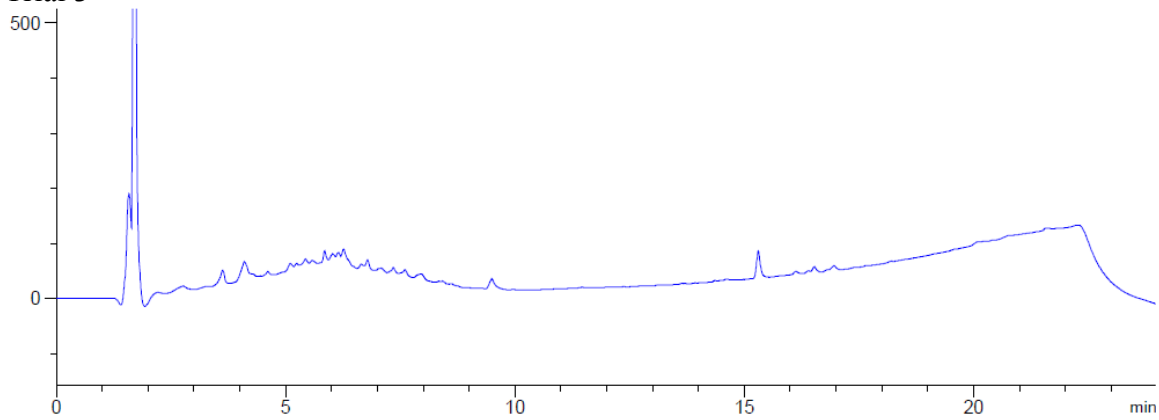
Trial 1



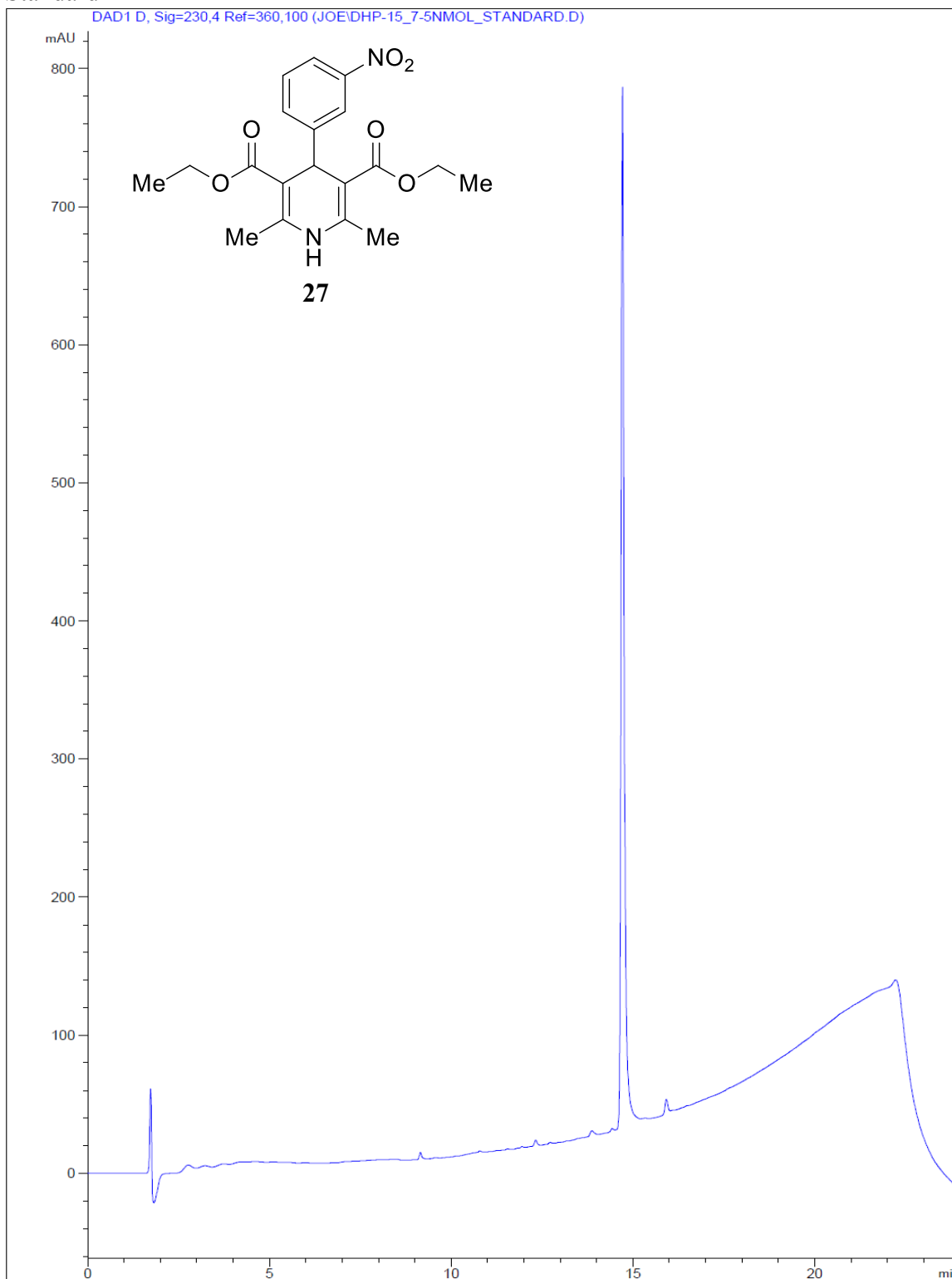
Trial 2



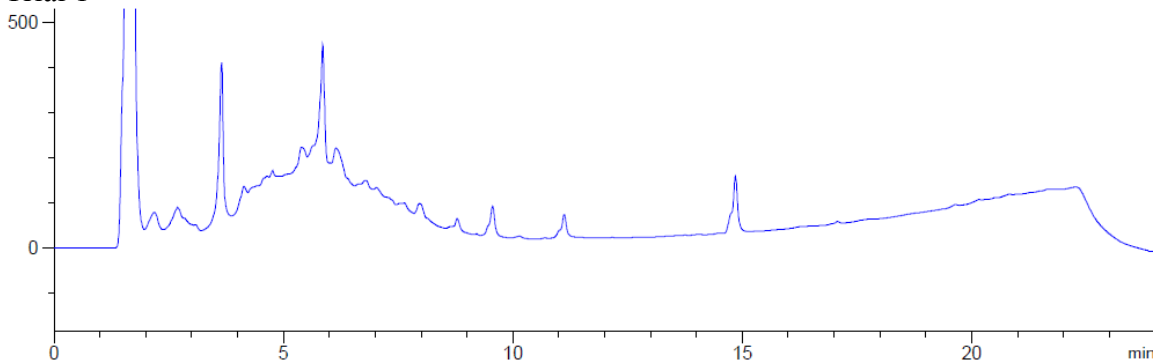
Trial 3



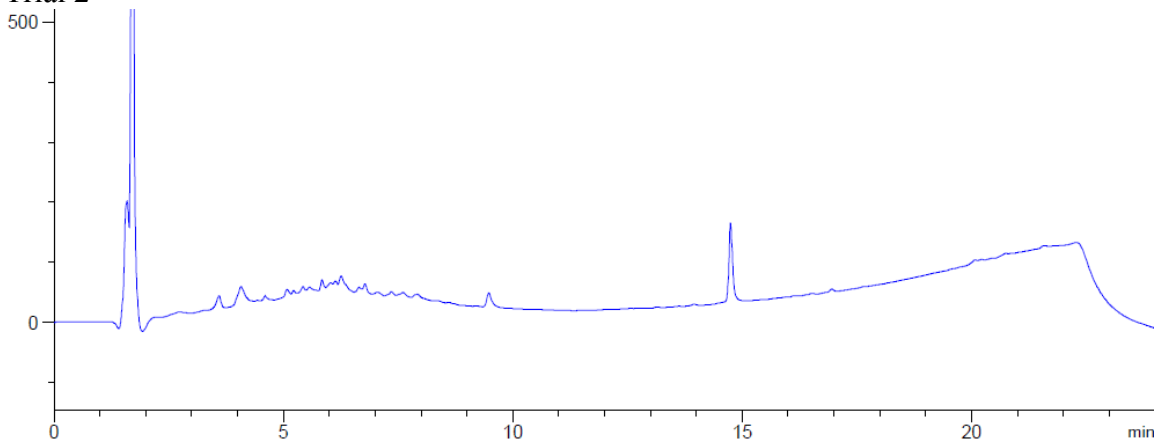
Standard



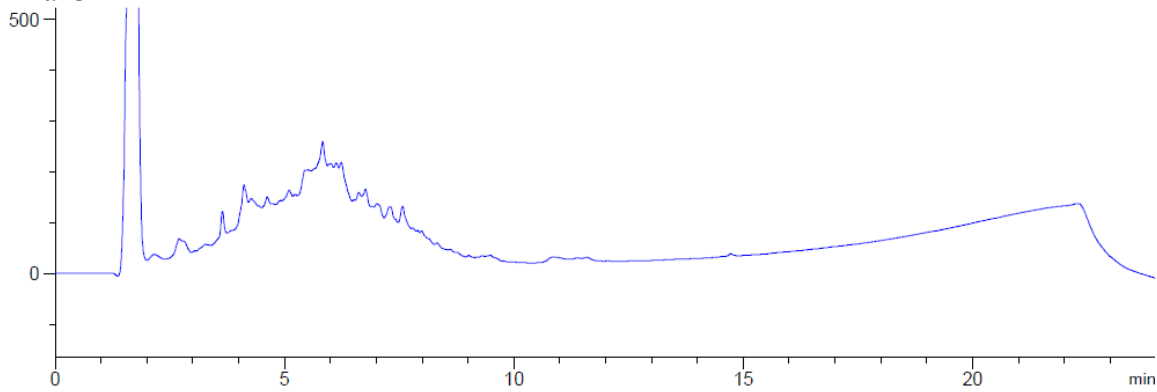
Trial 1



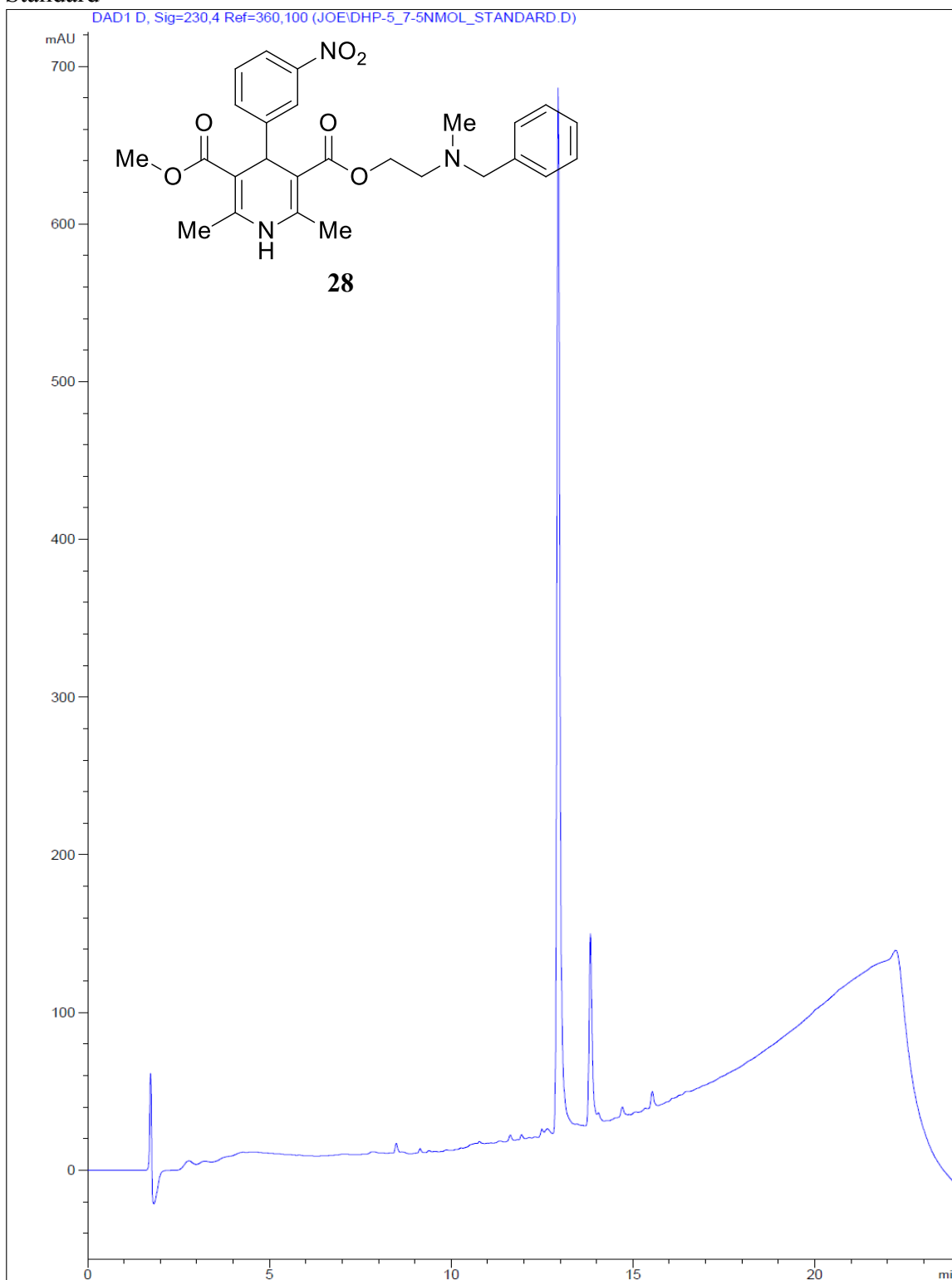
Trial 2



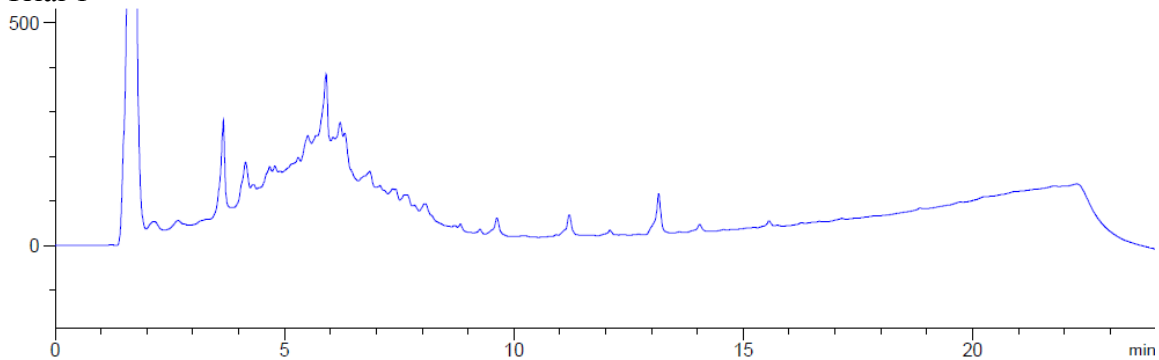
Trial 3



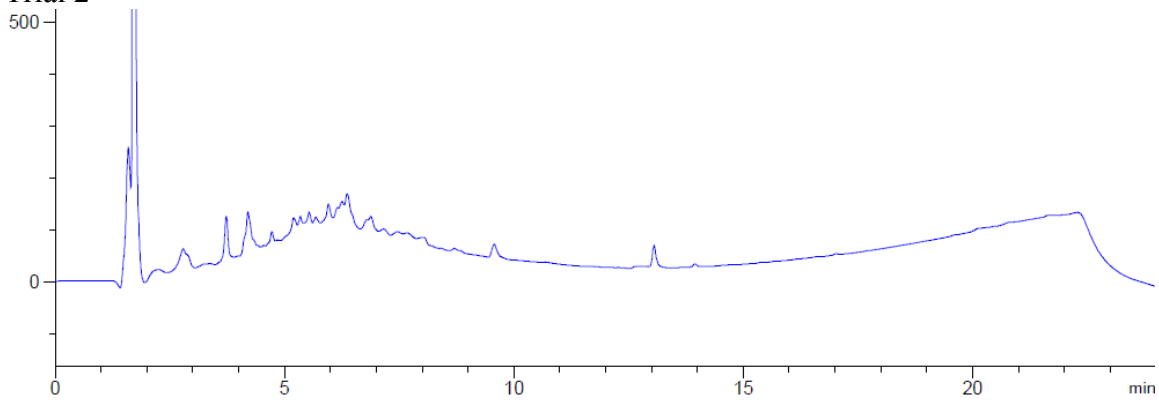
Standard



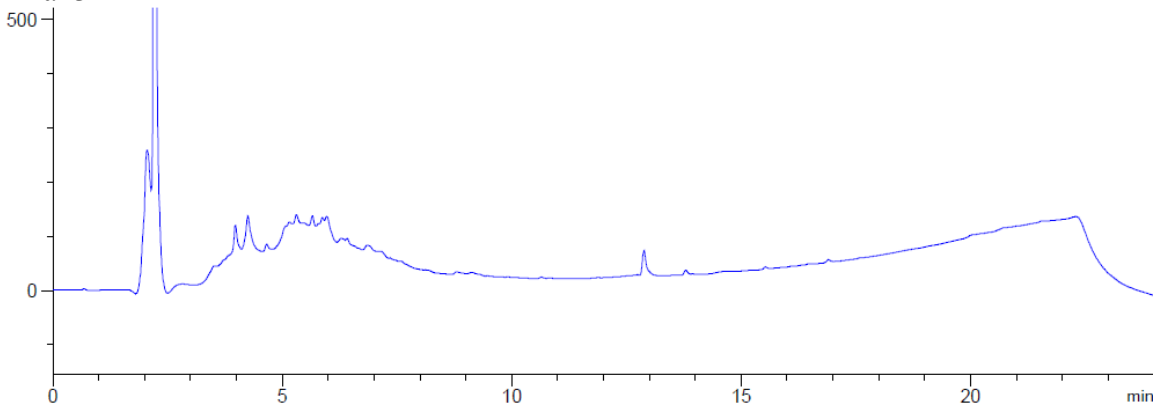
Trial 1



Trial 2

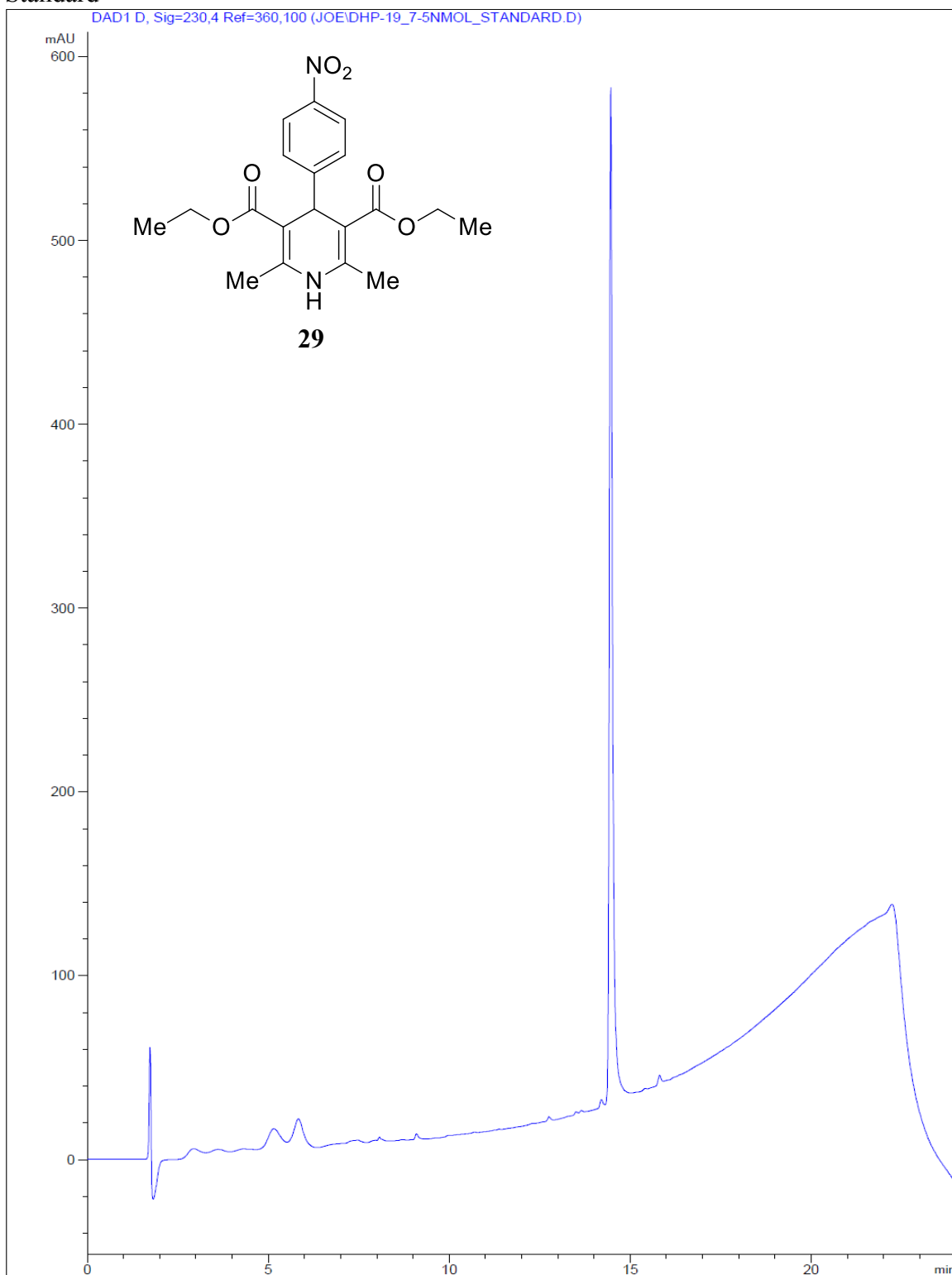


Trial 3

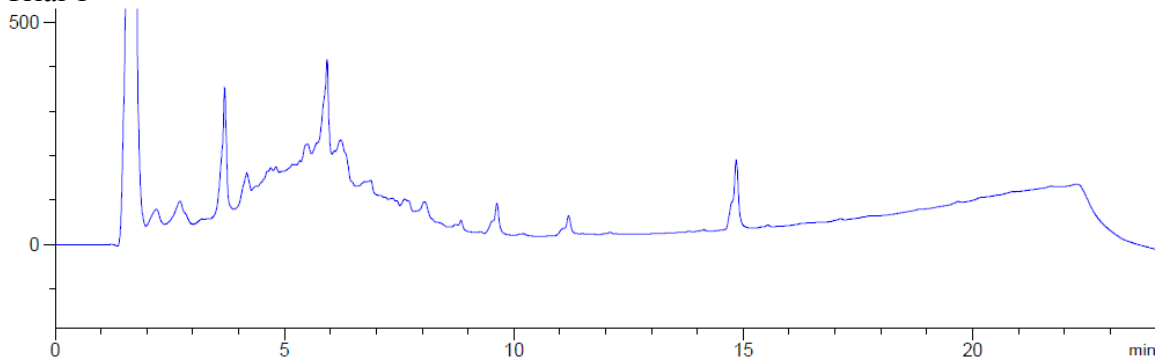


Standard

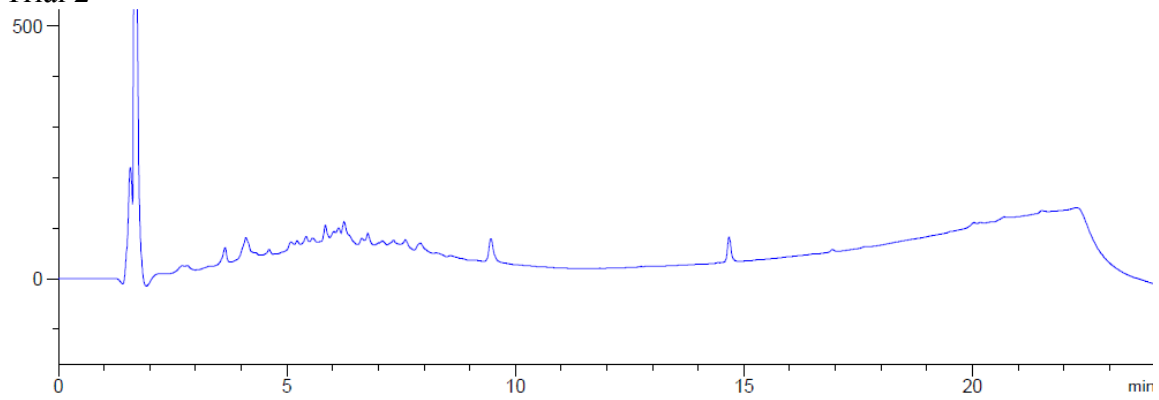
DAD1 D, Sig=230,4 Ref=360,100 (JOE/DHP-19_7-5NMOL_STANDARD.D)



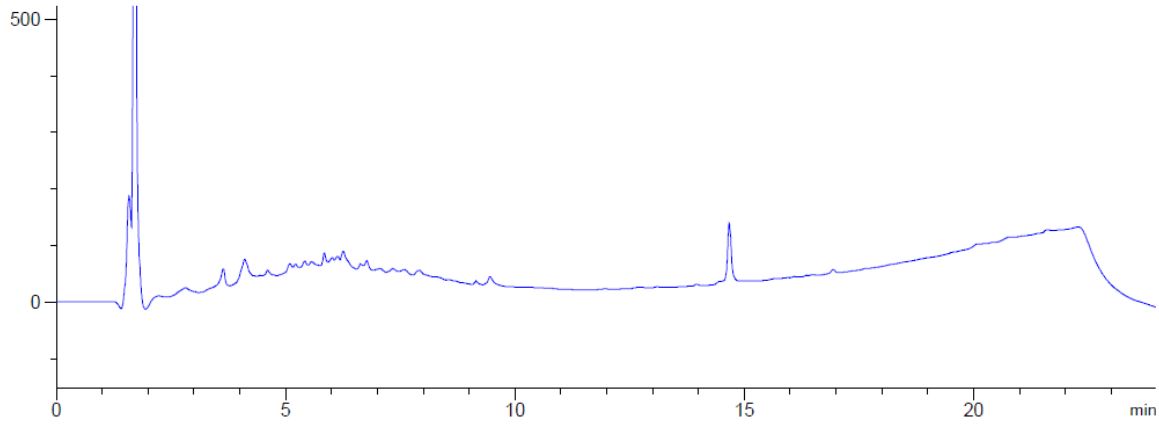
Trial 1



Trial 2

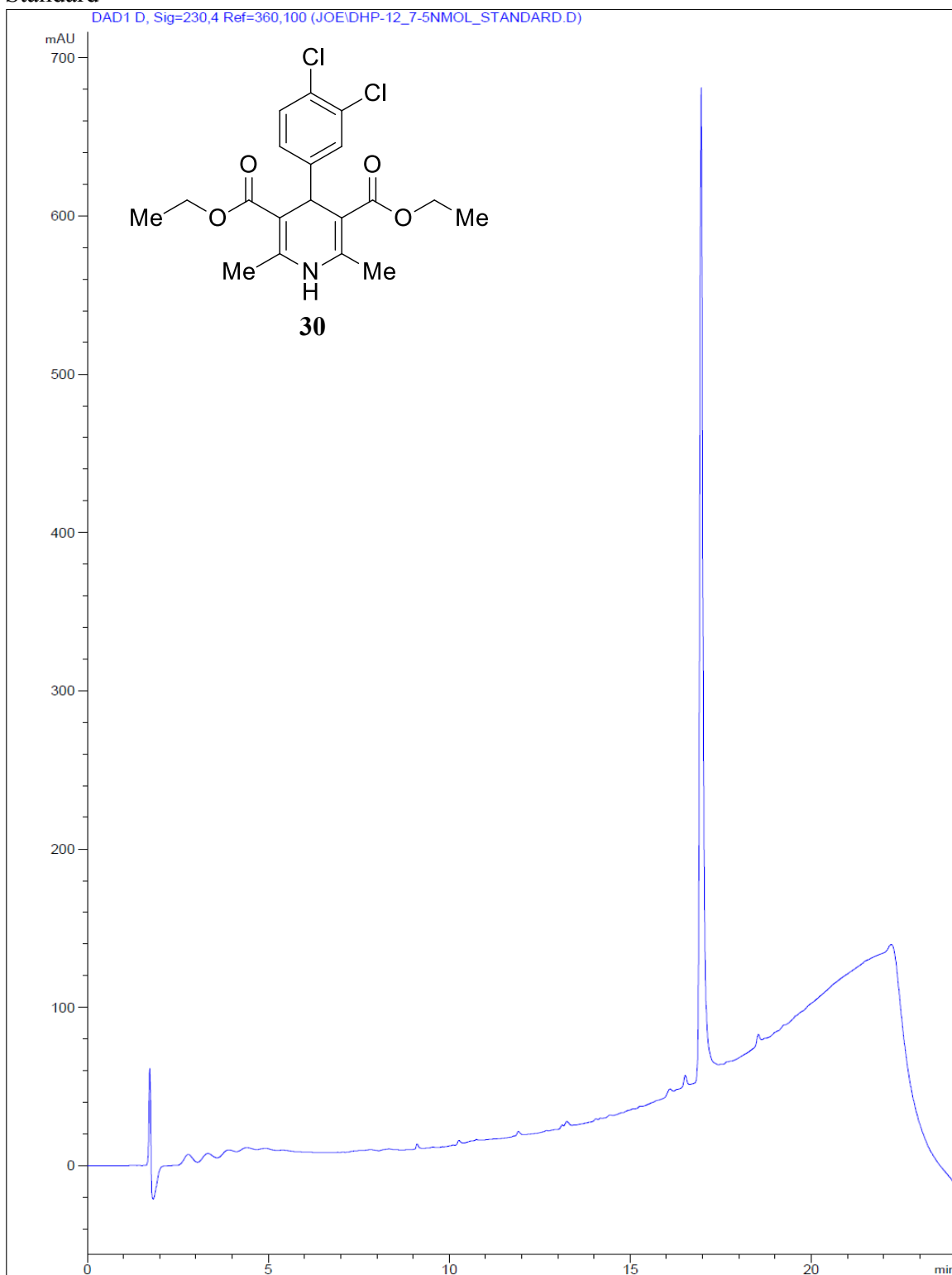


Trial 3

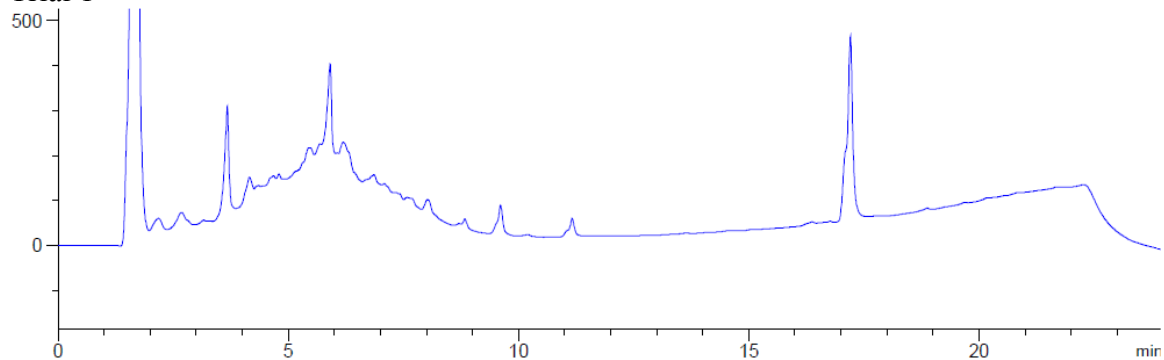


Standard

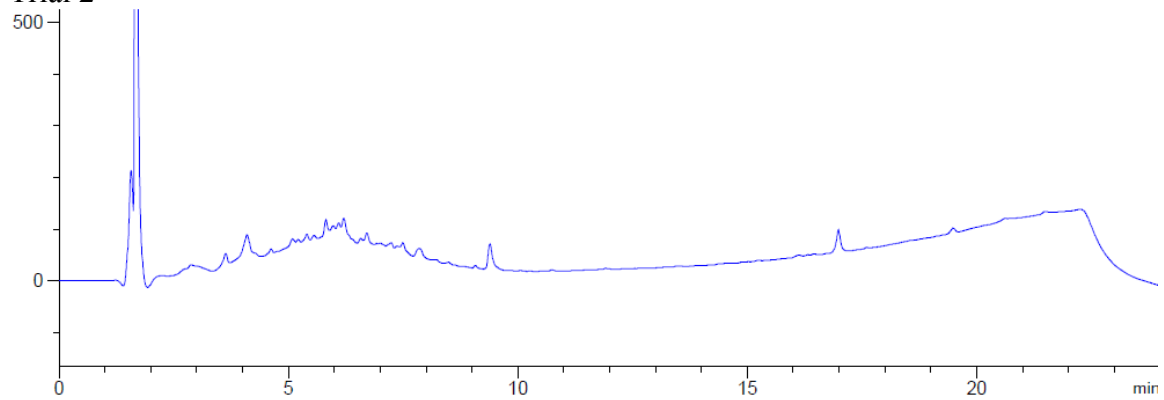
DAD1 D, Sig=230,4 Ref=360,100 (JOE/DHP-12_7-5NMOL_STANDARD.D)



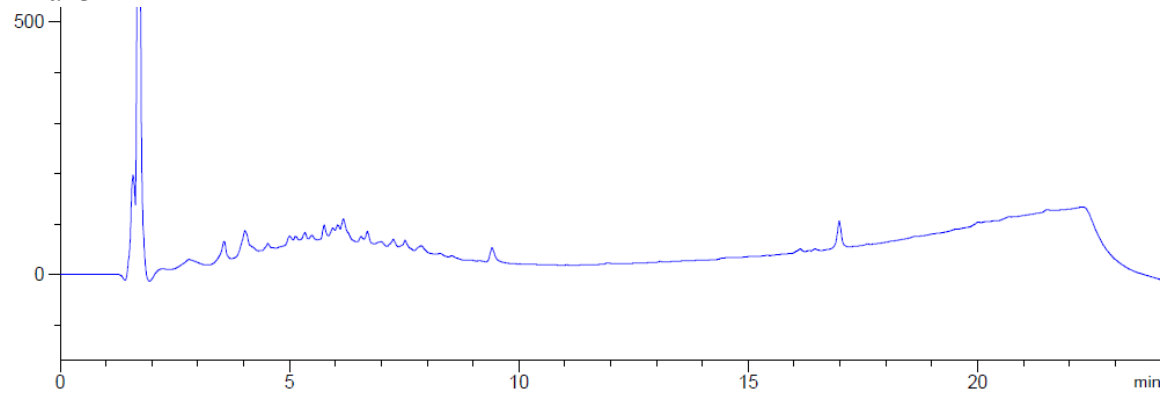
Trial 1



Trial 2

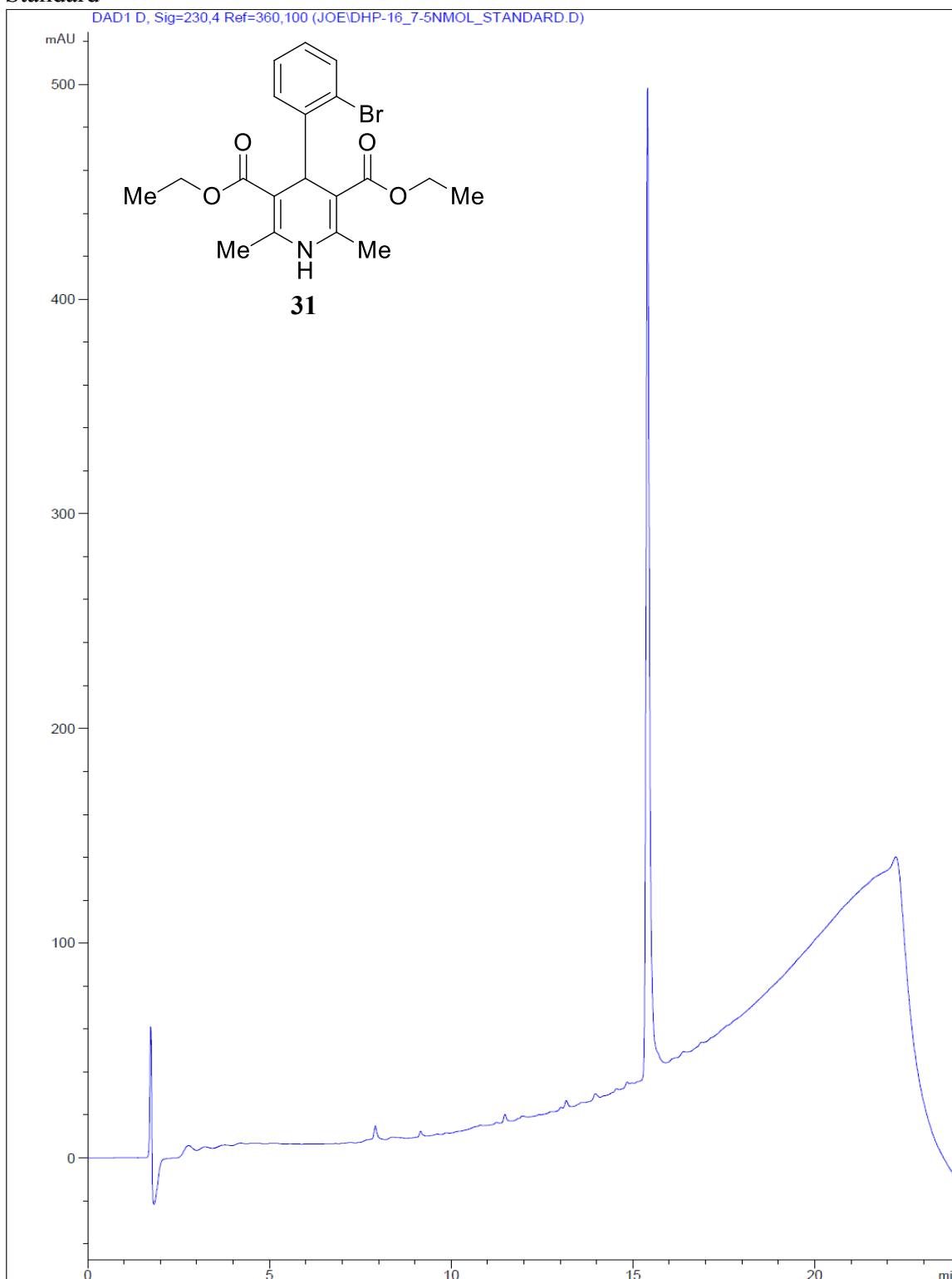


Trial 3

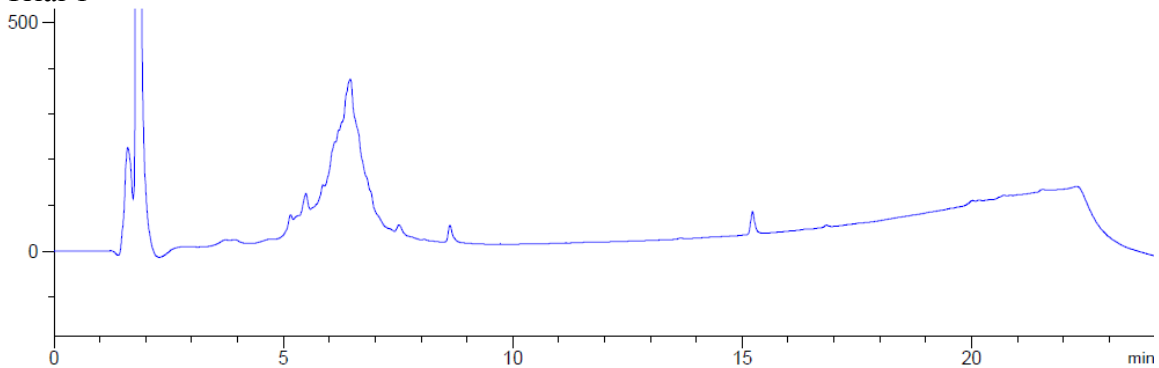


Standard

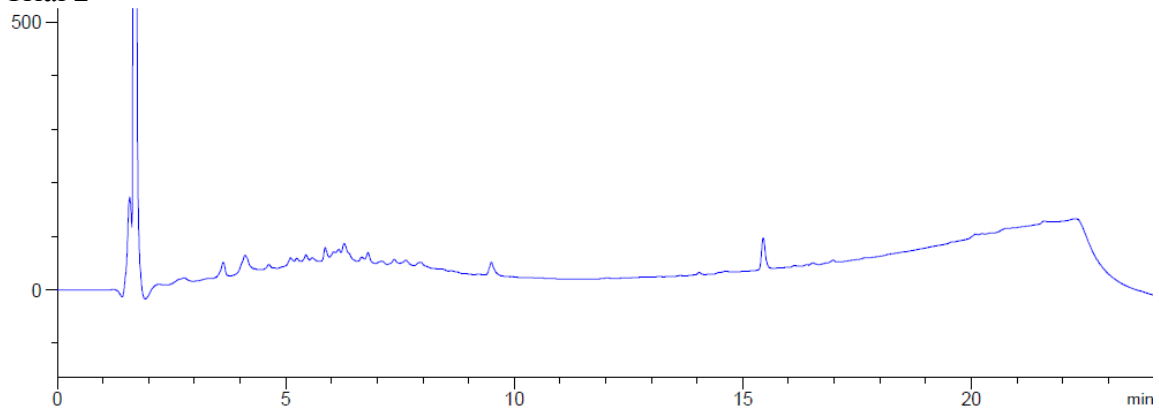
DAD1 D, Sig=230,4 Ref=360,100 (JOE/DHP-16_7-5NMOL_STANDARD.D)



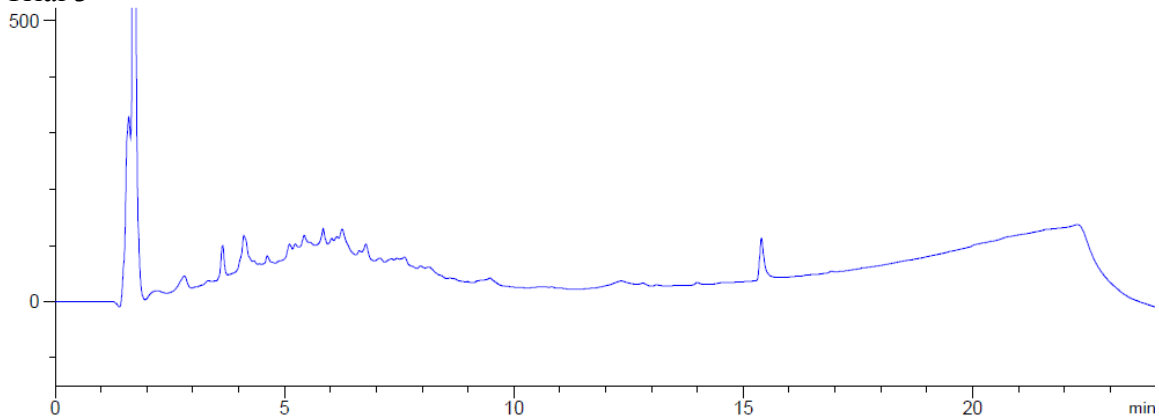
Trial 1



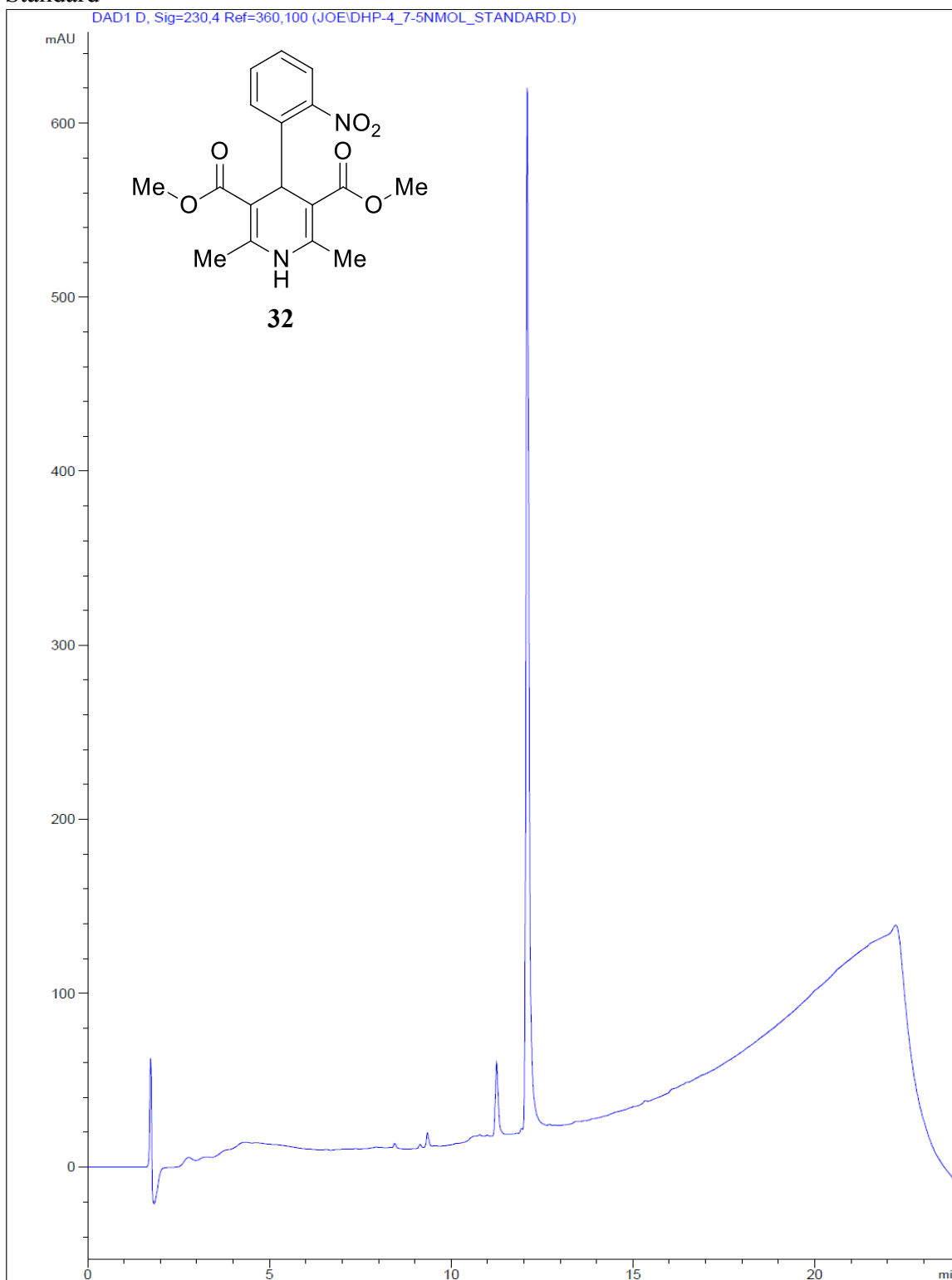
Trial 2

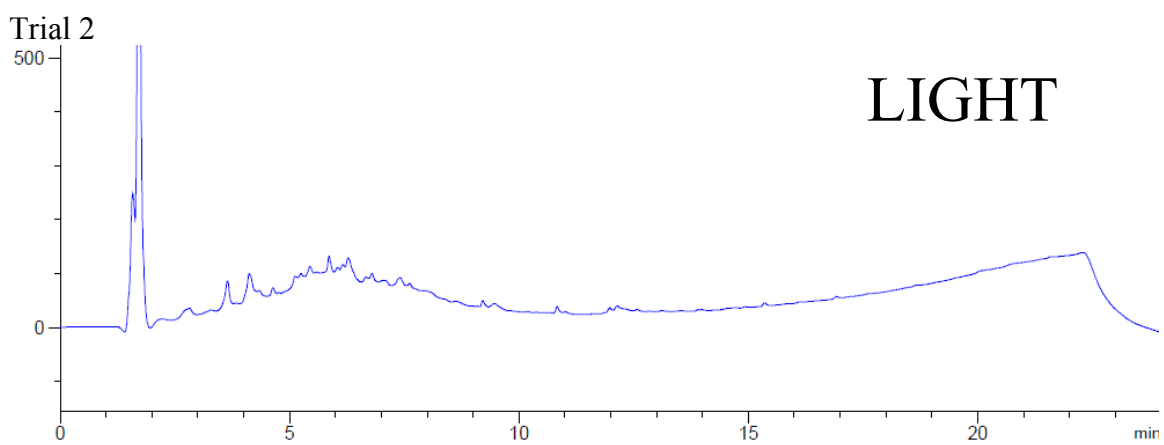
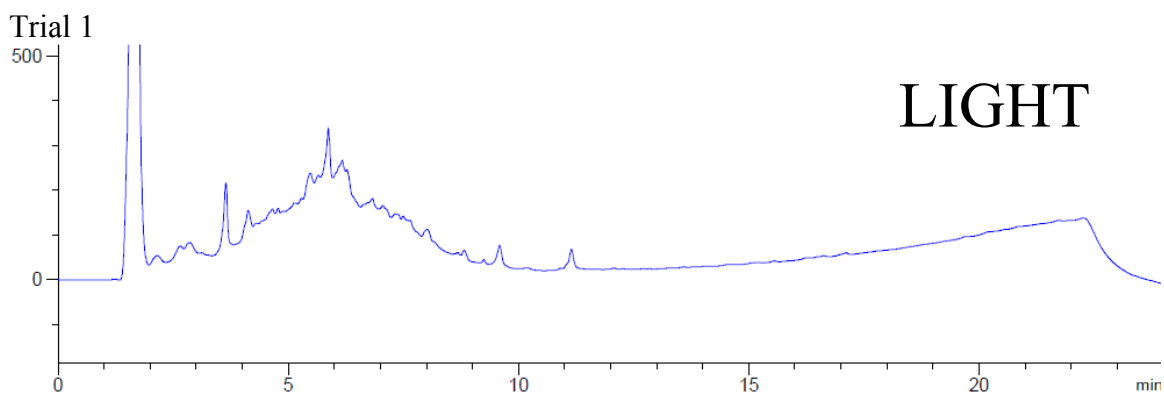


Trial 3

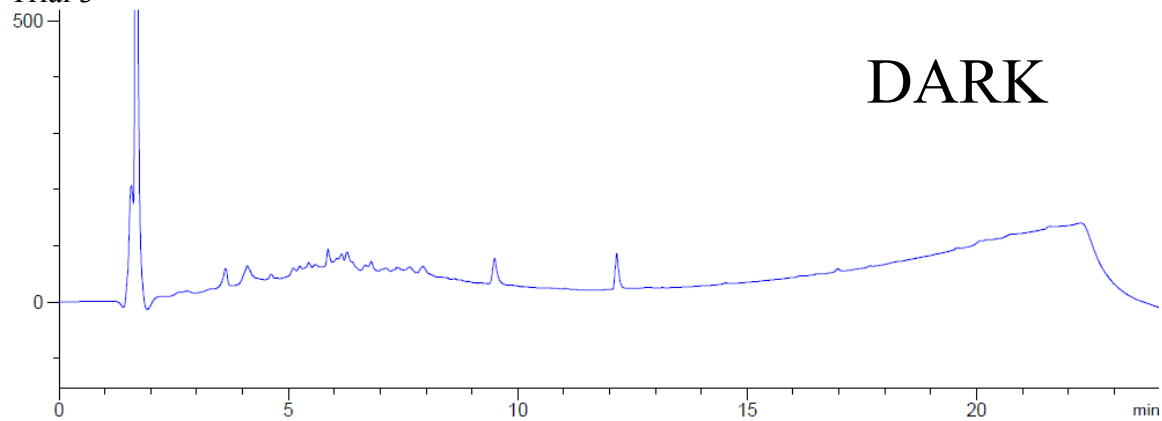


Standard

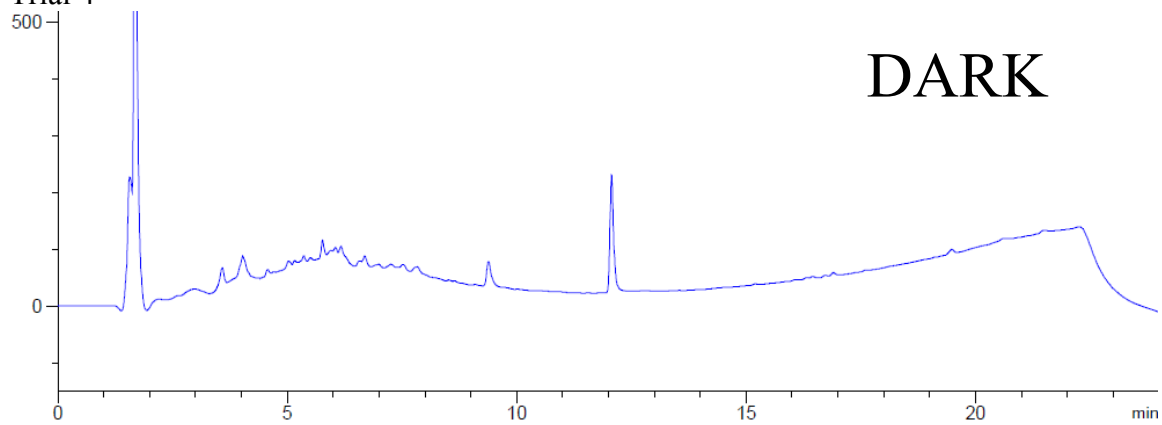




Trial 3

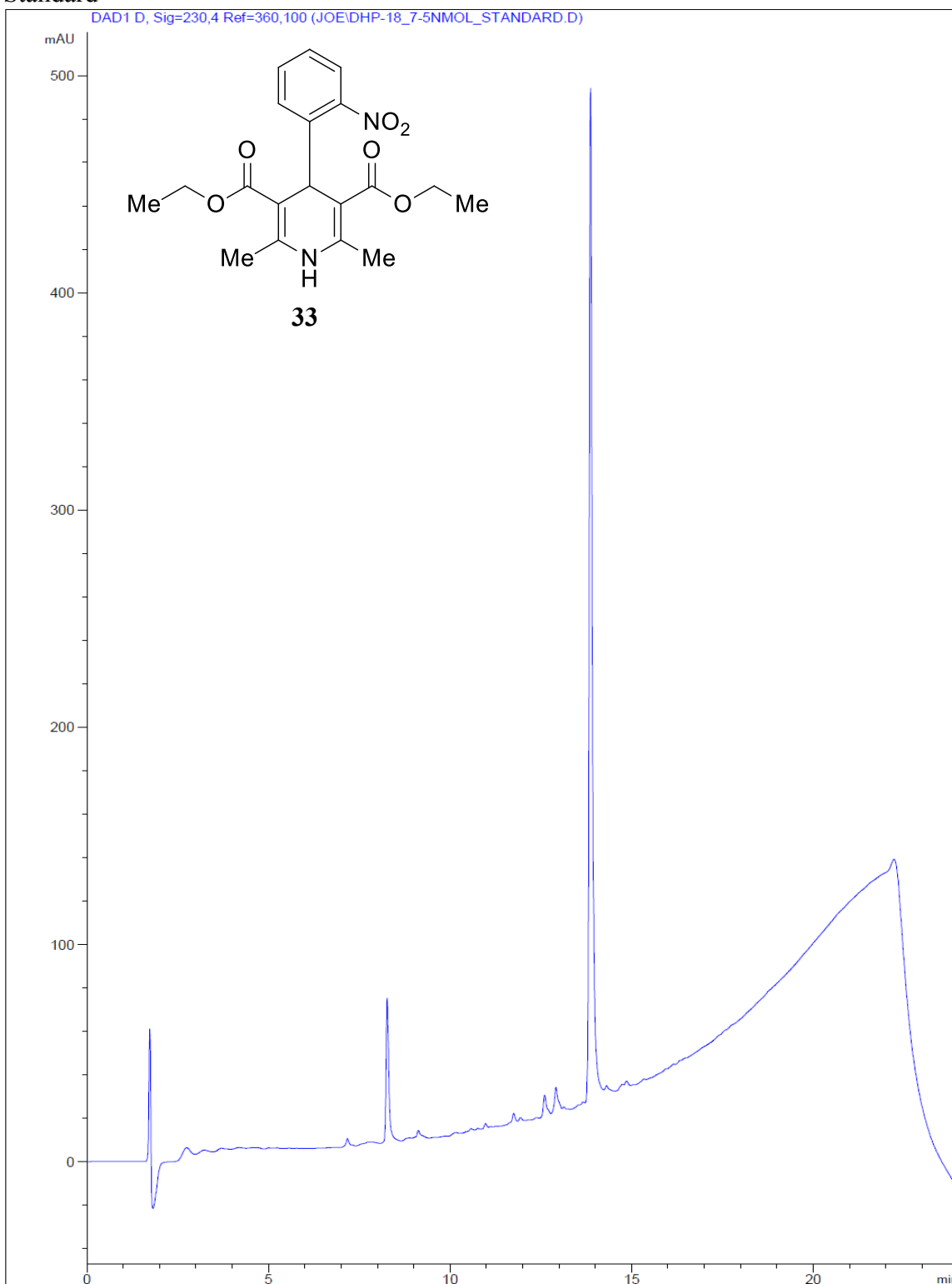


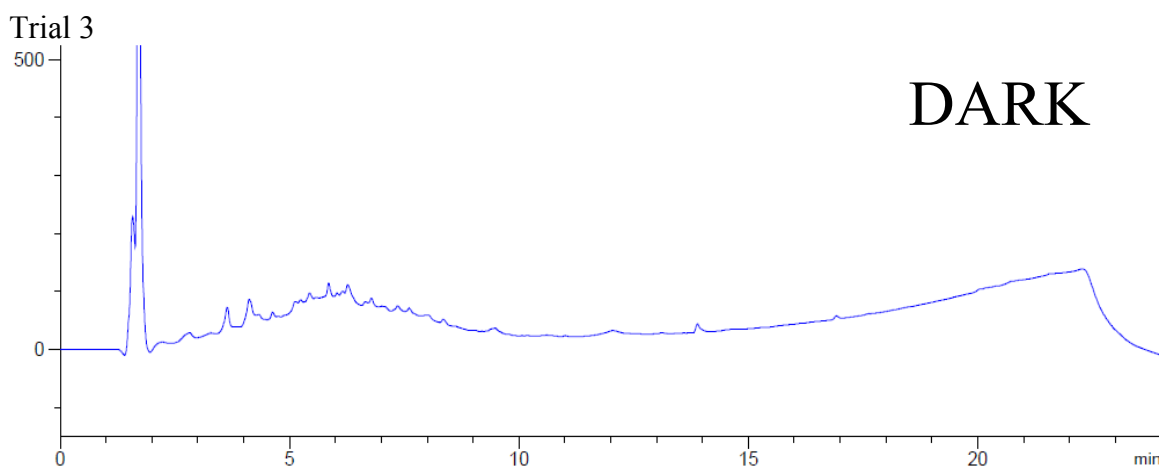
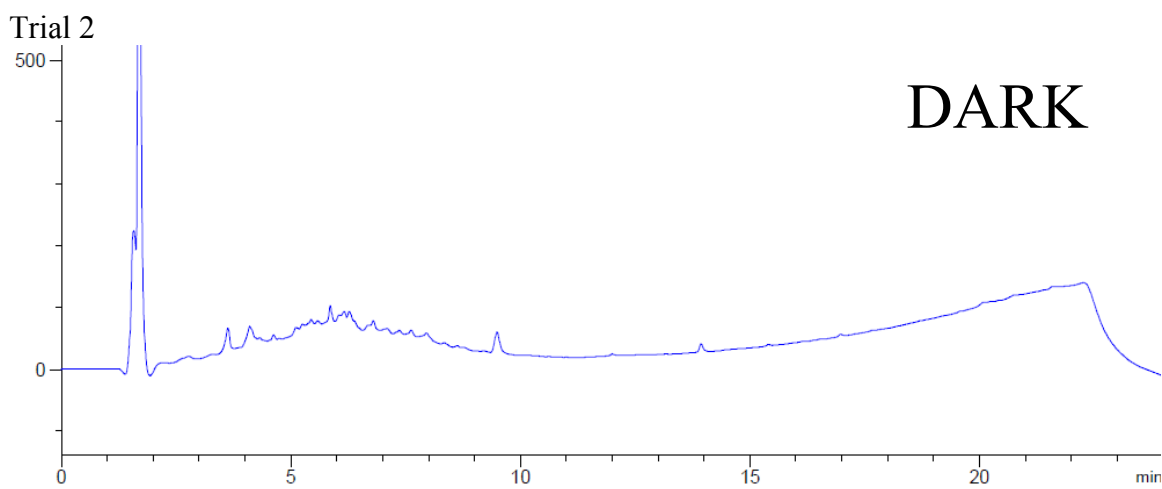
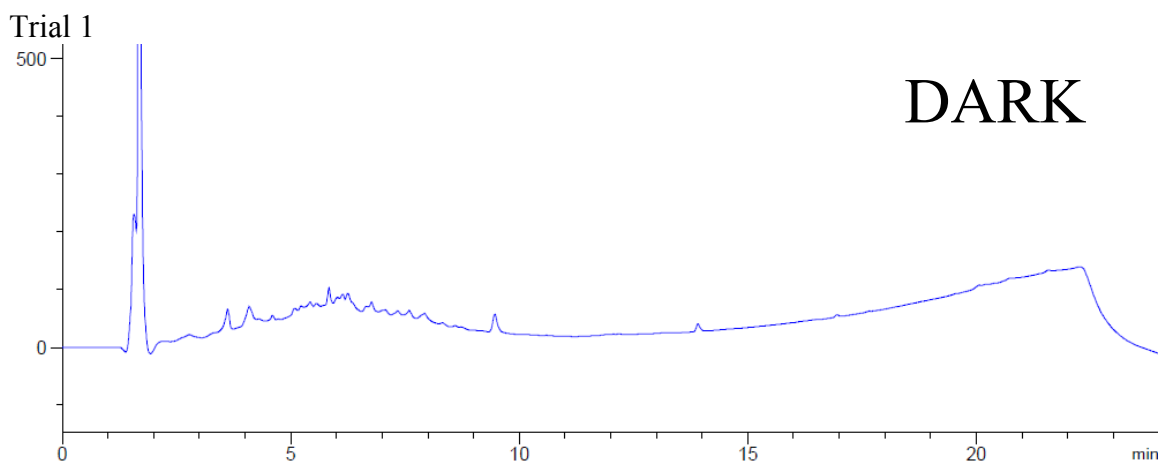
Trial 4



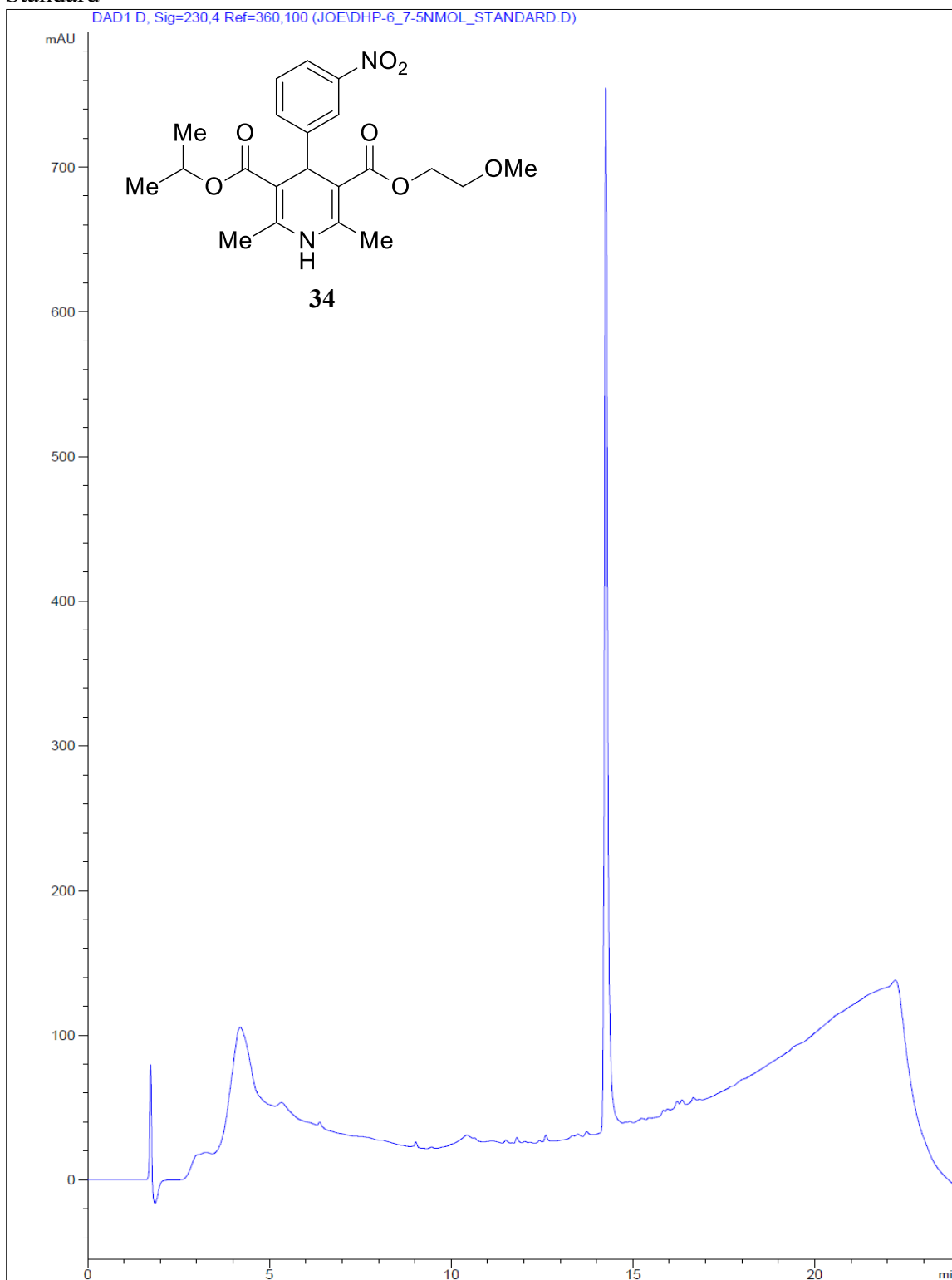
Standard

DAD1 D, Sig=230,4 Ref=360,100 (JOE\DHP-18_7-5NMOL_STANDARD.D)

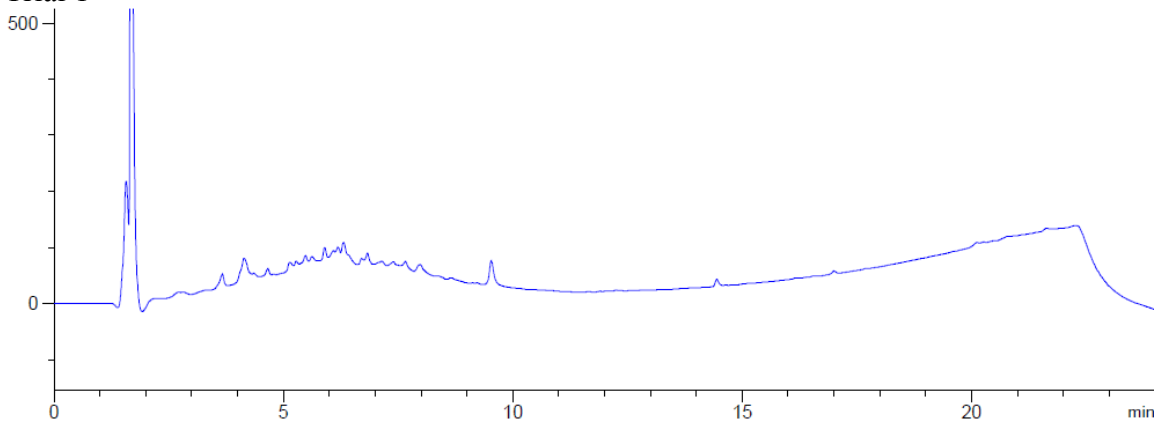




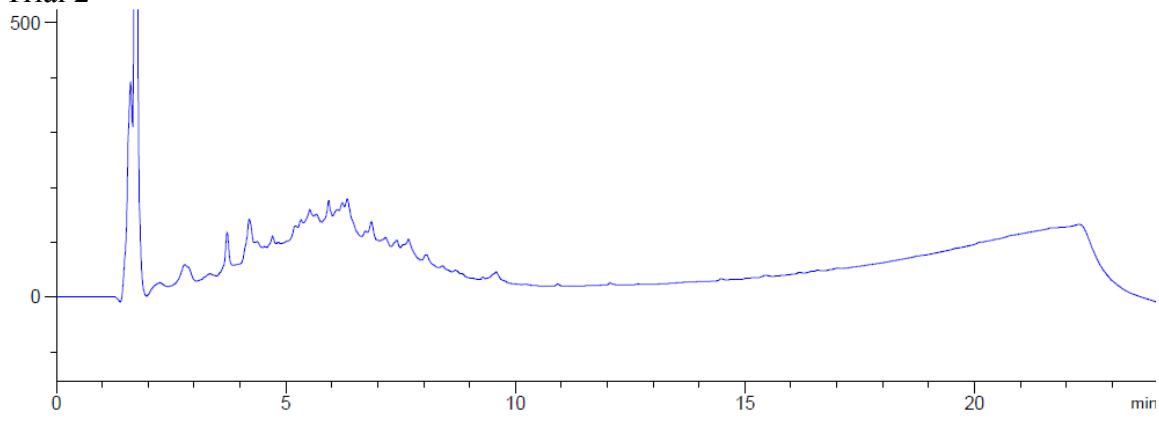
Standard



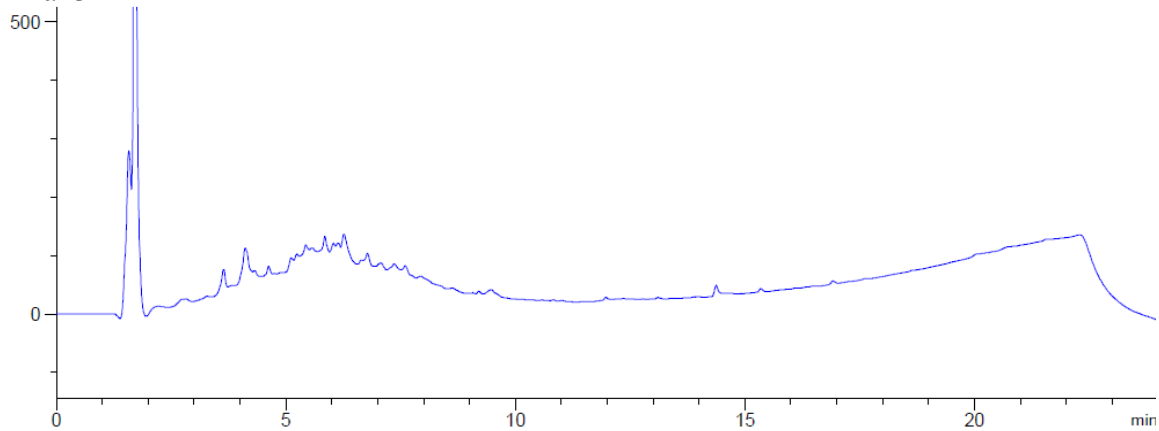
Trial 1



Trial 2

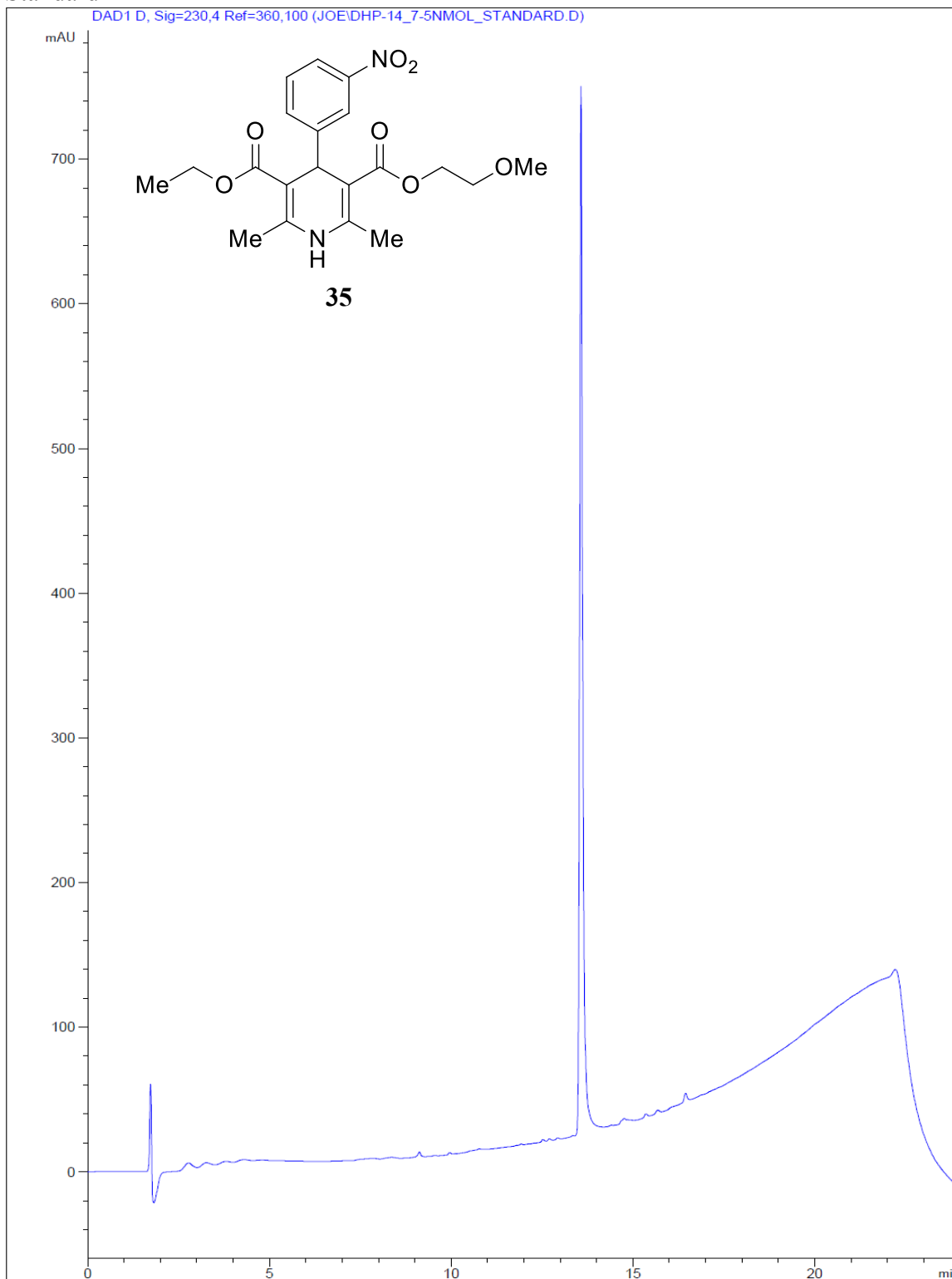


Trial 3

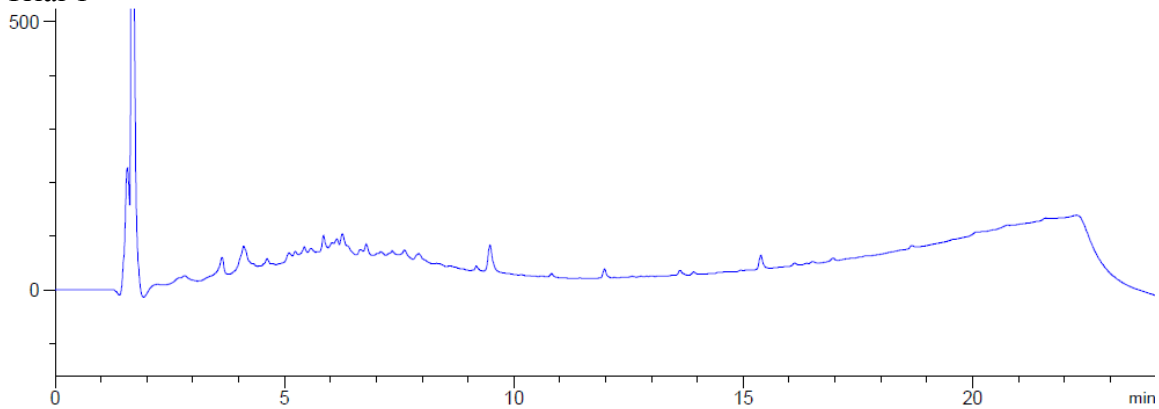


Standard

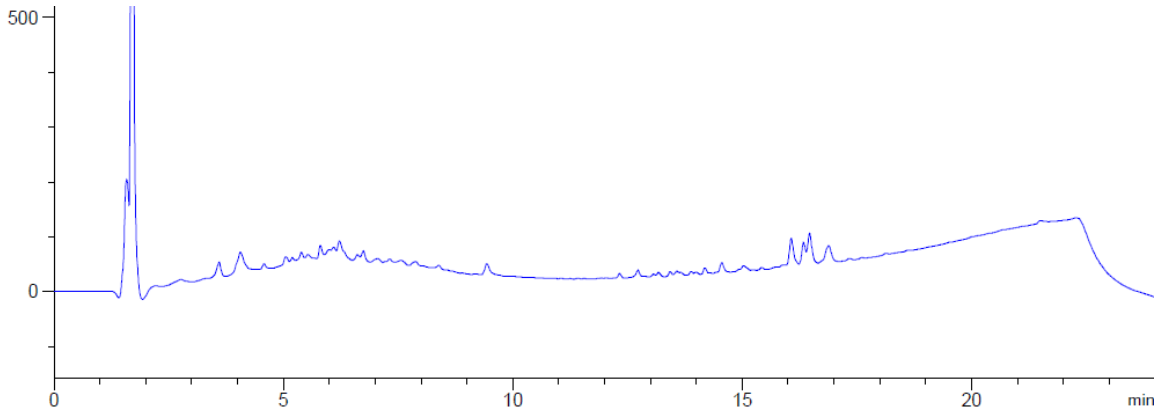
DAD1 D, Sig=230,4 Ref=360,100 (JOEIDHP-14_7-5NMOL_STANDARD.D)



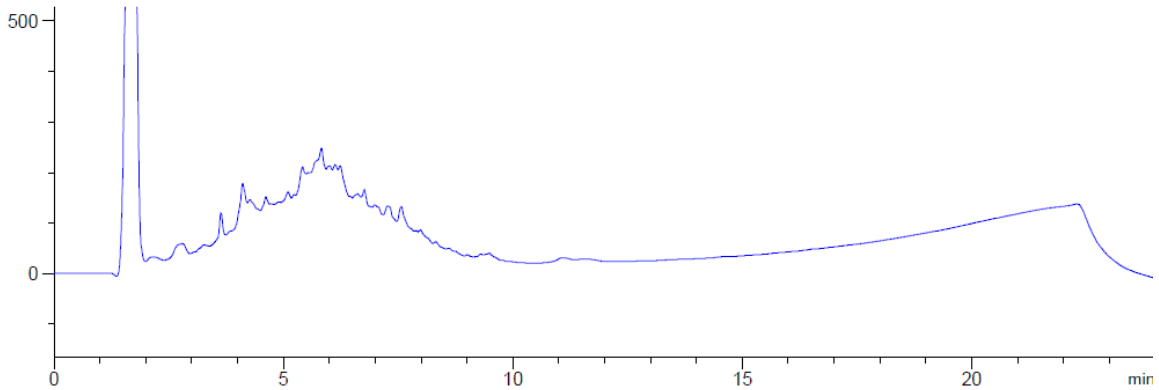
Trial 1



Trial 2

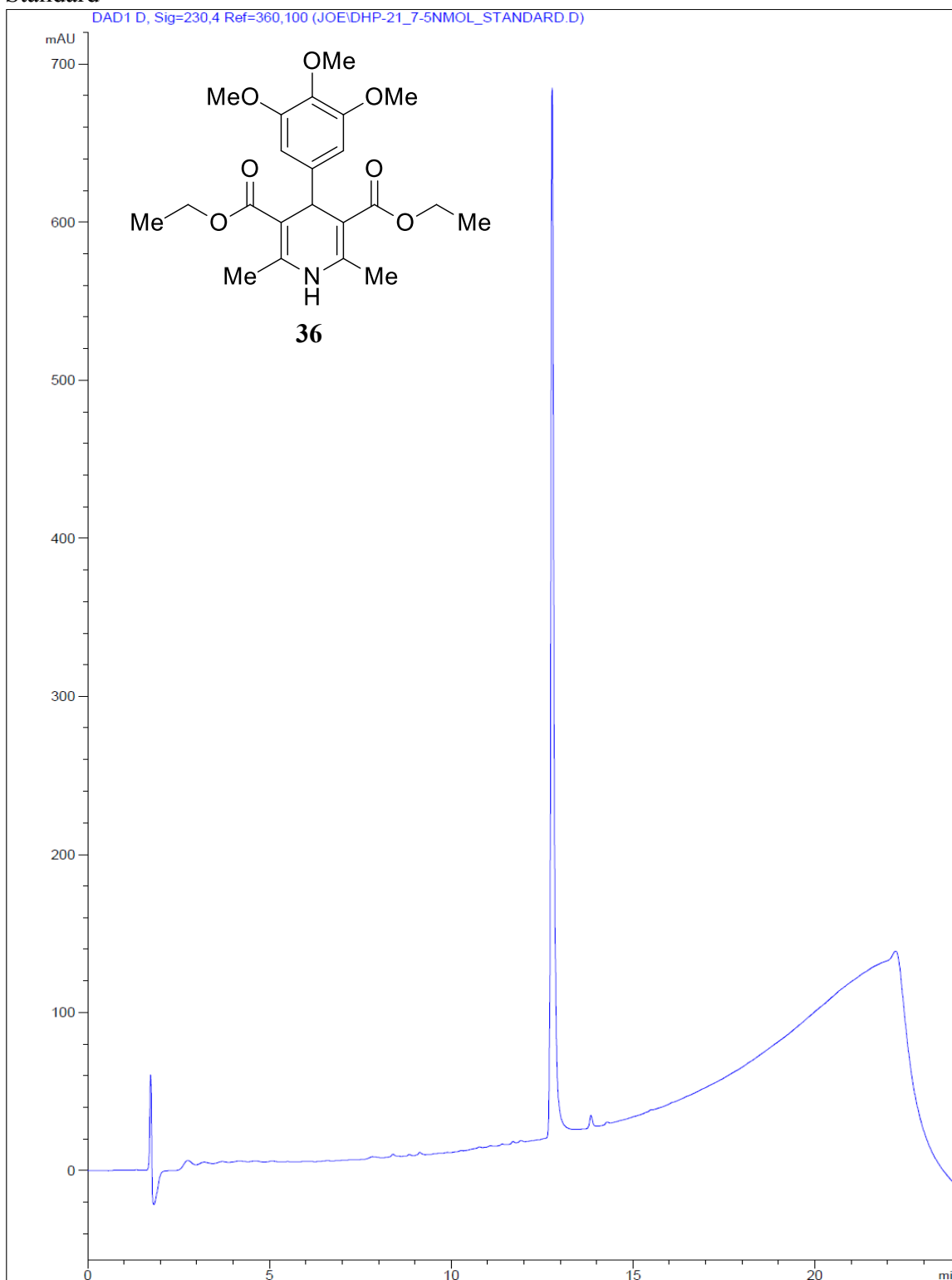


Trial 3

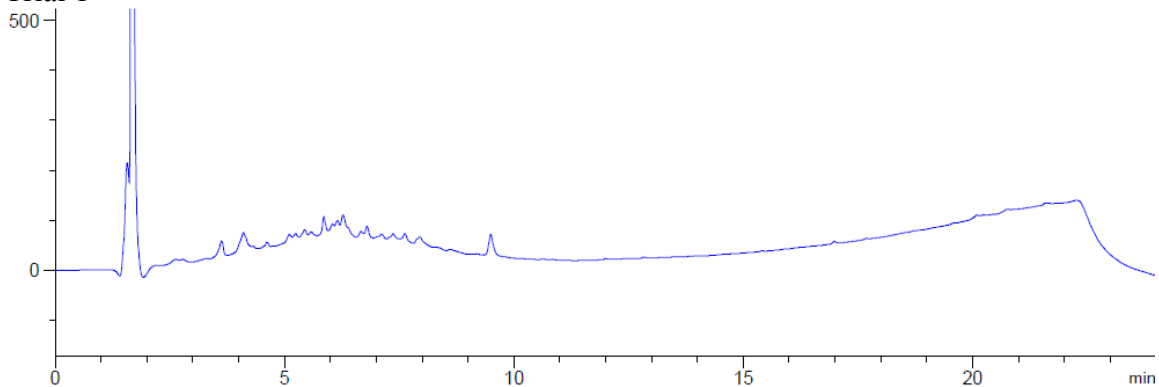


Standard

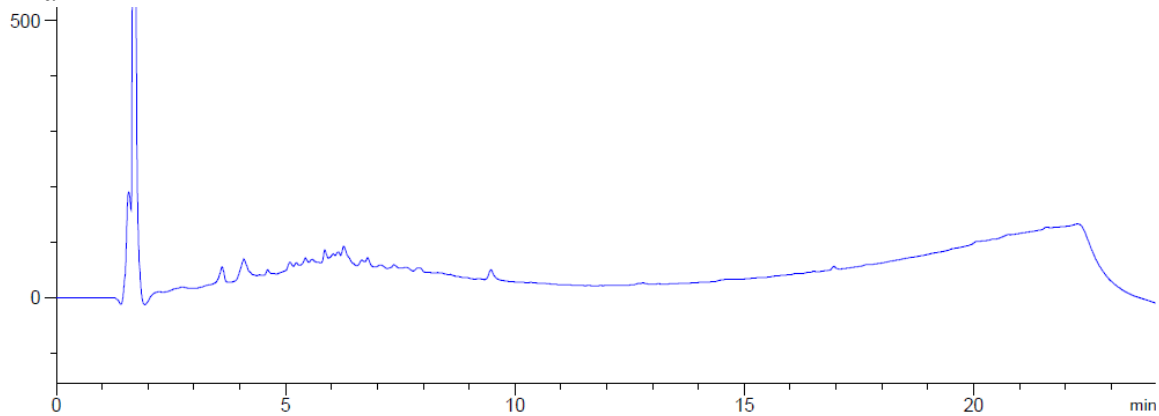
DAD1 D, Sig=230,4 Ref=360,100 (JOE/DHP-21_7-5NMOL_STANDARD.D)



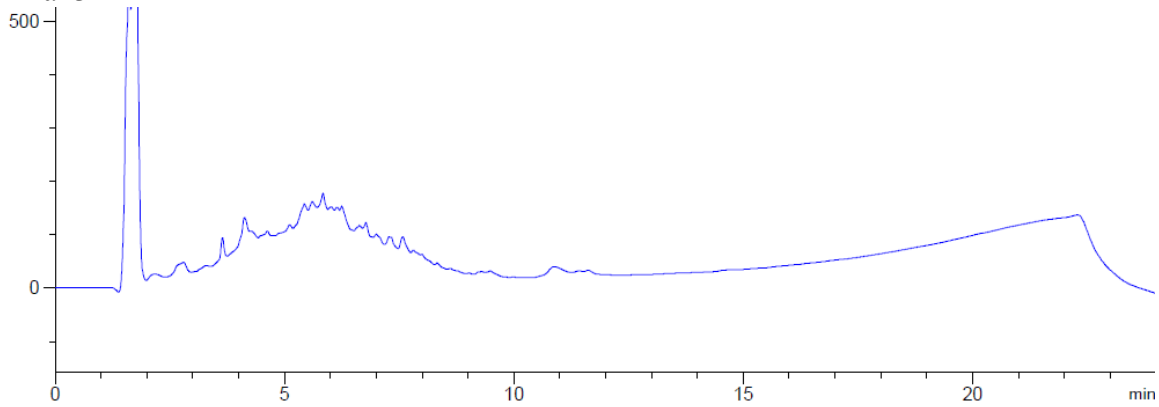
Trial 1



Trial 2

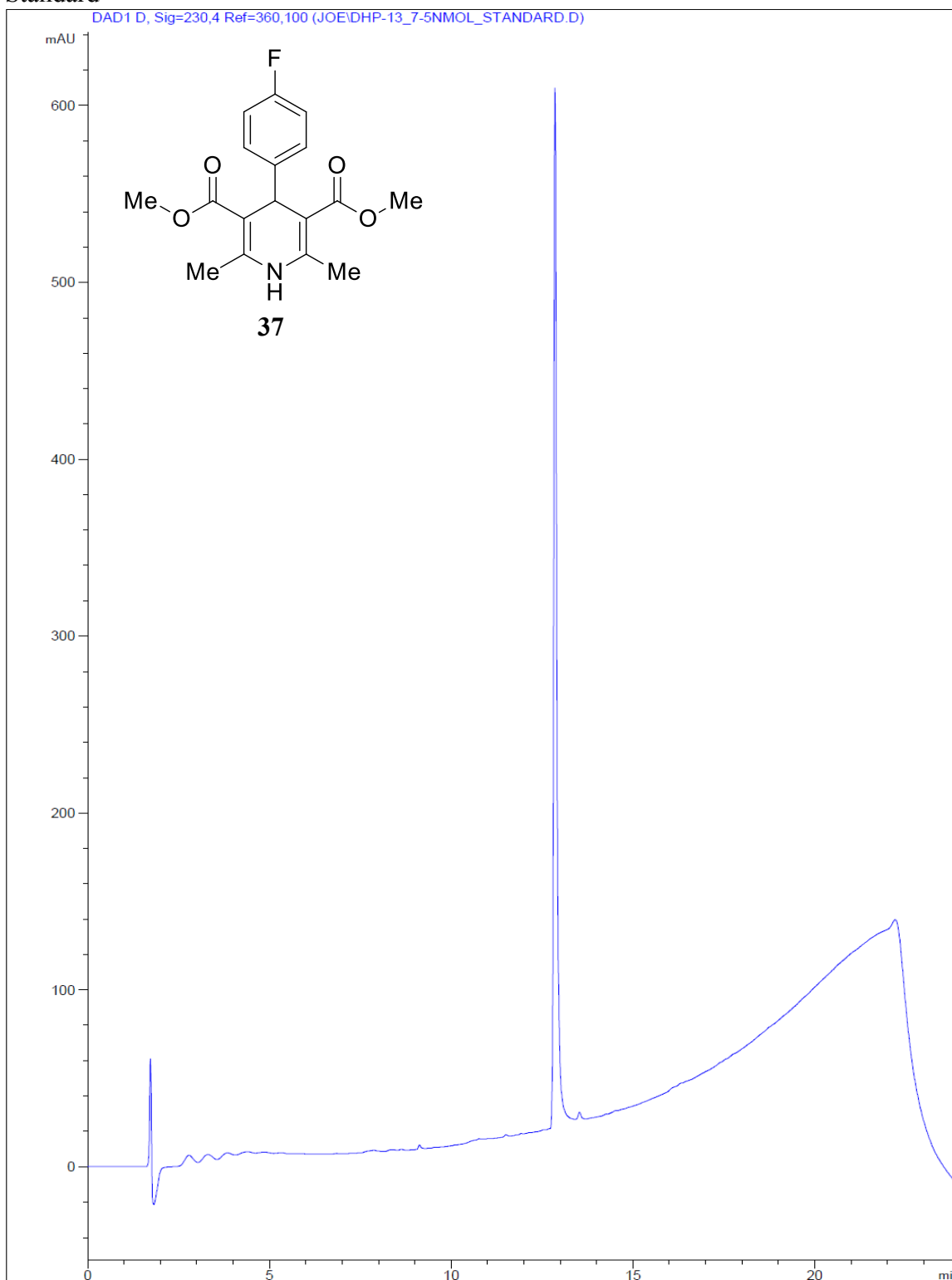


Trial 3

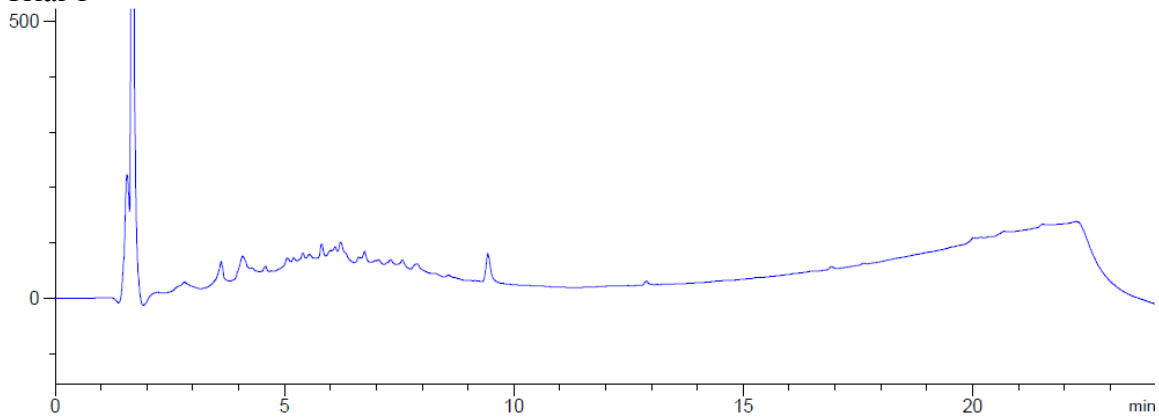


Standard

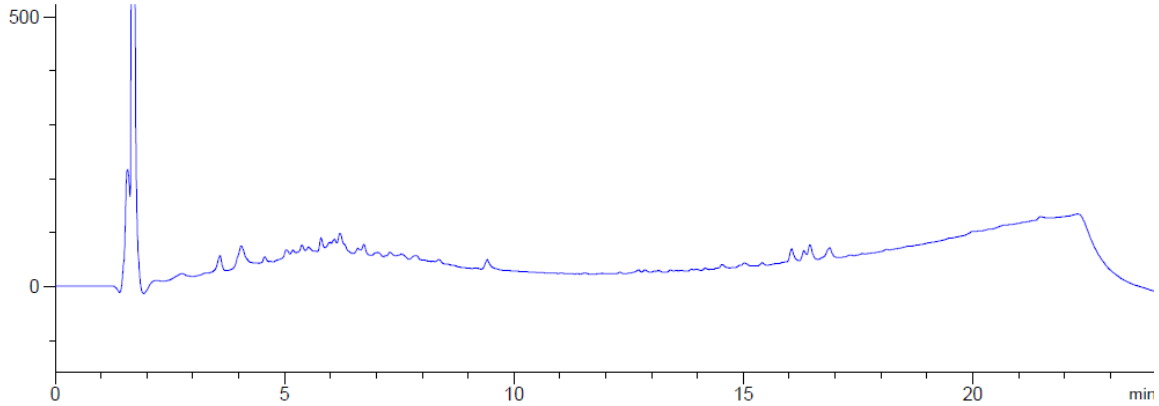
DAD1 D, Sig=230,4 Ref=360,100 (JOE/DHP-13_7-5NMOL_STANDARD.D)



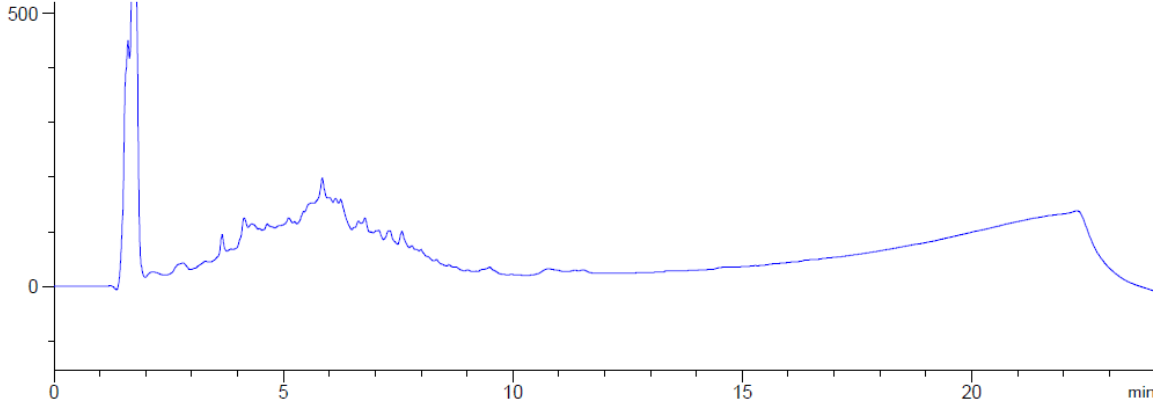
Trial 1



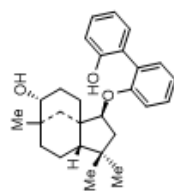
Trial 2



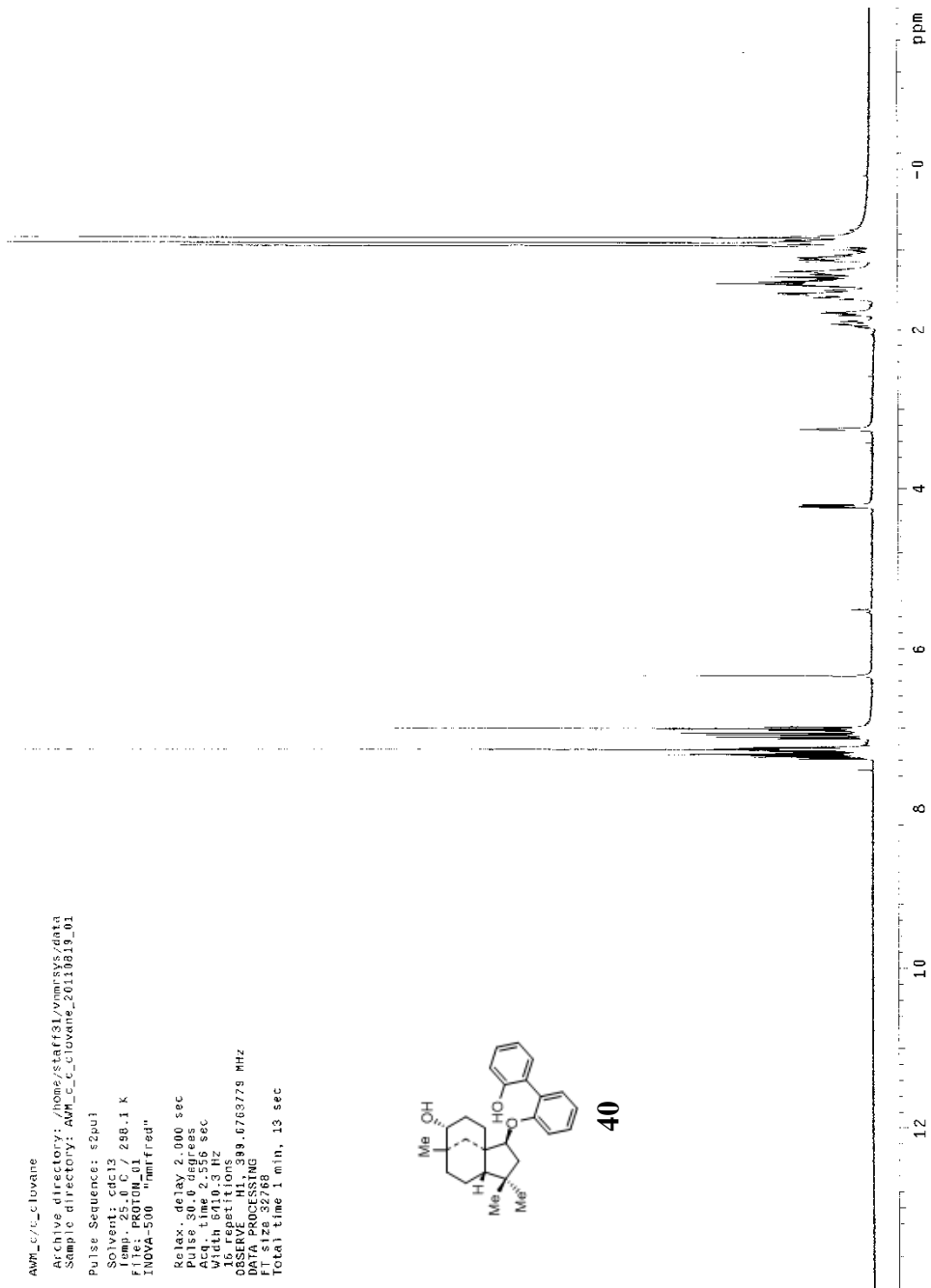
Trial 3



AMP_C7C_clovane
Archive directory: /home/staff31/vnmrSYS/data
Sample directory: AMP_C7C_clovane_20110919_01
Pulse Sequence: e2pul
Solvent: cdcl3
Temp: 25.0 C / 298.1 K
File: PROTON_01
INDYA-500 "nmrfred"
Relax. delay 2.000 sec
Pulse 30.0 degrees
Acq. time 2.330 sec
Width 6010.3 Hz
16 repetitions
OBSERVE H1, 399.6763779 MHz
DATA PROCESSING
F1 732.988
Total time 1 min, 13 sec

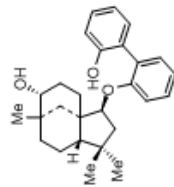


40

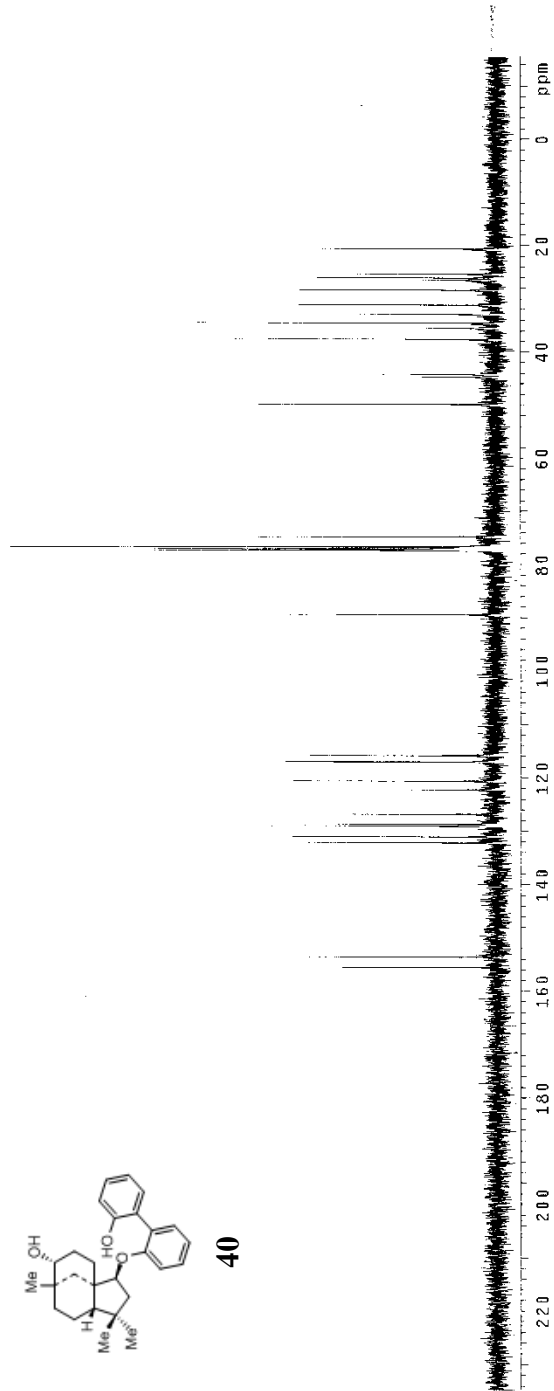


13C OBSERVE

Pulse Sequence: s2pul
Solvent: CDCl3
Ambient temperature
Mercury-400BB "nmr5"
Relax delay 2.000 sec
K1 20.000 sec
Acq: time 1.280 sec
Width 25188.9 Hz
250 repetitions
SOLVENT CH3 40.672277 MHz
DECUPLE H1 400.268355 MHz
Power 38 dB
Continuously on
WALTZ16 simulated
WALTZ16 setting
Line broadening 1.0 Hz
FT size 65536
Total time 4 hr., 42 min., 36 sec

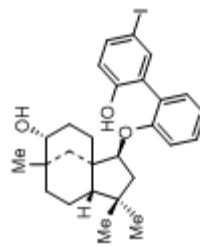


40

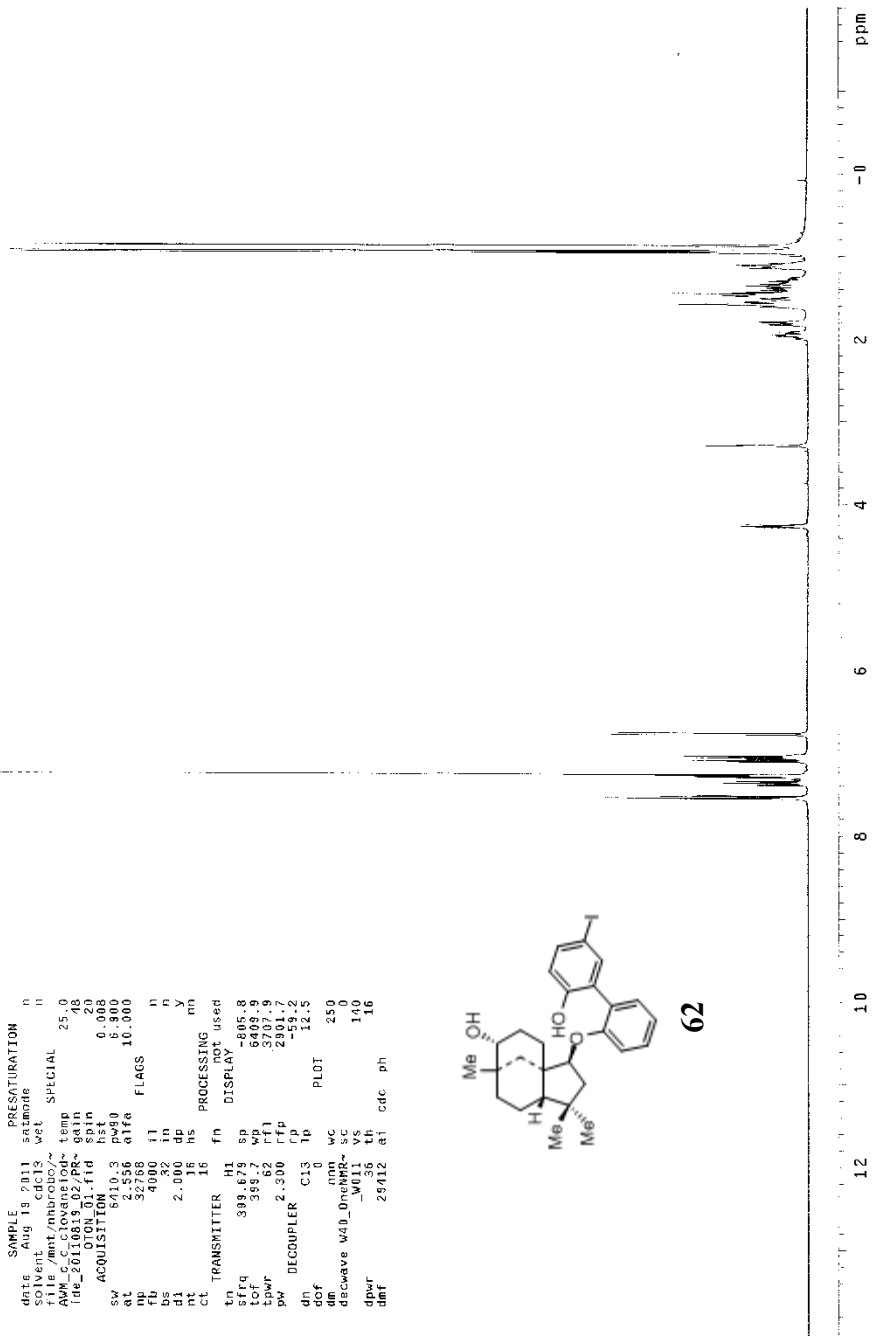


AWH_C/c_clovastatinolide

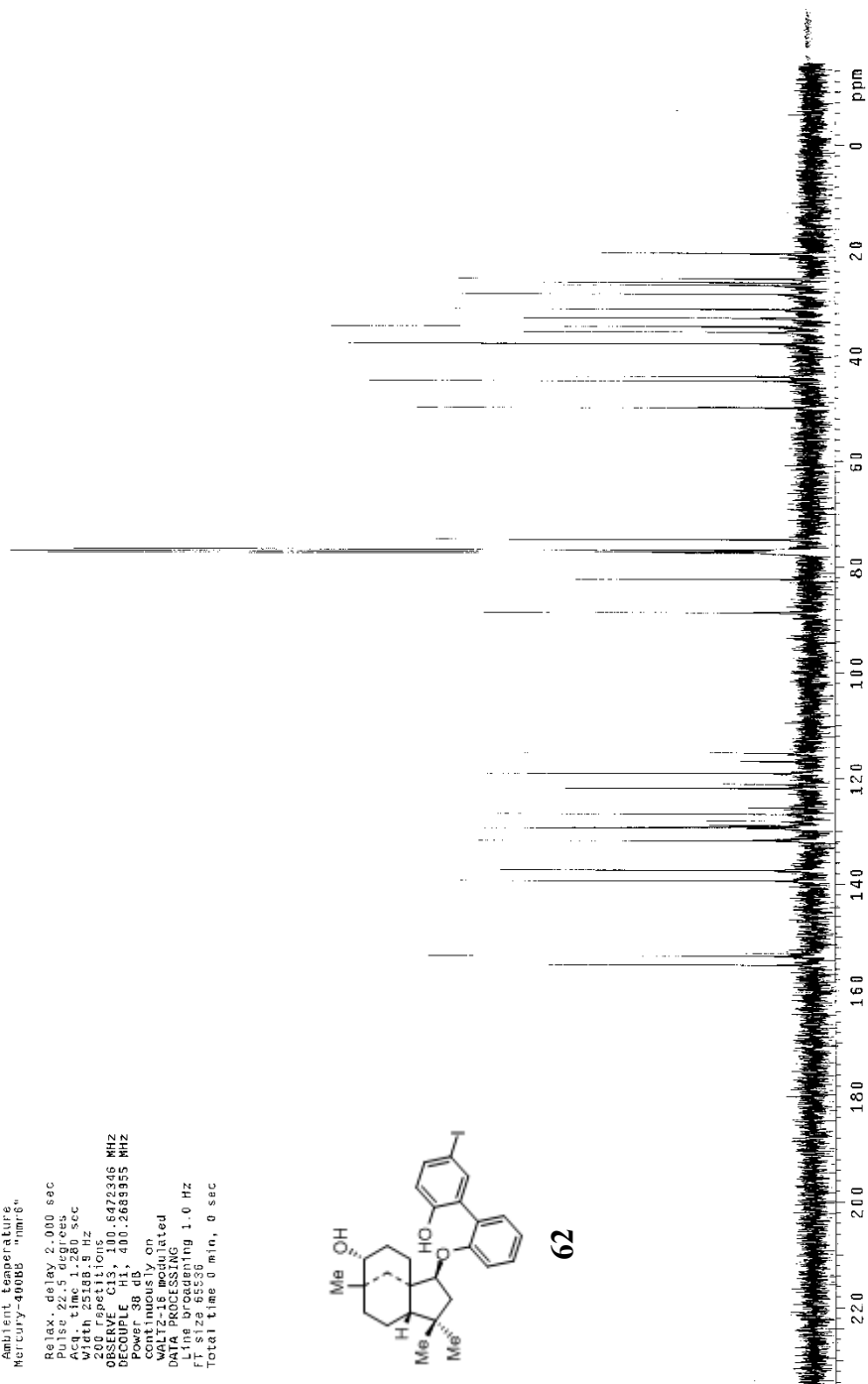
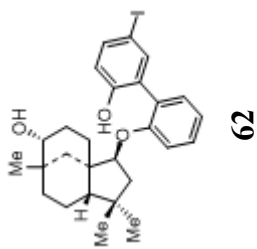
```
exp1  PRUTON
-----
date      Aug 19 2011
solvent   Aug 19 2011
file      /mnt/mbroto/~
AWM_C-Clovastatinolide
Title    20110819_02/PR-
=====
ACQUISITION
-----
sw      6410.3  pw80  5.800
ap      32768  f1    0.008
bs      4192   in    n
d1      2.000  dp    y
nt      16    hs
ct      16    fn
-----
TRANSMITTER HI  fn  PROCESSING  m
-----
tn      16    fn  used
-----
sfrq    399.679  sp    -605.8
tof     398.7  wp    6409.9
tpr     2.62  f1    3707.9
pw      2.500  cp    259.2
-----
dh      C13  tp    12.5
def     0
db      0
deconv  wd0_Dmch
dpr     36  th    140
def     29412  at  cdc  ph  16
-----
```



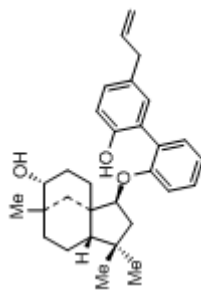
62



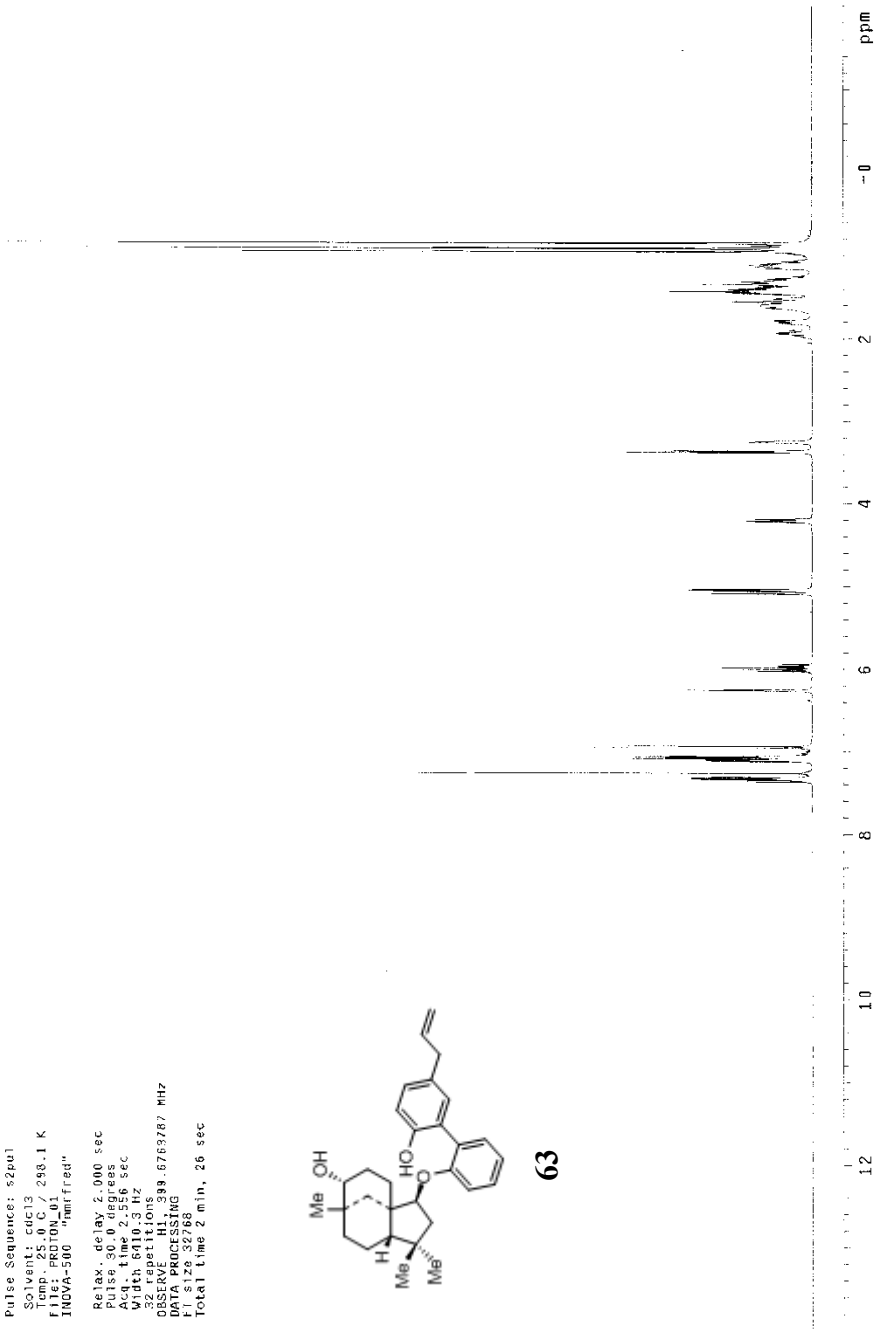
clovane iodide
 Pulse Sequence: s2pul
 Solvent: CDCl3
 Ambient temperature
 Mercury-400088 "nmr6"
 Relax delay: 2.000 sec
 Pulse: 22.5 degrees
 Width: 11.500 sec
 Width: 25146.5 Hz
 200 repetitions
 OBSERVE: C13, 100.6272365 MHz
 INVERT: 48
 Power: 38 dB, 400.2683335 MHz
 continuously on
 WALTZ-16 modulated
 DATA PROCESSING
 F1 size 65536
 F2 size 65536
 Total time 0 min, 0 sec



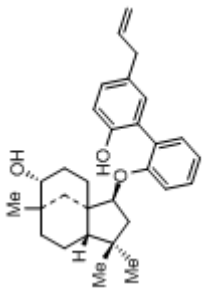
allyliclovane
 Archive directory: /home/staff31/vmatsys/data
 Sample directory: AMW_allyliclovane_20111116_01
 Pulse Sequence: s2pul
 Solvent: cdcl3
 Temp: 25.0 C / 298.1 K
 File: PRDTON_01 "hmrfreq"
 INOVA-500 "hmrfreq"
 Relax. delay: 2.000 sec
 Acq: 30.0 degrees
 Acq: 2.000 sec
 Width: 6010.3 Hz
 32 repetitions
 OBSERVE: H1, 399.6763787 MHz
 DATA PROCESSING
 File: 20111116_01
 Total time: 2 min, 26 sec



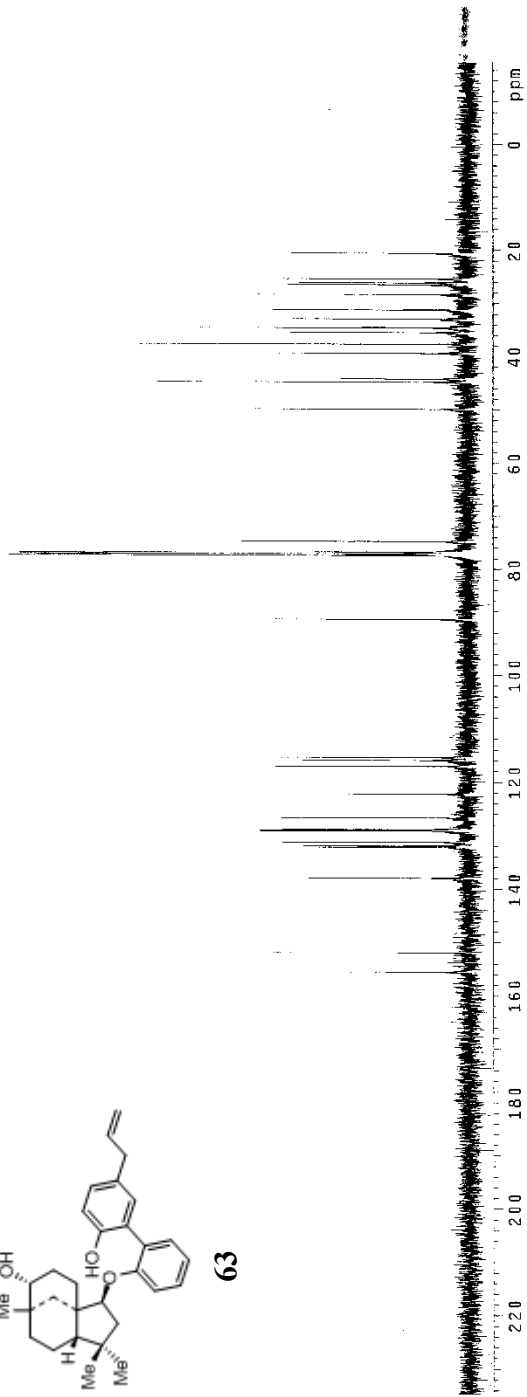
63



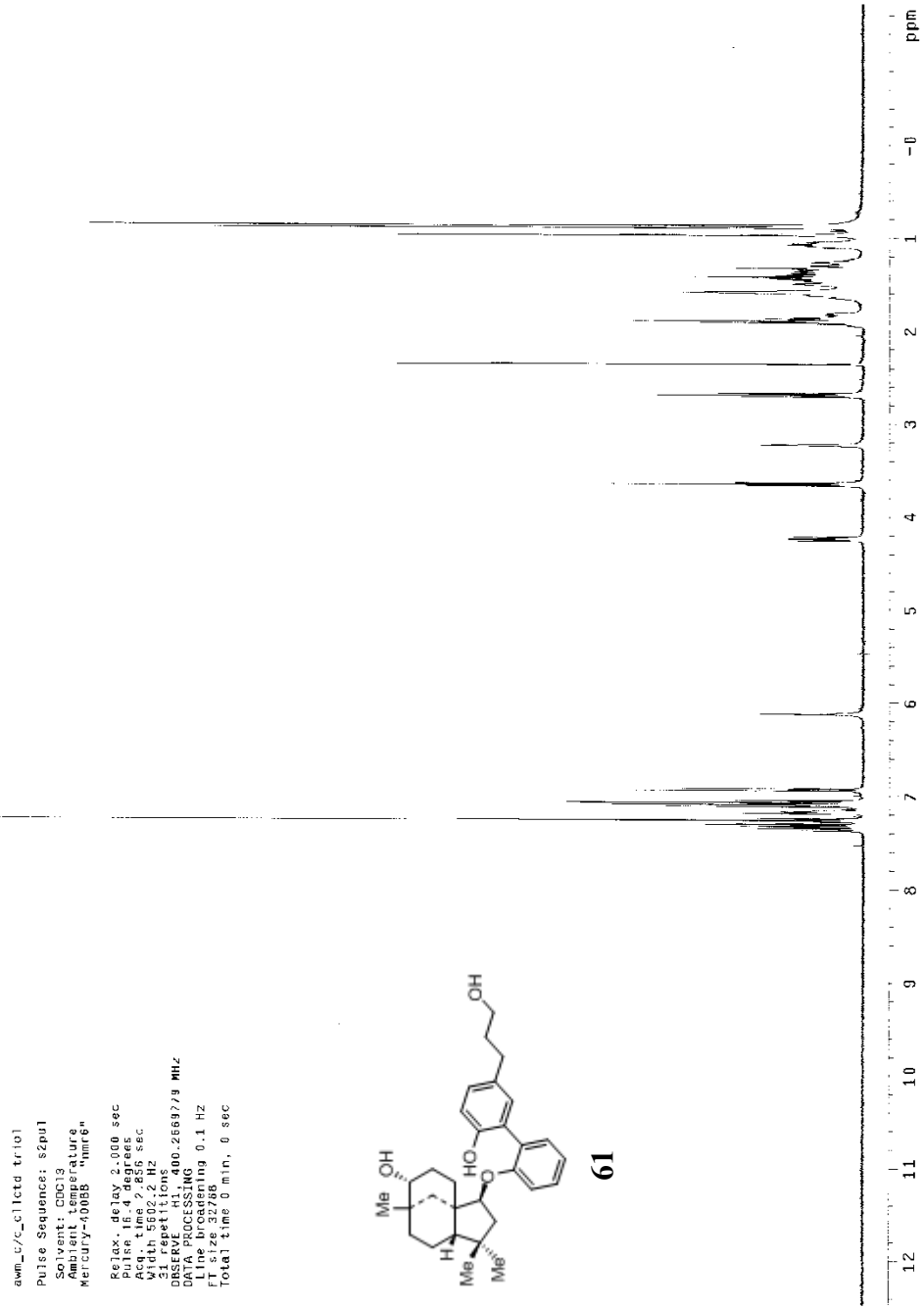
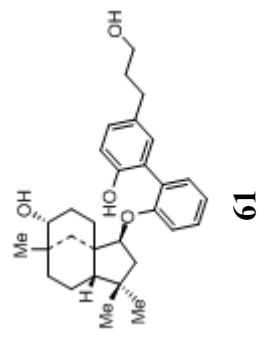
allyl clovanc
Pulse Sequence: zgpg30
Solvent: CDCl3
Acquire Date: 11/11/03
Acquire Time: 10:00:00
Mercury-400BBB "nmr5"
Relax. delay 2.000 sec
Pulse 22.5 degrees
Acq. time 0.200 sec
Width 20483.9 Hz
Waltz 200.000 Hz
250 repetitions
OBSERVE C13, 100.647232 MHz
DECOUPLE H1, 400.2683955 MHz
Spectrum by
continuity on
WALTZ-16 modulated
DATA PROCESSING
Line broadening 1.0 Hz
F2 - 125.760300 MHz
Total time 4 hr., 42 min., 36 sec



63



awm_c/c-cllctd triol
 Pulse Sequence: s2pu1
 Solvent: CDCl3
 Ambient Temperature
 Mercury-00058 "nmr6"
 Relax, delay 2.000 sec
 Pulse PB 4 degrees
 Width 5802.2 Hz
 31 repetitions
 OBSERVE H1, 400.2569779 MHz
 ULTRA PROCESSING
 FT size 32788
 Total time 0 min, 0 sec



clovene triol

Pulse Sequence: s2pul

Solvent: CDCl3

Ambient temperature

Mercury-400MHz "hmr6"

Relax. delay 2.000 sec

Pulse 22.5 degrees

Acq. time 0.260 sec

Width 25166.9 Hz

250 repetitions

OBSERVE C13, 100.6472307 MHz

PCPDPR 38 Hz, 400.2689355 MHz

continuously on

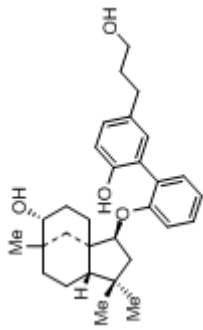
WALTZ-16 modulated

DATA PROCESSING

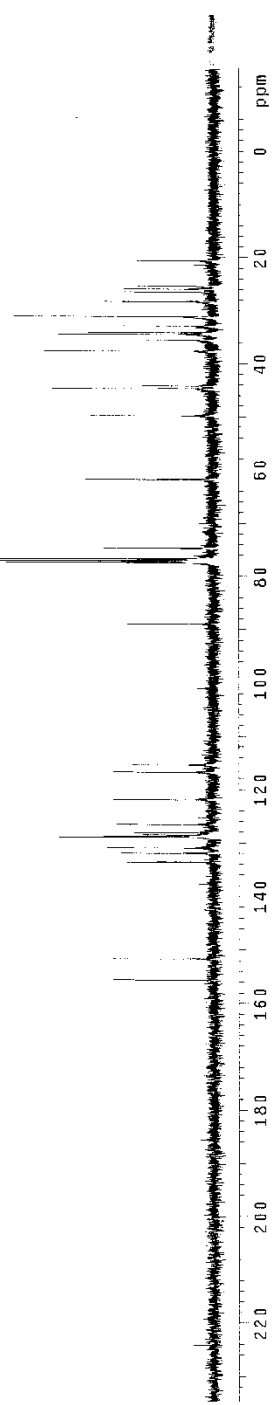
Time Domain

ft of 65531

Total time 4 hr., 42 min., 35 sec



61



References

1. Christopher and Dana Reeve Foundation. *One Degree of Separation: Paralysis and Spinal Cord Injury in the United States* **2009**.
2. DeVivo, M. J., Causes and costs of spinal cord injury in the United States. *Spinal Cord* **1997**, 35 (12), 809-813.
3. Kadoya, K.; Tsukada, S.; Lu, P.; Coppola, G.; Geschwind, D.; Filbin, M. T.; Blesch, A.; Tuszynski, M. H., Combined Intrinsic and Extrinsic Neuronal Mechanisms Facilitate Bridging Axonal Regeneration One Year after Spinal Cord Injury. *Neuron* **2009**, 64 (2), 165-172.
4. McDonald, J. W.; Christopher Reeve Paralysis Foundation., Repairing the damaged spinal cord. *Sci.Am.* **1999**, 281 (3), 64-73.
5. Wilson, R. M.; Danishefsky, S. J., Applications of total synthesis to problems in neurodegeneration: Fascinating chemistry along the way. *Acc Chem Res* **2006**, 39 (8), 539-549.
6. Hawryluk, G. W. J.; Rowland, J.; Kwon, B. K.; Fehlings, M. G., Protection and repair of the injured spinal cord: a review of completed, ongoing, and planned clinical trials for acute spinal cord injury. *Neurosurg. Focus* **2008**, 25 (5).
7. Fehlings, M. G.; Wilson, J. R.; Frankowski, R. F.; Toups, E. G.; Aarabi, B.; Harrop, J. S.; Shaffrey, C. I.; Harkema, S. J.; Guest, J. D.; Tator, C. H.; Burau, K. D.; Johnson, M. W.; Grossman, R. G., Riluzole for the treatment of acute traumatic spinal cord injury: rationale for and design of the NACTN Phase I clinical trial. *J. Neurosurg.-Spine* **2012**, 17, 151-156.
8. Casha, S.; Zygun, D.; McGowan, M. D.; Bains, I.; Yong, V. W.; Hurlbert, R. J., Results of a phase II placebo-controlled randomized trial of minocycline in acute spinal cord injury. *Brain* **2012**, 135, 1224-1236.

9. Hay, M.; Thomas, D. W.; Craighead, J. L.; Economides, C.; Rosenthal, J., Clinical development success rates for investigational drugs. *Nat. Biotechnol.* **2014**, *32* (1), 40-51.
10. Maden, M., Retinoic acid in the development, regeneration and maintenance of the nervous system. *Nat. Rev. Neurosci.* **2007**, *8* (10), 755-765.
11. Corcoran, J.; Shroot, B.; Pizzey, J.; Maden, M., The role of retinoic acid receptors in neurite outgrowth from different populations of embryonic mouse dorsal root ganglia. *J. Cell Sci.* **2000**, *113* (14), 2567-2574.
12. Taha, M. O.; Rosseto, M.; Fraga, M. M.; Mueller, S. F.; Fagundes, D. J.; Novo, N. F.; Caricati-Neto, A., Effect of retinoic acid on tibial nerve regeneration after anastomosis in rats: Histological and functional analyses. *Transplant. Proc.* **2004**, *36* (2), 404-408.
13. Arrieta, O.; Garcia-Navarrete, R.; Zuniga, S.; Ordonez, G.; Ortiz, A.; Palencia, G.; Morales-Espinosa, D.; Hernandez-Pedro, N.; Sotelo, J., Retinoic acid increases tissue and plasma contents of nerve growth factor and prevents neuropathy in diabetic mice. *Eur. J. Clin. Invest.* **2005**, *35* (3), 201-207.
14. Wong, L. F.; Yip, P. K.; Battaglia, A.; Grist, J.; Corcoran, J.; Maden, M.; Azzouz, M.; Kingsman, S. M.; Kingsman, A. J.; Mazarakis, N. D.; McMahon, S. B., Retinoic acid receptor beta 2 promotes functional regeneration of sensory axons in the spinal cord. *Nat. Neurosci.* **2006**, *9* (2), 243-250.
15. Wani, M. C.; Taylor, H. L.; Wall, M. E.; Coggon, P.; McPhail, A. T., Plant antitumor agents. VI. The isolation and structure of taxol, a novel antileukemic and antitumor agent from *Taxus brevifolia*. *J Am Chem Soc* **1971**, *93* (9), 2325-2327.
16. Vuorinen, V.; Roytta, M.; Raine, C. S., The Acute Effects of Taxol Upon Regenerating Axons After Nerve Crush. *Acta Neuropathol.* **1988**, *76* (1), 26-34.
17. Hellal, F.; Hurtado, A.; Ruschel, J.; Flynn, K. C.; Laskowski, C. J.; Umlauf, M.; Kapitein, L. C.; Strikis, D.; Lemmon, V.; Bixby, J.; Hoogenraad, C. C.; Bradke,

- F., Microtubule stabilization reduces scarring and causes axon regeneration after spinal cord injury. *Science* **2011**, *331* (6019), 928-931.
18. Erturk, A.; Hellal, F.; Enes, J.; Bradke, F., Disorganized microtubules underlie the formation of retraction bulbs and the failure of axonal regeneration. *J. Neurosci.* **2007**, *27* (34), 9169-9180.
 19. Sengottuvel, V.; Leibinger, M.; Pfreimer, M.; Andreadaki, A.; Fischer, D., Taxol facilitates axon regeneration in the mature CNS. *J Neurosci* **2011**, *31* (7), 2688-2699.
 20. Sengottuvel, V.; Fischer, D., Facilitating axon regeneration in the injured CNS by microtubules stabilization. *Communicative & integrative biology* **2011**, *4* (4), 391-393.
 21. Gao, Y.; Deng, K. W.; Cao, Z. X.; Graziani, E. I.; Gilbert, A. M.; Koehn, F. E.; Wood, A.; Doherty, P.; Walsh, F. S., Amphotericin B, identified from a natural product screen, antagonizes CNS inhibitors to promote axon growth via activation of an Akt pathway in neurons. *J. Neurochem.* **2010**, *113* (5), 1331-1342.
 22. Weng, M. S.; Liao, C. H.; Yu, S. Y.; Lin, J. K., Garcinol promotes Neurogenesis in Rat Cortical Progenitor Cells through the Duration of Extracellular Signal-Regulated Kinase Signaling. *J. Agric. Food Chem.* **2011**, *59* (3), 1031-1040.
 23. Fujita, M.; Sashida, Y.; Itokawa, H., Honokiol, A New Phenolic Compound Isolated from the Bark of *Magnolia obovata* THUNB. *Chem. Pharm. Bull.* **1972**, *20* (1), 212-213.
 24. Fukuyama, Y.; Nakade, K.; Minoshima, Y.; Yokoyama, R.; Zhai, H.; Mitsumoto, Y., Neurotrophic activity of honokiol on the cultures of fetal rat cortical neurons. *Bioorg Med Chem Lett* **2002**, *12* (8), 1163-1166.
 25. Fukuyama, Y.; Otsoshi, Y.; Kodama, M.; Hasegawa, T.; Okazaki, H., Structure of Clovanemagnolol, a Novel Neurotrophic Sesquiterpene-Neolignan from *Magnolia obovata*. *Tetrahedron Lett.* **1990**, *31* (31), 4477-4480.

26. Fukuyama, Y.; Otsoshi, Y.; Miyoshi, K.; Nakamura, K.; Kodama, M.; Nagasawa, M.; Hasegawa, T.; Okazaki, H.; Sugawara, M., Neurotrophic Sesquiterpene-Neolignans from *Magnolia obovata* - Structure and Neurotrophic Activity. *Tetrahedron* **1992**, *48* (3), 377-392.
27. Khaing, Z.; Kang, D.; Camelio, A. M.; Schmidt, C. E.; Siegel, D., Hippocampal and cortical neuronal growth mediated by the small molecule natural product clovanemagnolol. *Bioorg. Med. Chem. Lett.* **2011**, *21* (16), 4808-4812.
28. Cheng, X.; Harzdorf, N.; Khaing, Z.; Kang, D.; Camelio, A. M.; Shaw, T.; Schmidt, C. E.; Siegel, D., Neuronal growth promoting sesquiterpene-neolignans; syntheses and biological studies. *Org. Biomol. Chem.* **2012**, *10* (2), 383-393.
29. Cheng, X.; Harzdorf, N. L.; Shaw, T.; Siegel, D., Biomimetic Syntheses of the Neurotrophic Natural Products Caryolanemagnolol and Clovanemagnolol. *Org. Lett.* **2010**, *12* (6), 1304-1307.
30. Kumagai, K.; Hosotani, N.; Kikuchi, K.; Kimura, T.; Saji, I., Xanthofulvin, a novel semaphorin inhibitor produced by a strain of *Penicillium*. *J Antibiot (Tokyo)* **2003**, *56* (7), 610-616.
31. Takahashi, T.; Fournier, A.; Nakamura, F.; Wang, L. H.; Murakami, Y.; Kalb, R. G.; Fujisawa, H.; Strittmatter, S. M., Plexin-neuropilin-1 complexes form functional semaphorin-3A receptors. *Cell* **1999**, *99* (1), 59-69.
32. Aoki, M.; Itezono, Y.; Shirai, H.; Nakayama, N.; Sakai, A.; Tanaka, Y.; Yamaguchi, A.; Shimma, N.; Yokose, K.; Seto, H., Structure of a Novel Phospholipase C Inhibitor, Vinaxanthone (RO 09-1450), Produced by *Penicillium vinaceum*. *Tetrahedron Lett.* **1991**, *32* (36), 4737-4740.
33. Kikuchi, K.; Kishino, A.; Konishi, O.; Kumagai, K.; Hosotani, N.; Saji, I.; Nakayama, C.; Kimura, T., In vitro and in vivo characterization of a novel semaphorin 3A inhibitor, SM-216289 or xanthofulvin. *J. Biol. Chem.* **2003**, *278* (44), 42985-42991.
34. Kaneko, S.; Iwanami, A.; Nakamura, M.; Kishino, A.; Kikuchi, K.; Shibata, S.; Okano, H. J.; Ikegami, T.; Moriya, A.; Konishi, O.; Nakayama, C.; Kumagai, K.;

- Kimura, T.; Sato, Y.; Goshima, Y.; Taniguchi, M.; Ito, M.; He, Z. G.; Toyama, Y.; Okano, H., A selective Sema3A inhibitor enhances regenerative responses and functional recovery of the injured spinal cord. *Nat. Med.* **2006**, *12* (12), 1380-1389.
35. Zhang, L.; Kaneko, S.; Kikuchi, K.; Sano, A.; Maeda, M.; Kishino, A.; Shibata, S.; Mukaino, M.; Toyama, Y.; Liu, M. G.; Kimura, T.; Okano, H.; Nakamura, M., Rewiring of regenerated axons by combining treadmill training with semaphorin3A inhibition. *Mol. Brain* **2014**, *7*, 17.
36. Omoto, M.; Yoshida, S.; Miyashita, H.; Kawakita, T.; Yoshida, K.; Kishino, A.; Kimura, T.; Shibata, S.; Tsubota, K.; Okano, H.; Shimmura, S., The Semaphorin 3A Inhibitor SM-345431 Accelerates Peripheral Nerve Regeneration and Sensitivity in a Murine Corneal Transplantation Model. *PLoS One* **2012**, *7* (11), 9.
37. Lee, J. K.; Chow, R.; Xie, F.; Chow, S. Y.; Tolentino, K. E.; Zheng, B. H., Combined Genetic Attenuation of Myelin and Semaphorin-Mediated Growth Inhibition Is Insufficient to Promote Serotonergic Axon Regeneration. *J. Neurosci.* **2010**, *30* (32), 10899-10904.
38. Bleicher, K. H.; Bohm, H. J.; Muller, K.; Alanine, A. I., Hit and lead generation: Beyond high-throughput screening. *Nat. Rev. Drug Discov.* **2003**, *2* (5), 369-378.
39. Brenner, S., Genetics of *Caenorhabditis elegans*. *Genetics* **1974**, *77* (1), 71-94.
40. Altun, Z. F.; Hall, D. H., Introduction. *WormAtlas*, doi:10.3908/wormatlas.1.1 **2009**.
41. Sulston, J. E.; Horvitz, H. R., Post-Embryonic Cell Lineages of the Nematode *Caenorhabditis elegans*. *Dev. Biol.* **1977**, *56* (1), 110-156.
42. Sulston, J. E.; Schierenberg, E.; White, J. G.; Thomson, J. N., The Embryonic Cell Lineage of the Nematode *Caenorhabditis elegans*. *Dev. Biol.* **1983**, *100* (1), 64-119.

43. Hulme, S. E.; Whitesides, G. M., Chemistry and the Worm: *Caenorhabditis elegans* as a Platform for Integrating Chemical and Biological Research. *Angew. Chem.-Int. Edit.* **2011**, *50* (21), 4774-4807.
44. Ardiel, E. L.; Rankin, C. H., An elegant mind: Learning and memory in *Caenorhabditis elegans*. *Learn. Mem.* **2010**, *17* (4), 191-201.
45. Raizen, D. M.; Zimmerman, J. E.; Maycock, M. H.; Ta, U. D.; You, Y. J.; Sundaram, M. V.; Pack, A. I., Lethargus is a *Caenorhabditis elegans* sleep-like state. *Nature* **2008**, *451* (7178), 569-U566.
46. Chalfie, M.; Tu, Y.; Euskirchen, G.; Ward, W. W.; Prasher, D. C., Green Fluorescent Protein as a Marker for Gene Expression. *Science* **1994**, *263* (5148), 802-805.
47. Stiernagle, T., Maintenance of *C. elegans*. *WormBook : the online review of C. elegans biology* **2006**, 1-11.
48. *C. elegans* Sequencing Consortium., Genome sequence of the nematode *C. elegans*: A platform for investigating biology. *Science* **1998**, *282* (5396), 2012-2018.
49. Kenyon, C., The first long-lived mutants: discovery of the insulin/IGF-1 pathway for ageing. *Philos. Trans. R. Soc. B-Biol. Sci.* **2011**, *366* (1561), 9-16.
50. Hengartner, M. O.; Horvitz, H. R., *C. elegans* Cell Survival Gene *ced-9* Encodes a Functional Homolog of the Mammalian Protooncogene *bcl-2*. *Cell* **1994**, *76* (4), 665-676.
51. Kaletta, T.; Hengartner, M. O., Finding function in novel targets: *C. elegans* as a model organism. *Nat. Rev. Drug Discov.* **2006**, *5* (5), 387-398.
52. Harris, T. W.; Chen, N. S.; Cunningham, F.; Tello-Ruiz, M.; Antoshechkin, I.; Bastiani, C.; Bieri, T.; Blasiar, D.; Bradnam, K.; Chan, J.; Chen, C. K.; Chen, W. J.; Davis, P.; Kenny, E.; Kishore, R.; Lawson, D.; Lee, R.; Muller, H. M.; Nakamura, C.; Ozersky, P.; Petcherski, A.; Rogers, A.; Sabo, A.; Schwarz, E. M.;

- Van Auken, K.; Wang, Q. H.; Durbin, R.; Spieth, J.; Sternberg, P. W.; Stein, L. D., WormBase: a multi-species resource for nematode biology and genomics. *Nucleic Acids Res.* **2004**, *32*, D411-D417.
53. Fire, A.; Xu, S. Q.; Montgomery, M. K.; Kostas, S. A.; Driver, S. E.; Mello, C. C., Potent and specific genetic interference by double-stranded RNA in *Caenorhabditis elegans*. *Nature* **1998**, *391* (6669), 806-811.
54. Kamath, R. S.; Fraser, A. G.; Dong, Y.; Poulin, G.; Durbin, R.; Gotta, M.; Kanapin, A.; Le Bot, N.; Moreno, S.; Sohrmann, M.; Welchman, D. P.; Zipperlen, P.; Ahringer, J., Systematic functional analysis of the *Caenorhabditis elegans* genome using RNAi. *Nature* **2003**, *421* (6920), 231-237.
55. Artal-Sanz, M.; de Jong, L.; Tavernarakis, N., *Caenorhabditis elegans*: A versatile platform for drug discovery. *Biotechnology Journal* **2006**, *1* (12), 1405-1418.
56. Silverman, G. A.; Luke, C. J.; Bhatia, S. R.; Long, O. S.; Vetica, A. C.; Perlmutter, D. H.; Pak, S. C., Modeling Molecular and Cellular Aspects of Human Disease Using the Nematode *Caenorhabditis elegans*. *Pediatr. Res.* **2009**, *65* (1), 10-18.
57. Lakso, M.; Vartiainen, S.; Moilanen, A. M.; Sirvio, J.; Thomas, J. H.; Nass, R.; Blakely, R. D.; Wong, G., Dopaminergic neuronal loss and motor deficits in *Caenorhabditis elegans* overexpressing human alpha-synuclein. *J. Neurochem.* **2003**, *86* (1), 165-172.
58. Lublin, A. L.; Link, C. D., Alzheimer's disease drug discovery: in vivo screening using *Caenorhabditis elegans* as a model for beta-amyloid peptide-induced toxicity. *Drug discovery today. Technologies* **2013**, *10* (1), e115-119.
59. Dempsey, C. M.; Mackenzie, S. M.; Gargus, A.; Blanco, G.; Sze, J. Y., Serotonin (5HT), fluoxetine, imipramine and dopamine target distinct 5HT receptor signaling to modulate *Caenorhabditis elegans* egg-laying behavior. *Genetics* **2005**, *169* (3), 1425-1436.
60. Alegado, R. A.; Campbell, M. C.; Chen, W. C.; Slutz, S. S.; Tan, M. W., Characterization of mediators of microbial virulence and innate immunity using

- the *Caenorhabditis elegans* host-pathogen model. *Cell Microbiol.* **2003**, *5* (7), 435-444.
61. Siddiqui, S. S.; Loganathan, S.; Krishnaswamy, S.; Faoro, L.; Jagadeeswaran, R.; Salgia, R., *C. elegans* as a model organism for in vivo screening in cancer: effects of human c-Met in lung cancer affect *C. elegans* vulva phenotypes. *Cancer Biol. Ther.* **2008**, *7* (6), 856-863.
 62. Culetto, E.; Sattelle, D. B., A role for *Caenorhabditis elegans* in understanding the function and interactions of human disease genes. *Hum. Mol. Genet.* **2000**, *9* (6), 869-877.
 63. Perkins, L. A.; Hedgecock, E. M.; Thomson, J. N.; Culotti, J. G., Mutant Sensory Cilia in the Nematode *Caenorhabditis elegans*. *Dev. Biol.* **1986**, *117* (2), 456-487.
 64. Smith, H.; Campbell, W. C., Effect of ivermectin on *Caenorhabditis elegans* larvae previously exposed to alcoholic immobilization. *J. Parasitol.* **1996**, *82* (1), 187-188.
 65. Choy, R. K. M.; Kemner, J. M.; Thomas, J. H., Fluoxetine-resistance genes in *Caenorhabditis elegans* function in the intestine and may act in drug transport. *Genetics* **2006**, *172* (2), 885-892.
 66. Rand, J. B.; Johnson, C. D., Genetic pharmacology: Interactions between drugs and gene products in *Caenorhabditis elegans*. *Methods in Cell Biology, Vol 48* **1995**, *48*, 187-204.
 67. Gaud, A.; Simon, J. M.; Witzel, T.; Carre-Pierrat, M.; Wermuth, C. G.; Segalat, L., Prednisone reduces muscle degeneration in dystrophin-deficient *Caenorhabditis elegans*. *Neuromusc. Disord.* **2004**, *14* (6), 365-370.
 68. Giacomotto, J.; Segalat, L., High-throughput screening and small animal models, where are we? *Br. J. Pharmacol.* **2010**, *160* (2), 204-216.
 69. Jones, A. K.; Buckingham, S. D.; Sattelle, D. B., Chemistry-to-gene screens in *Caenorhabditis elegans*. *Nat. Rev. Drug Discov.* **2005**, *4* (4), 321-330.

70. Lackner, M. R.; Kindt, R. M.; Carroll, P. M.; Brown, K.; Cancilla, M. R.; Chen, C. Y.; de Silva, H.; Franke, Y.; Guan, B.; Heuer, T.; Hung, T.; Keegan, K.; Lee, J. M.; Manne, V.; O'Brien, C.; Parry, D.; Perez-Villar, J. J.; Reddy, R. K.; Xiao, H. J.; Zhan, H. J.; Cockett, M.; Plowman, G.; Fitzgerald, K.; Costa, M.; Ross-Macdonald, P., Chemical genetics identifies Rab geranylgeranyl transferase as an apoptotic target of farnesyl transferase inhibitors. *Cancer Cell* **2005**, *7* (4), 325-336.
71. Kwok, T. C. Y.; Ricker, N.; Fraser, R.; Chan, A. W.; Burns, A.; Stanley, E. F.; McCourt, P.; Cutler, S. R.; Roy, P. J., A small-molecule screen in *C. elegans* yields a new calcium channel antagonist. *Nature* **2006**, *441* (7089), 91-95.
72. Waggoner, L. E.; Dickinson, K. A.; Poole, D. S.; Tabuse, Y.; Miwa, J.; Schafer, W. R., Long-term nicotine adaptation in *Caenorhabditis elegans* involves PKC-dependent changes in nicotinic receptor abundance. *J. Neurosci.* **2000**, *20* (23), 8802-8811.
73. Davies, A. G.; Pierce-Shimomura, J. T.; Kim, H.; VanHoven, M. K.; Thiele, T. R.; Bonci, A.; Bargmann, C. I.; McIntire, S. L., A central role of the BK potassium channel in behavioral responses to ethanol in *C. elegans*. *Cell* **2003**, *115* (6), 655-666.
74. Simpson, V. J.; Johnson, T. E., Genetic models in the study of anesthetic drug action. *International Review of Neurobiology*, Vol 39 **1996**, *39*, 223-241.
75. Ranganathan, R.; Sawin, E. R.; Trent, C.; Horvitz, H. R., Mutations in the *Caenorhabditis elegans* serotonin reuptake transporter MOD-5 reveal serotonin-dependent and -independent activities of fluoxetine. *J. Neurosci.* **2001**, *21* (16), 5871-5884.
76. Nguyen, M.; Alfonso, A.; Johnson, C. D.; Rand, J. B., *Caenorhabditis elegans* Mutants Resistant to Inhibitors of Acetylcholinesterase. *Genetics* **1995**, *140* (2), 527-535.
77. Bargmann, C. I., Neurobiology of the *Caenorhabditis elegans* genome. *Science* **1998**, *282* (5396), 2028-2033.

78. White, J. G.; Southgate, E.; Thomson, J. N.; Brenner, S., The Structure of the Nervous System of the Nematode *Caenorhabditis elegans*. *Philos. Trans. R. Soc. Lond. Ser. B-Biol. Sci.* **1986**, *314* (1165), 1-340.
79. Varshney, L. R.; Chen, B. L.; Paniagua, E.; Hall, D. H.; Chklovskii, D. B., Structural Properties of the *Caenorhabditis elegans* Neuronal Network. *PLoS Comput. Biol.* **2011**, *7* (2), 21.
80. Mohamed, A. M.; Boudreau, J. R.; Yu, F. P. S.; Liu, J.; Chin-Sang, I. D., The *Caenorhabditis elegans* Eph Receptor Activates NCK and N-WASP, and Inhibits Ena/VASP to Regulate Growth Cone Dynamics during Axon Guidance. *PLoS Genet.* **2012**, *8* (2).
81. Ishii, N.; Wadsworth, W. G.; Stern, B. D.; Culotti, J. G.; Hedgecock, E. M., UNC-6, A Laminin-Related Protein, Guides Cell and Pioneer Axon Migrations in *C. elegans*. *Neuron* **1992**, *9* (5), 873-881.
82. Gabel, C. V.; Antonie, F.; Chuang, C. F.; Samuel, A. D. T.; Chang, C., Distinct cellular and molecular mechanisms mediate initial axon development and adult-stage axon regeneration in *C. elegans*. *Development* **2008**, *135* (6), 1129-1136.
83. El Bejjani, R.; Hammarlund, M., Neural Regeneration in *Caenorhabditis elegans*. *Annu. Rev. Genet.* **2012**, *46*, 499-513.
84. Yanik, M. F.; Cinar, H.; Cinar, H. N.; Chisholm, A. D.; Jin, Y. S.; Ben-Yakar, A., Neurosurgery - Functional regeneration after laser axotomy. *Nature* **2004**, *432* (7019), 822-822.
85. Ghosh-Roy, A.; Chisholm, A. D., *Caenorhabditis elegans*: A New Model Organism for Studies of Axon Regeneration. *Dev. Dyn.* **2010**, *239* (5), 1460-1464.
86. Rao, G. N.; Kulkarni, S. S.; Koushika, S. P.; Rau, K. R., In vivo nanosecond laser axotomy: cavitation dynamics and vesicle transport. *Opt. Express* **2008**, *16* (13), 9884-9894.

87. Bourgeois, F.; Ben-Yakar, A., Femtosecond laser nanoaxotomy properties and their effect on axonal recovery in *C. elegans* (vol 15, pg 8521, 2007). *Opt. Express* **2008**, *16* (8), 5963-5963.
88. Chen, L. Z.; Wang, Z. P.; Ghosh-Roy, A.; Hubert, T.; Yan, D.; O'Rourke, S.; Bowerman, B.; Wu, Z. L.; Jin, Y. S.; Chisholm, A. D., Axon Regeneration Pathways Identified by Systematic Genetic Screening in *C. elegans*. *Neuron* **2011**, *71* (6), 1043-1057.
89. Chen, L. Z.; Chisholm, A. D., Axon regeneration mechanisms: insights from *C. elegans*. *Trends Cell Biol.* **2011**, *21* (10), 577-584.
90. Hammarlund, M.; Nix, P.; Hauth, L.; Jorgensen, E. M.; Bastiani, M., Axon Regeneration Requires a Conserved MAP Kinase Pathway. *Science* **2009**, *323* (5915), 802-806.
91. Ghosh-Roy, A.; Wu, Z. L.; Goncharov, A.; Jin, Y. S.; Chisholm, A. D., Calcium and Cyclic AMP Promote Axonal Regeneration in *Caenorhabditis elegans* and Require DLK-1 Kinase. *J. Neurosci.* **2010**, *30* (9), 3175-3183.
92. Samara, C.; Rohde, C. B.; Gilleland, C. L.; Norton, S.; Haggarty, S. J.; Yanik, M. F., Large-scale in vivo femtosecond laser neurosurgery screen reveals small-molecule enhancer of regeneration. *Proc. Natl. Acad. Sci. U. S. A.* **2010**, *107* (43), 18342-18347.
93. Burns, A. R.; Wallace, I. M.; Wildenhain, J.; Tyers, M.; Giaever, G.; Bader, G. D.; Nislow, C.; Cutler, S. R.; Roy, P. J., A predictive model for drug bioaccumulation and bioactivity in *Caenorhabditis elegans*. *Nature Chemical Biology* **2010**, *6* (7), 549-557.
94. Leeson, P. D.; Springthorpe, B., The influence of drug-like concepts on decision-making in medicinal chemistry. *Nat. Rev. Drug Discov.* **2007**, *6* (11), 881-890.
95. Anniyappan, M.; Muralidharan, D.; Perumal, P. T., Synthesis of Hantzsch 1,4-dihydropyridines under microwave irradiation. *Synthetic Communications* **2002**, *32* (4), 659-663.

96. Xia, J. J.; Wang, G. W., One-pot synthesis and aromatization of 1,4-dihydropyridines in refluxing water. *Synthesis-Stuttgart* **2005**, (14), 2379-2383.
97. Squella, J. A.; Nunezvergara, L. J., Polarography as a Technique for Determining Photodegradation in Calcium Antagonists. *Bioelectrochemistry and Bioenergetics* **1990**, 23 (2), 161-166.
98. Guengerich, F. P.; Brian, W. R.; Iwasaki, M.; Sari, M. A.; Baarnhielm, C.; Berntsson, P., Oxidation of Dihydropyridine Calcium Channel Blockers and Analogs by Human Liver Cytochrome P-450 IIIA4. *Journal of Medicinal Chemistry* **1991**, 34 (6), 1838-1844.
99. Oleary, D. D. M.; Stanfield, B. B.; Cowan, W. M., Evidence that the Early Postnatal Restriction of the Cells of Origin of the Callosal Projection is due to the Elimination of Axonal Collaterals Rather than to the Death of Neurons. *Dev. Brain Res.* **1981**, 1 (4), 607-617.
100. Stanfield, B. B.; Oleary, D. D. M.; Fricks, C., Selective Collateral Elimination in Early Postnatal Development Restricts Cortical Distribution of Rat Pyramidal Tract Neurons. *Nature* **1982**, 298 (5872), 371-373.
101. Cohen-Cory, S.; Kidane, A. H.; Shirkey, N. J.; Marshak, S., Brain-Derived Neurotrophic Factor and the Development of Structural Neuronal Connectivity. *Dev. Neurobiol.* **2010**, 70 (5), 271-288.
102. Page, A. P.; Johnstone, I. L., The cuticle. *WormBook : the online review of C. elegans biology* **2007**, 1-15.
103. Aebi, A.; Barton, D. H. R.; Lindsey, A. S., Sesquiterpenoids. 3. The Stereochemistry of Caryophyllene. *Journal of the Chemical Society* **1953**, 3124-3129.
104. Aebi, A.; Barton, D. H. R.; Burgstahler, A. W.; Lindsey, A. S., Sesquiterpenoids. 5. The Stereochemistry of the Tricyclic Derivatives of Caryophyllene. *Journal of the Chemical Society* **1954**, 4659-4665.

105. Zlotkowski, K.; Eliassen, A. M.; Mitra, A.; Siegel, D., Small-Molecule Mechanism of Action Studies in *Caenorhabditis elegans*. *ChemBioChem* **2013**, *14* (17), 2338-2344.
106. Vanfleteren, J. R., Large-Scale Cultivation of a Free-Living Nematode (*Caenorhabditis elegans*). *Experientia* **1976**, *32* (8), 1087-1088.
107. Gbewonyo, K.; Rohrer, S. P.; Lister, L.; Burgess, B.; Cully, D.; Buckland, B., Large-Scale Cultivation of the Free-Living Nematode *Caenorhabditis elegans*. *Bio-Technology* **1994**, *12* (1), 51-54.
108. Bhaskaran, S.; Butler, J. A.; Becerra, S.; Fassio, V.; Girotti, M.; Rea, S. L., Breaking *Caenorhabditis elegans* the easy way using the Balch homogenizer: An old tool for a new application. *Anal. Biochem.* **2011**, *413* (2), 123-132.
109. Leslie, B. J.; Hergenrother, P. J., Identification of the cellular targets of bioactive small organic molecules using affinity reagents. *Chem. Soc. Rev.* **2008**, *37* (7), 1347-1360.
110. Rauthan, M.; Ranji, P.; Pradenas, N. A.; Pitot, C.; Pilon, M., The mitochondrial unfolded protein response activator ATFS-1 protects cells from inhibition of the mevalonate pathway. *Proc. Natl. Acad. Sci. U. S. A.* **2013**, *110* (15), 5981-5986.
111. Min, J.; Kim, Y. K.; Cipriani, P. G.; Kang, M.; Khersonsky, S. M.; Walsh, D. P.; Lee, J. Y.; Niessen, S.; Yates, J. R.; Gunsalus, K.; Piano, F.; Chang, Y. T., Forward chemical genetic approach identifies new role for GAPDH in insulin signaling. *Nature Chemical Biology* **2007**, *3* (1), 55-59.
112. Wang, X.; Imber, B. S.; Schreiber, S. L., Small-molecule reagents for cellular pull-down experiments. *Bioconjugate Chem.* **2008**, *19* (3), 585-587.
113. Tanaka, H.; Kuroda, A.; Marusawa, H.; Hatanaka, H.; Kino, T.; Goto, T.; Hashimoto, M.; Taga, T., Structure of FK506 - A Novel Immunosuppressant Isolated from *Streptomyces*. *J. Am. Chem. Soc.* **1987**, *109* (16), 5031-5033.

114. Holt, D. A.; Luengo, J. I.; Yamashita, D. S.; Oh, H. J.; Konialian, A. L.; Yen, H. K.; Rozamus, L. W.; Brandt, M.; Bossard, M. J.; Levy, M. A.; Eggleston, D. S.; Liang, J.; Schultz, L. W.; Stout, T. J.; Clardy, J., Design, Synthesis, and Kinetic Evaluation of High-Affinity FKBP Ligands and the X-ray Crystal Structures of their Complexes with FKBP12. *J. Am. Chem. Soc.* **1993**, *115* (22), 9925-9938.
115. Mutz, M.; Barr, K. J.; Gestwicki, J. PROTEASE INHIBITORS International Patent WO 2010/077317 A2. July 8, 2010.
116. Siekierka, J. J.; Hung, S. H. Y.; Poe, M.; Lin, C. S.; Sigal, N. H., A Cytosolic Binding Protein for the Immunosuppressant FK506 has Peptidyl-Prolyl Isomerase Activity But is Distinct from Cyclophilin. *Nature* **1989**, *341* (6244), 755-757.
117. Liu, J.; Farmer, J. D.; Lane, W. S.; Friedman, J.; Weissman, I.; Schreiber, S. L., Calcineurin is a Common Target of Cyclophilin-Cyclosporine A and FKBP-FK506 Complexes. *Cell* **1991**, *66* (4), 807-815.
118. Kang, C. B.; Ye, H.; Dhe-Paganon, S.; Yoon, H. S., FKBP Family Proteins: Immunophilins with Versatile Biological Functions. *Neurosignals* **2008**, *16* (4), 318-325.
119. Ong, S. E.; Schenone, M.; Margolin, A. A.; Li, X. Y.; Do, K.; Doud, M. K.; Mani, D. R.; Kuai, L.; Wang, X.; Wood, J. L.; Tolliday, N. J.; Koehler, A. N.; Marcaurelle, L. A.; Golub, T. R.; Gould, R. J.; Schreiber, S. L.; Carr, S. A., Identifying the proteins to which small-molecule probes and drugs bind in cells. *Proc. Natl. Acad. Sci. U. S. A.* **2009**, *106* (12), 4617-4622.
120. Hernandez, P.; Muller, M.; Appel, R. D., Automated protein identification by tandem mass spectrometry: Issues and strategies. *Mass Spectrom. Rev.* **2006**, *25* (2), 235-254.
121. Zlotkowski, K.; Pierce-Shimomura, J.; Siegel, D., Small-Molecule-Mediated Axonal Branching in *Caenorhabditis elegans*. *ChemBioChem* **2013**, *14* (3), 307-310.
122. Sakamoto, R.; Byrd, D. T.; Brown, H. M.; Hisamoto, N.; Matsumoto, K.; Jin, Y., The *Caenorhabditis elegans* UNC-14 RUN domain protein binds to the kinesin-1

- and UNC-16 complex and regulates synaptic vesicle localization. *Mol. Biol. Cell* **2005**, *16* (2), 483-496.
123. Lin, S.; Liu, M.; Son, Y. J.; Himes, B. T.; Snow, D. M.; Yu, W. Q.; Baas, P. W., Inhibition of Kinesin-5, a Microtubule-Based Motor Protein, As a Strategy for Enhancing Regeneration of Adult Axons. *Traffic* **2011**, *12* (3), 269-286.
 124. Timmons, L.; Court, D. L.; Fire, A., Ingestion of bacterially expressed dsRNAs can produce specific and potent genetic interference in *Caenorhabditis elegans*. *Gene* **2001**, *263* (1-2), 103-112.
 125. Axelrod, A.; Eliassen, A. M.; Chin, M. R.; Zlotkowski, K.; Siegel, D., Syntheses of Xanthofulvin and Vinaxanthone, Natural Products Enabling Spinal Cord Regeneration. *Angew. Chem.-Int. Edit.* **2013**, *52* (12), 3421-3424.
 126. Chin, M. R.; Zlotkowski, K.; Han, M.; Patel, S.; Eliassen, A. M.; Axelrod, A.; Siegel, D., Expedited Access to Vinaxanthone and Chemically Edited Derivatives Possessing Neuronal Regenerative Effects through Ynone Coupling Reactions. *ACS Chemical Neuroscience* **2015**.
 127. Wu, Z.; Ghosh-Roy, A.; Yanik, M. F.; Zhang, A. Z.; Jin, Y. S.; Chisholm, A. D., *Caenorhabditis elegans* neuronal regeneration is influenced by life stage, ephrin signaling, and synaptic branching. *Proc. Natl. Acad. Sci. U. S. A.* **2007**, *104* (38), 15132-15137.
 128. Goodman, M. B.; Schwarz, E. M., Transducing touch in *Caenorhabditis elegans*. *Annu. Rev. Physiol.* **2003**, *65*, 429-452.
 129. Syntichaki, P.; Tavernarakis, N., The biochemistry of neuronal necrosis: Rogue biology? *Nat. Rev. Neurosci.* **2003**, *4* (8), 672-684.
 130. Chalfie, M.; Sulston, J., Developmental Genetics of the Mechanosensory Neurons of *Caenorhabditis elegans*. *Dev. Biol.* **1981**, *82* (2), 358-370.

131. Chalfie, M.; Sulston, J. E.; White, J. G.; Southgate, E.; Thomson, J. N.; Brenner, S., The Neural Circuit for Touch Sensitivity in *Caenorhabditis elegans*. *J. Neurosci.* **1985**, *5* (4), 956-964.
132. Richardson, P. M.; Issa, V. M. K., Peripheral Injury Enhances Central Regeneration of Primary Sensory Neurons. *Nature* **1984**, *309* (5971), 791-793.
133. Parikh, P.; Hao, Y. H.; Hosseinkhani, M.; Patil, S. B.; Huntley, G. W.; Tessier-Lavigne, M.; Zou, H. Y., Regeneration of axons in injured spinal cord by activation of bone morphogenetic protein/Smad1 signaling pathway in adult neurons. *Proc. Natl. Acad. Sci. U. S. A.* **2011**, *108* (19), E99-E107.
134. Neumann, B.; Nguyen, K. C. Q.; Hall, D. H.; Ben-Yakar, A.; Hilliard, M. A., Axonal Regeneration Proceeds Through Specific Axonal Fusion in Transected *C. elegans* Neurons. *Dev. Dyn.* **2011**, *240* (6), 1365-1372.